IN VITRO ASSESSMENT OF THE PHYSIOLOGICAL BIOCORROSION BEHAVIOUR OF MAGNESIUM-BASED BIOMATERIALS

A thesis
submitted in partial fulfilment
of the requirements for the Degree of

DOCTOR OF PHILOSOPHY IN MECHANICAL ENGINEERING
AT THE
UNIVERSITY OF CANTERBURY

BY

NICHOLAS TRAVIS KIRKLAND

University of Canterbury

2011

Preface

This thesis is submitted as a partial requirement for the degree of Doctor of Philosophy in Mechanical Engineering. The research covered in this thesis was conducted under the supervision of Dr. Mark P. Staiger in the Mechanical Engineering Department, University of Canterbury, between October 2007 and December 2010.

Abstract

Magnesium (Mg) and its alloys provide numerous unique benefits as potential resorptive biomaterials and present the very real possibility of replacing current metallic implant materials in a variety of roles. However, considerable research remains before Mg alloys may be accurately screened and used *in vivo*. Most critically, a more comprehensive understanding of the corrosion of Mg alloys *in vitro* is needed.

This research program critically examined the types of *in vitro* experiments that may be performed on Mg alloys, investigated the numerous variables that affect Mg biodegradation when undertaking these experiments, explored the electrochemical performance of several biocompatible Mg alloys, and developed a novel process for producing ordered Mg structures.

The benefits and drawbacks of a range of *in vitro* tests were first investigated. The key strengths and weaknesses of each test were identified and recommendations provided for their respective use in the quest to determine Mg alloy biodegradation. The most common variables applicable to all *in vitro* experiments were then explored in detail, and their effect on the biocorrosion of a number of Mg alloys was determined. Recommendations were then made for the appropriate control of the different experimental variables based on these findings.

For the first time, the mechanistic control of Mg biodegradation by the microstructure of biocompatible alloys has been examined. This allows for greater understanding of the reasons for varied corrosion of alloys in bio-electrolytes, and is a step towards the effective design of Mg alloys for different bio-applications.

A novel method to produce ordered Mg structures was developed, with relevant processing parameters investigated in light of their effect on biocorrosion and mechanical performance.

Overall, the results and findings from this research further our understanding of the potential of Mg alloys as suitable biomaterials, and advance our knowledge of how to proceed towards the goal of using such alloys for biological applications.

Acknowledgements

I would like to thank all individuals and organisations that assisted and supported me in the completion of my PhD thesis.

First and foremost I would like to acknowledge my supervisors, Dr. Mark Staiger, Dr. Timothy Woodfield, and Dr. George Dias, for their guidance, continual support and encouragement over the course of my entire candidature.

I would also like to thank my external supervisor, Dr. Nick Birbilis of Monash University, for all the time, money and support he has provided me with. Without significant investment on his part, I would not have accomplished half of what I have done.

In addition, I would like to thank Kevin Stobbs, Mike Flaws, Julian Philips, Paul Southward, Karl Buchanan, Jay Waterman, Jemimah Walker, Shaylin Shadanbaz, Kristeen Nield-Patterson, Thanh Nguyen and the entire workshop for all the help and training they have provided over the past years.

I would like to acknowledge the funding of this research by the Foundation for Research, Science and Technology (FRST) and the University of Canterbury Department of Mechanical Engineering.

Most of all I would like to thank my family, without whose support I would not have been able to start nor finish my work. I owe you everything.

Publications

Kirkland, N. T., Staiger, M. P., Nisbet, D., Davies, C. H. J., and Birbilis, N., *Performance-driven Design of Biocompatible Mg Alloys* , JOM, *article in press*.

Kirkland, N. T., Kolbeinsson, I., Woodfield, T., Dias, G., and Staiger, M. P., *Synthesis and Properties of Topologically-ordered Porous Magnesium*, Journal of Materials Science and Engineering B: Advanced Functional Solid-State Materials, *article in press*.

Sudholz, A. D., Kirkland, N. T., Buchheit, R. G., and Birbilis, N., *Electrochemical Properties of Intermetallic Phases and Common Impurity Elements in Magnesium Alloys*, Electrochemical and Solid-State Letters, 2011, 14(2):C5-C7.

Staiger, M. P., Kolbeinsson, I., Kirkland, N. T., Nguyen, T., Dias, G., and Woodfield, T., *Synthesis of Topology-Ordered Open-Cell Porous Magnesium*, Materials Letters, 2010, 64:2572-2574.

Kirkland, N. T., Birbilis, N., Walker, J., Woodfield, T., Dais, G., and Staiger, M. P., *In Vitro Dissolution of Magnesium-Calcium Binary Alloys*, Journal of Biomedical Materials Research Part B: Applied Biomaterials, 2010, 95B:91-100.

Kirkland, N. T., Lespagnol, J., Birbilis, N., Staiger, M. P., *A Survey of Bio-Corrosion Rates of Magnesium Alloys*, Corrosion Science, 2010, 52:287-291.

Kirkland, N. T., Kolbeinsson, I., Staiger, M. P., Dias, G. and Woodfield, T., *Processing-Property Relationships of As-Cast Magnesium Foams with Controllable Architecture*, International Journal of Modern Physics B, 2008, 23(6):1002-1008.

Presentations

Kirkland, N. T., Waterman, J., Staiger, M.P., Birbilis, N., *Effect of Buffering System on Biological Performance of Magnesium Alloys*, National Association of Corrosion Engineers Expo, Houston,13-17 March 2011, *presentation.*

Kirkland, N. T., Dias, G., Woodfield, T., Birbilis, N., Staiger, M.P., *Toward Standardized In Vitro Performance Testing of Mg Alloys*, 23rd European Society for Biomaterials (ESB) Conference, Tampere (Finland), 11-15th September 2010, *presentation.*

Kirkland, N. T., Walker, J., Dias, G., Woodfield, T., Birbilis, N., Staiger, M.P., *Losses in Mass and Yield Strength of Mg-Based Biomaterials Due to Biodegradation Environment*, 23rd European Society for Biomaterials (ESB) Conference, Tampere (Finland), 11-15th September 2010, *poster.*

Kirkland, N. T., Birbilis, N., Dias, G., Woodfield, T., Staiger, M., *Predictive in vitro assessment of Mg-based biomaterials*, 2nd Symposium on Biodegradable Metals, Maratea (Italy), 1-3 September 2010, *presentation.*

Kirkland, N. T., *Biocorrosion Behavior of Mg-Ca Binary Alloys*, National Association of Corrosion Engineers Expo, San Antonio,14-18 March 2010, *poster.*

Kirkland, N. T., Staiger, M. P., Birbilis, N., Woodfield, T., Dias, G., *Biocorrosion Behaviour of Mg-Ca Binary Alloys*, 20th Annual Conference of the ASBTE, Brisbane, 10-12 February 2010, *presentation/poster*.

Kirkland, N. T., Staiger, M. P., Walker, J., Dias, G. and Woodfield, T., *Biocompatibility Screening Methods For Magnesium Alloys in Orthopaedic Applications*, 19th Annual Conference of the ASBTE, Sydney, 21-23 January 2009, *poster*.

Staiger, M. P, Kirkland, N. T., Kolbeinsson, I., Walker, J., Dias, G. and Woodfield, T., *A Manufacturing Route for Cellular Magnesium With Ordered Architecture Aimed At Orthopaedic Applications*, 19th Annual Conference of the ASBTE, Sydney, 21-23 January 2009, *presentation.*

Kirkland, N. T., *Corrosion Behaviour And Biocompatibility Data Of A Number of Mg Alloys*, New Zealand Medical Research Society (NZMRS), Christchurch, 8 December, 2008, *presentation.*

Kirkland, N. T., Kolbeinsson, I., Staiger, M. P., Dias, G. and Woodfield, T., *Processing-Property Relationships of As-Cast Magnesium Foams with Controllable Architecture*, Conference on Advanced Materials and Processing 5, Harbin, China, 2-5 September, 2008, *presentation.*

Table of Contents

List of Figures

List of Tables

List of Equations

List of Abbreviations

Abbreviation	Meaning
AA	Amino acids
BSA	Bovine serum albumin
BSS	Balanced salt solutions
CPE	Constant phase element
CytoC	Cytochrome C
E_{corr}	Corrosion potential
EBSD	Electron backscatter diffraction
EBSS	Earle's balanced salt solution
EDL	Electrical double layer
EDS	Energy-dispersive X-ray spectroscopy
EIS	Electrochemical impedance spectroscopy
FTIR	Fourier transform infrared spectroscopy
G	Gibbs free energy
H_2^{evo}	Hydrogen evolution experiment
HBSS	Hanks' balanced salt solution
HP	Human plasma
i_{corr}	Corrosion potential
KBM	Kirkland's biocorrosion medium
MEM	Minimum essential medium
MEM+BSA	MEM with bovine serum albumin
MEM+FBS	MEM with foetal bovine serum
ML	Mass loss experiment
OCP	Open circuit potential
PBS	Phosphate-buffered solution
QCM	Quartz crystal microbalance
R_{CT}	Charge transfer resistance
R_f	Film resistance
R_{tot}	Total resistance
R_{P-B}	Pilling-Bedworth ratio
RP	Rapid prototype
SB/CO^2	Sodium bicarbonate with CO^2 environment buffer
SEM	Scanning electron microscope
T_{phy}	Physiological temperature
T_{rm}	Room temperature
TOPM	Topologically ordered porous magnesium
TR	Template-rough scaffold

CHAPTER 1: Introduction

1.1. Overview

Magnesium (Mg) has been investigated as a potential biodegradable implant material for more than a century [1]. Although early trials displayed varying levels of success, there has recently been a surge of renewed interest in Mg biomaterials. Mg breaks the paradigm of biometal science, an area traditionally dominated by permanent, bio-inert fixtures, as it offers a ground-breaking approach to implant design by providing a temporary structural material which can be used in a wide variety of applications.

The potential for Mg biomaterials, particularly in orthopaedic applications, is clear. Mg is the fourth most abundant metal ion found within the human body, is a vital nutrient for life and is present in every cell type for all organisms [2-7]. Mg is a fundamental dietary requirement, and is efficiently controlled in the body by homeostatic mechanisms [8, 9]. As a result, toxicity of Mg implants is generally not considered to be a problem.

Mg and its alloys offer a number of other potential benefits over current implant materials. These include: low density, high damping capacity, ease of machinability, elastic modulus close to that of bone, biocompatibility and osteogenicity. However, what truly separates Mg from current metallic implants is its ability to biodegrade *in vivo*. This creates the potential for designing implants that remain in the body only long enough to perform their intended function without the eventual need for surgical retrieval. In orthopaedic applications, implants have been dominated by load-bearing designs based on permanent, non-biodegradable metals such as stainless steel and titanium. The benefits of such a temporary, biodegradable approach to implant design are numerous. Most importantly, they save the patient and healthcare provider time and money, and they lessen the likelihood of complications associated with implant removal or revision.

The renewed interest in investigating the potential of Mg alloys as biomaterials has been due in part to decreased impurity levels – a problem that plagued early trials [10-19]. In its much purer forms, Mg exhibits substantially decreased rates of corrosion [20]. Nevertheless,

despite renewed interest there still exist significant barriers to the development of Mg and its alloys as effective implant materials.

These barriers are manifold. The development of a clinically relevant biomedical implant would ideally require thorough *in vivo* testing, first using animal models but followed later by trials in humans. Unfortunately, several factors significantly hinder the effective use of these tests, including time, cost, and most notably the potential harm and discomfort such studies can cause to experimental animals. Government agencies around the world strictly regulate the approval of *in vivo* studies, generally requiring the material to exhibit significant potential promise as an implant before animal studies can be commenced. Thus, it is vital to first undertake appropriate *in vitro* tests to screen Mg alloys for potential problems before proceeding to *in vivo* studies.

In vitro tests for Mg alloys have generally focused on either: (i) degradation behaviour, or (ii) toxicity. However, the latter is strongly related to the former, as rapid degradation can lead to concentration toxicity and associated problems. Degradation experiments appear to hold the key to determining the suitability of a given Mg alloy (assuming mechanical and structural properties are met), since acceptable biocompatibility (*i.e.* non-toxicity) of Mg has been reported [3, 8, 21-26].

There are several commonly used *in vitro* tests for examining Mg degradation behaviour, from simple immersion or mass loss experiments to electrochemical investigations, which provide mechanistic information on how Mg degrades. The various *in vitro* methods each have their own unique benefits and limitations. It will be shown through the present work that studies in the literature have frequently made wide-ranging and imprecise assumptions by utilising unsuitable *in vitro* tests not designed for the intended use. Inappropriate testing and the interpretation of the consequent results could potentially justify the use of *in vivo* experiments where they are not warranted. It is therefore crucial to fully understand the correct usages of each type of experiment, and, perhaps even more important, the shortcomings that need to be considered before drawing conclusions. In this thesis, a primary aim is to elucidate the principal benefits and drawbacks of each experiment with respect to its role in the investigation of Mg biodegradation.

The literature also appears to exhibit a lack of understanding as to the impact that different variables may have on the results of Mg *in vitro* experiments. Many studies have overlooked important aspects that have the potential to seriously affect the derived outcomes and conclusions. Some variables (*e.g.* pH, temperature, medium) are common to all *in vitro* experiments and play crucial roles in the degradation mechanisms of any metal. However, these variables are particularly influential with respect to Mg alloys, since these alloys corrode rapidly in even mildly aggressive environments. The absence of sufficient emphasis on the effects of these variables within the literature suggests that most studies to date have drawn inaccurate conclusions with regard to the biodegradable nature of Mg *in vitro*. Thus, a real need exists to more clearly determine the relative importance of *in vitro* test variables on Mg biodegradation. This thesis attempts to do this.

Over the years, a wide range of Mg alloys have been investigated as potential implant materials, especially those containing aluminium, calcium, and zinc. Due to the limited solubility of these elements in Mg, many of these alloys contain secondary phases consisting of a mix of Mg and the element(s). Although the performance of these alloys has been investigated on a macro-scale, very little work has been done to clarify the individual contribution of each phase to the degradation mechanisms. Therefore, developing a greater understanding of these mechanisms is a necessary step on the path to effectively identifying an alloy for eventual implantation. This thesis contributes to this understanding by illustrating some of the effects that alloying can have on Mg degradation performance.

One aspect of Mg biomaterial design that has been largely overlooked in the literature is a suitable method to produce the variety of shapes required by different biomedical applications. Open cell designs provide numerous benefits in the biomaterials field, such as allowing the channelling of bone growth and providing a larger surface area for cellular attachment. To this end, considerable work has been performed on a variety of materials from titanium to bio-active hydroxyapatite-based materials to create a wide range of 3D structures [27]. However, until recently no method has been available to produce optimised ordered Mg structures both accurately and safely for use as potential implants. This has severely limited the possible applications for alloys that show promise, as many applications (such as spinal fusion) significantly benefit from an ordered porous macro-topology, which can lead to increased osteogenesis and bone integration. A novel method, developed in part by the author, shows real potential as a prospective process for producing a variety of ordered

shapes using only biocompatible materials, opening the possibility for development of appropriate Mg implant designs.

To summarise, the overall aim of this study was to critically assess and discuss the various *in vitro* tests that are currently available and to explicate the impact of important variables related to these tests. In addition, this study endeavours to determine the effects of some common alloying additions on biodegradation mechanisms. Finally, an innovative ordered structure technique is investigated to determine its potential as a production method for Mg cellular implants.

1.2. Outline of thesis

The chapters of this work are summarised as follows:

Chapter 2 provides an overview of magnesium and its alloys and their potential as biomaterials. Background is provided on both corrosion science techniques and the biological aspects of the body that affect implant success. Finally an overview of current *in vitro* test methods is provided.

Chapter 3 outlines the research goals of this dissertation based on a critical review of the available literature.

Chapter 4 explains how the Mg alloys used in this study were produced, prepared, tested and analysed. Details are provided on the mechanics of several experimental methods in order to provide a basis for understanding the interpretation of the results.

Chapter 5 provides an investigation into the most common *in vitro* test methods used today. The benefits and drawbacks of each are discussed in light of the data that is obtained.

Chapter 6 critically assesses the common experimental variables *in vitro*. The effects of temperature, pH, buffering system, media, medium flow rate and sample preparation are examined and discussed. Experimental data are provided to elucidate their relative importance to Mg corrosion *in vitro*. Some recommendations are made on the appropriate control of experimental variables based on these findings.

Chapter 7 investigates the effect of several common biocompatible alloying elements on the corrosion properties of Mg in various simulated body fluids. The contributions of individual phases are clarified with respect to their effect on the degradation mechanism.

Chapter 8 presents a synthesis of topologically-ordered porous Mg that is aimed at orthopaedic applications. Processing parameters are investigated for the purpose of explaining their effect on the corrosion and mechanical performance of the resultant porous structures.

Chapter 9 presents the overall conclusions of the research.

Chapter 10 discusses areas for future research that need to be undertaken to eventually develop an appropriate *in vitro* screening test for using Mg alloys for biomedical applications.

Appendix A describes the standard "reference human" in terms of macroscopic parameters and mechanical and physiochemical conditions.

Appendix B provides a table of the main *in vivo* tests that were collected and analysed as part of this work.

Appendix C provides a table of the main *in vitro* tests that were collected and analysed as part of this work.

Appendix D displays a table of the elemental composition of all alloys created in this work.

Appendix E describes the preparation protocol used to create a novel *in vitro* corrosion medium first presented in this dissertation.

Appendix F provides a list of common techniques used to determine protein adhesion.

Appendix G provides a list of all references used in the appendix.

1.3. References

[1] Huse, E.C. *A New Ligature?* Chicago Medical Journal and Examiner 1878;37:171.

[2] Staiger, M.P., A.M. Pietak, J. Huadmai, G. Dias. *Magnesium and Its Alloys as Orthopedic Biomaterials: A Review*. Biomaterials 2006;27:1728.

[3] Saris, N.-E.L., E. Mervaala, H. Karppanen, J.A. Khawaja, A. Lewenstam. *Magnesium: An Update on Physiological, Clinical and Analytical Aspects*. Clinica Chimica Acta 2000;294:1.

[4] Song, G. *Control of Biodegradation of Biocompatable Magnesium Alloys*. Corrosion Science 2007;49:1696.

[5] Seiler, H.G., H. Sigel. *Handbook of Toxicity of Inorganic Compounds*. New York, USA: Marcel Dekker Inc., 1988.

[6] Leroy, J. *Necessite Du Magnesium Pour La Croissance De La Souris*. Comptes Rendus de Seances de la Societe de Biologie 1926;94:431.

[7] Lusk, J.E., R.J.P. Williams, E.P. Kennedy. *Magnesium and the Growth of Escherichia Coli*. Journal of Biological Chemistry 1968;243:2618.

[8] Vormann, J. *Magnesium: Nutrition and Metabolism*. Molecular Aspects of Medicine 2003;24:27.

[9] Sojka, J.E., C.M. Weaver. *Magnesium Supplementation and Osteopososis*. Nutrition Review 1995;53:71.

[10] Shi, P., W.F. Ng, M.H. Wong, F.T. Cheng. *Improvement of Corrosion Resistance of Pure Magnesium in Hank's Solution by Microarc Oxidation with Sol-Gel Tio2 Sealing*. Journal of Alloys and Compounds 2009;469(1-2):286.

[11] Duygulu, O., R.A. Kaya, G. Oktay, A.A. Kaya. *Investigation on the Potential of Magnesium Alloy Az31 as a Bone Implant*. Materials Science Forum 2007;546-549:421.

[12] Lopez, H.Y., D.A. Cortes, S. Escobedo, D. Mantovani. *In Vitro Bioactivity Assessment of Metallic Magnesium*. Key Engineering Materials 2006;309-311:453.

[13] Witte, F., H. Ulrich, M. Rudert, E. Willbold. *Biodegradable Magnesium Scaffolds: Part 1: Appropriate Inflammatory Response*. Journal of Biomedical Materials Research Part A 2007:748.

[14] Willliams, D. *New Interests in Magnesium*. Medical device technology 2006;17:9.

[15] Witte, F., J. Nellesen, H.-A. Crostack, V. Kaese, A. Pisch, F. Beckmann, H. Windhagen. *In Vitro and in Vivo Corrosion Measurements of Magnesium Alloys*. Biomaterials 2006;27:1013.

[16] Witte, F., V. Kaese, H. Haferkamp, E. Switzer, A. Meyer-Lindenberg, C.J. Wirth, H. Windhagen. *In Vivo Corrosion of Four Magnesium Alloys and the Associated Bone Response*. Biomaterials 2005;26:3557.

[17] Denkena, B., C. Podolsky, A. Lucas, T. Hassel, F. Witte, O. Palm, C. Hurschler. *Degradable Implants Made of Magnesium Alloys*. 5th Euspen International Conference, vol. 6. Montpellier, France, 2005.

[18] Witte, F., N. Hort, C. Vogt, S. Cohen, K.U. Kainer, R. Willumeit, F. Feyerabend. *Degradable Biomaterials Based on Magnesium Corrosion*. Current Opinion in Solid State and Materials Science 2008;12:63.

[19] Zeng, R., W. Dietzel, F. Witte, N. Hort, C. Blawert. *Progress and Challenge for Magnesium Alloys as Biomaterials*. Advanced Engineering Materials 2008;10:B3.

[20] Lee, J.-Y., G. Han, Y.-C. Kim, J.-Y. Byun, J.-i. Jang, H.-K. Seok, S.-J. Yang. *Effects of Impurities on the Biodegradation Behavior of Pure Magnesium*. Metals and Materials International 2009;15:955.

[21] Blokhuis, T.J., M. Termaat, H.J. Haarman. *Properties of Calcium Phosphate Ceramics in Relation Fo Their in Vivo Behaviour*. The Journal of Trauma, Injury, Infection and Critical Care 2007;48.

[22] Allan, B. *Closer to Nature : New Biomaterials and Tissue Engineering*. British Journal of Opthamology 1999;83:1235.

[23] Merck International. *Water, Electrolyte Mineral, and Acid/Base Metabolism*. In: Porter, R.S., Kaplan, J.L., editors. Merck Manual of Diagnosis and Therapy. Merck & Co., Inc., 2006.

[24] Okuma, T. *Magnesium and Bone Strength*. Nutrition 2001;17:679.

[25] Wolf, F.I., A. Cittadini. *Chemistry and Biochemistry of Magnesium*. Molecular Aspects of Medicine 2003;24:3.

[26] Hartwig, A. *Role of Magnesium in Genomic Stability*. Mutation Research/Fundamental and Molecular Mechanisms of Mutagenesis 2001;475:113.

[27] Stevens, M.M. *Biomaterials for Bone Tissue Engineering*. Materials Today 2008;11:18.

CHAPTER 2: Literature Review

2.1. Introduction to magnesium and its alloys

By molarity, magnesium (Mg) is the eighth most abundant element in the world, constituting approximately 2.5% of the earth's crust [1]. Whilst first discovered by chemist Joseph Black in 1755, it was isolated by Sir Humphrey Davy in 1808. He created the metal electrolytically from a mixture of magnesium and mercury-oxide. In 1831 Antoine Bussy prepared Mg in its coherent form by mixing magnesium chloride (MgCl) and potassium (K), which precipitates Mg and KCl [2]. Several years later Michael Faraday reduced dehydrated MgCl by electrolysis obtaining pure Mg [3]. Magnesium production has since grown to a >1.17 Mton/yr industry [4].

2.1.1. Production history

To the mid 1990's, Mg was primarily obtained by extraction from fused chloride compounds using electrical current to oxidise the chloride, resulting in the reduction of the Mg metal [5]. However, as Chinese manufacturers began to dominate the global production market, the Pidgeon process has become more common. This involves thermally extracting the magnesium metal from magnesia (MgO) using a high temperature reaction with silicon (Si). This produces silica and Mg vapour that is condensed into solid Mg metal. This process consumes comparative energy to the reduction method, but results in a highly pure metal extraction [6]. Presently, China produces 65% of Mg metal globally, with the US, Russia, Canada, Norway and Israel also having a significant Mg industry [7].

2.1.2. History of use

Mg usage has historically been limited by three factors: i) difficulties with isolation, ii) rapid corrosion, and iii) relatively poor mechanical properties. With yield and ultimate tensile strengths which are poorer than most structural metals, Mg was ignored by industry for many years and considered primarily a curiosity [5]. It remained in production principally for pyrotechnical/photographical use, such as lighting wires for flash photography [8] and for use as the principal alloying element in the majority of aluminium alloys (in which it improves

the range of properties). However, the advent of aviation and the two World Wars resulted in an increase in interest - Mg's low density (1.738 g/cm^2) and moderate yield strength enabled it to be employed in several aircraft with success. The Northrop XP-56 is an example of such implementation and was the first plane made almost entirely of Mg alloys (Figure 2-1).

Figure 2-1 : Northrop XP-56, the first Mg plane. [9]

However, the renewed interest in Mg was short lived as, after the 1940's, other materials such as aluminium proved more economically viable [5]. Although the Mg industry attempted to develop a number of new applications the majority failed to be successful, with the notable exception of Ferdinand Porsche's engine for the VW Beetle. It was not until the 1990's that serious efforts were made to attempt to solve some of the issues limiting the widespread use of Mg alloys. This was driven primarily by automobile manufacturers working with Mg producers to develop new alloys and coatings to provide necessary properties to meet modern vehicle needs, with the main benefit being significant weight savings in the context of 'green engineering' and reduced emissions. The advent of high purity Mg, and its concomitant improvement in corrosion resistance, has also enabled the possibility of new areas of research, such as biomaterials, to be conducted [5].

2.1.3. Properties of pure Mg

Magnesium is an alkaline earth metal (found in Group 3 of the periodic table) which displays a similar electronic structure to beryllium (Be), calcium (Ca), strontium (Sr) , barium (Ba) and radium (Ra). The atomic and physical properties of pure Mg are shown in Table 2-1.

Table 2-1 : Atomic and physical properties of Mg.

Atomic	
Property	**Value**
Elemental Symbol	Mg
Atomic Number	12
Atomic Weight	24.3050
Atomic Diameter	0.320 nm
Atomic Volume	14.0 cm^3/mol
Atomic Isotopes	
78.99%	^{24}Mg
10.0%	^{25}Mg
11.01%	^{26}Mg
Physical	
Property	**Value**
Melting Point	650°C ± 2
Boiling Point	1107°C ± 10
Latent Heat of Fusion	0.37 MJ/kg
Latent Heat of Evaporation	5.25 MJ/kg
Heat of Combustion	25.1 MJ/kg
Specific Heat	
At 20°C	1030 J/(kg K)
At 600°C	1178 J/(kg K)
Electrical Resistivity at 20°C	4.45 μΩ cm
Thermal Conductivity at 25°C	155 W/(kg K)
Linear Coefficient of Thermal Expansion at 20°C	25.2 x 10^{-6} K^{-1}
Density	
at 20°C	1.738 g/cm^3
at 600°C	1.622 g/cm^3
at 650°C (solid)	1.65 g/cm^3
at 650°C (liquid)	1.58 g/cm^3
Volume Change During Solidification	4.2%

Data from [5, 8, 10-12]

The crystal structure of pure magnesium is hexagonal close-packed (HCP). The unit cell and principle crystallographic planes for an HCP crystal are shown in Figure 2-2.

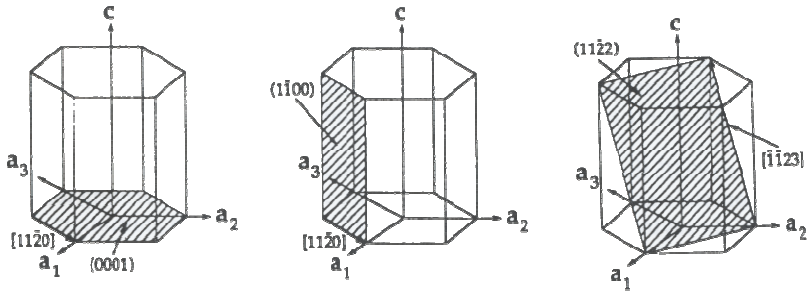

Figure 2-2 : Unit cell and principal planes. [5]

Selected mechanical properties of pure Mg are shown in Table 2-2 after various processing routes.

Table 2-2 : Mechanical properties of pure Mg at 20°C.

	Tensile Strength (MPa)	**Tensile Yield Strength [0.2%] (MPa)**	**Compressive Yield Strength [0.2%] (MPa)**	**Elongation (%) [1]**	**Brinell Hardness [2]**
Sand Cast (13mm)	90	21	21	2-6	30
Extrusion (13mm)	165-205	69-105	43-55	5-8	35
Hard Rolled Sheet	180-220	115-140	105-115	2-10	45-47
Annealed Sheet	160-195	90-105	69-83	3-15	40-41

[1] for 50 mm, [2] for 500 kg load, 10 mm diameter ball
Data from [8, 10]

2.1.4. Composition and properties of Mg alloys

In reality, very few commercial items are made of pure Mg. Alloying is mainly used to improve physical and mechanical properties, such as creep resistance and compressive strength. For example, if the elements remain in solid solution, they can result in solid solution strengthening [5, 8, 13]. Secondary or minor phases form when the solid solubility of any alloying element is exceeded; these phases further enhance strength *via* precipitate strengthening. However, the presence of these minor phases often leads to a reduction in corrosion resistance through micro-galvanic corrosion [14, 15]. Additionally, alloying

provides grain refinement, particularly for cast alloys, which strengthens Mg through grain-boundary strengthening (exploiting the Hall-Petch relationship) and improves ductility [16].

Mg will form solid solutions with many elements although the most common commercial alloys are based on additions of aluminium (Al) and zinc (Zn), with minor additions of calcium (Ca), manganese (Mn), cerium (Ce), lithium (Li), silver (Ag), zirconium (Zr) and rare earth elements (RE) [11]. A summary of some of the most common alloying systems and their properties is presented in Table 2-3.

Table 2-3 : Mg alloying systems and basic properties.

Alloying System (Series)	Solid Solubility in Mg (wt. %)	Background	Key Advantages	Disadvantages
Mg-Al (AE, AZ, AM, AS)	12	• Widely used • One of few elements to form extensive solid solution [17] • Most contain Zn (AZ series)	• Grain refinement • β-phase results in significant increase in strength • Ease of casting • Corrosion improvement	• Susceptibility to microporosity, micro-shrinkage • Mechanical properties can decrease significantly at higher temperature (>120 °C)
Mg-Zn (ZM, ZE)	6.2	• Not extensively used	• Solid-solution strengthening • Corrosion improvement [18]	• Grain refinement difficult by superheating / inoculation
Mg-Zn-Cu (ZC)		• Cu added to improve ductility • Forms $Mg(Cu, Zn)_2$ phase reducing negative effect of Cu	• High tensile strength • Fatigue strength • Good castability • Limited micro-shrinkage	• Relatively poor corrosion resistance
Mg-Mn	0.1	• Mn can be added to stabilize aging process	• Sequesters Fe from solid solution, improving corrosion	
Mg-Zr	0.6	• Rarely used without other elements • Cannot be used with Al or Mn	• Significant grain refinement	• Low strength
Mg-Zn-Zr (ZK)		• Few applications due to limitations	• Excellent grain refinement • High strength	• Microporosity • Poor weldability
Mg-Th (ZH, HZ)	10		• Ease of casting • Good weldability	
Mg-Ag (QE)	15	• Most widely used is QE22	• Low tensile properties	
Mg-RE-Zn-Zr (EZ, ZE)		• Role of Zn not fully understood but beneficial	• Ease of casting • Grain refinement • Good weldability	
Mg-Y (WE)	12.5	• Typically added with other RE	• Improved strength and ductility • Grain refinement	

Data from [5, 8, 11]

2.1.5. Corrosion of metals

All metals exposed to an aqueous environment will undergo electrochemical reactions at the surface, commonly referred to as REDOX reactions. This process is composed of the cathodic (reduction) reaction, which involves the gaining of electrons from the anodic (oxidation) reaction. Both these reactions must occur simultaneously.

The tendency for REDOX reactions to take place is based on the electropotential of the material. The electrochemical series is the most commonly used reference to rank the potentials of cathodic reactions of various elements in comparison to the equilibrium of H_2 [19]. The series is measured at 25 °C and 1 atm with the hydrogen gas dissolution arbitrarily set to 0.00 V (Table 2-4).

Table 2-4 : Electrochemical series for a number of elements versus a standard hydrogen electrode.

Element	**Electrode Potential (V_{SHE})**
Gold	1.692
Platinum	1.18
Palladium	0.951
Silver	0.7996
Copper	0.521
Hydrogen	0.00
Iron	-0.037
Lead	-0.1262
Nickel	-0.257
Cobalt	-0.28
Chromium	-0.744
Zinc	-0.7618
Manganese	-1.185
Titanium	-1.37
Zirconium	-1.53
Aluminium	-1.662
Magnesium	-2.372
Sodium	-2.71
Calcium	-2.868

The magnitude of this potential is indicative of the reaction's tendency to proceed, whilst the sign designates the direction of that tendency. Therefore, elements which possess a strong tendency to be reduced will possess a large positive potential (noble), and elements with a tendency to be oxidised possess a large negative potential (active). Mg has a very large negative potential and therefore reacts readily in mildly aggressive environments. The greater the potential difference, the larger the driving force for a reaction to proceed [20]. This is revealed by a change in Gibb's free energy, which is controlled by the potential difference as shown in Equation 2-1.

$$\Delta G = -nFE \qquad \text{Equation 2-1}$$

Where ΔG is the change in Gibb's free energy, n is the number of equivalents, F is Faraday's constant, and E is the electrochemical potential. With a decrease in Gibb's free energy the likelihood of a change in state also decreases.

2.1.6. Mg electrochemical behaviour

The anodic reaction for Mg is given according to Equation 2-2.

$$Mg_{(S)} \rightarrow Mg^{2+}_{(Aq)} + 2e^{-} \qquad \text{Equation 2-2}$$

This process reduces the ion to its base element [21]. The element that is reduced depends on the reaction pathways available. When Mg is placed in the presence of water with pH < 11, the cathodic reaction involves the evolution of hydrogen gas (H_2) according to Equation 2-3.

$$2H_2O + 2e^{-} = H_2 + 2OH^{-} \qquad \text{Equation 2-3}$$

The OH^{-} is normally ignored as it is considered a "spectator ion" [22], leading to Equation 2-4.

$$2H^{+}_{(Aq)} + 2e^{-} \rightarrow H_2 \qquad \text{Equation 2-4}$$

These reactions can be combined into the overall reaction shown in Equation 2-5 [23-25].

$$Mg_{(S)} + 2H_2O = Mg(OH)_2 + H_2 \qquad \text{Equation 2-5}$$

Equation 2-5 reveals the origins of a magnesium hydroxide ($Mg(OH)_2$) layer that develops on the Mg substrate.

However, in an electrolyte, metal ions (Mg^{2+}) are surrounded by water molecules upon entering into solution. These shield the ions from the attractive forces of the excess electrons ($2e^-$) at the metal surface, allowing metal ions to diffuse away from the substrate. Positively charged ions in the electrolyte ($2H^+$) are then attracted to the negatively charged metal surface, where electrons are consumed to produce H_2. In general, a corroding metal is never in equilibrium so that metal atoms will continue to be oxidised if not protected by a passivation layer.

2.1.7. Passivation layer and general corrosion of Mg

In moist air, magnesium alloys form a thin (< 1 µm) surface layer, primarily consisting of $Mg(OH)_2$. Whereas Al forms a continuous inert oxide layer that protects the underlying metal from further oxidation, the layer that forms on Mg is discontinuous, offering little corrosion protection [12, 26]. The irregular nature of the $Mg(OH)_2$ layer is due to the hexagonal close-packed (HCP) unit cell of Mg that creates a volumetric mismatch with the constituents of the passivation layer. The Pilling-Bedworth ratio ($R_{P\text{-}B}$) which is given by the ratio of volume of the unit cell of metal oxide to that of the corresponding metal from which the oxide is created [27], is only 0.81 for Mg [5]. In comparison, the value for Al is 1.38 which results in complete coverage of the metal surface.

Mg does not form a passivated layer at pH values under 11, as depicted on the Pourbaix diagram (Figure 2-3). This is one of the reasons for the continued dissolution of Mg and its alloys in even slightly aggressive solutions. The MgO layer, or $Mg(OH)_2$ in solution, has an equilibrium pH at 10.4 and is therefore stable in most bases, but will rapidly break down in the presence of acids [28]. However, at pH values of between 8.5 and 11.5 Mg can form a semi-protective $Mg(OH)_2$ layer.

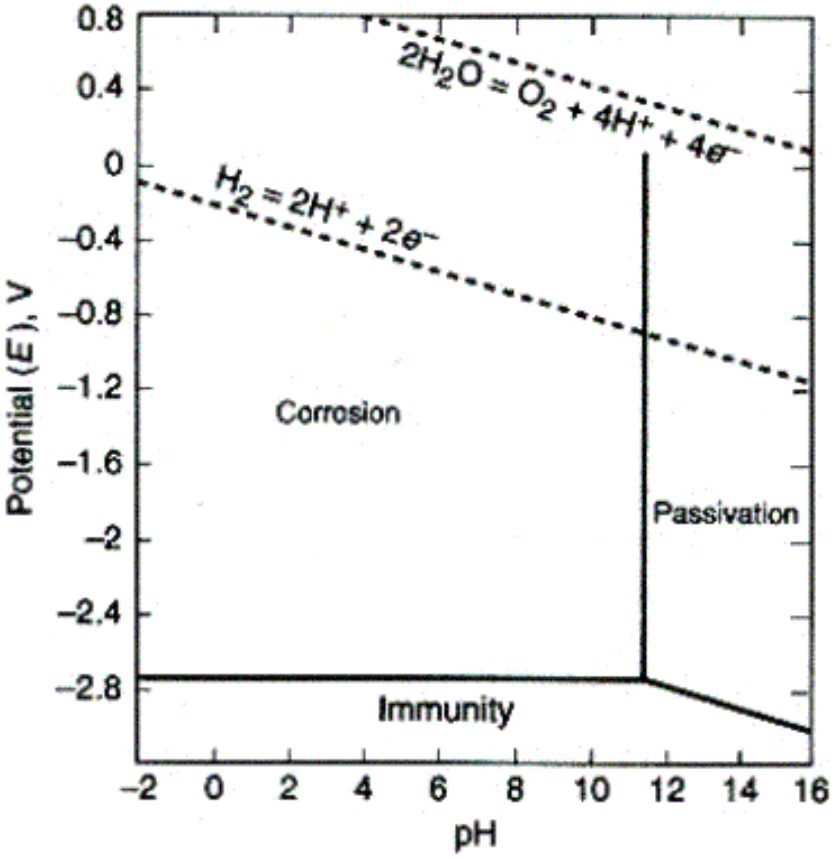

Figure 2-3 : Pourbaix diagram for pure Mg in water at 25 °C. [28]

Corrosion of Mg in neutral environments (ph of ~7) is often described as localised corrosion [29-32]. It is typically initiated as irregular localised corrosion that spreads laterally and covers the whole surface, primarily via pitting corrosion [33]. In general, however, there is not much tendency for deep pitting [29].

Metallurgical factors play a significant role in the corrosion of magnesium. For example, the rate of dissolution can be increased with the addition of trace amounts of impurities, particularly iron (Fe), nickel (Ni) and copper (Cu) [5, 34]. The acceleration of corrosion due to these impurities is primarily due to galvanic corrosion [34]. The impurities typically support the cathodic reaction very well, which in turn speeds the dissolution of the Mg matrix. A summary of the effect of common alloying elements and impurities can be seen in Figure 2-4.

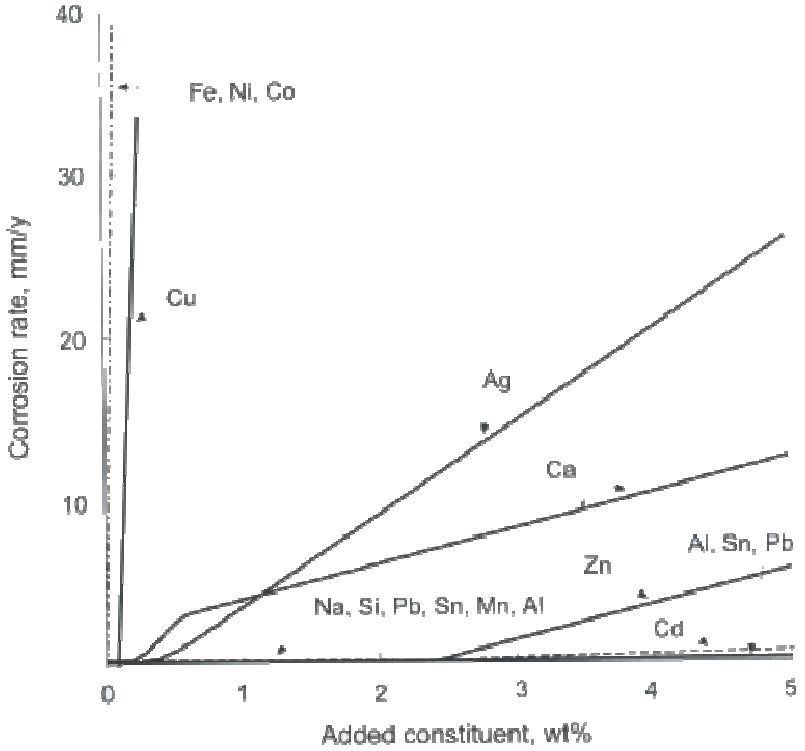

Figure 2-4 : Corrosion rates of binary Mg alloys due to immersion in 3% NaCl aqueous solution. [29]

Overall, the combination of a soluble, cracked and sparse Mg oxide layer and large negative potential means that Mg suffers continued degradation in any ionogenic (*i.e.* capable of forming ions) solution [3].

2.1.8. Mg corrosion in chloride solutions

The vast majority of solutions that are utilised to test the corrosion properties of Mg alloys contain chloride (Cl^-). Immersion, electrochemical and salt-spray testing of Mg is usually carried out in the presence of Cl^- as it is commonly encountered in the natural environment. Cl^- greatly influences the corrosion of Mg at solution concentrations greater than 30 mmol/L [26]. The $Mg(OH)_2$ layer's low density and susceptibility to cracking results in a weak ability to protect the Mg subsurface. In addition $Mg(OH)_2$ is soluble in the presence of Cl^-, and the halide magnesium chloride ($MgCl_2$) is formed more favourably due to the higher electronegativity of Cl^- compared to $(OH)^-$ (Equation 2-6).

$$2Cl^- + Mg(OH)_2 \rightarrow 2OH^- + MgCl_2 \qquad \text{Equation 2-6}$$

$MgCl_2$ is highly water soluble due to its strong tendency to form hydrogen bonds, resulting in the release of the chloride back into solution where it can continue to attack the Mg substrate.

2.1.9. Overview

When considering Mg for traditional structural and industrial applications there are a number of significant issues to overcome. Although a wide range of alloying systems have been developed, offering improvements in properties such as creep resistance or strength, the relatively rapid dissolution of Mg in even mildly aggressive environments has severely limited its use and implementation. This is especially important for long-term applications where the lifetime of the material is of key importance. Combined with relatively poor mechanical properties, significant increase in corrosion due to minute impurity levels, and a relatively under-developed understanding of the specific effects of alloying elements and processes (when compared to the aluminium or steel industries), Mg presents many challenges which hinder its widespread use. However, many of these issues and limitations may be beneficial in the biomedical industry.

2.2. Magnesium as a biomaterial

2.2.1. An introduction to biomaterials

At the outset, it is useful to define what is meant by "biomaterial". Although there are many different definitions, there does not seem to be one that is universally accepted. A broad classification defines it as a "synthetic material used to replace part of a living system or to function in intimate contact with living tissue" [35]. However, this does not include natural biomaterials, which are of particular importance to tissue engineering. One of the more commonly accepted definitions, proposed by the Clemson University Advisory Board for Biomaterials, defines it as "a systematically and pharmacologically inert substance designed for implantation within or incorporation with living systems" [36]. Again this definition does not include those biomaterials that are not inert within the body. Therefore it is unsurprising that one of the most relevant definitions is also one of the longest, namely "materials of synthetic as well as natural origin in contact with tissue, blood, and biological fluids, and intended for use for prosthetic, diagnostic, therapeutic, and storage applications without adversely affecting the living organism and its components" [37].

Biomaterials have been used in societies for thousands of years. The Romans, Aztecs and ancient Chinese all used gold in dentistry, while glass eyes have appeared in historical references for almost as long [36]. However, designs and material choices progressed very little until the turn of the last century. Increased scientific knowledge and improved equipment have seen the number of biomaterials and their implementation dramatically increase. For example, after World War 2, experimentation was carried out using parachute cloth as a vascular prosthesis [38]. It was also in this century that orthopaedic biomaterials truly started to be clinically tested and understood. John Charnley's experimentation with the use of poly(methyl methacrylate) (PMMA) and stainless steel for total hip replacement improved the human condition and spurred further interest in orthopaedic biomaterials replacements [39, 40]. A summary of common currently used biomaterials and their applications is given in Table 2-5.

Table 2-5 : Comparison of several current biomaterials and applications.

Biomaterial	Applications	Advantages	Disadvantages
Polymers: Dacron Nylon Teflon	• Blood vessels • Ligament replacement • Ear & nose replacement • Soft tissue applications	• Ease of fabrication • Processability • Low cost • Resilient • Part biodegradable	• Low compressive strength / hardness • Deformation over time • Degradation
Ceramics: Alumina Hydroxyapatite Carbides	• Dentistry • Hip sockets	• High compressive strength • Biocompatible • Bone conducting	• Difficult to manufacture • Brittle • Not resilient
Composites: Carbon-carbon	• Heart valves • Joint implants	• Mechanical strength	• Difficult to manufacture
Metals: Stainless steel Titanium Co-Cr alloy Gold	• Joint replacement • Bone fixation • Maxillofacial applications	• Mechanical strength • Wear resistance • Ductile	• Corrodes (metal ions) • Dense • High modulus (stress shielding)
Data from [35, 41]			

Biocompatibility is the primary concern when considering the suitability of any material as an implant. Most of the commonly used elements that are included in the composition of metallic implants (*e.g.* iron (Fe), chromium (Cr), nickel (Ni), titanium (Ti), tantalum (Ta), niobium (Nb), molybdenum (Mo), tungsten (W), cobalt (Co)) can only be tolerated in the body at low levels [42]. Although the presence of these elements may be vital to bodily functions, only trace concentrations are tolerable.

The biocompatibility of metals is of considerable importance where there is some susceptibility to corrosion *in vivo*. Corrosion of metal implants over extended periods can lead to implant failure and release of particles; the latter of which may result in problems including inflammation and localised toxicity.

Implant materials are exposed to a harsh environment in the human body – an oxygenated saline solution with a salt (NaCl) content of ~0.9 wt. % at a pH of 7.4 and temperature of 37.1 °C [43]. Bodily fluids consist of water, dissolved oxygen, complex compounds, large amounts of sodium, potassium, calcium, magnesium, phosphate, sulphate, amino acids, proteins, plasma, and a number of other substances [43]. Moreover, the *in vivo* environment can change dramatically in the immediate area of an implant after a surgery, further

complicating the expected biomaterial conditions. Consequently it is vital that in such an aggressive environment the release of elements is accommodated by the physiological system without side effects.

2.2.2. Mg and the body

Recent studies have cited Mg and its alloys as potential materials for biomedical orthopaedic implants [44-53]. The advantages of Mg-based materials include non-toxicity, biocompatibility, mechanical compatibility with bone, and biodegradability in the body [54] (see Chapter 2.2.4.). However, it is first necessary to elucidate the role of Mg in the body, as foreign body toxicity is the primary factor in determining the *in vivo* compatibility of any biomaterial.

Mg is the most abundant free divalent cation (Mg^{2+}) and fourth most abundant metal ion found within cells in the human body [55]. Mg is a vital nutrient for life and is known to be present in all cell types [56-58]. As an intricate part of cellular metabolism, Mg^{2+} dependant enzymes are in almost every metabolic pathway [59]. A significant amount of nucleic acid biochemistry requires Mg, where Mg^{2+} often functions as a signalling molecule [60]. Adenosine triphosphate (ATP), the main source of energy in cells, is bound to Mg^{2+} in order to become biologically active (commonly referred to as Mg-ATP) [61, 62].

The importance of Mg to the physiological system cannot be overstated. The US Food and Nutrition board recently re-established the recommended daily allowance (RDA) of Mg as 420 mg/d and 320 mg/d for men and women, respectively [63]. Mg depletion has been attributed to cardiac arrhythmias, development of artherosclerosis, vasoconstriction of coronary arteries and increased blood pressure [64]. Mg deficiency is also implicated as a risk factor for osteoporosis [65], with Mg supplementations resulting in significantly increased bone density and strength [66]. Along with calcium (Ca), sodium (Na) and potassium (K), Mg is efficiently controlled in the body by homeostatic mechanisms and toxicity is normally not a problem [67].

When Mg is implanted it is hypothesized that the corrosion products are phagocytosed (engulfed) by multinucleated cells [50]. An excess of Mg in serum is controlled by the body using bone and muscle areas to store Mg and excretion *via* the kidneys [68].

2.2.3. History of Mg as a biomaterial

In the late 1800s, American physician Edward C. Huse used Mg as a biomedical implant material. In this seminal work, Mg wires were used in the form of a ligature to stop bleeding vessels in three patients [69]. Huse was excited by the potential of Mg after observing its biodegradable nature *in vivo* [69]. Later in 1892, Austrian physician Erwin Payr began experiments on Mg resorption [70]. Payr was the first to propose that the combination of dissolved salts, tissue oxygen, water content and chemical processes in cells were responsible for *in vivo* corrosion of Mg [70, 71]. In 1907 Albin Lambotte used a plate of pure Mg, with steel nails, to secure a lower leg fracture [72]. The Mg implant was not successful, with the implant surviving only 8 days, along with a large amount of gas liberated subcutaneously. Jean Verbrugge, an assistant to Lambotte, also continued to investigate Mg with a number of animal and clinical studies [73-75].

In 1934 Verbrugge found that a Mg-8Al alloy dissolved completely in the body, producing a large amount of gas [76]. A later study by Troitskii and Tsitrin reported 34 surgeries in which Mg-Cd alloy plates and screws were used [77]. Of these, 9 of the procedures were unsuccessful, with the failures attributed to infection and inadequate treatment of the subcutaneous gas. Further, this work was one of the first written records of the potential bioactivity of Mg with respect to new bone formation. Mg-Cd alloys were observed to stimulate the formation of a hard callous at the fracture site [77] with total resorption of the material occurring after 10-12 months. Znamenski found that devices based on Mg-10Al alloys fused the fractures of 2 patients in 6 weeks and that the screws and plates were completely resorbed after 4 and 6 weeks, respectively [78]. It is noted that in all of these studies no systematic toxicity-instigated reactions or acute inflammatory response were reported. A thorough historical account of the early studies of Mg as a biomaterial is provided by Witte [79].

In some cases the early accounts of Mg biomaterials reported poor performance, primarily due to a fast biodegradation rate. The rapid biodegradation of Mg was primarily due to high levels of impurities that can lead to subcutaneous gas bubbles close to the surgical site. Recent production of high purity Mg combined with advances in alloy design and microstructure control has allowed a renewed interest into the potential for Mg as a biomaterial.

2.2.4. Benefits of Mg biomaterials

Magnesium and its alloys have a number of advantages over other metals in biomedical applications, including:

Low density / High specific strength

Mg is the lightest of all structural metals, at 1.738 g/cm^3 compared to 2.7 g/cm^3 for aluminium or 7.85 g/cm^3 for low carbon steel [80]. Despite the obvious benefits in commercial applications, low density is beneficial in the biomaterial field as it allows the use of Mg for large orthopaedic implants with a minimal increase in weight. The specific gravity of pure Mg is very close to that of bone, which ranges between 1.75-2.1 g/cm^3 [81]. For comparison, common medical-grade titanium alloys are typically 50% denser (4.5 g/cm^3) [82].

Pure Mg has a strength to weight ratio of approximately 130 kN•m/kg, however rapidly cooled alloys can reach 490 kN•m/kg [83]. This is 2 x greater than one of the most commonly used titanium alloys, Ti6Al4V (260 kN•m/kg). As a result less material may be used to provide a similar mechanical function in the body.

High damping capacity

Mg is unique due to its extremely high damping capacity (ability to absorb energy), the highest of any metal [8]. In the biomedical field this can be very important in heavy load-bearing applications, where the shock and vibration absorbing properties of Mg could provide significant benefit over other materials.

Machinability and dimensional stability

Mg is recognized as the easiest structural metal to machine, and stable final dimensions are easy to achieve [13]. Consequently complex shapes are easily producible. This is crucial for the often intricate shapes that are required for medical applications, which frequently have to be tailored individually to fit each patient.

Stress shielding

The mammalian skeletal system is constantly remodelling its bone mass and density in response to changes in the load-bearing environment. If physiological loads are increased in a region, the skeletal system responds by increasing bone tissue density in those areas required, and vice versa when load is reduced. The introduction of a metallic implant can upset the normal remodelling process due to differences in modulus to that of natural bone. A relatively stiff implant will transfer loads away from the adjacent bone, causing a reduction in bone density (also known as stress shielding). Stress shielding is known to be a problem with current orthopaedic devices based on stainless steel or titanium [84]. These materials have a density, elastic modulus, and yield strength an order of magnitude higher than that of bone [84]. This can cause poor integration with the surrounding bone with a correspondingly higher risk of fatigue or loosening of the implant [85-88].

Pure Mg has an elastic modulus of ~45 GPa, which is much closer to that of human cortical bone (~20 GPa) than most common Ti alloys (110-120 GPa) [54]. Combined with a density very close to that of bone, stress shielding related problems can be greatly reduced for many orthopaedic implants, most critically in high load bearing areas.

Biocompatibility and osteogenesis

Current biomaterials such as pure Ti are relatively inert in the body, meaning they exhibit little host response, positive or negative [89, 90]. In contrast, Mg is considered biocompatible and non-toxic [55, 67, 91-94], and has been shown to increase the rate of bone formation [92, 95]. Mg is also an important ion in the formation of the biological apatites that make up the bulk of bone mineral, a key part to new bone formation [96, 97]. Mg is known to have a positive influence on bone fragility and strength [46, 92, 98]. Over 50% of the Mg in an adult is found within bone, while the remainder is mainly located in muscle and soft tissue [99].

This close relationship with the formation and maintenance of healthy bone provides Mg significant advantages over other inert materials. The most obvious of these benefits is a potential for faster bone formation, as the Mg would not only provide a base for attachment but actually supply some of the necessary elements for new bone.

Safe degradation

Current metallic implants, made of titanium, stainless steel, and Co-Cr, are not designed to degrade safely in the body. However, all surgically implanted metal alloys undergo some electrochemical degradation due to the complex and corrosive environment of the body [43]. Combined with significant wear that can occur in load-bearing applications, particles of the implant can be released into the surrounding tissues, causing discomfort and potential health risks [100, 101]. In addition this wear and corrosion can lead to the need for a second implant during the patient's lifetime.

Although the bulk material may be considered bio-inert, the way in which the particles are metabolised within the body can lead to acute inflammation and eventually implant failure [102].

Mg has the unique position of being able to minimise all these issues. The gradual release of Mg ions in the body is dealt with effectively [55, 67, 91-94]. The corrosion of Mg in the body would result in an eventual complete degradation. This means the implant would not remain in the body for longer than is needed to perform its task and/or be replaced by bone. This also means that patients would benefit from only temporary exposure to a "foreign" object in their body. This is extremely crucial, as over time complications can and do occur for many implants, with more issues likely to arise the longer an implant remains *in vivo* [103].

2.2.5. Problems facing Mg biomaterials

A number of problems face current Mg alloys, limiting their immediate use in biomedical applications.

Low elastic modulus

Although the lower elastic modulus of Mg may be beneficial with respect to stress shielding, it also means that there may be a greater chance of failure in high-load applications, such as the spine where compressive loads during certain activities may exceed 3500 N [104]. It is vital to ensure that any implant is designed to sustain its load without deformation. However this aspect is even more vital when considering degradable materials, as an appropriate

mechanical support is required throughout the entire bioresorption and bone remodelling process.

Rapid degradation

Mg implants are intended to completely degrade but at a rate that reduces H_2 gas formation and that is similar to bone remodelling. The rapid degradation of Mg implants observed early in the last century [73, 76] has been greatly reduced by recent advances in controlling the purity of Mg and alloying elements [105, 106]. It may be possible to further reduce this rate when these factors are combined with a greater understanding of corrosion mechanisms, alloying and coating technologies [52].

Resorption problems

The rapid degradation of Mg alloys may cause an adverse biological response as Mg and other element ions are released too quickly into the surrounding tissues. All of the alloying elements will eventually enter the patient and must be selected with non-toxicity as a primary factor. However, elements normally present in the body (***e.g.*** Zn, Ca, Mn) can also be toxic if the release rate is too high as the levels cannot be dealt with appropriately (***e.g.*** excess Mg ***via*** kidneys, hydrogen gas ***via*** soft tissues). Thus, a truly biocompatible Mg alloy is required to avoid the use of toxic alloying elements and ensure an appropriate release rate for other elements, even those which are naturally occurring.

Hydrogen evolution

The release of H_2 and subsequent cyst formation following implantation of Mg can cause various problems. Gas pockets may form next to the implant that cause separation of tissue and/or tissue layers [107, 108]. H_2 bubbles may delay healing at the surgical site, leading to necrosis of surrounding tissue [109]. In the worst case scenario, gas bubbles could block the blood stream, causing death [53]. If the degradation is too rapid, the amount of H_2 produced will accumulate where it cannot diffuse through the surrounding soft tissues at a sufficient rate [48].

However, it has been shown that H_2 is able to be fully absorbed within the body without significantly reducing blood flow [70, 71]. Lespinasse produced Mg rings that were used for

connecting two blood vessels (anastomosis); these showed that hydrogen was resorbed at the same rate that it was produced [110]. Numerous *in vivo* studies, from the early 1900s to the present day, have found that hydrogen "bubbles" are often resorbed within a few weeks of appearing [77, 111-113]. Witte *et al.* reported that subcutaneous gas bubbles visible at 1 week following surgery were resorbed within 2-3 weeks [114].

Hydrogen gas pockets can also be removed by drawing off the gas with a subcutaneous needle [48]. The *in vitro* hydrogen evolution rate for various Mg alloys containing Zn, Al, and Mn are reported to be within tolerable rates (*i.e.* < 0.01 ml/cm^2/day) [8]. However it should be noted that these rates may depend strongly on the location of the implant, with certain applications (such as stents) allowing increased rates of H_2 evolution due to blood flow. There does not appear to be an absolute rate, and each alloy must be investigated in relation to its intended function. Consequently, it is reasonable to expect that hydrogen evolution during Mg degradation will not present a problem, provided that the corrosion rate of the Mg-based device is controlled.

2.2.6. Biocompatibility of Mg alloying elements

It is crucial to take into account the toxicity of all alloying elements and compounds that may form when considering Mg alloys for possible biomedical implant materials. All elements would need to be effectively and safely metabolised when released into the body as the implant degrades over time.

The vast majority of current Mg alloys that have been investigated for potential use as a biomaterial have been developed for commercial use. The emphasis for these commercial alloys has focussed on improving the castability, ductility, and high temperature creep of Mg as demanded by automotive applications [5]. The toxicity of alloying elements is generally not considered in engineering alloy design since this is less important for the end use.

The addition of any alloying element to provide significant benefit to Mg is futile unless the element is non-toxic. Al, Ca, Li, Mn, RE, Y, Zn and Zr have been alloyed with pure Mg to create alloys specifically aimed at biomaterials [23, 115-123]. Of these, Ca, Zn, Mn, Li and possibly very small amounts of RE are known to be tolerated in the body [64]

It is also important to consider the impurity levels of Mg-based biomaterials, particularly if Cu, Fe, Ni or beryllium (Be) are present; low levels of these impurities can dramatically reduce the corrosion resistance of Mg [33]. The level of impurities in the final product can depend both on the actual composition of the alloying elements (***e.g.*** in what compounds they are added to the melt), as well as the technology and materials used for production, where pickup of impurities may occur [124]. In general, 100-300 parts per million (ppm) of Cu, 35-50 ppm of Fe, 20-50 ppm of Ni and 4 ppm of Be are acceptable in many engineering applications [34, 125].

However, the control over impurity levels needs to be stricter in Mg alloys that are aimed at biomedical applications. Elements such as beryllium and nickel should be completely avoided as they can lead to acute sensitivity and cancer [126, 127]. In addition, the increased corrosion rate caused by impurities can lead not only to implant failure but also serious complications in the body if too much of a single element is released rapidly. Finally, it is important to control carefully the impurity levels so that comparisons between alloy designs are permitted without their behaviour being dominated by variations in trace impurities.

A comprehensive list of common Mg alloying elements and impurities, along with their biological and toxicological properties, is provided in Table 2-6.

Table 2-6 : Biological and toxicological characteristics of common Mg alloying elements and impurities.

Element	Toxicology / Biological Properties	Reference
Mg	• Normal blood serum level: 0.73-1.06 mmol/L	[128]
	• Toxic dosage: 500 mg/day	[129]
	• Influences growth factor effectiveness	[130]
	• Regulator of over 350 proteins	[131]
	• Co-regulator of energy metabolism, cell proliferation, protein and DNA synthesis	[130, 132]
	• Co-regulator and activator of integrins (cell migration)	[133-135]
	• Long-term influence on cellular reactions	[136]
	• Cellular up-take via transient receptor potential (TRP) ion channels	[137]
Al	• Normal blood serum level: 2.1-4.8 µg/L	[138]
	• Toxic dosage: 0.2-0.4 mg/Kg	[139]
	• Alloying element in titanium implants	[140, 141]
	• Risk in generation of Alzheimer's disease	[142-144]
	• Linked to possible reproductive and developmental problems	[145]
	• Can cause muscle fibre damage	[146]
	• Decrease osteoclast viability	[147]
	• In Mg, mild foreign body reactions *in vivo*	[47]
	• Al^{3+} ions combine with inorganic phosphate resulting in reduced phosphates	[145]

	• Majority of Al ingested passes through the body	[144]
	➢ **In spite of above issues, Al-containing alloys are most commonly invested in bio-Mg literature.**	
Zn	• Normal blood serum level: 12.4-17.4 µmol/L	[148]
	• Toxic dosage: 150 mg/day	[129]
	• One of the most abundant essential elements	[149]
	• Essential for the immune system	[150]
	• Co-factor for specific enzymes in bone and cartilage	[151, 152]
	• Neurotoxic at higher concentrations	[153]
	• Found to prevent bone loss by stimulating osteoblastic formation	[154]
	• Mg-Zn alloys have been found to perform well *in vitro* and *in vivo*	[123, 155]
	➢ **Overall, Zn demonstrates excellent potential as an alloying element for Mg-based biomaterials**	
Ca	• Normal blood serum level: 0.919-0.993 mg/L	[156]
	• Toxic dosage: 2500 mg/day	[129]
	• Most abundant mineral in the human body (1-1.1 Kg)	[156]
	• Mostly stored in bone and teeth	[156]
	• Tightly regulated by homeostasis of skeletal, renal, and intestinal mechanism	[156]
	• Ca-rich compounds (***e.g.*** hydroxyapatite) play crucial role in bone formation	[157]
	➢ **Likely most biocompatible alloying element, Ca displays significant promise for Mg biomaterials**	
RE	• Normal blood serum level: N/A	
	• Toxic dosage: N/A	
	• Many rare earth elements exhibit anti-carcinogenic properties	[158, 159]
	• Not known to play role in any biological function in the body	
	• Lanthanum (La) and cerium (Ce) exhibited cytotoxicity *in vitro*	[160]
	• Yttrium (Y) considered potential lung cancer risk if inhaled	[161]
	• Gadolinium (Gd) can induce nephrogenic systematic fibrosis in renal failure patients	[162]
	• RE have been observed to remain in bone for extended periods	[163]
	• Mg-Y stent has been successfully implemented in clinical trials	[164]
	• No accumulated RE surround bone tissue in studies of LAE442 and WE42 in rabbits	[165]
	• Gd has exhibited low toxicity in presence of osteoblast-like cells	[160]
	➢ **At present, it remains inconclusive as to whether RE are suitable for Mg-based biomaterials.**	
Li	• Normal blood serum level: 2-4 ng/g	[166]
	• Toxic dosage: 40 mg/day	[129]
	• Compound of psychiatric drugs for treatment of mania and depression	[167, 168]
	• Only prescribed when absolutely necessary	[169]
	• Over dosage can cause kidney and lung dysfunction	[170, 171]
	• Possible teratogenic effects	[172]
	• Side-effects include renal failure, hypothyroidism, and kidney damage	[173]
	• Therapeutic levels of Li are often close to the toxicity limit	
	• Displayed no negative effects in cytotoxicity tests	[160]
	• Slowed corrosion and displayed good cell viability in rabbits	[174, 175]
	➢ **All studies to date have indicated a more in-depth understanding of toxicity is required before Li can be used for implants.**	
Mn	• Normal blood serum level: <0.8 µg/L	[176]
	• Toxic dosage: 11 mg/day	[129]
	• Essential trace element	[177]
	• Important in metabolic cycle	[177]
	• Influences the function of the immune system, bone growth, and blood clotting	[177]
	• Scavenger of free radicals as manganese superoxide dismutase	[178]
	• Neurotoxic in higher concentrations (manganism)	[179]
	• Plays a primary role in activation of a number of enzyme systems	[180]

	• Shown to decrease corrosion rate *in vitro* and *in vivo*	[181-183]
	➢ **Based on potential benefits, Mn warrants further investigation.**	
Zr	• TiZr commonly investigated due to good biocompatibility	[184]
	• ZrO widely used in dental implants	[185]
	• Mg-Zr caused decreased cell viability but increased platelet adhesion	[123, 160]
	• Zr ion concentrations below 10^{-3} mol/L did not induce toxicity in cell studies	[186]
	• Toxicity of Zr is considered low despite no biological function association	[187]
	➢ **Further investigation of Zr is warranted, especially due to importance in improving mechanical properties.**	
	Impurities	
Be	• Normal blood serum level: N/A	
	• Toxic dosage > $2\mu g/m^3$	[188]
	• Induces metal sensitivity, highly carcinogenic	[189, 190]
Cu	• Normal blood serum level: 74-131 µmol/L	[191]
	• Toxic dosage: 10 mg/day	[129]
Fe	• Normal blood serum level: 5-17.6 g/L	[192, 193]
	• Toxic dosage: 1500 mg/day	[129]
	• Essential for life and metabolically regulated/stored	[192, 193]
	• Generator of age related diseases by reactive oxygen species	[194]
Ni	• Normal blood serum level: 0.05-0.23 µg/L	[195]
	• Strong allergenic agent which can induce sensitivity	[196]
	• Carcinogenic and genotoxic	[196]

2.2.7. Overview of Mg biomaterials

Mg shows great promise as a potential biomaterial. However, its key advantages over current materials, such as biodegradability and low specific strength (reduced stress shielding), are also some of the most challenging considerations. The fact that Mg and its alloys may degrade safely also means that the implant is constantly changing shape and mechanical properties over its entire life, adding another layer of complexity to carrying out a full life-cycle design. However, the benefits that Mg alloys offer over current materials are clear and the potential pitfalls of working with Mg may be overcome through systematic exploration and careful planning.

Pure Mg is not capable of providing all necessary properties for a wide range of implant applications. Therefore the many potential alloying elements need to be carefully considered. The toxicity and potential long-term problems associated with Al, the most common alloying element, mean that it will not be heavily investigated in this work. Any positive physical properties such alloys possess would be overshadowed by potentially disastrous issues for a patient. Further study may be warranted when their cytotoxicity is better understood.

Although lithium has been used in medicine for almost 150 years [169] it has not been employed widely in implanted materials. It is also extremely difficult (and dangerous) to alloy with due to its extremely high reactivity [197]. For these reasons it was not investigated in this work. Rare Earths are also not investigated due to the uncertainty surrounding the short and especially the long-term toxicity and side-effects.

However, the other four elements, Ca, Zn, Mn, and Zr, all show promise without the major shortfalls of Al, Li and REs.

2.2.8. Cellular biomaterial structures – Importance of design and manufacture

It is not only important to select a suitable material but also an appropriate shape and structure for the desired implant site when considering biomaterials for specific applications. Various locations in the body require different implant designs based on a number of factors, particularly mechanical stresses and loads. In some cases, the topology of the implant may be tailored to each individual patient to ensure maximum success. Therefore it is vital to consider the design of the implant throughout the process of materials selection.

Metal foams or cellular metals have been increasingly used across a wide variety of industries, such as in lightweight structures, acoustic and mechanical damping, electrical screening, filtration and recently, biomaterials for orthopaedic implants [184, 198, 199]. With correct material choice cellular structures can offer ample mechanical and structural properties with a fraction of the weight and cost. Cellular metals can offer unique advantages when implemented in biological roles that have traditionally been dominated by solid structures.

Permanent metal implants for supporting tissue in-growth have been at the forefront of classical biomaterials research and the orthopaedic medical device industry for decades. Traditionally, methods for tissue replacement have included the use of auto- or allograft tissue or permanent external materials, with each approach having its limitations. Procedures requiring auto/allo-grafting of tissue or organs can result in significant donor-site morbidity and risk of disease transfer, as well as requiring undesirable additional surgery. Furthermore, there are limitations to the amount of auto- or allo-graft tissue that is available.

The most common causes for failure of synthetic implants over time are adverse body response, stress shielding, wear and fatigue, all of which can eventually cause failure, particularly in load-bearing applications [200]. Although a cellular structure for a biomaterial may play little role in its biological response, it can help greatly in minimising the other issues facing solid implants. Such a structure may be designed to offer strength in areas only where it is needed and in turn reduce the amount of material to which the body is exposed. Tailoring of design may also alleviate the problem of stress shielding; a common issue that faces many current orthopaedic implants (see Chapter 2.2.4.). In addition, an increased surface area may be extremely beneficial to a biocompatible or bioactive material, as it provides more sites for cellular attachment and faster healing. In applications where bone is to be fused, such as spinal fusion, the topology of an implant may be designed to allow for appropriately sized channels to connect the two opposing bone surfaces. This would allow for controlled and focussed growth of bone, leading to a reduced healing time and better fixture. Overall cellular metal foams offer the potential for an implant device that is strong yet lightweight and provides an appropriate stiffness and pore architecture to promote rapid implant fixation and tissue growth.

Production of cellular metals

The advantages of cellular metal in various applications have provided a stimulus for the rapid development of fabrication routes for commercial production of closed- and open-cell metal foams [201]. However, the majority of these fabrication routes generate a random cell structure, yielding broad distributions in cell size and shape, with the result that material properties are unpredictable over the range of a few hundred microns to a few millimetres [202-209]. This is especially true for cellular metals, where high temperatures required to form structures limit the techniques available for their fabrication [202-207].

Manufacturing routes for cellular metals with controlled, as opposed to random, pore architectures are less well developed and are typically more difficult and costly to produce. Currently, the primary route for the fabrication of controlled cellular structures is to use rapid prototyping (RP) techniques. Cellular metals can be directly fabricated by incorporating selective laser melting (SLM) or selective electron beam melting (SEBM) into the RP process. Ordered cellular titanium [210, 211] and stainless steel [212] structures have been fabricated using these methods. Ceramic scaffolds have also been used to cast CoCr [213,

214] and titanium [215] alloys for orthopaedic applications, where the ceramic moulds are either directly fabricated or cast into polymeric RP scaffolds. Another alternative to fabricate titanium implants is to infiltrate polymer RP scaffolds with titanium powder slurry [200, 215-218]. This is followed by heat treatment to allow for wax removal and sintering of the Ti particles. NaCl has also been established as a possible spacer material for random foams [47, 219], and plaster has been used recently to cast controlled cellular Mg [220, 221]. However, it has been reported that plaster deposits remain on many strut surfaces on porous metal after the removal process, creating a potential biocompatibility issue [222].

A number of studies have attempted to generate optimized porous microstructures to meet global scaffold design criteria such as porosity, stiffness and permeability [223, 224]. These optimized architectures are often complex to fabricate and therefore have remained in a concept phase. Few studies have physically manufactured porous metal implants using solid freeform fabrication (SFF) methods for mechanical testing and validation of optimized models [13]. There remains a significant gap in the production capabilities available to create ordered Mg structures.

2.3. Magnesium and the *in vivo* environment

In vivo is a term that is commonly used to refer to experiments that use an entire living organism as a test environment. From the Latin for "within the living", the term is used to describe clinical trials where animals or humans are used as test subjects. Initially, *in vivo* testing occurs in small animals such as rats or rabbits for the assessment of new implant materials. Heavily inbred species, such as New Zealand white rabbits, are preferably used to eliminate some of the variables that affect the performance of an implant when it is placed *in vivo*.

2.3.1. The body – A brief overview

As a reference, the human body is normally considered in terms of a 70 kg man in his mid-30s. More detailed studies look at the differences that exist between different sexes, races, and age groups. However, for the sake of simplicity, this is the reference that will be used for

all comparisons in this work. It is important to have an understanding of the body as a system when designing any implant, as it can affect more than the local area.

As with any complex system, different locations and tissues have very different chemical and mechanical properties. These parameters all play a crucial role in the success or failure of an implant, as they can affect the corrosion rate (pH, temperature, gases) and also mechanical performance (stress, stress cycles) of the material. Each material must therefore be designed for a certain range or specific location to allow for these differences. The overall parameters of a reference human and a number of properties of anatomical locations are summarised in Appendix A.

2.3.2. Placing an implant in vivo

Based on interface reactions, biomaterials may be classified as resorptive, bioactive, biologically inactive or toxic [225]. This is important because the biocompatibility of a material is directly related to the reactions at the interface of the surface of the material as well as the inflammatory host response [226]. Numerous uncontrollable factors can contribute to this including general health, age and tissue perfusion [227]. Other factors that play a role pertain to the implant material itself. These include surface roughness, porosity, the corrosion properties of the material and its toxicity.

What happens when a foreign material is placed in the body can be divided into two main categories: host response and material interface response. These can also be considered as macro (host) and micro (material interface) responses. A number of references can provide a more detailed discussion of these behaviours [35, 36, 228], however the main ideas are summarised here.

Host response

Host response refers to how the surrounding tissue reacts to the implanted material as well as the surgical procedure and any contingent damage. If the operation is heavily invasive, this response can be primarily due to the disturbance of the biological environment rather than the actual material implanted itself. A summary of a typical host response for ideal and non-ideal materials is shown in Table 2-7.

Table 2-7 : Typical host response to implantation and ideal/non-ideal material reactions.

Time	Biological Responses
0-3 days	• Implant covered in blood clot [41] • Inflammatory reaction eliminates damage to tissue, bacteria, clots • Foreign debris/material purged by inflammatory cells • White blood cells remove larger debris [42] • Macrophages release enzymes promoting fibroblasts to form a fibrous capsule around implant. [229]
After 2-3 days	• For bone, stem cells develop into osteoblasts, which form layer close to implant with fibroblasts • Osteoblasts, fibroblasts, and capillaries penetrate blood clot, replace it, fill in the space between implant and bone [230] • Collagen-rich extracellular matrix (ECM) is mineralised • If well accepted, calcium-rich small ECM sacs form (vesicles) • Vesicles rupture, and apatite crystals unite and form calcifying structures [231] • Microscopic tissue beams (trabecular) grow and mineralise, reaching implant [232]
	Ideal and Non-ideal Materials
Ideal	• Implant is entirely covered by bone tissue, not fibrous capsule • Large amounts of ECM is mineralised, with fast proliferation and close attachment to implant [233] • Bone accepts material as part of ECM, leading to continuity between bone and implant (bone bonding) [232]
Non-ideal	• Fibrous layer remains between implant and bone • Thickness and longevity of layer varies depending on material and location, can only be determined through clinical trials • Resorption of bone matrix by osteoclasts (osteolysis) [234] • If toxic material is used, tissue in immediate area will die (tissue necrosis) • Even if non-toxic, micro-particles can trigger an inflammatory response [235, 236]

Material interface response

As soon as an implant is placed in the body and comes into contact with blood, serum proteins will start to adhere to the surface. This process is known as protein adsorption, where adsorption means the “adherence of a molecule to the surface of a solid” [237]. Initially the adsorption is influenced primarily by protein diffusion with the proteins possessing the highest affinity to the material surface being the first to come into contact [238]. However, over time lower-affinity proteins can replace the higher-affinity proteins through a complex dynamic process.

The implant is completely coated in a monolayer of proteins by the time that cells arrive at the surface if the material is biocompatible [239, 240]. Thus, the cells will not come into direct contact with the surface but rather a protein layer. The cells interact with proteins by

directly binding using receptors on the cell membrane; cells do not have receptors for a material surface free of proteins. This means that the proteins provide a platform for the cells to adhere to on the surface. Increased protein attachment usually leads to an increase in cell adhesion [229]. Thus, proteins are required to initiate new bone growth.

The amount of protein adhering to an implant is a factor of both the makeup of the biological solution and the implant surface properties, which are outlined below.

Biological solution effects

The material interface response in a certain solution is mainly controlled by: i) protein concentration, ii) rate of diffusion, and iii) protein affinity to the surface. In general, protein adsorption is heavily affected by its concentration in a solution. For simple single protein solutions (unlike those found in the body), an increased concentration of proteins leads to more proteins attached to the surface [237]. However, the effect is more complicated when several proteins are in the solution due to protein-protein interactions. Except during coagulation, the majority of serum proteins will not adhere to one another on a material surface [241].

Other factors that affect material performance include: (i) rate of diffusion of proteins, controlled primarily by protein size, (ii) affinity of protein to substrate [237], and (iii) difference in protein concentration. Proteins themselves interact with a material surface through a number of mechanisms including: i) ionic bonds (between positive and negative charges), ii) intramolecular bonds, such as hydrophobic interactions, and iii) charge transfer [242]. The strength of these bonds can vary widely depending on the physical and chemical properties of the protein (Table 2-8).

Table 2-8 : Properties of proteins that affect adsorption on materials.

Protein Property	Description
Size	Smaller proteins will diffuse more quickly and arrive at material surface faster. They will, however, form fewer contact points with the material surface than larger proteins. Thus, the size of the protein may also affect its affinity.
Charge	Charged proteins preferentially adsorb to a surface with an opposite charge. On most surfaces, however, proteins adsorb the most at their isoelectric point where they are at neutral charge in the solution.
Hydrophobicity / Hydrophilicity	More hydrophilic side chains are present on the outside of a protein molecule in aqueous media so they may interact with a substrate surface. Hydrophilic protein domains tend to adsorb to hydrophilic surfaces, while hydrophobic domains adsorb more to hydrophobic surfaces.
Structural Stability	Proteins that are less structurally stable normally exhibit greater unfolding upon adsorption and form more contact points. Proteins that unfold quickly form bonds with the surface before other proteins arrive.

Data from [239, 240] , adapted from [237]

Implant surface effects

The material surface itself can greatly influence the type, quantity and function of the proteins that adsorb. Water molecules from the biological environment interact with the material before proteins even have time to attach to a surface. For hydrophobic materials, a "shell" of water molecules will form in which the molecules will interact with each other more than the hydrophobic surface. It has been postulated that the surrounding water molecules have a decreased state of entropy, and disruption of this layer by proteins is energetically favourable due to a concomitant increase in entropy. It is this increase in entropy that is the primary motivating force behind the protein adhesion onto materials that are hydrophobic [237]. On hydrophilic surfaces water molecules can easily form hydrogen bonds with the surface and compete with the proteins. Thus, in general, hydrophobic surfaces tend to adsorb more proteins [239].

Other factors of the material surface that affect adsorption include: (i) distribution of charge, where oppositely charged surface/proteins attract, although amino acids can themselves be polar [237]; (ii) topographical layout, where increased surface roughness provides more surface area for attachment, and (iii) chemical composition at the material surface. An example of several material surface functional groups and some observed effects on proteins can be seen in Table 2-9. The effects of surface properties on protein adhesion are summarized in Table 2-10.

Table 2-9 : Effect of material surface functional groups on proteins and cells.

Functional Group	Charge / Phobicity	Effect on Proteins and Cells
-OH	Neutral / Hydrophilic	- Decreased affinity for plasma proteins - Induces exposure of cell adhesive domains on fibronectin, - Increases differentiation of osteoblasts
-CH_3	Neutral / Hydrophobic	- High affinity/binding with fibrinogen, - Binds strongly with immunoglobulin G (IgG), - Increased leukocyte adhesion/phagocyte migration
-NH_2	Positive / Hydrophilic	- High affinity for fibronectin - Increased myoblast proliferation - Increases differentiation of osteoblasts - Promotes endothelial cell proliferation
-COOH	Negative / Hydrophilic	- Increased affinity for fibronectin and albumin.

Adapted from [237]

Table 2-10 : Effect of material surface properties on protein adsorption.

Surface Property	Description
Chemistry	The chemical composition of a substrate surface will dictate the types of bonds between the material surface and the protein
Charge	Opposite charges between the protein and the surface promote increased protein adsorption, while like charges will reduce adsorption.
Hydrophobicity / Hydrophilicity	Hydrophobic surfaces tend to adsorb more proteins, hydrophilic surfaces tend to resist protein adsorption
Topography	Increased surface roughness and topological features provide increased material surface area for protein adsorption. For example, a micrometre sized hole on the surface can accommodate millions of blood serum proteins.

Data from [239, 240] , adapted from [237]

With knowledge of the conditions facing implants when they enter the physiological environment, it was possible to start reviewing the current literature on Mg alloys tested both *in vitro* and *in vivo*.

2.3.3. Summary of review of Mg biomaterial literature in an abridged format

As part of the analysis of the available literature on Mg alloys for biomedical purposes, a catalogue was created that outlined the parameters of each study, including:

- Alloys investigated
- Solutions used
- Buffering system
- Coatings or work applied to samples
- Atmosphere of test (*e.g.* 5% CO_2)
- Value and control of pH
- Period experiment was performed over
- Experimental techniques performed (mass loss, PDP, etc.)
- Analysis techniques (optical, SEM, EDS, etc.)

This allowed comparisons to be made between similar studies with relative ease. The majority of the literature that was collected was obtained from online databases such as ScienceDirect® and EngineeringVillage®, ProQuest® and ISI Web of Knowledge®. As research progressed new searches were performed, and a large number of reference alerts were set up to ensure all new publications relevant to the area were obtained as soon as they were available. Significant effort was made to ensure that as much pertinent literature as possible was considered.

Whenever references are made to the available literature, it is based on this collation. Part of the information collected on the majority of the studies considered for this work can be seen in Appendix B and Appendix C.

2.3.4. In vivo testing of Mg and its alloys

A new biomaterial must be tested in applicable animal models before it can be approved for safe use in humans in line with the various standards that have been set up for this purpose. *In vivo* testing is considered mandatory for assessment of degradation and toxicity.

Of over thirty *in vivo* studies that have been performed on Mg alloys, the vast majority have used implantation into the femur of rabbits or guinea pigs. AZ alloys have been the most commonly investigated, with 13 different experiments carried out in rabbits, guinea pigs and sheep. Mg-Ca and two RE alloys, LAE442 and WE43, have also been investigated by 9, 8, and 4 studies, respectively. Other alloys that have been researched include Mg-Zn-Mn (4) AE21 (1), Mg-Zn (1), pure Mg (1) and 2 proprietary alloys. These do not include the historical tests of the early 1900's, but the few available investigations of Mg implants into humans were also recorded.

A summary of the basic findings of each of these tests is shown in Table 2-11, along with the alloy, animal model and implant location.

Table 2-11 : *In vivo* tests on Mg alloys.

Primary Author	Main Findings	Material / Animal / Location	Ref.
Duygulu	• Mg alloys have "significant potential" as implant materials	AZ31 / Sheep / Hips	[45]
Heublein	• AE21 is a "realistic alternative to permanent implants"	AE21 / Pigs / Stents	[243]
Krause	• Mg-0.8Ca use may be limited • WE43 corrosion is too non-uniform for orthopaedic applications • LAE442 shows good promise as biomaterial	Mg-0.8Ca, WE43, LAE442 / Rabbit / Tibia	[174]
Krause	• Mg-0.8 showed promise • WE43 fracture strength is unpredictable and not good for orthopaedics • LAE442 shows good corrosion/strength potential	Mg-0.8Ca, WE43, LAE442 / Rabbit / Tibia	[115]
Li	• Alloy showed very good promise as potential implant, • Secondary phases may be implemented to control corrosion	Mg-Ca(1,2,3) / Rabbit / Femora	[112]
Reifenrath	• AZ91 is a "fast degrading biomaterial that cannot sufficiently replace subcondral bone plate during the first 12 weeks (of implantation)" • However, appropriate coatings may slow the corrosion allowing proper adhesion and success	AZ91 / Rabbit / Knee	[244]
Ren	• Alloy displayed appropriate degradation rate and low hydrogen release. • Would degrade slow enough to "form calcium phosphate around the implant with a Ca/P ratio close to natural bone"	AZ31B / Rabbit / Femora	[245]
Thomopoulos	• Mg based bone adhesive (MBA) displayed a negative reaction. • Failure could be because of "allergic response or to increased chronic inflammation resulting from the foreign materials"	MBA / Dog / Distal phalange	[246]
Von Der Hoh	• "In summary, it can be said that all magnesium implants investigated were well tolerated"	Mg-0.8Ca / Rabbits / Femora	[247]
Von Der Hoh	• All implants were well tolerated by the animals, with no redness or excess pain • Wound healing was early and complication free • Callus formation was observed around implants	Mg-Ca (0.4-2 %) / Rabbits / Femora	[248]

Witte	• No allergenic reactions were observed in skin biopsies • No skin sensitizing potential was detected using the applied methods	AZ31,AZ91,WE43, LAE442 / Guinea Pigs / Intradermal	[249]
Witte	• "Both alloys showed direct contact with newly formed bone, which proves the biocompatibility of these materials"	AZ91D, LAE442 / Guinea Pig / Femora	[165]
Witte	• "All magnesium implants have been observed in direct bone contact and without a fibrous capsule"	LAE442 / Rabbits / Femora	[250]
Witte	• High mineral apposition rates and increase bone mass were observed surround the magnesium • No bone was induced in soft surrounding tissue • "there is a strong rationale that in this research model, high magnesium ion concentration could lead to bone cell activation"	AZ31,AZ91,WE43, LAE442 / Guinea Pig / Femora	[50]
Witte	• "Alloys had direct contact with bone which showed good compatibility"	AZ91D,LAE442 / Guinea Pig / Femora	[49]
Witte	• Alloys degraded too rapidly *in vivo* to allow cartilage repair • "However the surrounding cartilage tissue was not negatively affected by the rapid degradation process and new bone formation was observed " • Initial corrosion should be slowed to allow cartilage growth	AZ91 / Rabbits / Knee	[114]
Witte	• Even fast-degrading Mg induced extended peri-implant bone remodelling with a good biocompatibility	AZ91D / Rabbits / Knee	[219]
Witte	• "Magnesium alloys based on implants are therefore a very promising approach in the development of mechanically suitable and open porous scaffolds for the replacement of subchondral bone in cartilage tissue engineering"	AZ91D / Rabbits / Knee	[47]
Wong	• New bone formation was observed • No inflammation, necrosis or accumulated hydrogen gas was recorded,	AZ91 / Rabits / Trochanter	[251]
Xu	• Ca-P coated Mg alloy provided a significantly good surface bioactivity and promoted early bone growth at the bone/implant interface	Mg-1.2Mn-1Zn / Rabbits / Femora	[119]
Xu	• After 18 weeks, all implants were fixed and no inflammation was visible • Element analysis found the Mn and Zn distributed homogenously in the implant, degradation layer and surrounding bone tissue, indicating they were easily absorbed	Mg-1.2Mn-1Zn / Rats / Femora	[182]
Zarter	• "Magnesium is generally well tolerated and even in our patient with her low bodyweight and reduced renal function, serum levels were only modestly elevated"	AMS Proprietary / Human Baby / Stent	[252]
Zhang	• New bone was in tight contact with implant due to good osteoconductivity of phosphate layer • More bone tissue was observed around the implant • No apparent increase in the (fibrous) membrane was found with increasing implantation time • Little change was recorded in blood composition	Mg-1Zn-0.8Mn / Rats / Femora	[183]
Zhang	• "*In vivo* degradation did not harm the important organs" • No adverse effects of the generated hydrogen or released Zn was observed	Mg-6Zn / Rabbits / Femora	[155]

A number of studies have suggested potential problems and issues facing Mg implants that need to be addressed. These include the need for a greater understanding of the corrosion

mechanisms that are occurring *in vivo*, as well as larger and more systematic studies of individual alloys. However, the overall conclusions were that the Mg alloys that have been tested have performed very well *in vivo* and warrant further study.

2.3.5. The relationship between in vitro and in vivo results

A limited number of studies have systematically carried out comparisons of Mg alloys both *in vivo* and *in vitro* [49, 112, 113, 119, 155, 245, 251]. Much of the available results show significant differences between *in vitro* and *in vivo* corrosion rates. However, it remains unclear as to what exactly are the most crucial *in vivo* parameters to emulate *in vitro*.

A summary of setup and findings of these correlation studies can be seen in Table 2-12 and Table 2-13.

Table 2-12 : Comparison of reported corrosion parameters for studies with *in vitro* and *in vivo* tests.

Primary Author [Ref]	Alloy(s)	*In vitro*				*In vivo*		
		Sample area (cm^2)	**Solution amount / type**	**Time (hours)**	**Corrosion rates (mm/year)**	**Animal**	**Area**	**Corrosion rates (mm/year)**
Witte [49]	AZ91D LAE442	3.39	25 L / Artificial Ocean Water	240	PDP = 2.8, ML = -0.267 PDP = 6.9, ML = 5.535	Rabbit	Femur	SRμCT = 3.5×10^{-4} SRμCT = 1.21×10^{-4}
Zhang [155]	HP Mg Mg-6Zn	1	N/S / Basic SBF	720	PDP = 0.2, ML = 0.1-0.4 PDP = 0.16, ML = 0.07-0.2	Rabbit	Femur	 ML = 2.32
Li [112]	Mg-1Ca Mg-2Ca Mg-3Ca	2.19	N/S / Kokubo's SBF	250	PDP = 12.56 PDP = 12.98 PDP = 25.00	Rabbit	Femur	ML = 1.27[A]
Wong [251]	AZ91	1	N/S / Basic SBF	1440	ML = 5.9×10^{-6}	Rabbit	Trochanter	ML = 1.2×10^{-10} [B]
Ren [245]	AZ31B	9.6	N/S / Hanks	720	ML = 0.2-0.7	Rabbit	Femur	-
Ren [113]	HP Mg	11.8	N/S / Hanks	720	ML = 0.2-0.6	Rabbit	Femur	-
Xu [119]	Mg-1.2Mn-1Zn	1.57	N/S / PRI1640	120	-	Rabbit	Femur	-

N/S = the values were not stated in the work, [A] = degradation rate converted from reported $mg/mm^2/y$, [B] = converted to mm/year using ASTM G31 [253]

Table 2-13 : Summary of results of studies that performed *in vitro* and *in vivo* experiments concurrently.

Primary Author [Ref]	Study Overview	Key Findings
	Quantitative Studies	
Witte [49]	• Unphysiological pH (8.2), not controlled (or stated) • Assumed *in vitro* tests were performed at room temperature (not stated) • Gain in recorded mass loss was due to build-up of corrosion product, which should be removed before weighing • Authors have since rectified some of these issues [116, 254]	• No correlation between *in vitro* and *in vivo* • Artificial sea water is an inappropriate SBF due to lack of inorganic salts
Zhang [155]	• Physiological pH (7.44) and temperature (37 °C) • pH not controlled during experiment, lead to value of 9 after 24 hrs. This would provide significant protection to surface	• Electrochemical and immersion corrosion rates were similar • *In vivo* rates were up to 40x faster
Li [112]	• Physiological pH (7.4) and temperature (37 °C) • In some cases, pH rose to 12 within 24 hrs (Deviation from physiological) • Solution amount based on ASTM G31[253], which states solution to surface ratio of 0.2-0.4 ml/mm^2. This is not an appropriate standard for Mg.	• *In vivo* only performed on Mg-1Ca • *In vitro* displayed 10x faster rate of corrosion • Minimal discussion of reasons for corrosion rate
Wong [251]	• Physiological pH (7.4) and temperature (37 °C) • pH was not controlled over the entire 2 months of study, and quickly rose to above 8 for some samples. • µCT is of limited use to determine actual corrosion due to problems discerning between corrosion product and remaining implant. Especially relevant given the minimal corrosion (0.33%) that occurred over the test. • No SBF constituents were given, just “standard simulated body fluid”. • Did not report mass loss results or perform Tafel-type analysis	• Mg ion loss, converted to mass loss, was extremely small. • Barely noticeable (through µCT) amounts of corrosion occurred *in vivo*
	Qualitative Studies	
Ren [245]	• Physiological and controlled pH (7.5) and temperature (37 °C) • Unknown amount of solution used *in vitro* • Only *in vitro* corrosion rates reported	• *In vitro* samples displayed “acceptable” corrosion rates (according to author) • *In vivo* alloy showed good CaP build-up around implant
Ren [113]	• Physiological and controlled pH (7.5) and temperature (37 °C) • Unknown amount of solution used *in vitro* • Only *in vitro* corrosion rates reported	• 10x increase in corrosion rate (*in vitro*) if pH was not controlled • *In vivo* Mg displaced good thromboresistant properties and tissue compatibility • CaP build-up around implant
Xu [119]	• Tests primarily used to determine toxicity effects of alloy *in vitro* and *in vivo*	• CaP coatings on Mg resulted in good surface bioactivity (*in vitro*) and early bone growth (*in vivo*)

2.3.6. The need for appropriate in vitro tests

As previously mentioned, there have only been a few studies that have compared Mg alloys in both *in vitro* and *in vivo* environments, most of which found little correlation between corrosion rates (see Chapter 2.3.5.). However, these tests have also all suffered from some major shortcomings, primarily relating to the choice of solution and control of the pH.

In vitro tests will likely never be able to fully emulate every complexity of the human body. Many of the multifaceted reactions that occur between the numerous compounds, proteins, amino acids, and other attributes would be nearly impossible to recreate outside a living organism. Any setup would be extremely complex, requiring control over many variables.

However this is not necessarily a problem. *In vitro* tests have been developed and widely employed to investigate many currently used biomaterials, such as titanium, with relative success [255]. These tests have allowed approval for systematic *in vivo* studies and eventual use in humans.

The development of physiologically relevant *in vitro* tests is appealing as these can provide a means for relatively cost-effective and rapid collection of data. Succeeding in the development of a predictive *in vitro* test would allow assessment of the *in vivo* performance, biodegradation rate and material-body interactions with constituents such as proteins and cells. In his book on the biological performance of materials, Jonathan Black stated that “all materials should be tested *in vitro* before being implanted in animals” [42]. He regarded the necessity “to attempt to replicate the environment that the material will encounter after implantation” as crucial to the success of any material.

This is the real benefit of *in vitro* tests, as they can offer an effective screening technique for unsuitable materials, requiring a reduced number of animal and human trials. Non-animal experiments also offer a number of benefits including reduced cost, controllability, ease of monitoring/recording of data, and reproducibility (see Chapter 2.4.1.). The problem that exists is that there are no such experiments that can effectively predict the *in vivo* performance of degradable metals.

It is apparent from the current literature that there is a significant gap in the understanding of the variables that are most important to the performance of Mg alloys *in vivo*. All the current comparisons have overlooked several key variables in their experimental design, such as pH control. It is clear that there needs to be a greater understanding of which aspects of the *in vivo* environment most affect the performance of the Mg alloys, especially the corrosion rate. Given the inconsistencies from one experiment to another, it appears that the general bio-Mg community does not have a full appreciation of the important parameters that affect the final results of *in vitro* tests.

Although a single definitive test to check all Mg alloys for all situations may be difficult, it is apparent that certain basic properties of the body, such as Cl^- content and pH control, are vital to the corrosion performance *in vitro* and should be regulated. However, the solution makeup is also critical, and the interactions with proteins and amino acids can have a considerable role in both the corrosion and the successful integration of the implant into the surrounding tissues.

What is required is a systematic study of the key performance parameters for Mg alloys, both qualitative and quantitative, to determine which variables are critical and their level of significance. This would provide an important platform on which future tests could be based, allowing clearer, more reproducible, and in many ways much more useful information for the community as a whole. Only with this basic framework is significant progress possible in the near future.

2.4. *In vitro* testing of magnesium

2.4.1. Disadvantages of in vivo tests

Since its first recorded use by Aristotle in the 4th Century B.C., animal research has produced significant advances in medicine [256-258]. It is arguable that the benefits obtained from selected *in vivo* experiments have been and will continue to be immense [259]. However, it is equally important to minimise the number of experiments carried out to only the most promising of materials and applications. There are many disadvantages to *in vivo* experiments that are minimised or eliminated using *in vitro* methods (Table 2-14).

Table 2-14 : Disadvantages of *in vivo* experiments.

Disadvantage	Description
Discomfort to test animals	• If not properly tested beforehand, material may cause significant pain/discomfort to the animal • Majority of countries world-wide have strict policies regarding requirements before *in vivo* tests may be performed
Cost	• Intrinsically high cost to perform • Multiple samples for statistical accuracy • Failed experiments more common due to uncontrollable factors/variations • No simple cost-to-benefit ratio exists worldwide [260]
Time	• Experiments often cannot commence for long periods while approval is obtained from regulatory body
Difficulty to analyse in situ	• Possible to use X-ray and µCT, but greater qualitative/quantitative analysis requires animal sacrifice • In contrast, *in vitro* tests may be stopped, analysed, and restarted with little problem
Choice of animal model	• Especially important in orthopaedic applications, where mechanical conditions play role in biomaterial performance (eg. Rabbit may not be suitable for spinal implant material) • For cartilage repair, no current animal species replicates all of the bio-properties [261] • Extrapolation across species is difficult • Choice of most appropriate model is often problematic
Ethical issues	• Animal rights is closely followed and a popular issue in modern culture • Rationalisation of studies depends on "potential human benefit and justification for their exploitation" [260]

2.4.2. In vitro environments

The term "*in vitro*" is often used to refer to a wide range of experiments, some of which could be considered "standard" tests if they were not being investigated in reference to biological performance. An example of this would be the many experiments performed on Mg alloys using immersion in NaCl solutions [116, 262]. The only physical difference between these tests and most general purpose corrosion tests that are performed on Mg alloys is the concentration of NaCl and the conclusions drawn [263].

The simplest way to divide different *in vitro* corrosion environments would be based on how realistically they emulate the body. The degree of realism can vary depending on the limitations of the implant environment and material. Black *et al.* distinguished between four "classes of exposure environment" (Table 2-15) [42].

Table 2-15 : Classes of exposure environment.

Environment	Description	Example
Physiological	Chemical (inorganic) and thermal conditions controlled to be normative mammalian values for the intended applications	HBSS, EBSS, PBS
Bio-physiological	Physiological conditions with the addition of appropriate types and concentrations of initially non-denatured (active) cell products (serum proteins, enzymes). This includes amino acids.	MEM, MEM+FBS/BSA
Biological	Bio-physiological conditions with the addition of appropriate viable, active cells.	Cell culture, toxicity tests
Pericellular (Circumcellular)	A special case of biological: the conditions in the immediate vicinity of appropriate, viable, active cells	

Adapted from [42]

The vast majority of *in vitro* testing on Mg has been carried out in physiological or bio-physiological conditions. This is primarily due to the relative ease with which these tests may be performed. Cellular tests require many additional steps, such as the growth, maintenance, and transplantation of suitable cells. This adds significantly to the cost and introduces a number of variables that can result in problems and cause experimental failure.

2.4.3. Types of in vitro corrosion experiments

The biodegradation behaviour of Mg is the most important factor in determining if it will succeed or fail as an implant material. Thus, a detailed understanding of the biodegradation of Mg and its alloys in a biological or simulated environment is vital to its eventual implementation.

There are a range of different *in vitro* experiments that may be performed to elucidate the possible *in vivo* performance of Mg alloys; some of which are unique to Mg or biodegradable metals (*e.g.* the measurement of hydrogen evolution). *In vitro* corrosion tests can be collated into two categories; i) immersion and ii) electrochemical. The former typically records physical loss of mass or evolution of hydrogen and provides information on the physical corrosion that has taken place. Other than pH measurement, electrochemical tests normally require the use of an electronic instrument called a potentiostat. Since all metals undergo electrochemical corrosion, these methods are frequently employed not only to obtain corrosion rates but to gather information on the mechanism of corrosion.

Mass loss

Often referred to as weight loss, mass loss (ML) experiments require only a sample and solution and an accurate microbalance. The sample is placed in a selected solution for set period(s) of time, after which it is removed and mass loss is measured. Normally a mixture, such as chromic acid, is used to remove any corrosion product on the surface. This test has been used in over 40 different journal papers in the bio-Mg literature.

Hydrogen evolution

For Mg, the overall corrosion reaction at its corrosion potential may be represented by Equation 2-7 [264].

$$Mg + 2H_2O = Mg^{2+} + 2OH^- + H_2 \qquad \text{Equation 2-7}$$

This indicates that 1 atom of Mg generates 1 hydrogen gas molecule. Thus, the evolution of 1 mol of hydrogen gas (22.4 L) directly corresponds to the dissolution of 1 mol of Mg (24.31 g). In theory, measuring the volume of H_2 gas produced is equivalent to measuring the mass loss of the Mg.

The setup of a typical hydrogen evolution (H_2^{evo}) experiment is very similar to that of a standard mass loss experiment. A sample is submerged in a solution and a "collector" is placed above. Most setups use an inverted funnel and burette or graduated tube [265-268]. The burette is filled with the test solution, and as the H_2 gas evolves it rises and replaces the solution in the burette. H_2^{evo} has been used in more than 35 studies to determine Mg *in vitro* performance.

pH measurement

The most simple electrochemical test is pH measurement of the solution. The corrosion rate of an Mg alloy can be indicated qualitatively by the rise in pH of the solution in which the sample is immersed [46, 113, 269, 270]. Measurement may be performed remotely or close to the surface of the sample.

Potentiodynamic polarisation

Potentiodynamic polarisation (PDP) literally means multiple or changing potentials. It is a form of linear polarisation and is the most commonly used electrochemical technique for studying *in vitro* corrosion of Mg alloys, performed in over 70 studies.

Typically the test starts with a set period of time where the open circuit potential (OCP) is recorded. This allows the material to "stabilise" with the electrolyte and reach a steady corrosion potential (see Chapter 4.3.5.). After this, a voltage difference is applied by controlling the current flowing between the working and counter electrode. The voltage is altered at a controlled rate (*e.g.* 1 mV/s) and the current required for this change to occur is recorded. Normally for Mg the voltage is initially set to be more negative (cathodic) and sweeps to become more positive (anodic) than the OCP. This is to limit the effect of the increased Mg dissolution that occurs in the anodic region. The test provides both thermodynamic information, from the corrosion potential (E_{corr}), and kinetic information from the corrosion current density (i_{corr}) [271].

Electrochemical impedance spectroscopy

A corrosion analysis technique that has become increasingly popular in recent years is electrochemical impedance spectroscopy (EIS) which has been utilised in over 50 studies on

the bio-performance of Mg alloys. EIS is an AC technique and uses a range of low magnitude polarising voltages that cycle from peak anodic to peak cathodic using a spectra of voltage frequencies. Resistance and capacitance values are obtained for each frequency. These can then be used to elucidate a number of phenomena and properties of the metal surface.

There are a number of other experiments that may also be used to study the *in vitro* behaviour of Mg, such as OCP recording or electrical noise measurement. However these are not currently widely used in the Mg biocorrosion literature, have several significant drawbacks and consequently were not investigated in this work.

2.4.4. Corrosive media

When performing *in vitro* tests it is important to select an appropriate simulated body fluid (SBF). These can range significantly in makeup, from basic salt solutions to media containing physiological amounts of proteins and even cells.

For Mg biocorrosion experiments, the vast majority of test solutions have been "off the shelf" cell culture media. Many of the cell culture media in use are based on solutions originally conceived in the middle of the last century by Hanks [272, 273], Earle [274], and Dulbecco and Vogt [275]. Some have since been revised [276], and there are many different modifications that are available to suit specific needs. Although each medium was originally designed to perform specific studies, most are similar in inorganic composition.

A number of the solutions and constituents that have been used in the literature are discussed below.

Sodium chloride

The simplest solution that has been used to attempt to mimic the body's environment is effectively just salt water. Water containing physiological amounts of NaCl has been widely used in the literature in the study of Mg alloy bio-performance. To date, over 25 separate studies have been performed on Mg in NaCl solutions for biomedical purposes. The concentration of NaCl in the solution varied from 0.27% [277] to 3% [278], although studies on the effects of varying NaCl amounts have looked at between 0.05% and 5% [279].

However, the majority of studies have used a 0.9% NaCl solution, which is the amount of NaCl that is found in physiological saline.

Cl^- is important for the continued dissolution of Mg with increasing amounts facilitating amplified attack. It is crucial then that any saline solution contains the correct amount of Cl^- as found in the body, because increasing or decreasing the concentration will have a significant effect on corrosion [279]. The utility of NaCl solutions is somewhat limited, since they do not contain basic components, such as potassium and calcium ions; elements that have been shown to have a significant effect on the corrosion process [280].

Balanced salt solutions

Balanced salts solutions (BSS) come in a variety of compositions, but most contain similar amounts of the majority of the inorganic salts that are found in the body. They typically contain physiological concentrations of calcium chloride ($CaCl_2$), potassium chloride (KCl), magnesium sulphate ($MgSO_4$), and NaCl. Phosphate buffered saline (PBS), Hank's balance salt solution (HBSS) and Earle's balance salt solution (EBSS) are the most frequently used commercially available BSS in the literature. Of the three, HBSS is the most commonly used in the *in vitro* Mg literature with 26 separate studies employing it. Seven studies have used PBS, and 1 study has used EBSS. A number of other works have used different versions of a SBF developed by Tadashi Kokubo [281, 282], however they often do not state which version they used or just call the solution a "basic SBF". The overall makeup of this solution is similar to both HBSS and EBSS.

BSS are another step towards simulating human blood or plasma. Containing physiological amounts of ions that are found in the body, they can have a significant effect on not only the corrosion rate but also the oxides that form on the surfaces of Mg alloys [280]. For example, these salts facilitate the formation of calcium phosphates (CaP) that are commonly found on the surfaces of Mg samples *in vivo*. They are useful as they can be made quickly and have a low cost.

However, the BSS are all hindered by their lack of some of the other constituents of the body, primarily amino acids and proteins. The solutions are considered inorganic. Amino acids, and to a great extent proteins, have been known to play a significant role in the degradation of

other implant materials [283, 284], and have more recently been investigated on Mg alloys [285, 286]. However, overall the BSS solutions may still elucidate underlying corrosion properties of the alloy and due to their simplicity still have a significant role in the *in vitro* testing of Mg alloys.

Minimum essential medium

Originally developed by Harry Eagle, minimum essential medium (MEM) is one of the most widespread cell culture media in use. It contains the same salts that are found in the BSS, but also includes glucose, vitamins and, most importantly, amino acids. Amino acids (AA) are the building blocks of proteins, and perform many functions in the body's metabolism [41]. AA are also known to be pH regulators, although are not as effective as carbonic buffering [287]. They may influence corrosion behaviour of Mg alloys by adsorbing onto the sample surface, following the Langmuir isotherm [288, 289]. They have also been found to form a complex with metal cations (positive ions), which may encourage the dissolution of metal [290, 291]. Yamamoto discussed this in the case of Mg dissolution, where the chelating (metal atom attached to large molecule) of the Mg with an organic compound will "inhibit the formation of insoluble salts, suggesting that the reduction of the retardation by insoluble salt layer on the magnesium disk surface" [280]. She suggested that organic compounds, like the amino acids, may reduce the corrosion resistance effect of the insoluble salt layer that forms on Mg.

However, Gu found that amino acid adsorbed onto the surface of Mg alloys increased the resistance to polarisation and reduced the corrosion current density [285]. An increased corrosion resistance has also been reported for steel and aluminium [288, 289, 292]. To date it appears the specific role of amino acids on Mg biomaterials is unclear, and warrants further study.

Only 4 studies have used MEM to analyse the bio-performance of Mg. Several other studies have used similar solutions; McCoy's medium [293, 294], PRMI1640 [119] and a simulated blood plasma [120]. The reason for the lack of widespread use of MEM in the bio-Mg literature may stem from its traditional function as a base medium for protein of cell cultures. However, MEM provides a link between a completely inorganic salt solution and one containing proteins, and is a necessary solution in the understanding of Mg corrosion *in vivo*.

Addition of proteins

As discussed in Chapter 2.3.2. , proteins play a vital part in the success of any implant in the body. Their attachment to the surface is crucial as they provide attachment sites upon which cells are able to bind [295]. A number of tests have been performed on Mg with the addition of proteins to a base simulated body fluid. These are summarised in Table 2-16.

Table 2-16 : Summary of Mg *in vitro* tests that have included proteins.

Author	Year	Base Medium	Protein Addition	Reference
Gu	2009	MEM	10% FBS	[285]
Witte	2007	MEM	10% FBS	[254]
Yamamoto	2009	E-MEM	10% FBS	[280]
Pietak	2007	MEM	15% FBS	[296]
Liu	2007	Basic SBF (not specified)	1 g/L BSA	[286]
Mueller	2007	PBS	1/10 g/L BSA	[122]
Mueller	2010	PBS	1/10 g/L BSA	[293]
Mueller	2009	PBS	0.1/1/10 g/L BSA	[297]
Rettig	2008	Oyane m-SBF[A]	40 g/L BSA	[298]
Rettig	2009	Oyane m-SBF[A]	40 g/L BSA	[299]

[A] = solution based on modified SBF by Oyane [300]

Apart from a range of base solutions, the key differences between these experiments have been the amount of and method by which proteins have been added. Foetal bovine serum (FBS), also known as foetal calf serum, is the part of plasma that is left after the coagulation of blood. It is widely used in cell cultures due to its low amounts of antibodies and ample amount of growth factors [301]. FBS typically contains a total of between 30-45 g/L of proteins [302]. Of these, bovine serum albumin (BSA), a large globular protein, makes up the majority [303]. Its human equivalent, human serum albumin, is the most common protein in the body, comprising of just over half [303]. BSA may be purified from bovine blood relatively cheaply and easily, and is a more inexpensive option than FBS, which has to be extracted from living or freshly deceased foetuses.

In the literature the amount of protein added to solutions has varied widely, from approximately 0.1 g/L [297] to 40 g/L [299]. It is important to note that when added in FBS

form the proteins are not solely BSA, and a 10% FBS solution would be equivalent to adding a total of ~4 g/L of protein. Thus all FBS experiments had between 4-6 g/L of protein. Although none of the experiments justified why this amount was chosen, it is a commonly used amount in cell cultures and FBS is expensive [304].

As it is in virtually pure form, directly adding BSA proteins results in the same amount of protein in solution. Most experiments that used BSA additions also did not specify why a certain amount was chosen, however Mueller ***et al.*** chose three different amounts with which to make comparisons [297]. Rettig and Virtanen chose to use 40 g/L in two separate experiments, the most realistic amount investigated to date [298, 299]. This was justified as it would be equivalent to the physiological amount of HSA in the body.

Although the effect of proteins has been widely investigated for a number of biomaterials, studies of their influence on Mg alloys has been extremely limited. Apart from the tests mentioned above, very few studies have looked at how they might affect the corrosion properties of the alloys ***in vitro***. As one of the key parameters determining the success of an implant in the body, protein interaction with the surface of Mg alloys is not well understood. This is an area that will be explored in this work.

Human plasma

Complete or mixed human plasma may also be used to test Mg alloys ***in vitro***. However it carries a number of health risks that are not posed by bovine and other plasmas and must be handled with extreme care. There is also more possibility for variation between batches, depending on how it is collected.

2.4.5. Test environment

The environment in which ***in vitro*** tests are carried out plays a large role in the accuracy and magnitude of the results obtained. Factors including the temperature of the test solution, the pH, the buffer used, and the atmosphere surrounding the solution are all necessary considerations when designing appropriate experiments.

Temperature

Of all environmental factors, temperature is perhaps the most important yet often overlooked. Room temperature is generally between 20-25 °C, however the temperature in the body is normally kept at 37 °C. This difference of 12-17 °C may alter not only the corrosion rate but also the formation of protective layers on the Mg and the interaction of proteins. It has been well established that an increase in temperature can lead to a significant increase in corrosion rate for metals in general [305]. The increase from 20 °C to 37 °C has the potential to more than double the rate of electrochemical reactions, following the Arrhenius equation [306].

However, only a limited number of studies have looked at the role of temperature on degradation performance of metals for biological applications. Burstein ***et al.*** found that, for titanium (Ti) in Ringer's solution, nucleation of corrosion pits rose significantly with an increase in temperature from 20°C [307]. This was attributed to the increased speed with which Cl^- ions were migrating across the passivating oxide film. An increase in temperature from 26°C to 40 °C was also found to decrease the corrosion resistance of stainless steel in a PBS + BSA solution from 16 $k\Omega/cm^2$ to 6 $k\Omega/cm^2$ [308]. Similarly, an increase from 25°C to 36°C increased the corrosion rate of aluminium by 230% [289].

Very few publications have examined the corrosion rate of Mg alloys as a function of temperature. In his review paper, Ghali reported that increases in temperature from 25°C to 50°C promoted increased localised corrosion attack on pure Mg in NaCl solutions [309]. Zeng ***et al.*** studied AZ31, AZ91 and WE43 in 0.9% NaCl solution and Hanks using OCP and PDP techniques [310]. It was reported that the corrosion rates of AZ31 and WE43 in the NaCl solution increased by 390% and 460%, respectively, with a rise in temperature from 20°C to 37°C. Interestingly, the same increase in temperature caused the corrosion rates of AZ31 and WE43 in Hanks to decrease by 50% and 20%, respectively. It is suggested that other ions in the solution (***i.e.*** Ca^{2+}, HCO_3^-, $H_2PO_4^-$, and SO_4^-) suppress the detrimental impact of the Cl^- ions [32]. Zeng ***et al.*** concluded that the corrosion rates of the alloys are very sensitive to the temperature of the solution [310].

In addition to affecting the degradation rate, temperature may also influence the corrosion mechanisms of the metal. Gerasimov ***et al.*** found that temperature had a substantial effect on the anodic and cathodic contributions to the corrosion for a range of metals [305]. In an

example of copper they found the reactions to be primarily cathodically controlled below 50°C while anodically controlled above 80°C. Ashassi-Sorkhabi *et al.* found that an increase in temperature causes a shift in the corrosion potential (E_{corr}) to more negative values for pure aluminium (Al) [289]. Lunder *et al.* observed filiform corrosion of AZ91 to occur between 20-30°C in a 3% NaCl solution; however, pitting was the main form of corrosion observed outside this range [311].

The individual components of a solution may also be affected by its temperature. For example, the behaviour of proteins has been found to be highly dependent on the temperature of the test solution. In low temperature experiments Yin *et al.* calculated the adsorbtion rate of BSA on hydroxyapatite (HaP) to be 15% higher at 15°C when compared with 5°C [312]. Jackson *et al.* found that almost 4 × as much BSA adhered to Ti at a temperature of 70°C compared with that at 43°C or below [313]. This was to some extent attributed to the reversible partial unfolding of proteins that occurs between 42°C and 50°C [314]. Omanovic *et al.* stated that the temperature affects the Gibbs free energy of adsorption for proteins, which plays a significant role in the number and affinity with which proteins adsorb to a surface [308].

pH

As discussed in Chapter 2.1.7. , the pH of the solution surrounding an Mg sample can have a significant effect on the formation of the $Mg(OH)_2$ layer. At pH values close to those of the body, 7.4-7.6, this layer is neither stable nor complete and will continue to dissolve. In more realistic SBFs, pH may also play a role in the absorption of proteins [312].

It has been suggested that due to implantation (in a bone fracture site) the pH of surrounding tissues can drop to 5.5 [267]. However, pH changes due to surgery are normally only temporary, unless significant tissue damage occurs or the implant is not well received [315]. Chakkalakal *et al.* found that after an orthopaedic operation the pH in the vicinity of the implant varied only ± 0.16 around the baseline value of 7.4 during the 30 post-operative days [316]. This was attributed to tissue repair during bone healing.

Buffering system

Associated with the pH is the implementation of a buffer in the chosen solution. Buffer solutions operate as neutralizing agents, containing both positive and negative ions of a weak acid. pH is kept constant when more acid is added to the solution as the H^+ ions will combine with a conjugate base, and similarly the OH^- ions will accept protons from the acid. Through this adsorption they will normally create water or another compound that will not affect the pH of the solution. The maximum amount of H^+ or OH^- that a buffer can accept is known as its buffering capacity. It should be noted that in more complex media, other components such as amino acids also act as buffers [287].

There are a number of buffer systems available specifically for use in the *in vitro* environment. Of these buffers, the most similar to the body's mechanism is a mix of sodium bicarbonate ($NaHCO_3$) in solution and a controlled partial carbon dioxide (CO_2) atmosphere. In the body, CO_2 and carbonic acid neutralize hydroxide ions, which would increase the pH of blood, and hydrogen ions, which decrease the pH. Through these processes the body's pH is kept constant.

In vitro typically 2.2 g/L of $NaHCO_3$ are added to an SBF that is kept in a 5-10% CO_2 environment. The CO_2 balances the CO_3^{2-}/HCO_3^- content of the solution. This is effective at keeping the pH balanced and is a very commonly used method in cell culture where control of the pH value is crucial to avoid cell death. The main benefit of using a sodium bicarbonate and CO_2 ($SB+CO_2$) system is its similarity to the *in vivo* buffering mechanisms. The use of a $SB+CO_2$ system is also relatively cheap and can provide chemical benefits to the cells [317]. However, an incubator is required to provide the correct environment and vented flasks must be used to allow the CO_2 to have an effect and regulate the pH.

The second category of buffering systems is typically based on a zwitterion, a highly water-soluble molecule that has both positive and negative charges, and typically contains both an acid and a base. The most common of these is *4-(2-hydroxyethyl)-1-piperazineethanesulfonic acid*, commonly referred to as HEPES. HEPES is one of twelve buffers described in the 1960's for maintaining pH during cell culture that has since become popular [318]. The main benefit of HEPES is the lack of requirement for a CO_2 environment. High concentrations (>50 mmol/L) of HEPES are toxic to some types of cells [317, 319]; however, HEPES also

strongly supports cell growth in comparison to some SB+CO_2 and TRIS buffered environments [320].

Other chemical buffers include *tris(hydroxymethyl)aminomethane*, or TRIS, borate buffer and citric acid, although these have been used in less than 8% of the Mg biocorrosion literature. Borate and citric acid buffers are normally used for pH control outside the physiological range and as such were not investigated in this work.

2.5. References

[1] Wedepohl, K.H. *Chemical Composition and Fractionation of the Continental Crust*. Geologische Rundschau 1991;80:207.

[2] Weeks, M.E. *Discovery of the Elements*. Journal of Chemical Education 1945;22.

[3] Roberts, C.S. *Magnesium and Its Alloys*. New York: Wiley, 1960.

[4] Kramer, D.A. *Magnesium*. 2008 Minerals Yearbook: U.S. Geological Survey, 2008.

[5] Friedrich, H.E. Magnesium Technology : Metallurgy, Design Data, Applications. Heidelberg: Springer, 2006.

[6] Gupta, C.K. *Chemical Metallurgy: Principles and Practise*. New York: Wiley-VCH, 2003.

[7] Kramer, D.A. *Magnesium in the Fourth Quarter 2009*. Mineral Industry Surveys: U.S. Geological Survey, 2009.

[8] Avedesian, M.M., H. Baker. *Magnesium and Magnesium Alloys*. Materials Park, Ohio: ASM International, 1999.

[9] US Airforce National Museum. *Northrop Xp-56*. 1943.

[10] ASM International. *Properties and Selection : Nonferrous Alloys and Special-Purpose Materials*. Metals Handbook, 10th Edition, vol. 2. Materials Park, OH: ASM International, 1990.

[11] Polmear, I.J. Light *Alloys : Metallurgy of the Light Metals*, Second Edition. Melbourne: Hodder & Stoughton, 1989.

[12] Kainer, K.U. *Magnesium Alloys and Their Application*. Sb. Int. Congress. Mnichov, 2000. p.534.

[13] Emley, E.F. *Principle of Magnesium Technology*: Pergammon Press, 1966.

[14] Blake, A.H., C.H. Caceres. *Solid Solution Effects on the Tensile Behaviour of Concentrated Mg-Zn Alloys*. San Francisco, CA, USA: Minerals, Metals & Materials Society, 2005. p.403.

[15] Ganeshan, S., S.L. Shang, Y. Wang, Z.K. Liu. *Effect of Alloying Elements on the Elastic Properties of Mg from First-Principles Calculations*. Acta Materialia 2009;57:3876.

[16] Birbilis, N., M.A. Easton, A.D. Sudholz, S.M. Zhu, M.A. Gibson. *On the Corrosion of Binary Magnesium-Rare Earth Alloys*. Corrosion Science 2009;51:683.

[17] Mordike, B.L., P. Lukac. *Physical Metallurgy*. In: Friedrich, H.E., Mordike, B.L., editors. Magnesium Technology : Metallurgy, Design Data, Applications. Heidelberg: Springer, 2006. p.63.

[18] Haferkamp, H., F.W. Bach, V. Kaese, K. Möhwald, M. Niemeyer, H. Schreckenberger. *Magnesium Corrosion-Processes, Protection of Anode and Cathode*. In: Kainer, K.U., editor. Magnesium : Alloys and Technology. Weinheim: Wiley-VCH, 2003. p.226.

[19] Bard, A.J., L.R. Faulkner. *Electrochemical Methods: Fundametals and Applications*: John Wiley and Sons, 2001.

[20] Jones, D.A. *Principles and Prevention of Corrosion*. Englewood Cliffs, NJ: Prentice-Hall, 1992.

[21] Wang, J. *Analytical Electrochemistry (Second Edition)*. New York: Wiley-VCH, 2002.

[22] Bothwell, M.R. *The Corrosion of Light Metals*. New York: John Wiley and Sons, 1967.

[23] Busk, R.S. *Magnesium Products Design*. New York: Marcell Dekker, 1986.

[24] Szklarska-Smialowska, Z. *Pitting Corrosion of Metals*. Houston: NACE, 1986.

[25] Perrault, G.G. In: Bard, A.J., editor. Encyclopedia of Electrochemistry of the Elements. New York: Marcell Dekker, 1978. p.262.

[26] Shaw, B.A. *Corrosion Resistance of Magnesium Alloys*. ASM Handbook 2003;13A Corrosion: Fundamentals, Testing, and Protection.

[27] Vermilyea, D.A. *On the Mechanism of the Oxidation of Metals*. Acta Metallurgica 1957;5:492.

[28] ASM International. *Corrosion : Fundamentals, Testing and Protection*. Materials Park: ASM International, 1987.

[29] Song, G.L., A. Atrens. *Corrosion Mechanisms of Magnesium Alloys*. Advanced Engineering Materials 1999;1:11.

[30] Song, G., A. Atrens. *Understanding Magnesium Corrosion : a Framework for Improved Alloy Performance*. Advanced Engineering Materials 2003;5:837.

[31] Song, G., A. Atrens, D. Stjohn, J. Nairn, Y. Li. *The Electrochemical Corrosion of Pure Magnesium in 1 N Nacl*. Corrosion Science 1997;39:855.

[32] Song, G., A. Atrens, D. St John, X. Wu, J. Nairn. *The Anodic Dissolution of Magnesium in Chloride and Sulphate Solutions*. Corrosion Science 1997;39:1981.

[33] Ghali, E. *Corrosion and Protection of Magnesium Alloys*. In: Kojima, Y., editor. Magnesium 2000, vol. 350-351. Nagaoka City, Japan: Trans Tech Publications, 2000. p.261.

[34] Ferrando, W. *Review of Corrosion and Corrosion Control of Magnesium Alloys and Composites*. Journal of Materials Engineering 1989;11:299.

[35] Park, J.B., J.D. Bronzino. *Biomaterials : Principles and Applications*. London: CRC Press, 2003.

[36] Park, J.B., R.S. Lakes. *Biomaterials : An Introduction*. New York: Springer, 2007.

[37] Bruck, S.D. *Properties of Biomaterials in the Physiological Environment*. Boca Raton, FL: CRC Press, 1980.

[38] Rather, B.D., A.S. Hoffman, F.J. FSchoen, J.E. Lemons. *Biomaterial Science*. London: Academic Press, 1996.

[39] Charnley, J. *Arithoplasty of the Hip : A New Operation*. The Lancet 1961;277:1129.

[40] Charnley, J. *Tissue Reactions to Polytetrafluorethylene*. The Lancet 1963;282:1379.

[41] Puleo, D.A., R. Bizios. *Biological Interactions on Materials Surfaces : Understanding and Controlling Protein, Cell and Tissue Responces*. London: Springer, 2009.

[42] Black, J. Biological Performance of Materials: Fundamentals of Biocompatibility. New York: Marcel Dekker, 2006.

[43] Mudali, U.K., B. Raj, T.M. Sridhar. *Corrosion of Bio Implants*. Sadhana - Academy Proceedings in Engineering Sciences 2003;28:601.

[44] Shi, P., W.F. Ng, M.H. Wong, F.T. Cheng. Improvement of Corrosion Resistance of Pure Magnesium in Hank's Solution by Microarc Oxidation with Sol-Gel Tio2 Sealing. Journal of Alloys and Compounds 2009;469(1-2):286.

[45] Duygulu, O., R.A. Kaya, G. Oktay, A.A. Kaya. *Investigation on the Potential of Magnesium Alloy Az31 as a Bone Implant*. Materials Science Forum 2007;546-549:421.

[46] Lopez, H.Y., D.A. Cortes, S. Escobedo, D. Mantovani. *In Vitro Bioactivity Assessment of Metallic Magnesium*. Key Engineering Materials 2006;309-311:453.

[47] Witte, F., H. Ulrich, M. Rudert, E. Willbold. *Biodegradable Magnesium Scaffolds: Part 1: Appropriate Inflammatory Response*. Journal of Biomedical Materials Research Part A 2007:748.

[48] Willliams, D. *New Interests in Magnesium*. Medical device technology 2006;17:9.

[49] Witte, F., J. Nellesen, H.-A. Crostack, V. Kaese, A. Pisch, F. Beckmann, H. Windhagen. *In Vitro and in Vivo Corrosion Measurements of Magnesium Alloys*. Biomaterials 2006;27:1013.

[50] Witte, F., V. Kaese, H. Haferkamp, E. Switzer, A. Meyer-Lindenberg, C.J. Wirth, H. Windhagen. *In Vivo Corrosion of Four Magnesium Alloys and the Associated Bone Response*. Biomaterials 2005;26:3557.

[51] Denkena, B., C. Podolsky, A. Lucas, T. Hassel, F. Witte, O. Palm, C. Hurschler. *Degradable Implants Made of Magnesium Alloys*. 5th Euspen International Conference, vol. 6. Montpellier, France, 2005.

[52] Witte, F., N. Hort, C. Vogt, S. Cohen, K.U. Kainer, R. Willumeit, F. Feyerabend. *Degradable Biomaterials Based on Magnesium Corrosion*. Current Opinion in Solid State and Materials Science 2008;12:63.

[53] Zeng, R., W. Dietzel, F. Witte, N. Hort, C. Blawert. *Progress and Challenge for Magnesium Alloys as Biomaterials*. Advanced Engineering Materials 2008;10:B3.

[54] Staiger, M.P., A.M. Pietak, J. Huadmai, G. Dias. *Magnesium and Its Alloys as Orthopedic Biomaterials: A Review*. Biomaterials 2006;27:1728.

[55] Saris, N.-E.L., E. Mervaala, H. Karppanen, J.A. Khawaja, A. Lewenstam. *Magnesium: An Update on Physiological, Clinical and Analytical Aspects*. Clinica Chimica Acta 2000;294:1.

[56] Seiler, H.G., H. Sigel. *Handbook of Toxicity of Inorganic Compounds*. New York, USA: Marcel Dekker Inc., 1988.

[57] Leroy, J. *Necessite Du Magnesium Pour La Croissance De La Souris*. Comptes Rendus de Seances de la Societe de Biologie 1926;94:431.

[58] Lusk, J.E., R.J.P. Williams, E.P. Kennedy. *Magnesium and the Growth of Escherichia Coli*. Journal of Biological Chemistry 1968;243:2618.

[59] Marschner, H. *Mineral Nutrition in Higher Plants.* . San Diego: Academic Press, 1995.

[60] Black, C.B., J.A. Cowan, editors. *Magnesium-Dependent Enzymes in General Metabolism*. New York: VCH, 1995.

[61] Ebel, H., T. Gunther. *Magnesium Metabolism: A Review*. Journal of Clinical Chemistry and Clinical Biochemistry 1980;18:257.

[62] Cowan, J.A. *Introduction to the Biological Chemistry of Magnesium*. New York: VCH, 1995.

[63] Institute of Medicine. *Magnesium*. Dietary Reference Intakes for Calcium, Phosphorus, Magnesium, Vitamin D, and Fluoride. National Adademy Press, 1997. p.190.

[64] Williams, D. *New Interests in Magnesium*. Medical device technology 2006;17:9.

[65] Gruber, H., R. Rude, L. Wei, A. Frausto, B. Mills, H.J. Norton. *Magnesium Deficiency: Effect on Bone Mineral Density in the Mouse Appendicular Skeleton*. BMC Musculoskeletal Disorders 2003;4:7.

[66] Sojka, J.E., C.M. Weaver. *Magnesium Supplementation and Osteopososis*. Nutrition Review 1995;53:71.

[67] Vormann, J. *Magnesium: Nutrition and Metabolism*. Molecular Aspects of Medicine 2003;24:27.

[68] Lothar, T. *Labor Und Diagnose*. Frankfurt: TH-Books, 2000.

[69] Huse, E.C. *A New Ligature?* Chicago Medical Journal and Examiner 1878;37:171.

[70] Payr, E. *Beiträge Zur Technik Der Blutgefäss- Und Nervennaht Nebst Mittheilungen Über Die Verwendung Eines Resorbirbaren Metalles in Der Chirurgie*. Arch Klin Chir 1900;62:67.

[71] Payr, E. *Blutgefäß- Und Nervennaht (Nebst Mittheilung Über Die Verwendung Eines Resorbirbaren Metalles in Der Chirurgie)*. Gesellschaft für Chirurgie, XXIX Kongress, Vol. 28. Langenbeck-Hause, 1901:31.

[72] Lambotte, A. *Technique Et Indications De La Prothèse Perdue Dans La Traitement Des Fractures.* 1909;17:321.

[73] Lambotte, A. *L'utilisation Du Magnesium Comme Materiel Perdu Dans L'osteosynthese*. Bull Mem Soc Nat Chir 1932;28:1325.

[74] Verbrugge, J. *La Tolérance Du Tissu Osseux Vis-À-Vis Du Magnésium Métallique*. Presse Med 1933;55:1112.

[75] Verbrugge, J. *L'utilisation Du Magnésium Dans Le Traitement Chirurgical Des Fractures*. Bull Mém Soc Nat Cir 1937;59:813.

[76] Verbrugge, J. Le Matériel Métallique Résorbable En Chirurgie Osseuse. La Press Medicale 1934;23:460.

[77] Troitskii, V.V., D.N. Tsitrin. *The Resorbing Metallic Alloy 'Osteosinthezit' as Material for Fastening Broken Bone*. Khirurgiia 1944;8:41.

[78] Znamenskii, M.S. *Metallic Osteosynthesis by Means of and Apparatus Made of Resorbing Metal*. Khirurgiia 1945;12:60.

[79] Witte, F. *The History of Biodegradable Magnesium Implants: A Review*. Acta Biomaterialia 2010;6:1680.

[80] The American Foundry Society Technical Department. *Magnesium Alloys*. Schaumburg, Illiniois: The American Foundry Society Technical Department,, 2006.

[81] Gibson, L.J., M.F. Ashby. *Cellular Solids : Structure and Properties*. Cambridge: Cambridge University Press, 1997.

[82] Krishna, B.V., S. Bose, A. Bandyopadhyay. *Low Stiffness Porous Ti Structures for Load-Bearing Implants*. Acta Biomaterialia 2007;3:997.

[83] Kim, S.G., A. Inoue, T. Masumoto. *Increase of Mechanical Strength of a Mg85zn12ce3 Amorphous Alloy by Dispersion of Ultrafine Hcp-Mg Particles*. Materials Transactions, JIM 1991;32:875.

[84] Rashmir-Raven, A.M., D.C. Richardson, H.M. Aberman, D.J.D. Young. *The Response of Cancellous and Cortical Canine Bone to Hydroxylapatite-Coated and Uncoated Titanium Rods*. Journal of Applied Biomaterials 1995;6:237.

[85] Wintermantel, E., H. Suk-Woo. *Biokompatible Werkstoffe Und Bauweisen (Biocompatible Material and Design)*. Springer Verlag 1998;2.

[86] Pietrzak, W.S., D. Sarver, M. Verstynen. *Bioresorbable Implants - Practical Considerations*. Bone 1996;19:S109.

[87] Vadapalli, S., K. Sairyo, V.K. Goel, M. Robon, A. Biyani, A. Khandha, N.A. Ebraheim. *Biomechanical Rationale for Using Polyetheretherketone (Peek) Spacers for Lumbar Interbody Fusion-a Finite Element Study*. SPINE 2006;31:E992.

[88] Tsantrizos, A., H.G. Baramki, S. Zeidman, T. Steffen. *Segmental Stability and Compressive Strength of Posterior Lumbar Interbody Fusion Implants*. SPINE 2000;25:1899.

[89] Blokhuis, T.J., M. Termaat, H.J. Haarman. *Properties of Calcium Phosphate Ceramics in Relation Fo Their in Vivo Behaviour*. The Journal of Trauma, Injury, Infection and Critical Care 2007;48.

[90] Allan, B. *Closer to Nature : New Biomaterials and Tissue Engineering*. British Journal of Opthamology 1999;83:1235.

[91] Merck International. *Water, Electrolyte Mineral, and Acid/Base Metabolism*. In: Porter, R.S., Kaplan, J.L., editors. *Merck Manual of Diagnosis and Therapy*. Merck & Co., Inc., 2006.

[92] Okuma, T. *Magnesium and Bone Strength*. Nutrition 2001;17:679.

[93] Wolf, F.I., A. Cittadini. *Chemistry and Biochemistry of Magnesium*. Molecular Aspects of Medicine 2003;24:3.

[94] Hartwig, A. *Role of Magnesium in Genomic Stability*. Mutation Research/Fundamental and Molecular Mechanisms of Mutagenesis 2001;475:113.

[95] Howlett, C.R., H. Zreiqat, R.O. Dell, J. Noorman, P. Evans, B.A. Dalton. *The Effect of Magnesium Ion Implantation into Alumina Upon the Adhesion of Human Bone Derived Cells*. Journal of Material Science: Materials in Medicine 1994;9:715.

[96] Li, L., J. Gao, Y. Wang. *Evaluation of Cyto-Toxicity and Corrosion Behavior of Alkali-Heat-Treated Magnesium in Simulated Body Fluid*. Surface and Coatings Technology 2004;185:92.

[97] Kuwahara, H., Y. Al-Abdullat, N. Mazaki, S. Tsutsumi, T. Aizawa. *Precipitation of Magnesium Apatite on Pure Magnesium Surface During Immersing in Hank's Solution*. Materials Transactions 2001;42:1317.

[98] Kim, S.R., J.H. Lee, Y.T. Kim, D.H. Riu, S.J. Jung, Y.J. Lee, S.C. Chung, Y.H. Kim. *Synthesis of Si, Mg Substituted Hydroxyapatites and Their Sintering Behaviors*. Biomaterials 2003;24:1389.

[99] Shils, M.E. *Magnesium*. In: Shils, M.E., Olson, J.A., Shike, M., editors. *Modern Nutrition in Health and Disease, 8th Edition*. Philadelphia: Lea & Febiger, 1994. p.164.

[100] Puleo, D.A., W.W. Huh. Acute Toxicity of Metal Ions in Cultures of Osteogenic Cells Derived from Bone Marrow Stromal Cells. Journal of Applied Biomaterials 1995;6:109.

[101] Granchi, D., G. Ciapetti, S. Stea, L. Savarino, F. Filippini, A. Sudanese, G. Zinghi, L. Montanaro. *Cytokine Release in Mononuclear Cells of Patients with Co-Cr Hip Prosthesis*. Biomaterials 1999;20:1079.

[102] Pholer, O.E.M. *Failure of Orthopaedic Metallic Implants*. Asm Handbook on Failure Analysis and Prevention, vol. 11. Metals Park, OH: ASM International, 1986. p.670.

[103] Bach, F.W. *Development of Biocompatible Magnesium Alloys and Investigation of the Degradation Behaviour*. Sustainable Bioresorbable and Permanent Implants of Metallic and Ceramic Materials. Medical University of Hanover, 2006.

[104] Davis, K.G., W.S. Marras, T.R. Waters. *Evaluation of Spinal Loading During Lowering and Lifting*. Clinical Biomechanics 1998;13:141.

[105] Polmear, I.J. *Magnesium and Magnesium Alloys*. In: International, A., editor. Asm Specialty Handbook. USA: The Materials Information Society, 1999. p.3.

[106] Inoue, H., K. Sugahara, A. Yamamoto, H. Tsubakino. *Corrosion Rate of Magnesium and Its Alloys in Buffered Chloride Solutions*. Corrosion Science 2002;44:603.

[107] Song, G. *Control of Biodegradation of Biocompatable Magnesium Alloys*. Corrosion Science 2007;49:1696.

[108] Seal, C.K., K. Vince, M.A. Hodgson. *Biodegradable Surgical Implants Based on Magnesium Alloys: A Review of Current Research*. IOP Conference Series: Materials Science and Engineering 2009:012011.

[109] Meyer-Lindenberg, A., H. Windhugen, F. Witte. *Us 200410241036.*

[110] Lespinasse, V.D. A Practical Mechanical Method of End-to-End Anastomosis of Blood-Vessels : Using Absorbable Magnesium Rings. Journal of The American Medical Association 1910;55:1785.

[111] Seelig, M.G. A Study of Magnesium Wire as an Absorbable Suture and Ligature Material. Archives of Surgery 1924;8:669.

[112] Li, Z., X. Gu, S. Lou, Y. Zheng. *The Development of Binary Mg-Ca Alloys for Use as Biodegradable Materials within Bone*. Biomaterials 2008;29:1329.

[113] Ren, Y., H. Wang, J. Huang, B. Zhang, K. Yang. *Study of Biodegradation of Pure Magnesium*. Key Engineering Materials 2007;342-343:601.

[114] Witte, F., J. Reifenrath, P.P. Müller, H.A. Crostack, J. Nellesen, F.W. Bach, D. Bormann, M. Rudert. *Cartilage Repair on Magnesium Scaffolds Used as a Subchondral Bone Replacement*. Materialwissenschaft und Werkstofftechnik 2006;37:504.

[115] Krause, C., D. Bormann, T. Hassel, F.W. Bach, H. Windhagen, A. Krause, C. Hackenbroich, A. Meyer-Lindenberg. *Mechanical Properties of Degradable Magnesium Implants in Dependence of the Implantation Duration.* In: Pekguleryuz, M., editor. Conference of Metallurgists : Magnesium Technology in the Global Age. Montreal, Quebec, Canada, 2006. p.329.

[116] Eliezer, A., F. Witte. *Corrosion Behaviour of Magnesium Alloys in Biomedical Environments*. Advanced Materials Research 2010;95:17.

[117] Denkena, B., A. Lucas. *Biocompatible Magnesium Alloys as Absorbable Implant Materials - Adjusted Surface and Subsurface Properties by Machining Processes.* CIRP Annals - Manufacturing Technology 2007;56:113.

[118] Brar, H.S., M.O. Platt, M. Sarntinoranont, P.I. Martin, M.V. Manuel. *Magnesium as a Biodegradable and Bioabsorbable Material for Medical Implants*. Jom 2009;61:31.

[119] Xu, L., F. Pan, G. Yu, L. Yang, E. Zhang, K. Yang. *In Vitro and in Vivo Evaluation of the Surface Bioactivity of a Calcium Phosphate Coated Magnesium Alloy*. Biomaterials 2009;30:1512.

[120] Yang, L., E. Zhang. *Biocorrosion Behavior of Magnesium Alloy in Different Simulated Fluids for Biomedical Application*. Materials Science and Engineering: C 2009;29:1691.

[121] Hänzi, A.C., M.M. Weder, B. Gerold, P.J. Uggowitzer. *New Bio-Absorbable Magnesium Alloys for Medical Applications*. Light Metals Technology Conference. Canada, 2007.

[122] Mueller, W.D., M.L. Nascimento, M. Zeddies, M. Córsico, L.M. Gassa, M.A.F.L. de Mele. *Magnesium and Its Alloys as Degradable Biomaterials: Corrosion Studies Using Potentiodynamic and Eis Electrochemical Techniques*. Materials Research 2007;10:5.

[123] Gu, X., Y. Zheng, Y. Cheng, S. Zhong, T. Xi. *In Vitro Corrosion and Biocompatibility of Binary Magnesium Alloys*. Biomaterials 2009;30:484.

[124] Blawert, C., D. Fechner, D. Höche, V. Heitmann, W. Dietzel, K.U. Kainer, P. Zivanovic, C. Scharf, A. Ditze, J. Gröbner, R. Schmid-Fetzer. *Magnesium Secondary Alloys: Alloy Design for Magnesium Alloys with Improved Tolerance Limits against Impurities*. Corrosion Science;In Press, Accepted Manuscript.

[125] Lee, J.-Y., G. Han, Y.-C. Kim, J.-Y. Byun, J.-i. Jang, H.-K. Seok, S.-J. Yang. *Effects of Impurities on the Biodegradation Behavior of Pure Magnesium*. Metals and Materials International 2009;15:955.

[126] U.S. Center for Disease Control. *Public Health Statement : Nickel*. vol. 2010.

[127] U.S. Center for Disease Control. *Beryllium Toxicity*.

[128] Speich, M., B. Bousquet, G. Nicolas. *Reference Values for Ionized, Complexed, and Protein-Bound Plasma Magnesium in Men and Women*. Clinical Chemistry 1981;27:246.

[129] Vojtěch, D. *Stents Production from Biodegradable Mg Alloys*. Prague: Institute of Chemical Technology, 2004.

[130] Rubin, H. *Magnesium: The Missing Element in Molecular Views of Cell Proliferation*. BioEssays 2005;27:311.

[131] Romani, A.M., A. Scarpa. *Regulation of Cellular Magnesium*. Front Biosci 2000;5:D720.

[132] Rubin, H. *Degrees and Kinds of Selection in Spontaneous Neoplastic Transformation: An Operational Analysis*. Proceedings of the National Academy of Sciences of the United States of America 2005;102:9276.

[133] Grzesiak, J.J., M.D. Pierschbacher. *Shifts in the Concentrations of Magnesium and Calcium in Early Porcine and Rat Wound Fluids Activate the Cell Migratory Response*. Journal of Clinical Investigation 1995;95:227.

[134] Liddington, R.C., M.H. Ginsberg. *Integrin Activation Takes Shape*. Journal of Cell Biology 2002;158:833.

[135] Grzesiak, J.J., M. Bouvet. *Activation of the Alpha2beta1 Integrin-Mediated Malignant Phenotype on Type I Collagen in Pancreatic Cancer Cells by Shifts in the Concentrations of Extracellular Mg2+ and Ca2+*. International Journal of Cancer 2008;122:2199.

[136] Rink, T.J., R.Y. Tsien, T. Pozzan. *Cytoplasmic Ph and Free Mg2+ in Lymphocytes*. Journal of Cell Biology 1982;95:189.

[137] Kraft, R., C. Harteneck. *The Mammalian Melastatin-Related Transient Receptor Potential Cation Channels: An Overview*. Pflugers Archives 2005;451:204.

[138] Tahan, J.E., V.A. Granadillo, R.A. Romero. *Electrothermal Atomic Absorption Spectrometric Determination of Al, Cu, Fe, Pb, V and Zn in Clinical Samples and in Certified Environmental Reference Materials*. Analytica Chimica Acta 1994;295:187.

[139] Studenikina, F., V. Kosova, V. Denisova. *Physicochemical Properties and Biological Characteristics of Some Metals Used in Medical Instruments*. Biomedical Engineering 1993;27:281.

[140] Morant, C., M.F. Lopez, A. Gutierrez, J.A. Jimenez. *Afm and Sem Characterization of Non-Toxic Vanadium-Free Ti Alloys Used as Biomaterials*. Applied Surface Science 2003;220:79.

[141] Okazaki, Y., S. Rao, Y. Ito, T. Tateishi. *Corrosion Resistance, Mechanical Properties, Corrosion Fatigue Strength and Cytocompatibility of New Ti Alloys without Al and V*. Biomaterials 1998;19:1197.

[142] Ferreira, P.C., A. Piai Kde, A.M. Takayanagui, S.I. Segura-Munoz. *Aluminum as a Risk Factor for Alzheimer's Disease*. Revista Latino-Americana de Enfermagem 2008;16:151.

[143] Lucey, T.D., B. Venugopal. *Metal Toxicity in Mammals*. New York: Plenum Press, 1977.

[144] Flatten, T.P. *Aluminium as a Risk Factor in Alzheimer's Disease, with Emphasis on Drinking Water*. Brain Research Bulletin 2001;55:187.

[145] Domingo, J.L. *Reproductive and Developmental Toxicity of Aluminum: A Review*. Neurotoxicology and Teratology 1995;17:515.

[146] Shingde, M., J. Hughes, R. Boadle, E.J. Wills, R. Pamphlett. *Macrophagic Myofasciitis Associated with Vaccine-Derived Aluminium*. Medical Journal of Australia 2005;183:145.

[147] Rousselle, A.V., D. Heymann, V. Demais, C. Charrier, N. Passuti, M.F. Basle. *Influence of Metal Ion Solutions on Rabbit Osteoclast Activities in Vitro*. Histology and Hispathology 2002;17:1025.

[148] Kiilerich, S., M.S. Christensen, J. Naestoft, C. Christiansen. *Determination of Zinc in Serum and Urine by Atomic Absorption Spectrophotometry: Relationship between Serum Levels of Zinc and Proteins in 104 Normal Subjects*. Clinica Chimica Acta 1980;105:231.

[149] Tapiero, H., K.D. Tew. *Trace Elements in Human Physiology and Pathology: Zinc and Metallothioneins*. Biomedicine & Pharmacotherapy 2003;57:399.

[150] Lastra, M.D., R. Pastelin, A. Camacho, B. Monroy, A.E. Aguilar. *Zinc Intervention on Macrophages and Lymphocytes Response*. Journal of Trace Elements in Medicine and Biology 2001;15:5.

[151] Rosenberg, K., H. Olsson, M. Morgelin, D. Heinegard. *Cartilage Oligomeric Matrix Protein Shows High Affinity Zinc-Dependent Interaction with Triple Helical Collagen*. Journal of Biological Chemistry 1998;273:20397.

[152] Saltman, P.D., L.G. Strause. *The Role of Trace Minerals in Osteoporosis*. Journal of the American College of Nutrition 1993;12:384.

[153] Post, J.I., J.K. Eibl, G.M. Ross. *Zinc Induces Motor Neuron Death Via a Selective Inhibition of Brain-Derived Neurotrophic Factor Activity*. Amyotrophic Lateral Sclerosis 2008;9:149.

[154] Yamaguchi, M. *Role of Zinc in Regulation of Osteoclastogenesis*. Biomedical Research on Trace Elements 2004;15:9.

[155] Zhang, S., X. Zhang, C. Zhao, J. Li, Y. Song, C. Xie, H. Tao, Y. Zhang, Y. He, Y. Jiang, Y. Bian. *Research of Mg-Zn Alloy as Degradable Biomaterial*. Acta Biomaterialia 2010;6:626.

[156] Renkema, K.Y., R.T. Alexander, R.J. Bindels, J.G. Hoenderop. *Calcium and Phosphate Homeostasis: Concerted Interplay of New Regulators*. Annals of Internal Medicine 2008;40:82.

[157] Ilich, J.Z., J.E. Kerstetter. *Nutrition in Bone Health Revisited : A Story Beyond Calcium*. Journal of the American College of Nutrition 2000;19:715.

[158] Ji, Y.J., B. Xiao, Z.H. Wang, M.Z. Cui, Y.Y. Lu. *The Suppression Effect of Light Rare Earth Elements on Proliferation of Two Cancer Cell Lines*. Biomedical and Environment Science 2000;13:287.

[159] Magda, D., R.A. Miller. *Motexafin Gadolinium: A Novel Redox Active Drug for Cancer Therapy*. Seminars in Cancer Biology 2006;16:466.

[160] Feyerabend, F., J. Fischer, J. Holtz, F. Witte, R. Willumeit, H. Drücker, C. Vogt, N. Hort. *Evaluation of Short-Term Effects of Rare Earth and Other Elements Used in Magnesium Alloys on Primary Cells and Cell Lines*. Acta Biomaterialia;In Press, Corrected Proof.

[161] US Department of Labour. *Occupational Safety and Health Guidline for Yttrium & Compounds*. vol. 2010: US Department of Labour, 2010.

[162] ten Dam, M.A., J.F. Wetzels. *Toxicity of Contrast Media: An Update.* Netherlands Journal of Medicine 2008;66:416.

[163] Wedeking, P., K. Kumar, M.F. Tweedle. *Dose-Dependent Biodistribution of [153gd]Gd(Acetate)N in Mice*. Nuclear Medicine and Biology 1993;20:679.

[164] Schranz, D., P. Zartner, I. Michel-Behnke, H. Akintürk. *Bioabsorbable Metal Stents for Percutaneous Treatment of Critical Recoarctation of the Aorta in a Newborn*. Catheterization and Cardiovascular Interventions 2006;67:671.

[165] Witte, F., J. Fischer, J. Nellesen, F. Beckmann. *Microtomography of Magnesium Implants in Bone and Their Degradation*. vol. 6318. San Diego, CA, United States: International Society for Optical Engineering, Bellingham WA, WA 98227-0010, United States, 2006. p.631806.

[166] Hamilton, E.I. *Review of the Chemical Elements and Environmental Chemistry: Strategies and Tactics*. Science of the Total Environment 1976;5:1.

[167] Loghin, F., A. Olinic, D.S. Popa, C. Socaciu, S.E. Leucuta. *Effects of Long-Term Administration of Lithium and Hydrochlorothiazide in Rats.* Metal-Based Drugs 1999;6:87.

[168] Bhagwagar, Z., G.M. Goodwin. *The Role of Lithium in the Treatment of Bipolar Depression*. Clinical Neuroscience Research 2002;2:222.

[169] Timmer, R.T., J.M. Sands. *Lithium Intoxication*. J Am Soc Nephrol 1999;10:666.

[170] Bichet, D.G. *Lithium, Cyclic Amp Signaling, a-Kinase Anchoring Proteins, and Aquaporin-2*. Journal of the American Society of Nephrology 2006;17:920.

[171] Sahin, O., O. Sulak, Y. Yavuz, E. Uz, I. Eren, Y. Ramazan. *Lithium Induced Lung Toxicity in Rats: The Effect of Caffeic Acid Phenethyl Ester (Cape)*. Pathology 2006;38:58.

[172] Giles, J.J., J.G. Bannigan. *Teratogenic and Developmental Effects of Lithium*. Current Pharmaceutical Design 2006;12:1531.

[173] Newman, P.K., M. Saunders. *Lithium Neurotoxicity*. Postgraduate Medical Journal 1979;55:701.

[174] Krause, A., N. von der Höh, D. Bormann, C. Krause, F.-W. Bach, H. Windhagen, A. Meyer-Lindenberg. *Degradation Behaviour and Mechanical Properties of Magnesium Implants in Rabbit Tibiae*. Journal of Materials Science 2010;45:624.

[175] Meyer-Lindenberg, A., M. Thomann, A. Krause, D. Bormann, B. von Rechenberg, H. Windhagen. *Investigation on the Use of a Magnesium Alloy as a New Resorbable Implant Material for Orthopaedic Surgery*. Kleintierpraxis 2010;55:349.

[176] Baruthio, F., O. Guillard, J. Arnaud, F. Pierre, R. Zawislak. *Determination of Manganese in Biological Materials by Electrothermal Atomic Absorption Spectrometry : A Review*. Clinical Chemistry 1988;34:227.

[177] Aschner, M., T.R. Guilarte, J.S. Schneider, W. Zheng. *Manganese: Recent Advances in Understanding Its Transport and Neurotoxicity*. Toxicology and Applied Pharmacology 2007;221:131.

[178] Gilca, M., I. Stoian, V. Atanasiu, B. Virgolici. *The Oxidative Hypothesis of Senescence*. Journal of Postgraduate Medicine 2007;53:207.

[179] Bock, N.A., F.F. Paiva, G.C. Nascimento, J.D. Newman, A.C. Silva. *Cerebrospinal Fluid to Brain Transport of Manganese in a Non-Human Primate Revealed by Mri*. 1198 2008.

[180] Helsen, J.A., H.J. Breme. *Metals as Biomaterials*. London: Wiley, 1998.

[181] Zhang, E., D. Yin, L. Xu, L. Yang, K. Yang. *Microstructure, Mechanical and Corrosion Properties and Biocompatibility of Mg-Zn-Mn Alloys for Biomedical Application*. Materials Science and Engineering: C 2009;29:987.

[182] Xu, L., G. Yu, E. Zhang, F. Pan, K. Yang. *In Vivo Corrosion Behavior of Mg-Mn-Zn Alloy for Bone Implant Application*. Journal of Biomedical Materials Research - Part A 2007;83:703.

[183] Zhang, E.L., L.P. Xu, G.N. Yu, F. Pan, K. Yang. *In Vivo Evaluation of Biodegradable Magnesium Alloy Bone Implant in the First 6 Months Implantation*. Journal of Biomedical Materials Research Part A 2009;90A:882.

[184] Wen, C.E., Y. Yamada, P.D. Hodgson. *Fabrication of Novel Tizr Alloy Foams for Biomedical Applications*. Materials Science and Engineering: C 2006;26:1439.

[185] Att, W., F. Komine, T. Gerds, J.R. Strub. *Marginal Adaptation of Three Different Zirconium Dioxide Three-Unit Fixed Dental Prostheses*. The Journal of Prosthetic Dentistry 2009;101:239.

[186] Yamamoto, A., R. Honma, M. Sumita. *Cytotoxicity Evaluation of 43 Metal Salts Using Murine Fibroblasts and Osteoblastic Cells*. Material Research 1998;39:331.

[187] Couture, P., C. Blaise, D. Cluis, C. Bastien. *Zirconium Toxicity Assessment Using Bacteria, Algae and Fish Assays*. Water, Air, & Soil Pollution 1989;47:87.

[188] Wambach, P.F., J.C. Laul. *Beryllium Health Effects, Exposure Limits and Regulatory Requirements*. Journal of Chemical Health and Safety 2008;15:5.

[189] Beyersmann, D., A. Hartwig. *Carcinogenic Metal Compounds: Recent Insight into Molecular and Cellular Mechanisms*. Archives of Toxicology 2008;82:493.

[190] Gordon, T., D. Bowser. *Beryllium: Genotoxicity and Carcinogenicity*. Mutation Research 2003;533:99.

[191] Makino, T., K. Takahara. *Direct Determination of Plasma Copper and Zinc in Infants by Atomic Absorption with Discrete Nebulization*. Clinical Chemistry 1981;27:1445.

[192] Crosby, W.H., V. Likhite, J.E. O'Brien, D. Forman. *Serum Iron Levels in Ostensibly Normal People*. Journal of The American Medical Association 1974;227:310.

[193] Statland, B.E., P. Winkel, H. Bokelund. *Variation of Serum Iron Concentration in Young Healthy Men: Within Day and Day to Day Changes*. Clinical Biochemistry 1976;9:26.

[194] Brewer, G.J. *Iron and Copper Toxicity in Diseases of Aging, Particularly Atherosclerosis and Alzheimer's Disease*. Exp Biol Med (Maywood) 2007;232:323.

[195] Nixon, D.E., T.P. Moyer, D.P. Squillace, J.T. McCarthy. *Determination of Serum Nickel by Graphite Furnace Atomic Absorption Spectrometry with Zeemaneffect Background Correction: Values in a Normal Population and a Population Undergoing Dialysis*. Analyst 1989;114:1671.

[196] Milavec-Puretic, V., D. Orlic, A. Marusic. *Sensitivity to Metals in 40 Patients with Failed Hip Endoprosthesis*. Archives of Orthopaedic Trauma Surgery 1998;117:383.

[197] Pekguleryuz, M. *Melting, Alloying, and Refining*. In: Friedrich, H.E., Mordike, B.L., editors. Magnesium Technology : Metallurgy, Design Data, Applications. Heidelberg: Springer, 2006. p.109.

[198] Gagliardi, F., L. Filice, D. Umbrello, R. Shivpuri. *Forging of Metallic Foams to Reproduce Biomechanical Components*. Materials Science and Engineering: A 2008;480:510.

[199] Hutmacher, D.W., D.F. Williams. *Scaffolds in Tissue Engineering Bone and Cartilage*. The Biomaterials: Silver Jubilee Compendium. Oxford: Elsevier Science, 2006. p.175.

[200] Ryan, G.E., A.S. Pandit, D.P. Apatsidis. *Porous Titanium Scaffolds Fabricated Using a Rapid Prototyping and Powder Metallurgy Technique*. Biomaterials 2008;29:3625.

[201] Banhart, J. *Manufacture, Characterisation and Application of Cellular Metals and Metal Foams*. Progress in Materials Science 2001;46:559.

[202] Solórzano, E., M. Hirschmann, M.A. Rodriguez-Perez, C. Körner, J.A. de Saja. *Thermal Conductivity of Az91 Magnesium Integral Foams Measured by the Transient Plane Source Method*. Materials Letters 2008;62:3960.

[203] Ashby, M.F., A. Evans, N.A. Fleck, L.J. Gibson, J.W. Hutchinson, H.N.G. Wadley. *Metal Foams: A Design Guide*. Woburn, MA: Butterworth Heinemann, 2000.

[204] Gibson, L.J., M.F. Ashby. *Cellular Solids: Structure and Properties*. Sydney: Pergamon Press, 1988.

[205] Campana, F., D. Pilone. *Effect of Wall Microstructure and Morphometric Parameters on the Crush Behaviour of Al Alloy Foams*. Materials Science and Engineering: A 2008;479:58.

[206] Peroni, L., M. Avalle, M. Peroni. *The Mechanical Behaviour of Aluminium Foam Structures in Different Loading Conditions*. International Journal of Impact Engineering 2008;35:644.

[207] Maurer, M., D. Koch, Z. Lidong, E. Lugscheider. *Metallographic Investigations of Composite Structures of Aluminum Foam with Thermally Sprayed Coatings*. Praktische Metallographie 2005;42:5.

[208] Adachi, T., Y. Osako, M. Tanaka, M. Hojo, S.J. Hollister. *Framework for Optimal Design of Porous Scaffold Microstructure by Computational Simulation of Bone Regeneration*. Biomaterials 2006;27:3964.

[209] Lin, C.-Y., C.-C. Hsiao, P.-Q. Chen, S.J. Hollister. *Interbody Fusion Cage Design Using Integrated Global Layout and Local Microstructure Topology Optimization*. SPINE 2004;29:1747.

[210] Wehmoller, M., P.H. Warnke, C. Zilian, H. Eufinger. *Implant Design and Production - a New Approach by Selective Laser Melting*. CARS 2005: Computer Assisted Radiology and Surgery 2005;1281:690.

[211] Heinl, P., A. Rottmair, C. Korner, R.F. Singer. *Cellular Titanium by Selective Electron Beam Melting*. Advanced Engineering Materials 2007;9:360.

[212] Meier, H., C. Haberland. *Experimental Studies on Selective Laser Melting of Metallic Parts*. Materialwissenschaft und Werkstofftechnik 2008;39:665.

[213] Curodeau, A., E. Sachs, S. Caldarise. *Design and Fabrication of Cast Orthopedic Implants with Freeform Surface Textures from 3-D Printed Ceramic Shell*. Journal of Biomedical Materials Research 2000;53:525.

[214] Melican, M.C., M.C. Zimmerman, M.S. Dhillon, A.R. Ponnambalam, A. Curodeau, J.R. Parsons. *Three-Dimensional Printing and Porous Metallic Surfaces: A New Orthopedic Application*. Journal of Biomedical Materials Research 2001;55:194.

[215] Lopez-Heredia, M.A., J. Sohier, C. Gaillard, S. Quillard, M. Dorget, P. Layrolle. *Rapid Prototyped Porous Titanium Coated with Calcium Phosphate as a Scaffold for Bone Tissue Engineering*. Biomaterials 2008;29:2608.

[216] Kruth, J.P., P. Mercelis, J. Van Vaerenbergh, L. Froyen, M. Rombouts. *Binding Mechanisms in Selective Laser Sintering and Selective Laser Melting*. Rapid Prototyping Journal 2005;11:26.

[217] Das, S. *Physical Aspects of Process Control in Selective Laser Sintering of Metals*. Advanced Engineering Materials 2003;5:701.

[218] Ryan, G., A. Pandit, D.P. Apatsidis. *Fabrication Methods of Porous Metals for Use in Orthopaedic Applications*. Biomaterials 2006;27:2651.

[219] Witte, F., H. Ulrich, C. Palm, E. Willbold. *Biodegradable Magnesium Scaffolds: Part 2: Peri-Implant Bone Remodeling*. Journal of Biomedical Materials Research Part A 2007;81A:757.

[220] Yamada, Y., C. Wen, K. Shimojima, H. Hosokawa, Y. Chino, M. Mabuchi. *Compressive Deformation Characteristics of Open-Cell Mg Alloys with Controlled Cell Structure*. Materials Transactions 2002;43:1298.

[221] Yamada, Y., K. Shimojima, Y. Sakaguchi, M. Mabuchi, M. Nakamura, T. Asahina, T. Mukai, H. Kanahashi, K. Higashi. *Processing of an Open-Cellular Az91 Magnesium Alloy with a Low Density of 0.05 G/Cm(3)*. Journal of Materials Science Letters 1999;18:1477.

[222] Brothers, A.H., D.C. Dunand. *Mechanical Properties of a Density-Graded Replicated Aluminum Foam*. Materials Science and Engineering a-Structural Materials Properties Microstructure and Processing 2008;489:439.

[223] Lin, C.Y., N. Kikuchi, S.J. Hollister. *A Novel Method for Biomaterial Scaffold Internal Architecture Design to Match Bone Elastic Properties with Desired Porosity*. Journal of Biomechanics 2004;37:623.

[224] Leong, K.F., C.K. Chua, N. Sudarmadji, W.Y. Yeong. *Engineering Functionally Graded Tissue Engineering Scaffolds*. Journal of the Mechanical Behavior of Biomedical Materials 2008;1:140.

[225] Hench, L.L. *Ceramics, Glasses, and Glass-Ceramics*. In: Lemons, J.E., editor. Biomaterials Science: An Introduction to Materials in Medicine, vol. 1. San Diego: Academic PRess, 1996. p.73.

[226] Thomsen, P., L.E. Ericson. *Inflammatory Cell Responce to Bone Implant Surfaces*. In: Davies, J.E., editor. The Bone Biomaterial Interface. Toronto: University of Toronto Press, 1991. p.153.

[227] Klinger, A., D. Steinberg, D. Kohavi, M.N. Sela. *Mechanism of Adsorption of Human Albumin to Titanium in Vitro*. Journal of Biomedical Materials Research 1997;36:387.

[228] Saltzman, W.M. *Tissue Engineering : Principles for the Design of Replacement Organs and Tissues*. New York: Oxford University Press, 2004.

[229] Anderson, J., A. Rodrigues, D. Chang. *Foreign Body Reaction to Biomaterials*. Seminars in Immunology 2008;20:86.

[230] Tarr, R.R., D.A. Wiss. *The Mechanics and Biology of Intramedullary Fracture Fixation*. Clinical Orthopaedics & Related Research 1986;212:10.

[231] Davies, J.E. *Early Extracellular Matric Synthesis by Bone Cells*. In: Davies, J.E., editor. The Bone-Biomaterial Interface. Toronto: University of Toronto Press, 1991. p.214.

[232] Davies, J.E. *Bone Bonding at Natural and Biomaterial Surfaces*. Biomaterials 2007;28:5058.

[233] Vrouwenvelder, W.C., C.G. Groot, G.K. de Groot. *Histological and Biochemical Evaluation of Osteoblasts Cultured on Bioactive Glass, Hydroxyapatite, Titanium Alloy, and Stainless Steel*. Journal of Biomedical Materials Research 1993;27:465.

[234] Santavirta, S., A. Ceponis, S.A. Solovieva, H. Hurri, J. Jin, M. Takagi, A. Suda, Y.T. Konttinen. *Periprosthetic Microvasculature in Loosening of Total Hip Replacement*. Archives of Orthopaedic Trauma Surgery 1996;115:286.

[235] Tang, L., T.P. Ugarova, E.F. Plow, J.W. Eaton. *Molecular Determinants of Acute Inflammatory Responces to Biomaterials*. Journal of Clinical Investigation 1996;97:1329.

[236] Shabalovskaya, S.A. *On the Nature of the Biocompatbility and on Medical Applications of Niti Shape Memory and Superelastic Alloys*. Biomedical Materials and Engineering 1996;6:267.

[237] Schmidt, D.R., H. Waldeck, W.J. Kao. *Protein Adsorption to Biomaterials*. In: Puleo, D.A., Bizios, R., editors. Biological Interactions on Materials Surfaces: Understanding and Controlling Protein, Cell, and Tissue Responce. New York: Springer, 2009. p.1.

[238] Latour, R.A. *Biomaterials: Protein-Surface Interactions*. In: Bowlin, G.L., editor. Encyclopedia of Biomaterails and Biomedical Engineering, vol. 1. London: Informa Healthcare, 2005. p.270.

[239] Dee, K.C., D.A. Puleo, R. Bizios. *Protein-Surface Interactions*. In: Dee, K.C., Puleo, D.A., Bizios, R., editors. An Introduction to Tissue-Biomaterial Interactions. Hoboken, Nj: John Wiley and Sons, 2002.

[240] Horbett, T.A. *The Role of Adsorbed Proteins in Tissue Responce to Biomaterials*. In: Ratner, B.D., Hoffman, A.S., Schoen, F.J., Lemons, J.E., editors. Biomaterials Science: An Introduction to Materials in Medicine. San Diego: Elsevier Academic Press, 2004. p.237.

[241] Nakanishi, K., T. Sakiyama, K. Imamura. *On the Adsorption of Proteins on Solid Surfaces, a Common but Very Complicated Phenomenon*. Journal of Bioscience and Bioengineering 2001;91:233.

[242] Bhaduri, A., K.P. Das. *Proteins at Solid Water Interface - a Review*. Journal of Dispersion Science and Technology 1999;20:1097.

[243] Heublein, B., R. Rohde, V. Kaese, M. Niemeyer, W. Hartung, A. Haverich. *Biocorrosion of Magnesium Alloys: A New Principle in Cardiovascular Implant Technology?* Heart 2003;89:651.

[244] Reifenrath, J., C. Palm, P. Muller, H. Hauser, H.A. Crostack, J. Nellesen, F.W. Bach, D. Besdo, M. Rudert, F. Witte. *Subchondral Plate Reconstruction by Fast Degrading Magnesium Scaffolds Influence Cartilage Repair in Osteochondral Defects*. In: Society, O.R., editor. 51st Annual Meeting of the Orthopaedic Research Society, vol. 30: Orthopaedic Research Society, 2005.

[245] Ren, Y., J. Huang, B. Zhang, K. Yang. *Preliminary Study of Biodegradation of Az31b Magnesium Alloy*. Frontiers of Material Science in China 2007;1:401.

[246] Thomopoulos, S., E. Zampiakis, R. Das, H.M. Kim, M.J. Silva, N. Havlioglu, R.H. Gelberman. *Use of a Magnesium-Based Bone Adhesive for Flexor Tendon-to-Bone Healing*. The Journal of Hand Surgery;34:1066.

[247] Von Der Höh, N., D. Bormann, A. Lucas, B. Denkena, C. Hackenbroich, A. Meyer-Lindenberg. *Influence of Different Surface Machining Treatments of Magnesium-Based Resorbable Implants on the Degradation Behavior in Rabbits*. Advanced Engineering Materials 2009;11:B47.

[248] Von Der Höh, N., A. Krause, C. Hackenbroich, D. Bormann, A. Lucas, A. Meyer-Lindenberg. *The Influence of Difference Surface Machining Treatments of Resorbable Implants of Different Magnesium Alloys - a Primary Study in Rabbits*. Biomaterialien 2006;7:122.

[249] Witte, F., I. Abeln, E. Switzer, V. Kaese, A. Meyer-Lindenberg, H. Windhagen. *Evaluation of the Skin Sensitizing Potential of Biodegradable Magnesium Alloys*. Journal of Biomedical Materials Research Part A 2008;86A:1041.

[250] Witte, F., J. Fischer, J. Nellesen, C. Vogt, J. Vogt, T. Donath, F. Beckmann. *In Vivo Corrosion and Corrosion Protection of Magnesium Alloy Lae442*. Acta Biomaterialia 2010;6:1792.

[251] Wong, H.M., K.W.K. Yeung, K.O. Lam, V. Tam, P.K. Chu, K.D.K. Luk, K.M.C. Cheung. *A Biodegradable Polymer-Based Coating to Control the Performance of Magnesium Alloy Orthopaedic Implants*. Biomaterials 2010;31:2084.

[252] Zartner, P., R. Cesnjevar, H. Singer, M. Weyand. *First Successful Implantation of a Biodegradable Metal Stent into the Left Pulmonary Artery of a Preterm Baby*. Catheterization and Cardiovascular Interventions 2005;66:590.

[253] ASTM International. Astm Standard G31-72, "Standard Practice for Laboratory Immersion Corrosion Testing of Metals". West Conshohocken, PA: ASTM International, 2004.

[254] Witte, F., F. Feyerabend, P. Maier, J. Fischer, M. Stormer, C. Blawert, W. Dietzel, N. Hort. *Biodegradable Magnesium-Hydroxyapatite Metal Matrix Composites*. Biomaterials 2007;28:2163.

[255] Wang, R.R., Y. Li. *In Vitro Evaluation of Biocompatibility of Experimental Titanium Alloys for Dental Restorations*. The Journal of Prosthetic Dentistry 1998;80:495.

[256] Prichard, R.W. *Animal Models in Human Medicine.* Animal Models of Thrombosis and Hemorrhagic Diseases, vol. 76-982. Washington DC: US Department of Health, Education, and Welfare, 1976. p.169.

[257] Bernard, C. *An Introduction to the Study of Experimental Medicine (English Translation)*. New York: Dover Publications, 1957.

[258] National Research Council. *Use of Laboratory Animals in Biomedical and Behavioral Research*. Washington DC: National Academy Press, 1988.

[259] Matfield, M. *Animal Experimentation: The Continuing Debate*. Nat Rev Drug Discov 2002;1:149.

[260] Auer, J., A. Goodship, S. Arnoczky, S. Pearce, J. Price, L. Claes, B. von Rechenberg, M. Hofmann-Amtenbrinck, E. Schneider, R. Muller-Terpitz, F. Thiele, K.-P. Rippe, D. Grainger. *Refining Animal Models in Fracture Research: Seeking Consensus in Optimising Both Animal Welfare and Scientific Validity for Appropriate Biomedical Use*. BMC Musculoskeletal Disorders 2007;8:72.

[261] Gill, T.J., P.C. McCulloch, S.S. Glasson, T. Blanchet, E.A. Morris. *Chondral Defect Repair after the Microfracture Procedure: A Nonhuman Primate Model*. American Journal of Sports Medicine 2005;33:680.

[262] Hassel, T., F.W. Bach, A.N. Golovko, A. Krause. *Investigation of the Mechanical Properties and the Corosion Behaviour of Low Alloyed Magnesium-Calcium-Alloys for Use as Absorbable Biomaterial in the Implant Technique*. In: Pekguleryuz, M., editor. Conference of Metallurgists : Magnesium Technology in the Global Age. Montreal, Quebec, Canada, 2006. p.359.

[263] Pardo, A., M.C. Merino, A.E. Coy, R. Arrabal, F. Viejo, E. Matykina. *Corrosion Behaviour of Magnesium/Aluminium Alloys in 3.5 wt.% Nacl*. Corrosion Science 2008;50:823.

[264] Shaw, B.A., R.C. Wolfe. *Corrosion of Magnesium and Magnesium-Base Alloys*. In: Cramer, S.D., Convino, B.S., editors. Asm Handbook, vol. 13B Corrosion: Materials. Metals Park: ASM International, 2005. p.205.

[265] Song, G., A. Atrens, D.H. St. John. *An Hydrogen Evolution Method for the Estimation of the Corrosion Rate of Magnesium Alloys*. In: Hyrn, J.N., editor. Magnesium Technology 2001 Symposium. New Orleans: Minerals, Metals & Materials Society, 2001. p.255.

[266] Xin, Y., C. Liu, X. Zhang, G. Tang, X. Tian, P.K. Chu. *Corrosion Behavior of Biomedical Az91 Magnesium Alloy in Simulated Body Fluids*. Journal of Materials Research 2007;22:2004.

[267] Ng, W.F., K.Y. Chiu, F.T. Cheng. *Effect of Ph on the in Vitro Corrosion Rate of Magnesium Degradable Implant Material*. Materials Science and Engineering: C 2010;30:898.

[268] Zhang, C.-Y., R.-C. Zeng, C.-L. Liu, J.-C. Gao. *Comparison of Calcium Phosphate Coatings on Mg-Al and Mg-Ca Alloys and Their Corrosion Behavior in Hank's Solution*. Surface and Coatings Technology;In Press, Accepted Manuscript.

[269] Liu, C., Y. Xin, G. Tang, P.K. Chu. *Influence of Heat Treatment on Degradation Behavior of Bio-Degradable Die-Cast Az63 Magnesium Alloy in Simulated Body Fluid*. Materials Science and Engineering: A 2007;456:350.

[270] Song, G., S. Song. *A Possible Biodegradable Magnesium Implant Material*. Advanced Engineering Materials 2007;9:298.

[271] Uhlig, H.H. *Corrosion and Corrosion Control*. New York: John Wiley & Sons Inc., 1963.

[272] Hanks, J.H. *The Longevity of Chick Tissue Cultures without Renewal of Medium*. Journal of Cellular Physiology 1948;31:235.

[273] Hanks, J.H., R.E. Wallace. *Relation of Oxygen and Temperature in the Preservation of Tissues by Refridgeration*. Proceedings of the Society for Experimental Biology and Medicine 1949;71:196.

[274] Earle, W.R. *A Technique for Adjustment of Oxygen and Carbon Dioxide Tensions, and Hydrogen Ion Conenctration, in Tissue Cultures Planted in Carrel Flasks*. Archiv fur Experimentelle Zellforschung, Besonders Gewebzuechtung. Jena. 1934;16:116.

[275] Dulbecco, R., M. Vogt. *Plaque Formation and Isolation of Pure Lines with Poliomyelitis Viruses*. The Journal of Experimental Medicine 1954;99:167.

[276] Hanks, J.H. *Hanks' Balanced Salt Solution and Ph Control*. Methods in Cell Science 1975;1:3.

[277] Yfantis, C.D., D.K. Yfantis, J. Anastassopoulou, T. Theophanides, M.P. Staiger. *New Magnesium Alloys for Bone Tissue Engineering: In Vitro Corrosion Testing*. WSEAS transactions on Environment and Development 2006;2:1110.

[278] Cui, F.Z., J.X. Yang, Y.P. Jiao, Q.S. Yin, Y. Zhang. *Calcium Phosphate Coating on Magnesium Alloy for Modification of Degradation Behavior* Frontiers of Material Science in China 2008;2:143.

[279] Hassel, T., F.W. Bach, C. Krause. *Influence of the Alloy Composition on the Mechanical and Electrochemical Properties of Binary Mg-Ca Alloys and Its Corrosion Behaviour in Solutions at Different Chloride Concentrations*. In: Kainer, K.U., editor. Magnesium : Proceedings of the 7th International Conference on Magnesium Alloys and Their Applications: Wiley-VCH, 2007. p.789.

[280] Yamamoto, A., S. Hiromoto. *Effect of Inorganic Salts, Amino Acids and Proteins on the Degradation of Pure Magnesium in Vitro*. Materials Science and Engineering: C 2009;29:1559.

[281] Kokubo, T. *Bioactive Glass Ceramics: Properties and Applications*. Biomaterials 1991;12:155.

[282] Kokubo, T., H. Takadama. *How Useful Is Sbf in Predicting in Vivo Bone Bioactivity?* Biomaterials 2006;27:2907.

[283] Cheng, X., S.G. Roscoe. *Corrosion Behavior of Titanium in the Presence of Calcium Phosphate and Serum Proteins*. Biomaterials 2005;26:7350.

[284] Contu, F., B. Elsener, H. Böhni. *Characterization of Implant Materials in Fetal Bovine Serum and Sodium Sulfate by Electrochemical Impedance Spectroscopy. Ii. Coarsely Sandblasted Samples*. Journal of Biomedical Materials Research Part A 2003;67A:246.

[285] Gu, X.N., Y.F. Zheng, L.J. Chen. *Influence of Artificial Biological Fluid Composition on the Biocorrosion of Potential Orthopedic Mg-Ca, Az31, Az91 Alloys*. Biomedical Materials 2009;4:8.

[286] Liu, C., Y. Xin, X. Tian, P.K. Chu. *Degradation Susceptibility of Surgical Magnesium Alloy in Artificial Biological Fluid Containing Albumin*. Journal of Materials Research 2007;22:1806.

[287] Malda, J., T.B.F. Woodfield, M. Radisic, S. Levenberg, C. Oomens, F.P. Baaijens, P. Svalander, G. Vunjak-Novakovic. *Cell Nutrition : In Vitro and in Vivo*. Tissue Engineering : A Textbook 2008:327.

[288] Ashassi-Sorkhabi, H., M.R. Majidi, K. Seyyedi. *Investigation of Inhibition Effect of Some Amino Acids against Steel Corrosion in Hcl Solution*. Applied Surface Science 2004;225:176.

[289] Ashassi-Sorkhabi, H., Z. Ghasemi, D. Seifzadeh. *The Inhibition Effect of Some Amino Acids Towards the Corrosion of Aluminum in 1 m Hcl + 1 m H2so4 Solution*. Applied Surface Science 2005;249:408.

[290] William, D.F., R.L. William. *Degradative Effects of the Biological Environment on Metals and Ceramics*. In: Ratner, B.D., Hoffman, A.S., Schoen, F.J., Lemons, J.E., editors. Biomaterials Science: An Introduction to Materials in Medicine. San Diego: Elsevier Academic Press, 2004. p.430.

[291] Bruneel, N., J.A. Helsen. *In Vitro Simulation of Biocompatibility of Ti-Al-V*. Journal of Biomedical Materials Research 1988;22:203.

[292] El-Shafei, A.A., M.N.H. Moussa, A.A. El-Far. *Inhibitory Effect of Amino Acids on Al Pitting Corrosion in 0.1m Nacl*. Journal of Applied Electrochemistry 1997;27:1075.

[293] Mueller, W.D., M. Lucia Nascimento, M.F. Lorenzo de Mele. *Critical Discussion of the Results from Different Corrosion Studies of Mg and Mg Alloys for Biomaterial Applications*. Acta Biomaterialia 2010;6:1749.

[294] Yun, Y., Z. Dong, D. Yang, M.J. Schulz, V.N. Shanov, S. Yarmolenko, Z. Xu, P. Kumta, C. Sfeir. *Biodegradable Mg Corrosion and Osteoblast Cell Culture Studies*. Materials Science and Engineering: C 2009;29:1814.

[295] Miller, R., V.B. Fainerman, M.E. Leser, M. Michel. *Kinetics of Adsorption of Proteins and Surfactants*. Current Opinion in Colloid & Interface Science 2004;9:350.

[296] Pietak, A.M., T. Mahoney, G. Dias, M.P. Staiger. *Bone-Like Matrix Formation on Magnesium and Magnesium Alloys*. Journal of Biomedical Materials Research 2007;19:407.

[297] Mueller, W.D., M.F.L. de Mele, M.L. Nascimento, M. Zeddies. *Degradation of Magnesium and Its Alloys: Dependence on the Composition of the Synthetic Biological Media*. Journal of Biomedical Materials Research Part A 2009;90A:487.

[298] Rettig, R., S. Virtanen. *Time-Dependent Electrochemical Characterization of the Corrosion of a Magnesium Rare-Earth Alloy in Simulated Body Fluids*. Journal of Biomedical Materials Research Part A 2008;85A:167.

[299] Rettig, R., S. Virtanen. *Composition of Corrosion Layers on a Magnesium Rare-Earth Alloy in Simulated Body Fluids*. Journal of Biomedical Materials Research - Part A 2009;88:359.

[300] Oyane, A., H.-M. Kim, T. Furuya, T. Kokubo, T. Miyazaki, T. Nakamura. *Preparation and Assessment of Revised Simulated Body Fluids*. Journal of Biomedical Materials Research Part A 2003;65A:188.

[301] Willmer, E.N. *Cells and Tissues in Culture: Methods, Biology, and Physiology*. London: Academic Press, 1965.

[302] Equitech-Bio Inc. *Sterile Filtered Fetal Bovine Serum, Us Origin*. vol. 2010: Equitech-Bio Inc,, 2010.

[303] Lentner, C. *Geigy Scientific Tables*. Basle: Ciba-Geigy, 1981.

[304] Helgason, C.D., C.L. Miller. *Basic Cell Culture Protocols*. Totowa, NJ: Humana Press, 2005.

[305] Gerasimov, V.V., I.L. Rozenfeld. *Effect of Temperature on the Rate of Corrosion of Metals* Russian Chemical Bulletin 1957;6.

[306] Kaesche, H. *Corrosion of Metals - Physiochemical Principles and Current Problems*. Berlin: Springer-Verlag, 2003.

[307] Burstein, G.T., C. Liu, R.M. Souto. *The Effect of Temperature on the Nucleation of Corrosion Pits on Titanium in Ringer's Physiological Solution.* Biomaterials 2005;26:245.

[308] Omanovic, S., S.G. Roscoe. *Electrochemical Studies of the Adsorption Behavior of Bovine Serum Albumin on Stainless Steel*. Langmuir 1999;15:8315.

[309] Ghali, E., W. Dietzel, K.-U. Kainer. *Testing of General and Localized Corrosion of Magnesium Alloys: A Critical Review*. Journal of Materials Engineering and Performance 2004;13:517.

[310] Zeng, R.C., J. Chen, W. Dietzel, N. Hort, K.U. Kainer. *Electrochemical Behavior of Magnesium Alloys in Simulated Body Fluids*. Transactions of Nonferrous Metals Society of China 2007;17:S166.

[311] Lunder, O., J.E. Lein, S.M. Hesjevik, T.K. Aune, K. Ni, scedil, ancio, gcaron, lu. *Corrosion Morphologies on Magnesium Alloy Az 91*. Materials and Corrosion/Werkstoffe und Korrosion 1994;45:331.

[312] Yin, G., Z. Liu, J. Zhan, F. Ding, N. Yuan. *Impacts of the Surface Charge Property on Protein Adsorption on Hydroxyapatite*. Chemical Engineering Journal 2002;87:181.

[313] Jackson, D.R., S. Omanovic, S.G. Roscoe. *Electrochemical Studies of the Adsorption Behavior of Serum Proteins on Titanium.* Langmuir 2000;16:5449.

[314] Rouhana, R., S.M. Budge, S.M. MacDonald, S.G. Roscoe. *Erratum: Electrochemical Studies of the Interfacial Behaviour of α-Lactalbumin and Bovine Serum Albumin*. Food Research International 1997;30:303.

[315] Waters, J.H., L.R. Miller, S. Clack, J.V. Kim. *Cause of Metabolic Acidosis in Prolonged Surgery*. Critical Care Medicine 1999;27:2142.

[316] Chakkalakal, D.A., A.A. Mashoof, J. Novak, B.S. Strates, M.H. McGuire. *Mineralization and Ph Relationships in Healing Skeletal Defects Grafted with Demineralized Bone Matrix*. Journal of Biomedical Materials Research 1994;28:1439.

[317] Sigma-Aldrich. *Fundamental Techniques in Cell Culture : A Laboratory Handbook*. vol. 2010: Sigma-Aldrich, 2010.

[318] Good, N.E., G.D. Winget, W. Winter, T.N. Connolly, S. Izawa, M.M. Singh. *Hydrogen Ion Buffers for Biological Research*. Biochemistry 1966;5:467.

[319] Masters, J.R.W., editor *Animal Cell Cultures*. Oxford: Oxfird University Press, 2000.

[320] Eley, J.H. *The Use of Hepes as a Buffer for the Growth of the Cyanobacterium Anacystis Nidulans*. Applied Microbiology and Biotechnology 1988;28:297.

CHAPTER 3: Research Aims

This chapter outlines the objectives of the project as a whole.

3.1. Purpose of investigation

The literature review provided in Chapter 2 highlights significant gaps in the current understanding of *in vitro* techniques utilised for Mg biomaterial investigations. Several studies have drawn potentially erroneous conclusions in reference to the behaviour of Mg based on findings derived from the use of inappropriate testing protocols. The majority of studies also appear to have overlooked key experimental parameters that affect corrosion. To date, although a number of alloys have been investigated, no significant study has been done to elucidate the role of phase microstructure on the biocorrosion mechanisms of Mg alloys. Furthermore, no investigations appear to have been dedicated to the development of a protocol for the production of ordered Mg structures. This is a necessary step in the eventual implementation of a wide range of implant types.

Consequently, it is the aim of this dissertation to:

- Demonstrate the potential pitfalls that are encountered when using different *in vitro* tests in Mg alloy corrosion investigations. Each experimental technique is explained in light of its role in elucidating the corrosion properties of Mg, whilst limitations are highlighted and discussed.

- Examine the role that different experimental variables play in the biocorrosion of a wide range of Mg alloys. A number of *in vitro* techniques are utilised to fully explore and understand these effects on both overall corrosion and electrochemical behaviour.

- Clarify the contribution and thus the role that alloy microstructure plays in corrosion mechanisms for some of the most common biocompatible Mg alloy systems.

- Investigate a novel production method for creating ordered Mg structures, whilst assessing the effects of different processing parameters on the corrosion rates and mechanical performance of the end structure.

3.2. Hypotheses

The following hypotheses have been made about the present work. The merit of each hypothesis will be assessed throughout the remaining chapters.

i. The choice of *in vitro* method is crucial to appropriately assess Mg alloy biocorrosion performance. A combination of the current techniques will always be needed to fully understand both the corrosion rates and mechanistic behaviour of the degradation processes. Each technique will have unique limitations and considerations that must be taken into account if it is to be properly utilised.

ii. All of the variables common to *in vitro* experiments have a considerable effect on Mg alloy corrosion. Even relatively minor changes, such as the difference between room and physiological temperatures, play a role in corrosion rate and in some cases the morphologies of corrosion layers that form in simulated body fluids. Idealised values may be possible for certain variables, while others will require choice depending on what is being investigated.

iii. Microelectrochemical techniques, in combination with normal electrochemical methods, can be used to elucidate the mechanisms that control the corrosion for the alloying systems investigated *in vitro*. Analysis of the electrochemical behaviour of the microstructure (*e.g.* phases) will allow control over degradation rates based on a better understanding of the corrosion reactions taking place.

iv. The novel method for production of Mg foams will provide a variety of surface topologies depending on the processing parameters investigated. The mechanical performance will be superior to random foams; however corrosion rates will likely be higher than with normal as-cast surfaces due to increased surface area.

CHAPTER 4: Experimental Methods

4.1. Materials and media

4.1.1. Mg alloys investigated

Unless otherwise stated, “pure Mg” refers to a high-purity form (99.99%) that was obtained specifically for this study (Timmenco Ltd., Toronto, Canada). The chemical composition of all Mg alloys was tested independently *via* inductively coupled plasma atomic emission spectroscopy mass spectroscopy (ICP-AES, Spectrometer Services, Coburg, VIC, Australia). The results of these tests can be found in Appendix D.

Alloys that were procured include Mg-28Ca, AZ31, AZ91 (Timmenco Ltd., Toronto, Canada), and Mg-33.3Zr (Zirmax®, Magnesium-Elektron, Manchester, UK). All other alloys were produced in-house using facilities at the University of Canterbury. Alloying elements and compounds that were employed included high purity zinc (99.99%) and manganese chloride (99.999%). Manganese chloride ($MnCl_2$) was chosen for alloy production of Mg-Mn alloys, due to the high melting temperature of pure Mn (1244 °C) that lies above the boiling/vapour point of Mg. Mg alloys were produced with an iron (Fe) level of less than 40 ppm to ensure that corrosion rates were not influenced by the presence of this impurity element [1].

4.1.2. Alloy preparation

All Mg alloys used in this work were created using the same equipment and casting process. Castings were prepared to have a final weight of 250 g. The bulk Mg and alloying elements were placed in a mild steel crucible of 60 mm diameter and 140 mm height. The crucible was kept dry in an oven at 120 °C to minimize moisture build-up. Any material that came into contact with the molten alloy, including the crucible, stirrer, thermocouple protector and mould, were coated with an alcohol-based graphite spray to minimise impurity pickup.

After pre-drying of the crucible and feedstock materials, a steel tube thermocouple-protector was placed inside the crucible. This prevented thermal damage to the k-type thermocouple from the molten alloy, yielding a more accurate reading of the melt temperature. The crucible

was then placed into the appropriate holder in the furnace chamber (Figure 4-1). Melting was performed in a purpose-built 10 kW induction furnace (Induktio GmBH, Ljubljana, Slovenia).

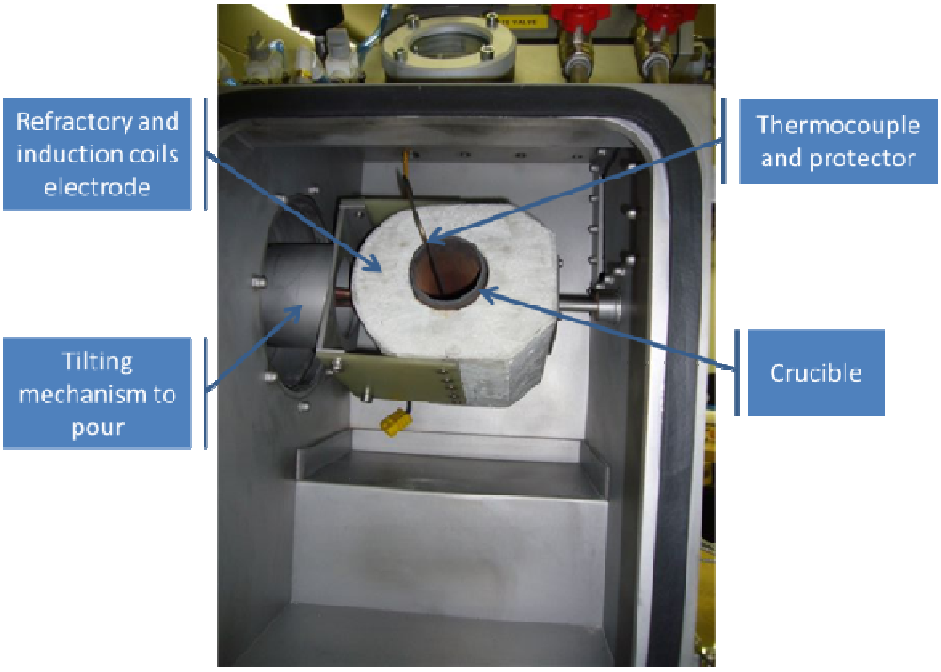

Figure 4-1 : Photograph of crucible inside the induction furnace.

The furnace chamber was evacuated to approximately 0.01 bar then filled with 0-Grade argon to create an inert environment and prevent the ignition of molten Mg that occurs in atmospheric conditions. The alloy was ramp-heated at approximately 3-5 °C/s to 350 °C, 500 °C, and then was held for 15-20 min at 700 °C whilst stirring vigorously. The furnace power was then shut down, while water continued to flow through the induction coils, helping to cool down the refractory surrounding the crucible. The castings cooled at an average rate of ~1 °C/s down to room temperature.

In the latter stages of the work, some alloys were prepared using a heated mould setup. The furnace was modified to accommodate the use of ten cartridge heaters and a thermocouple. In this case, the alloy was poured into a rectangular mould that had been preheated to 400 °C. Due to an enlarged surface area the measured cooling rate of the mould was ~1 °C/s without water flow. Figure 4-2 shows some of the parts of the heated mould and approximate dimensions.

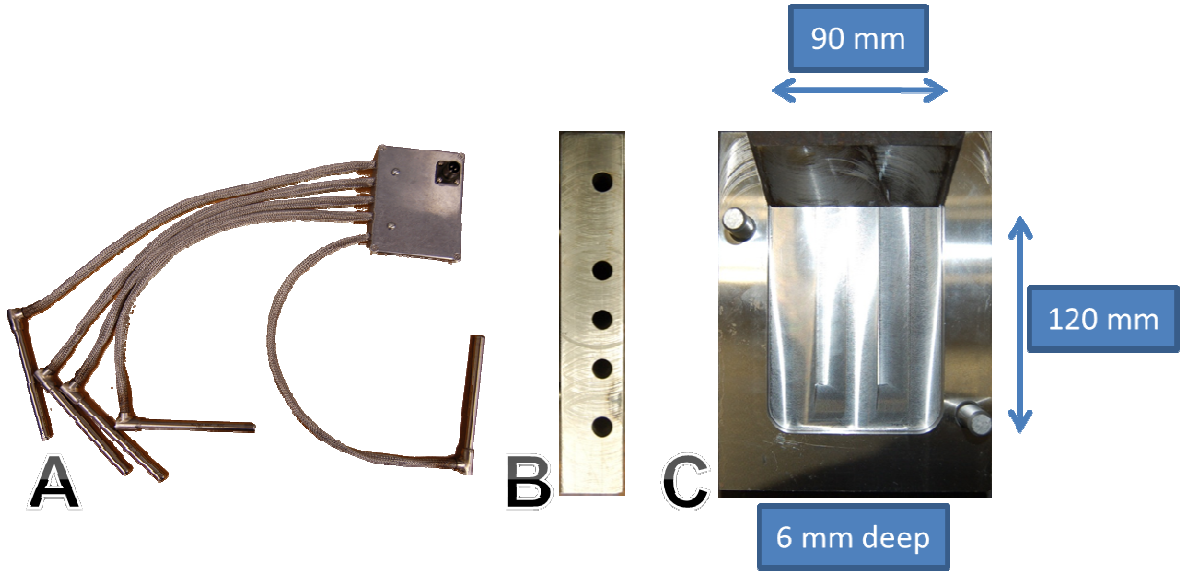

Figure 4-2 : (A) One of two cartridge heater units, (B) side view of mould with holes for cartridges, (C) male-half of heated mould with dimensions.

Unless stated otherwise, no alloy had any heat treatment or work performed on it after casting. As a result, alloys were tested in the 'as cast' state. Although further work could be beneficial in a number of ways, including decreasing the grain size and improving hardness, part of the overall focus of this work was to produce alloys that could be used with the ordered structure method discussed in Chapter 8. It would not be possible to work or heat-treat these structures, and so these methods were not investigated in this work.

4.1.3. Electrolytes and testing media

A range of corrosion media were employed including:

i. 8 g/L NaCl,
ii. Phosphate buffered saline (PBS),
iii. Hank's balanced salt solution (HBSS),
iv. Earle's balanced salt solution (EBSS),
v. Minimum essential medium (MEM),
vi. MEM containing 10 vol.% foetal bovine serum (MEM+FBS),
vii. MEM containing 20, 40, and 60 g/L bovine serum albumin (MEM+BSA) and
viii. PBS containing 50% human plasma (PBS+HP).

All solutions were prepared as instructed by the manufacturer. Normally this involved dissolving a powder form of the electrolyte in distilled water, adding a buffer or other component, and stirring at room temperature until completely dispersed. A list of the solutions used throughout this work and their constituents are reported in Table 4-1.

All solutions were buffered with 5.96 g/L of *2-(4-(2-hydroxyethyl)-1-piperazinyl) ethanesulfonic acid* (HEPES, H3375, Sigma Aldrich Co., Auckland, New Zealand) unless otherwise stated. HEPES is commonly employed to buffer cell culture media in air and is widely used in *in vitro* Mg experiments [2]. Additionally, long term experiments (> 3 days) and tests involving cell culture media were all filtered and stored according to the manufacturers' recommendation. This involved vacuum-assisted filtering using a 0.22 µm filter (Millipore Express PLUS Stericup®, Millipore Inc., Billerica, MA, USA). The pH was adjusted prior to testing to ensure the desired value (7.4) was achieved after sterilisation. During all testing, the pH was regulated to the desired value by adding controlled amounts of 1 M NaOH or 1 M HCl solutions. All filtering and sterilisation was performed in a Clemco CF631 HEPA-filtered laminar flow hood (Clemco Ultraviolet, Artarmon, NSW, Australia).

Due to limitations in facilities and the original scope of this thesis, *in vitro* toxicity tests were not performed as part of this work. However, the majority of the tested alloys have been tested for cytotoxicity concurrently by a member of the group at the University of Otago. Any relevant information has been stated.

Table 4-1 : Element and compound concentrations found in media used in this study.

Component	**Human Plasma (HP)**	**8 g/L NaCl (NaCl)**	**Phosphate Buffered Saline (PBS)[a]**	**Hank's Balanced Salt Solution (HBSS)[b]**	**Earle's Balanced Salt Solution (EBSS)[c]**	**Minimum Essential Medium (MEM)[d]**	**MEM + 10% Foetal Bovine Serum[e] (MEM+FBS)**	**MEM + Bovine Serum Albumin[f] (MEM+BSA)**	**PBS + 50% HP**
Na^+	142	136.86	154	145	151	117.4	119.66	117.4	148
Cl^-	103	136.86	140.6	144.6	135	123.5	121.15	123.5	121.8
K^+	5.0	-	2.7	5.8	5.4	5.4	5.36	5.4	3.85
Ca^{2+}	2.5	-	-	1.3	1.5	1.8	1.87	1.8	1.25
Mg^{2+}	1.5	-	-	0.4	0.4	0.4	0.46	0.4	0.75
HPO_4^{2-}	1.0	-	8.06	0.8	0.897	1	0.98	1	4.53
SO_4^{2-}	0.5	-	-	0.4	0.41	0.4	0.41	0.4	0.25
D-Glucose	5	-	-	5.5	5.5	5.5	5.45	5.5	2.5
Bicarbonate (HCO_3^-)	22-30	-	-	± 26.2	± 26.2	± 26.2	± 26.2	± 26.2	11-15
HEPES	-	± 25	± 25	± 25	± 25	± 25	± 25	± 25	25
Phenol Red	-	-	-	0.03	0.03	0.03	0.03	0.03	-
Albumin (g/L)	34-54	-	-	-	-	-	4-6	40	17-27

All concentrations in mmol/L unless otherwise stated.
Concentrations of inorganic blood contents given as in [3].
N/A = information not available
[a] (P5368, Sigma-Aldrich), [b] (H1641, Sigma-Aldrich), [c] (E7510, Sigma-Aldrich), [d] (56414C, Sigma-Aldrich), [e] (F2442, Sigma-Aldrich), [f] (MP Biomedical NZ Ltd)

4.2. Immersion tests

4.2.1. Mass loss

Mass loss experiments were performed either in a normal or a CO_2 atmosphere. The former were carried out in a water bath setup that utilised a Techne Tempette® TE-10D thermoregulator (Bibby Scientific Ltd., Stone, UK) in a double-hulled plastic container with a temperature variance of ± 1 °C. Experiments using this setup were carried out at both a room temperature of 20 °C (T_{rm}) and physiological temperature of 37 °C (T_{phy}). When sodium bicarbonate was used for buffering, experiments were carried out in a CO_2 incubator (Belco Glass, Vineland, NJ, USA) at T_{phy} with a temperature variance of 0.5 °C. This is standard practice for cell cultures using this buffer to maintain a physiological pH [4].

The mass of each sample was measured using a XP105 Analytical Balance (Mettler-Toledo Inc., Columbus, OH, USA) with an accuracy of 0.001 g. After removal from the solution, the corrosion products were dissolved by immersing the sample in a 2 M chromic acid solution (200 g/L CrO_3, 10g/L $AgNO_3$) for 10 min at 40 °C. This removal technique is commonly employed in magnesium corrosion studies [5].

4.2.2. Hydrogen evolution

Hydrogen evolution experiments were performed at both T_{rm} and T_{phy} using the water bath as described above (Figure 4-3). Holes in the lid of the box allowed 500 mL beakers to be placed so that the test solution was kept at temperature but did not come into contact with the heating water. A funnel (Ø 40 mm) was inserted into the open end of a 50 mL burette using Parafilm tape (Pechiney, Chicago, IL, USA) to create a tight fit. This was then inverted and placed directly above the sample so the lip of the funnel was 10 mm above the top surface. Each sample was placed in the centre of its beaker. This design allowed the entire solution to be mixed by hand stirring at each recording point, allowing more realistic measurement of pH and temperature. Measurements were typically taken every 30 min with an accuracy of ± 0.1 mL.

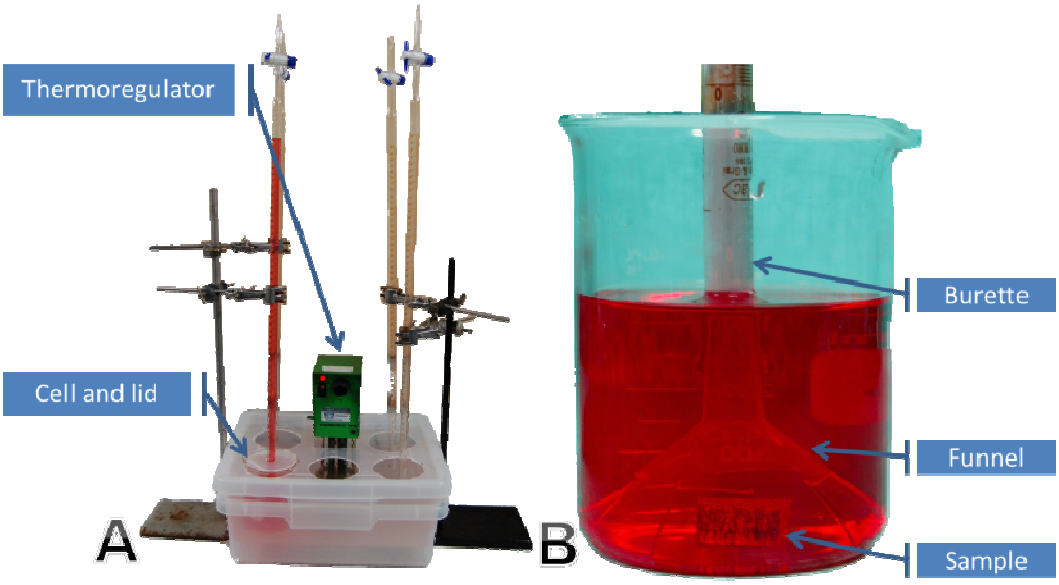

Figure 4-3 : Photographs of (A) the hydrogen evolution test rig and (B) beaker with sample, funnel and burette.

4.3. Electrochemical tests

Unless otherwise stated, all electrochemical tests were performed using a three electrode flat-cell (K0235, Princeton Applied Research, Oak Ridge, TN, USA) (Figure 4-4). The cell contained 300 mL of medium and had an exposed working electrode area of 1 cm^2. A separate glass well, immersed in the cell, contained the saturated calomel (SCE) reference electrode that is directed to the surface of the working electrode using a Luggin capillary tube. The counter electrode was platinum wire mesh. Elevated temperature experiments at T_{phy} ± 0.5 °C were carried out using heated water that was made to flow at 1 m/s through a clear silicone tube (ø 10 mm) wrapped around the cell. The temperature of the water was adjusted so it was constant at the desired level inside the cell when filled with solution.

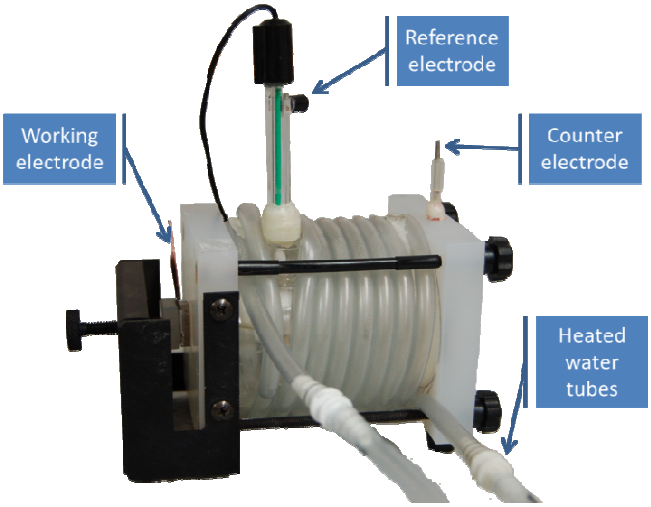

Figure 4-4 : Photograph of flat test cell with different parts labelled.

Electrochemical experiments were performed on either a BioLogic® SP-150 or a BioLogic® VMP-3Z potentiostat/galvanostat using EC-Lab 10.02 software (BioLogic Inc., Knoxville, TN, USA). The working voltage range for all tests was -3 V to 0 V to cover the full range of potentials encountered while maximising the resolution of the tests (50 µV). Electrochemical experiments were executed in a purpose-built faraday cage to minimise electrical noise.

4.3.1. pH monitoring

The evolution of the pH was recorded using a SevenEasy® S20 pH/Temperature meter and LabX pH meter software (Mettler-Toledo Inc., Columbus, OH, USA) (Figure 4-5). The measurement of pH and temperature was recorded at a frequency of 1 Hz. The recording of the pH near the sample was performed 3 mm above the surface using an adjustable stand/arm and a Mettler-Toledo InLab® Surface flat pH probe.

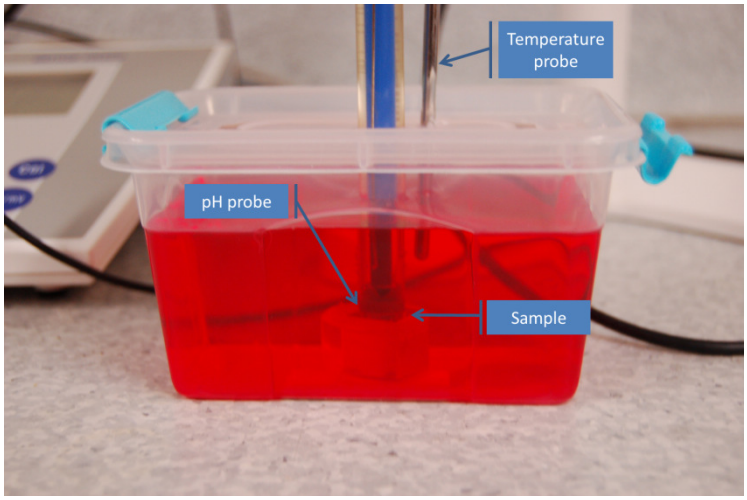

Figure 4-5 : Photograph of pH meter testing sample surface.

4.3.2. Open circuit potential recording

Open circuit potential (OCP) was recorded between the working electrode and the reference electrode without any current being passed through the counter electrode. The measurement shows the potential at which the anodic and cathodic reaction currents, occurring at the interface of the working electrode and solution, are balanced.

4.3.3. Potentiodynamic polarisation

Background theory

Potentiodynamic polarisation (PDP) tests rely on an applied overpotential to accelerate the rate of reaction at the working electrode (sample) surface. The applied potential and ensuing current are recorded as the test proceeds. Such tests allow one to yield a plot of the potential versus current density, providing information regarding the electrochemical behaviour of a metal in given electrolyte [6]. A typical representation of such data is the E-log(i) plot, also known as the Evans diagram.

Electrode reaction rates on the E-log(i) plot may be divided into oxidation (anodic) and reduction (cathodic) reactions, depending on the polarity of the polarising signal. At sufficiently large polarisation potentials in either direction from the open circuit potential (OCP), only one reaction will occur. If the slopes of each reaction can be obtained from the

recorded data, the slope of the linear regions approaching E_{corr} may be analysed by Tafel-type analysis.

An idealised schematic of a polarisation curve may be seen in Figure 4-6. The dotted lines represent actual data, and the solid blue lines are linear approximations which may be used to make a Tafel-type fit and estimate the corrosion current density (i_{corr}).

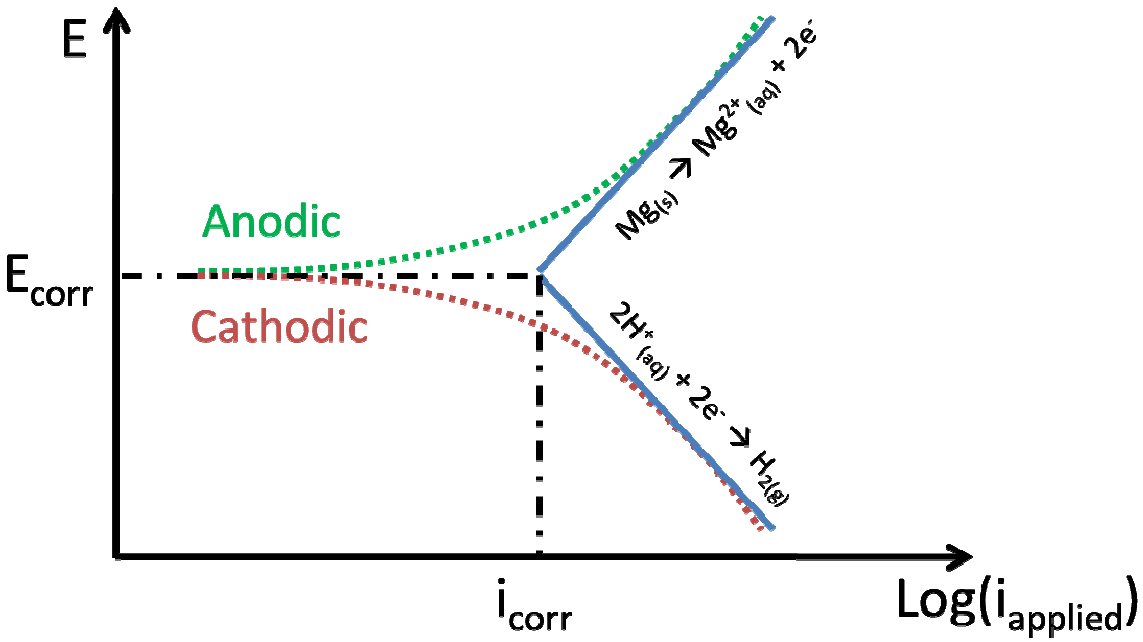

Figure 4-6 : Example of polarisation curve with a Tafel-type fit.

The i_{corr} value is the rate at which the electrode reactions are occurring, and this may be related to the corrosion rate expressed as a penetration *via* Equation 4-1 (from ASTM G102 [7]).

$$CR = K_1 \frac{i_{corr} W}{\eta \rho}$$

Equation 4-1

where CR is the corrosion rate, K_1 is a constant that defines the units for the corrosion rate (for mm/year : 3.27 x 10^{-3} mm g/µA cm year), i_{corr} is the corrosion current density (µA/cm^2), W is the atomic weight (Mg: 24.312), η is the number of electrons in the valence shell (equivalents) (Mg : 2), and ρ is the density (Mg: 1.74 g/cm^3).

It is important to note that the determination of CR assumes general (uniform) corrosion takes place. Typically Mg alloys corrode primarily through localised forms of attack and thus this must be considered when making estimates of life prediction.

Experimental design

In this work the software EC-Lab was used to perform Tafel-type analysis. This software is very powerful, allowing fits to individual anodic or cathodic data as well as entire curve portions, while also providing a predicted fitted slope. This also allowed reproducible and comparable results for all PDP experiments carried out regardless of which alloy or solution is used, or which user performed them.

PDP tests were performed after the OCP had been allowed to stabilise. Normally, stabilisation of the OCP required 15 min, which is similar to what was found in other studies [8, 9]. Running the test immediately after a sample is exposed to the solution may yield erroneous values (***i.e.*** higher currents measured) as the surface has not had time to stabilise in the new environment and establish a uniform double layer. However, it is equally important that the exposure time in the medium is minimised prior to the PDP test as excessive corrosion may alter the surface area of the sample. After extensive trial and error, a settling time of 15 min was deemed to be suitable for the magnesium alloys tested. During this time recordings were logged at 2 Hz.

Potentiodynamic scans were performed at a rate of 1 mV/s. Each test was carried out from -150 mV below the OCP to 500 mV above. It is necessary to start the scan on the cathodic (negative) side of the OCP as the forced corrosion during the anodic part could cause significant corrosion, altering values obtained later in the scan. The maximum current was limited to 2 mA. Values were recorded at 2 Hz for the entire test.

A minimum of 5 separate scans were performed for each data point to ensure reproducibility. Unless otherwise stated, Tafel-type analysis was performed at points ± 50 mV outside of the corrosion potential, which is based on best practice [6].

4.3.4. Microelectrochemical experiments

Microelectrochemical tests were carried out on certain alloys to evaluate the electrochemical response of the intermetallic phase present in isolation. The technique used was the micro-electrochemical cell method, as outlined previously in [10-12] and reviewed in [13]. In this method, the working electrode area is defined by the area of metal that comes into contact with the opening of a micro-capillary. The micro-capillary is filled with electrolyte (pre-heated for 37 °C experiments) whilst containing a small platinum-wire counter electrode (Ø 2 mm) and a saturated calomel reference electrode. A silicone seal was applied to the open end of the capillary in order to avoid any solution leakage and to allow an interference contact with the working electrode. The capillary opening is generally in the vicinity of 10-100 µm in diameter and will vary with each capillary - such a size being sufficient to individually isolate the majority of intermetallic particles in the alloys produced. The microcell used in these studies was incorporated into a lens-piece of an optical microscope in the arrangement illustrated in Figure 4-7.

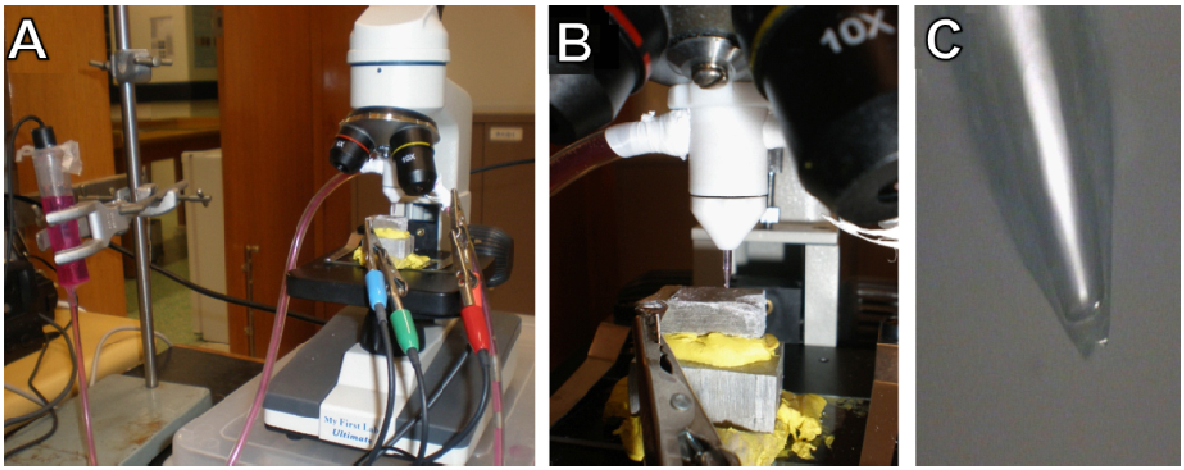

Figure 4-7 : Photographs of the microelectrochemical apparatus showing: (A) the entire setup, (B) microelectrode during testing and (C) a close-up of the micro-capillary.

All experiments were carried out using a VMP-3Z potentiostat and EC-Lab software (Bio-Logic). PDP was performed with an increased scan rate of 10 mV/s due to the decrease in surface area. All potentials quoted are in reference to the SCE. A minimum of 5 separate scans were performed for each reported measurement to ensure accuracy and reproducibility of the results.

4.3.5. Electrochemical impedance spectroscopy

Background theory

A phenomenon known as the electrical double layer (EDL) will develop at the surface of a corroding metal when it is placed in a solution (Figure 4-8). This phenomenon occurs as metal ions leave their lattice, which leaves electrons behind in the metal. Water molecules will surround (hydrate) the ions as they leave the lattice and allow them to diffuse away from the metal. The negative charge, caused by excess electrons on the metal surface, attracts positively charged metal ions and a number of them remain near the surface instead of completely diffusing in the bulk electrolyte. The water layer surrounding the ions prevents most from making direct contact with the surface electrons (and subsequently being reduced to metal atoms). In addition, other positive ions in the electrolyte may be attracted to the electronegative surface. Consequently, the layer of electrolyte directly adjacent to the electrode surface contains ions from the metal, electrolyte, and water molecules, and has a different chemical composition to the bulk electrolyte. The combination of the negatively charged surface and adjacent electrolyte layers are collectively referred to as the EDL.

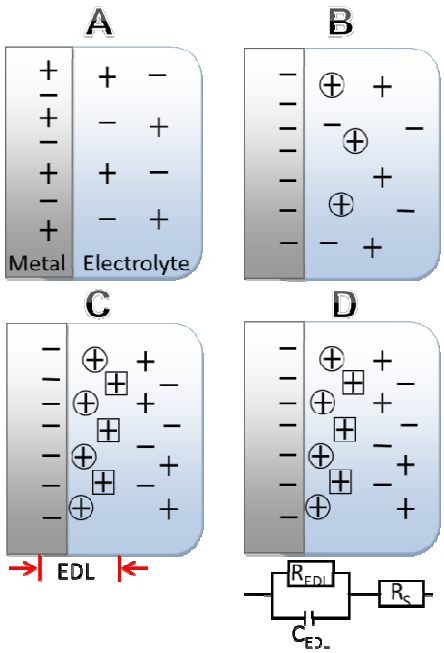

Figure 4-8 : Formation of the electrical double layer: (A) Non-corroded metal in equilibrium in electrolyte solution, (B) Metal ions are released as part of the corrosion process and are hydrated ⊕, (C) Hydrated metal ions, along with other ions in the electrolyte ⊞ are attracted to the metal surface but cannot re-enter the lattice. This creates the EDL (D), which may be represented by a circuit diagram.

Physically separating two oppositely charged planes produces an electrical capacitor. This is what occurs with the EDL, with the level of capacitance determined by the type of metal and electrolyte composition. During corrosion, charge moves through this layer. However, the metal will resist the transfer of its electrons to the electrochemically active species. Consequently, an EDL will display both capacitive and resistive properties, which are similar to those for a simple electrical circuit composed of a resistor and capacitor in parallel. In addition to this there will be a resistance to electron flow from the solution, which can be represented by a single resistor. The combined electrical circuit model of the EDL, any coatings, and the solution resistance is called the equivalent electrical circuit (EEC) (Figure 4-8D).

Electrochemical impedance spectroscopy (EIS) is a powerful technique that measures the frequency response of the electrochemical system. The frequency dependency of the system reveals unique time constants characteristic of electrochemical reactions. A reaction time constant is equal to the capacitance (Farads) multiplied by the corresponding parallel resistance (ohms). For an EDL, this will change over time as the layer properties change. Time constants are important when analysing EIS data, as each layer or coating on a surface will display a unique time constant based on its properties.

EIS data may be graphed in a number of different ways based on the vector magnitudes of the components, total impedance magnitudes, and phase angles. The three most common types are; a) complex plane or Nyquist plots, b) Bode magnitude, and c) Bode phase plots. The Nyquist plot is a graph of the real and imaginary impedance magnitudes for each frequency (Figure 4-9). From this it is possible to determine the resistance of the solution (R_S), the number of time constants and the resistance and impedance values of each time constant. It is also possible to fit an appropriate circuit to more complex plots to determine how the additional coatings or films are affecting the corrosion process. It should be noted that the value of solution resistance is a property of the solution and test cell geometry, and is not related to the corrosion mechanism.

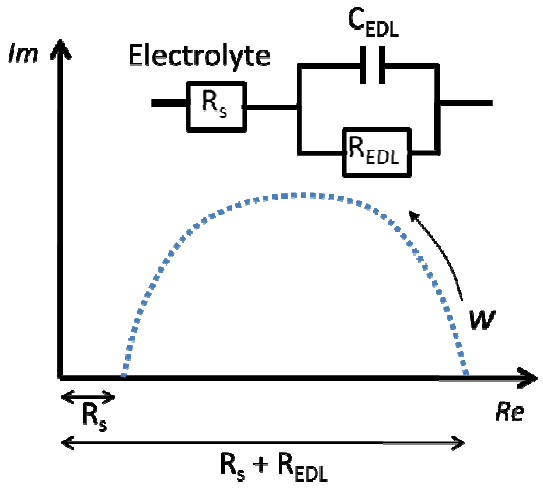

Figure 4-9 : Single time constant Nyquist plot, where R_s is the resistance of the electrolyte (Ω), R_{EDL} and C_{EDL} are the charge transfer resistance (Ω) and capacitance (F), and W is the angular frequency (s^{-1}).

The main disadvantage of displaying EIS data on the Nyquist plot is that the dependence of impedance on the frequency of the signal is not displayed. Thus, Bode plots are a necessary part of the analysis. In Bode plots, the log values of corresponding frequencies are plotted against those of the total impedance (log|Z|) for the magnitude plot and against the phase angle for the phase plot. Bode plots allow the detection of regions that are dominated by the resistive elements, shown by a slope of zero, and regions dominated by the capacitive elements where a slope of -1 is observed (in the ideal case). The plots can also be used to determine the likelihood of certain types of corrosion taking place. For example, it has been shown that pitting of stainless steel displays a capacitive response at low frequencies [14, 15]. For Mg, it has been reported that Bode plots allow the identification of the presence of high frequency electrochemical processes which are only present in the case of fast localized attack [16].

The Bode magnitude plot can potentially be used to determine the resistance values of the equivalent circuit (Figure 4-10A). However, it requires the polarisation to be entirely through the resistors, yielding a zero-slope line. This may be checked using the phase plot where a zero slope indicates the same thing (Figure 4-10B). However, a completely horizontal slope does not seem to occur commonly during tests on Mg, and the Nyquist plot is better suited to determine the resistance and capacitance values.

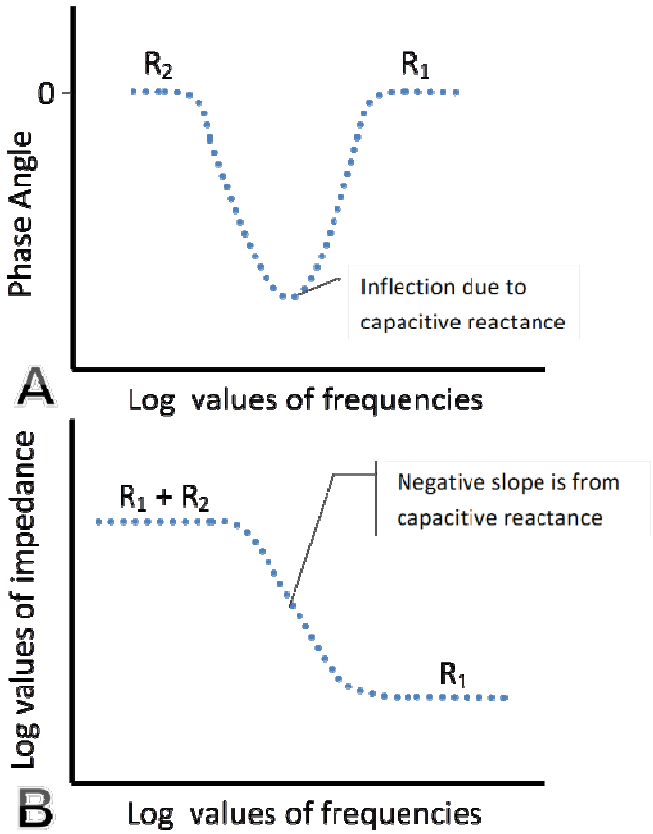

Figure 4-10 : (A) Idealised Bode magnitude plot for single time constant system, (B) corresponding Bode phase plot.

However, the majority of systems do not contain a single time constant, especially if a surface coating is present. Multi-time constant systems may often be divided into components of charge transfer (CT) and film (f) values. CT typically represents the components (R_{CT}, C_{CT}, etc.) of the electrical behaviour between the solution and the bare metal surface alone. Film components (R_f, C_f, etc.) represent the behaviour of each film or coating on the surface.

Experimental design

EIS scans were performed using the EC-Lab software. A frequency range of 10 kHz to 30 mHz was used for all experiments, with 10 points recorded per logarithmic decade. The scanning voltage amplitude was set to ±10 mV (7 mV RMS). Complete EIS scans took an average of 2 min to perform, and were carried out every 30 min for the lifetime of each test, unless stated otherwise. A minimum of 3 replicates of each test was performed for each data point to ensure reproducibility.

For most two time constant systems, an adapted form of the Randle's circuit was found to provide the closest fit to most of the data as well as the most appropriate equivalent circuit to represent the reactions at the surface (Figure 4-11). Randle's circuit is commonly used for a two time-constant system with an incomplete protective layer, as is the case for the Mg alloys in the investigated solutions. In this case, constant phase elements (CPE, Q) were used instead as they represent capacitance that is non-Debeye. This is because a perfect capacitor behaves in an exponential manner, which does not occur in reality, as the interface of the Mg surface and the solution is not atomically smooth. The data were fitted using the Nyquist impedance plot, and then the location and number of the time constants were checked using Bode impedance and admittance graphs.

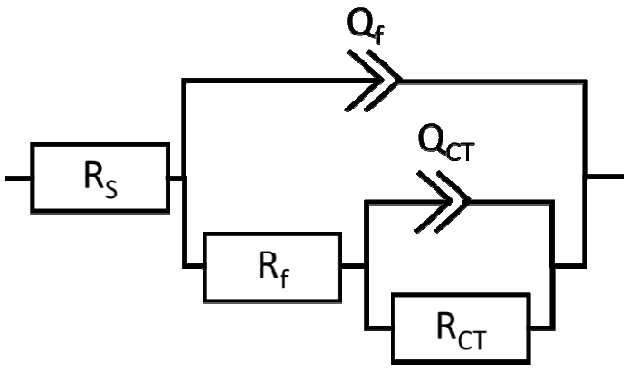

Figure 4-11 : Equivalent circuit used to analyse collected EIS data. R_S is the resistance of the solution, R_{CT} and Q_{CT} are the resistance and CPE of charger transfer to/from the Mg, and R_f and Q_f represent any film that is on the surface.

4.4. Metallographic preparation

After casting, samples were prepared in an appropriate size for the different tests that would be performed. A TechCut® 5 precision sectioning machine was used to cut samples into different shapes (Allied High Tech Products Inc., Rancho Dominguez, CA, USA). A diamond blade and moderate feed rate (2.5 mm/min) were used to ensure accurate cuts with minimal deformation to the subsurface.

Unless otherwise stated, samples were then nominally ground with 240, 600, and 1200 grit SiC paper to ensure consistency across all tests. High purity ethanol (99.5 %) was used to clean the samples between each polishing grade. Samples were then stored in a desiccator immediately after cleaning.

When necessary, further polishing was carried out on a Leco VP-160 polishing wheel (Leco Corporation, St. Joseph, MO, USA) using MetaDi® 9 and 3 µm diamond slurries on a MasterTex® 1000 polishing pad (Beuhler Inc., Lake Bluff, MI, USA). A soft polishing pad (Buehler Chemomet®) and colloidal silicon-based polishing slurry (Buehler MasterPolish® 2) were then used as a final step. At times, a Beuhler MiniMet® polisher was used to obtain a scratch-free surface.

As-polished surfaces were often observed to display different phases and grain boundaries without further treatment. This surface was appropriate for use in microelectrochemical experiments to determine different phases.

4.5. Material characterisation

4.5.1. Surface preparation

When necessary for optical or SEM analysis, samples were polished to 0.02 µm following steps outlined in Chapter 4.4. However, before these steps were taken, samples were mounted in EpoFix® epoxy resin (Struers Australia Pty, Milton, NSW, Australia). After pouring resin into containers with the samples they were placed in a desiccator and a vacuum was applied to remove any trapped air. All samples were set for a minimum of 24 hrs to allow complete curing of the resin.

When necessary, etching was used to illuminate the alloy microstructure. A solution was utilised containing 6 g of picric acid, 5 mL of acetic acid, 10 mL of distilled water and 100 mL of high purity ethanol (99.5 %). A sample would be exposed to the etchant for 20 s, washed with ethanol (99.5 %), then analysed under a light microscope. If required, further etching was carried out by repeating the same process.

4.5.2. Optical microscopy

Optical analysis was performed using a number of different methods. Samples were first examined using an Olympus B061 upright optical microscope (Olympus Inc. Center Valley, PA, USA). Grain analysis was performed primarily on a Leica DM IRM inverted microscope (Leica Microsystems GmbH, Wetzlar, Germany). An Axiocam® MR digital camera was

used to obtain images using computer-based capture software AxioVision® 4.8 (Carl Zeiss NZ Ltd., Auckland, New Zealand). Samples were also analysed using an Olympus BH2-RLA-2 upright microscope. Images were captured using a Spot Insight QE® digital camera and Spot 3.5.8 software (Diagnostic Instruments Inc., Sterling Heights, USA).

Stereo optical images were obtained using an Olympus SXH10 stereo microscope with a Polaroid DMC 2 digital camera (Polaroid Inc., Minnetonka, MN, USA). Images were attained using Corel Photo-Paint 3 software with a driver for the camera (Corel Pty Ltd, Sydney, NSW, Australia).

4.5.3. Electron microscopy and x-ray spectroscopy

The majority of SEM images were obtained using a JEOL 7000F field emission scanning electron microscope (JEOL Ltd., Tokyo, Japan). Accelerating voltages ranging from 12-20 kV were used to obtain images depending on the surface conditions. Higher voltages, such as 20 kV, "charged" the surface when non-conducting or low conducting layers were present, such as $Mg(OH)_2$.

Energy dispersive x-ray spectroscopy (EDS) was used to determine the chemical composition of the surface of the alloys before and after corrosion testing *via* a JEOL JED-2200 EDS attachment using JEOL Analysis Station 3.61.02 software.

Confocal microscopy was also used to analyse the surface topology of selected alloys. A Leica® TCS-SP5 confocal microscope provided digital images *via* LCS software (Leica Microsystems CMS GmbH, Mannheim, Germany). Surface roughness was measured using in-house image analysis software developed at the University of Canterbury, but based on well-defined techniques [17, 18].

Electron backscatter diffraction (EBSD) was used to identify the exact nature of the secondary and intermetallic phases *via* crystal structure determination. EBSD was carried out on a FEI Quanta 3D-FEG (FEI Company, Hillsboro, OR, USA) with a Hikari EBSD camera and TSL OIM software (EDAX Inc., Mahwah, NJ, USA). The heterogeneous nature of many of the alloys did not allow for ultra-high quality polishing required for EBSD analysis. In order to achieve high quality Kikuchi patterns, gentle localised ion milling was performed

immediately prior to collection of the pattern. The execution of spot EBSD was performed to identify the exact nature of the intermetallic phase via crystal structure determination.

4.5.4. Fourier transform infrared spectroscopy

Fourier transform infrared spectroscopy (FTIR) was performed on a Spectrum One® (Perkin Elmer, Waltham, MA, USA) using dedicated Spectrum software (Version 3.02). A total of 16 scans were performed per sample using a wavenumber range of 400 to 4000 cm^{-1}. The system had a resolution of 1 cm^{-1}. The system used potassium bromide (KBr) as a background spectrum and filler material. Approximately 2 mg of sample was used per 200 mg of KBr. A minimum of 3 samples exposed to the same conditions were analysed using this technique to ensure reproducibility.

4.5.5. Mechanical testing

Mechanical compression tests were performed on selected samples during the course of this work. Tests were carried out either on a MTS® 810 Material Test System (MTS, Eden Prairie, MN, USA) at the University of Canterbury, or an Instron 4505 Testing System (Instron, Norwood, MA, USA) at Monash University in Melbourne, Australia. For both instruments a 100 kN load cell was used. The initial strain rate was 10^{-3} s^{-1}. Flat platens were used and samples were prepared according to guidelines in ASTM E9-89a [19].

Where possible an extensometer was fitted to the samples to measure movement. Otherwise the crosshead displacement was used to calculate the strain. Both methods were investigated prior to use to ensure they provided accurate data. Data were recorded at a rate of 50 Hz using MTS TestSuite or Instron BlueHill 3.0 software.

4.6. Protein adsorption experiments

4.6.1. Protein staining

Protein staining is a common technique for determining the amount of protein in a solution or attached to a surface. In this work the possibility of using such a staining technique directly on the surface of Mg samples was investigated. It was hoped that staining of the proteins

would provide an immediate visual clue to the attachment or presence of proteins on the surface. A similar experiment was carried out on Ti and stainless steel in a solution containing FBS [20]. A dye that has become popular for use in biological staining, Coomassie brilliant blue, was chosen as it has been successfully used in studies of BSA [21].

Mg samples were prepared by polishing with 1200 grit paper and spraying them with a 70% ethanol solution. Samples were then placed in PBS either with or without the addition of 40g/L BSA in an incubator at T_{phy} and a pH of 7.4 ± 0.02. After 5, 15, 30, and 60 min samples were removed from the medium and washed twice in PBS. They were then placed in a 0.001% Coomassie Brilliant Blue (B7920, Sigma-Aldrich) solution for 5 min, removed and washed in distilled water before drying. Analysis was performed immediately after drying using an Olympus B061 upright optical microscope and images were obtained using a Spot Insight QE® digital camera.

4.6.2. Protein solute-depletion method

The solute-depletion method relies on detecting the reduction in protein concentration in solution after a set period. The protein loss is measured using a UV/visible spectrophotometer to determine the amount of light absorbed. It is well known that many proteins exhibit the greatest absorption at 280 nm [22]. Consequently by measuring the absorbance at this wavelength it is possible to determine the amount of proteins remaining in solution thereby allowing quantification of the amount attached by determining the difference between initial and final protein concentrations.

Mg discs with a total surface area of 130 mm^2 were prepared and polished to 1200 grit. All samples were triple washed in milli-q water and then PBS for 1 min. Each disc was placed in an individual Eppendorf pipette which was filled with 1 mL of a base solution of PBS with 0.25, 0.5, or 1 mg/mL of BSA (negative charge at 7.4) or cytochrome C (CytoC, positive charge at 7.4). Additional Eppendorf pipettes were filled with the same solutions without samples to provide base measurements and to determine the protein loss due to attachment to the inside of the pipette. Samples were placed on a rotating wheel to keep the solution flowing over the surface at approximately 0.25 Hz.

All Eppendorf pipettes were hard spun at 13,000 rpm for 5 min before sampling in order to remove other products that may absorb the same wavelength as proteins. Analysis of the change in protein concentration was carried out using a Nanodrop ND-1000 spectrophotometer and an Amersham Ultrospec 2100 pro spectrophotometer (GE Healthcare Ltd., Rydalmere, NSW, Australia). For the Nanodrop, test samples of each concentration were removed every 10 min for 1 hr and 2 µL of medium was extracted. The Ultrospec 2100 required a larger solution amount and 100 µL of the sample medium was extracted and diluted to a ratio of 1:1 with fresh PBS. Samples for these experiments were taken after 1 and 24 hrs.

The absorbance values from the tests were converted to mg/mL concentration using Equation 4-2.

$$\text{Concentration} = \frac{Abs_{280}}{\alpha} \qquad \text{Equation 4-2}$$

where Abs_{280} is the absorbance at 280 nm and α is the absorption coefficient of the protein (cm). For BSA this is 0.667 and Cytochrome-C this is 0.99.

4.6.3. Quartz crystal microbalance and sputtering

A quartz crystal microbalance (QCM) is a tool that has in recent years become widely used for determining tiny alterations in mass on a surface [23]. It measures the change in frequency for a quartz crystal as a layer is either put down on or removed from the surface. This has been used to measure the deposition of thin films as well as the affinity of molecules, such as proteins, to a coated surface. Using this technique, it is possible to measure mass densities to a level below 5 ng/cm^2 [24]. It is a real-time measurement system which makes it very useful for both short and long term experiments.

Background to quartz crystal microbalance theories and techniques may be found in numerous books [25, 26] and review papers [23].

Crystal preparation

In order to perform QCM experiments on Mg, it was first necessary to coat the quartz crystals. DC magnetron sputtering was selected as a suitable method due to previous success noted in the literature using the technique with Mg [27-29]. All sputtering was performed in an Auto 500 sputtering system (Edwards Inc., Tewksbury, MA, USA). A disc of high purity Mg (99.98 %) was prepared and quartz crystals (QSX 301, Q-Sense, Vastra Frolunda, Sweden) were mounted so 1 cm^2 of electrode surface was 15 cm away from the Mg disc. A range of applied bias voltages, from 150 V to 600V, were used to investigate their effect on the microstructure of the sputtered films. The processing conditions used in this work yielded a deposition rate of 1.7-8 nm/s.

An atmosphere of high purity argon (Grade 0) with a base pressure below 10^{-5} bar was used throughout the experiment. The crystals were positioned directly above the Mg source and at the start of each sputtering cycle the source was covered for 2-3 min to allow steady-state deposition rates to be reached. A target thickness of 2 µm of coating was desired as this was the value recommended by the QCM manufacturer as the maximum thickness that would allow protein-adhesion detection. Coating thickness was determined using a Dektak 150 stylus profiler (Bruker-AXS, Tuscan, AZ, USA) with a maximum resolution of 1 angstrom.

QCM experimental design

The Mg-coated crystals were analysed using a Q-Sense E4 flow QCM (Q-Sense, Vastra Frolunda, Sweden) and the bundled software (QSoft 4.01). All solutions and crystals were heated to T_{phy} ± 0.2 °C and a flow rate of 200 µL/min was used to fill each the 500 µL chamber and switch between media. For each experiment, high purity ethanol (99.8%) was first pumped through the chamber and the fundamental frequencies were measured. This is necessary to provide a base frequency/dissipation relationship that other solutions may be compared against, as no corrosion and limited interactions would happen in this environment.

After the frequencies were determined, MEM was pumped through separate chambers containing both Mg-coated and uncoated crystals for comparison with the fundamental frequencies which had been recorded previously. The change in viscosity between the MEM and ethanol resulted in a shift in the fundamental frequencies measured by the QCM crystals. Normally, a period of a few min is required for the frequencies to stabilise in the new

solutions. After 3-4 min, a further solution of MEM with 40 g/l BSA was pumped through the chamber. After a further 10 min, the MEM was again pumped through the chamber. This step was necessary to determine the amount of protein that had attached to the surface during immersion in MEM+BSA. A drop in frequency indicates an increase in the mass on the surface of the crystal. Thus, proteins still attached to the surface after immersion in the MEM+BSA medium would result in a lower frequency when MEM solution is re-pumped through the chamber. At the end of the experiment, ethanol was pumped through all chambers to compare the original base frequencies.

4.7. References

[1] Shaw, B.A., R.C. Wolfe. *Corrosion of Magnesium and Magnesium-Base Alloys*. In: Cramer, S.D., Convino, B.S., editors. Asm Handbook, vol. 13B Corrosion: Materials. Metals Park: ASM International, 2005. p.205.

[2] Yamamoto, A., S. Hiromoto. *Effect of Inorganic Salts, Amino Acids and Proteins on the Degradation of Pure Magnesium in Vitro*. Materials Science and Engineering: C 2009;29:1559.

[3] Warrel, D.A. *Oxford Textbook of Medicine*. New York: Oxford University Press, 2003.

[4] Helgason, C.D., C.L. Miller. *Basic Cell Culture Protocols*. Totowa, NJ: Humana Press, 2005.

[5] Friedrich, H.E. Magnesium Technology : Metallurgy, Design Data, Applications. Heidelberg: Springer, 2006.

[6] Bard, A.J., L.R. Faulkner. *Electrochemical Methods: Fundametals and Applications*: John Wiley and Sons, 2001.

[7] ASTM International. Astm Standard G102-89, "Standard Practice for Calculation of Corrosion Rates and Related Information from Electrochemical Measurements". West Conshohocken, PA: ASTM International, 2004.

[8] Lunder, O., J.E. Lein, S.M. Hesjevik, T.K. Aune, K. Ni, scedil, ancio, gcaron, lu. *Corrosion Morphologies on Magnesium Alloy Az 91*. Materials and Corrosion/Werkstoffe und Korrosion 1994;45:331.

[9] Zeng, R.C., J. Chen, W. Dietzel, N. Hort, K.U. Kainer. *Electrochemical Behavior of Magnesium Alloys in Simulated Body Fluids*. Transactions of Nonferrous Metals Society of China 2007;17:S166.

[10] Suter, T., H. Böhni. *Microelectrodes for Studies of Localized Corrosion Processes.* Electrochimica Acta 1998;43:2843.

[11] Birbilis, N., R.G. Buchheit. *Electrochemical Characteristics of Intermetallic Phases in Aluminum Alloys*. Journal of the Electrochemical Society 2005;152:B140.

[12] Lohrengel, M.M. *Electrochemical Capillary Cells*. Corrosion Engineering, Science and Technology 2004;39:53.

[13] Birbilis, N., B.N. Padgett, R.G. Buchheit. *Limitations in Microelectrochemical Capillary Cell Testing and Transformation of Electrochemical Transients for Acquisition of Microcell Impedance Data*. Electrochimica Acta 2005;50:3536.

[14] Hamdy, A.S., E. El-Shenawy, T. El-Bitar. *Electrochemical Impedance Spectroscopy Study of the Corrosion Behavior of Some Niobium Bearing Stainless Steels in 3.5% Nacl*. International Journal of Electrochemical Science 2006;1:171.

[15] Polo, J.L., E. Cano, J.M. Bastidas. *An Impedance Study on the Influence of Molybdenum in Stainless Steel Pitting Corrosion*. Journal of Electroanalytical Chemistry 2002;537:183.

[16] Quach, N.-C., P.J. Uggowitzer, P. Schmutz. *Corrosion Behaviour of an Mg-Y-Re Alloy Used in Biomedical Applications Studied by Electrochemical Techniques*. Comptes Rendus Chimie 2008;11:1043.

[17] Whitehouse, D. *Surfaces and Their Measurement*. London: Kogan Page Science, 2004.

[18] Udupa, G., M. Singaperumal, R.S. Sirohi, M.P. Kothiyal. *Assessment of Surface Geometry Using Confocal Scanning Optical Microscope*. Mechatronics 1998;8:187.

[19] ASTM International. Astm Standard E9-89a, "Standard Test Methods of Compression Testing of Metallic Materials at Room Temperature". 2000.

[20] Smith, R.A., M.W. Mosesson, A.U. Daniels, T.k. Gartner. *Adhesion of Microvascular Endothelial Cells to Metallic Implant Surfaces*. Journal of Materials Science: Materials in Medicine 2000;11:279.

[21] Sohl, J.L., A.G. Splittgerber. *The Binding of Coomassie Brilliant Blue to Bovine Serum Albumin: A Physical Biochemistry Experiment*. Journal of Chemical Education 1991;68:262.

[22] Aitken, A., M.P. Learmonth. *Protein Determination by Uv Absorption*. In: Walker, J.M., editor. The Protein Protocols Handbook. Humana Press, 2002. p.3.

[23] Marx, K.A. *Quartz Crystal Microbalance: A Useful Tool for Studying Thin Polymer Films and Complex Biomolecular Systems at the Solution-Surface Interface*. Biomacromolecules 2003;4:1099.

[24] Lu, C., A.W. Czanderna. *Applications of Piezoelectric Quartz Crystal Microbalances*. Amsterdam: Elsevier, 1984.

[25] Steinem, C., A. Janshoff, editors. *Piezoelectric Sensors*. Heidelberg: Springer-Verlag, 2007.

[26] Smith, A.L. *The Quartz Crystal Microbalance*. In: Brown, M.E., Gallagher, P.K., editors. Handbook of Thermal Analysis and Calorimetry Volume 5 : Recent Advances, Techniques, and Applications. Amsterdam: Elsevier, 2008.

[27] Huo, H., Y. Li, F. Wang. *Preparation and Corrosion Resistance of Magnesium Coatings by Magnetron Sputtering Deposition*. Journal of Materials Sciences and Technology 2003;19:459.

[28] Nieh, T.G., J. Wadsworth. *Magnesium Alloy Az31 Foil Prepared by Sputter Deposition at 200° C*. Journal of Materials Science Letters 1987;6:1150.

[29] Wu, G., W. Dai, L. Song, A. Wang. *Surface Microstructurization of a Sputtered Magnesium Thin Film Via a Solution-Immersion Route*. Materials Letters 2010;64:475.

CHAPTER 5: Critical Analysis of Common *In Vitro* Experiments – Advantages, Limitations and Considerations

5.1. Introduction

Corrosion is a complex process, requiring a combination of different techniques to fully characterise. For Mg, the various test methods may be grouped into two primary categories: (i) immersion and (ii) electrochemical. Care must be taken to ensure the chosen experiment is actually designed to investigate the intended corrosion attribute. Correct interpretation of data is often dependent on precise setup parameters that must be known and properly controlled.

The aim of this chapter is to clarify the use, limitations and considerations of the most common *in vitro* tests for Mg alloys. Part of the information provided was gathered over time as experiments were carried out and potential issues or drawbacks were observed. Other information comes from a review of pertinent literature and an analysis of methods that have been utilised by those authors. A detailed description of the setup of each experiment can be found in Chapters 2.4.3. , 4.2, and 4.3.

5.2. Immersion tests

5.2.1. Mass loss – A limited but necessary corrosion experiment

A mass loss (ML) measurement is the simplest of the *in vitro* methods for investigating the corrosion of Mg. Setup may vary depending on the experimental variables, such as choice of buffering system, but the same basic design is typically employed. This test is therefore very commonly used, with over 40 studies in which ML has been utilised to measure Mg corrosion *in vitro*.

Results obtained from ML tests are typically accurate, assuming issues with the removal of the corrosion layer are minimised. Depending on the design of the experiment it may also be

possible to perform other *in vitro* tests may be performed concurrently with ML, such as pH recording or even in certain situations electrochemical experiments.

5.2.1.1. Limitations and considerations when performing mass loss experiments

Mass loss experiments are able to reveal how much corrosion has occurred, but do not disclose any of the mechanisms. Consequently, while it may be observed that one alloy corrodes faster than another, ML does not provide the information required to determine why this happens. This is highlighted in Figure 5-1, where the total mass loss for two alloys (Mg-5Ca, Mg-10Zn) was very similar after 1 week immersion in HBSS. However, the polarisation curves clearly show that the alloys are corroding at dissimilar potentials due to different anodic and cathodic responses. This behaviour is particularly important in more "realistic" media, as the effects of organic components (***e.g.*** amino acid, proteins) may have varying effects on each partial reaction (see Chapter 5.3.2.), but cannot be seen using only a ML experiment.

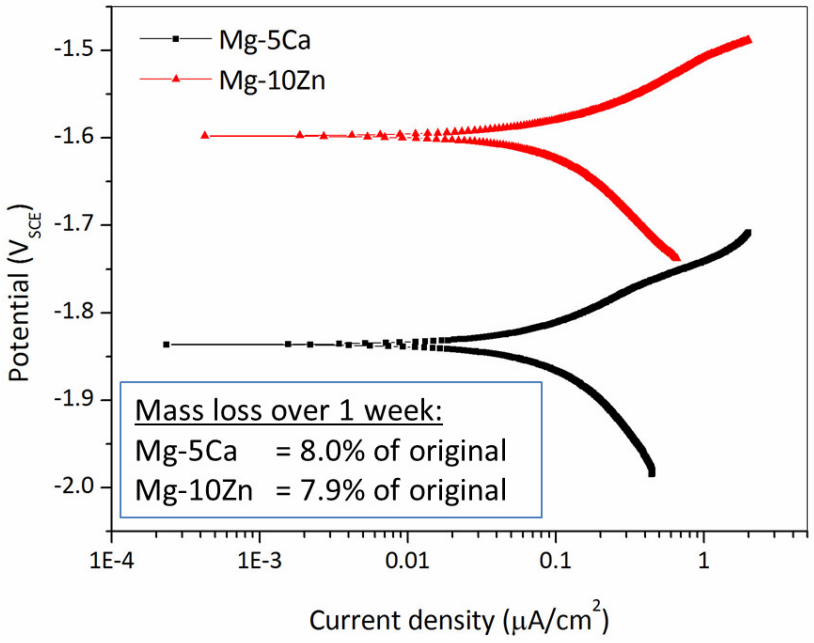

Figure 5-1 : Polarisation response and mass loss of Mg-5Ca and Mg-10Zn after 1 week immersion. (HBSS, T_{phy}, 7.4)

Similarly, though SEM analysis after immersion may provide some information on the corrosion mechanisms, any time-dependant behaviour involved in the creation or degradation of a given layer on the surface cannot be exposed by ML. This information is particularly

important for Mg in SBF; layers such as calcium phosphate are known to be crucial to the degradation performance of virtually any Mg alloy.

Due to the significant corrosion that is necessary for measurements of drop in mass, multiple samples are needed to provide accuracy for ML experiments. Because there may be significant variation between samples, comprehensive control of each preparation step is vital. Given the rapid corrosion rates of many Mg alloys in the aggressive SBF environments, even minor discrepancies between samples (***e.g.*** location of sample within original ingot) may result in large variances in obtained results.

There are a number of concerns and variables that need to be considered when performing ML experiments. The corrosion of Mg will release Mg^{2+} and reduce H^{+} in the corrosion medium, so the surface area to medium ratio must be taken into account. If this ratio is too large, the measured corrosion rate may be affected by the rising pH. This was shown in an experiment on pure Mg in HBSS at T_{phy} over 1 week (Figure 5-2). A variety of solution to surface area ratios were investigated (5-500 mL/cm^2) and pH was adjusted every 30 min to 7.4 using a 1 M NaOH solution. A large rise in measured mass loss was found as the amount of solution increased, until 50 ml/cm^2. Thereafter the mass loss levelled off at ~ 7 wt. % of the original. This disparity was due to the rapid increases in pH that occurred in-between the re-adjustments to 7.4, allowing a thicker $Mg(OH)_2$/CaP layer to form on the Mg samples in the low solution to surface area ratio tests. Although this layer would have partially dissolved when the solution pH was readjusted to 7.4, it is likely that a significant amount remained, reducing the overall corrosion rate of the Mg.

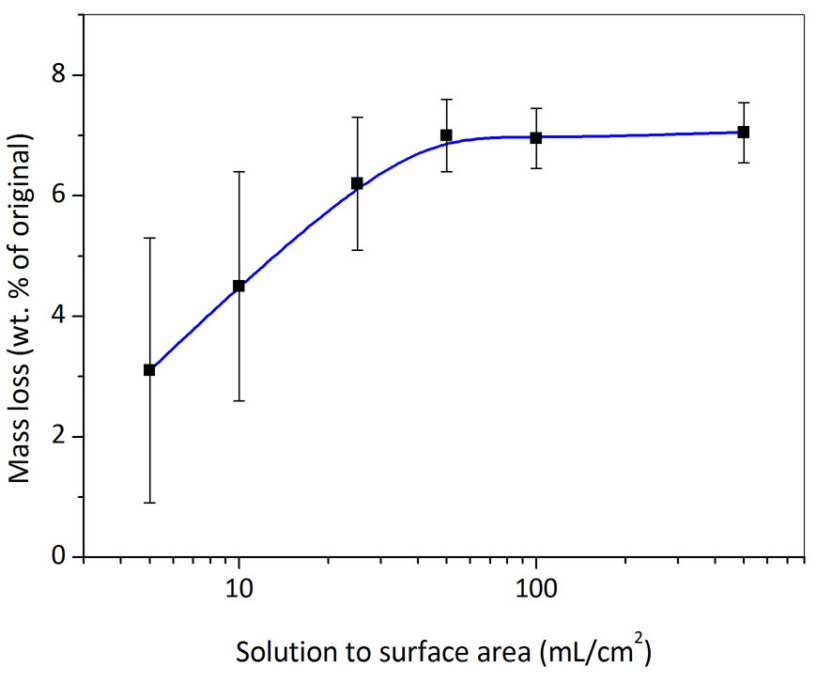

Figure 5-2 : Mass loss as a function of solution to surface area for pure Mg after 1 week immersion. (HBSS, T_{phy}, 7.4)

The variation of pH in ML tests may be minimised by changing the solution frequently. Furthermore, the use of a ratio based on proposed end implant size and the exchange of a portion of the solution at regular intervals, as performed by Yamamoto [1] and in this work (Chapter 6.5), is a credible method of more accurately simulating physiological conditions. Standards outlined by the American Society for Testing and Materials (ASTM) are not suitable for Mg as they recommend solutions far too small (0.2-0.4 mL/mm^2) for the rapid change in pH that typically occurs [2, 3].

It is also important to remove the corrosion product after immersion. Early studies did not incorporate this step, and some even reported a net gain in weight due to a hydrated corrosion layer on the surface [2, 4]. Typically a mixture of CrO_3 and $AgNO_3$ (chromic acid) is used to remove this layer as it has been found to cause little additional corrosion to the underlying Mg surface [5-7].

5.2.2. Hydrogen evolution – A valuable corrosion measurement technique with many considerations

Most hydrogen evolution (H_2^{evo}) experiments reported in the literature utilise the same basic setup as ML tests, though they also include a funnel and burette for collecting the evolving hydrogen. Similarly, H_2^{evo} is likewise frequently utilised, as it is included in more than 35 papers reporting on the *in vitro* testing of Mg and its alloys.

H_2^{evo} tests are relatively easy to set up. As opposed to ML, H_2^{evo} measurement is unaffected by the corrosion product and does not require its removal at the end of the experiment to obtain results. The primary advantage of H_2^{evo} tests is the ability to take measurements at any time point. This presents an overall picture of the progression of the degradation, allowing analysis of the changes in corrosion rate that may occur over the lifetime of the test – information not obtained *via* a simple ML experiment. For example, a mass loss test may show that an alloy (*X*) has corroded less than alloy (*Y*). However, a H_2^{evo} test is able to show that alloy *X* started to more rapidly degrade near the end of the ML experiment, and would likely have surpassed alloy *Y* in overall corrosion. This information would have been lost if only the ML data was relied upon.

In this work, it was observed that several Mg alloys show three distinct regions of differing H_2 evolution rate over 48 hrs, from ~0.4 mL/hr (i) to ~0.08 mL/hr (iii) (Figure 5-3). The difference in corrosion rate was attributed to the formation of corrosion layers on the surface, slowing the rate of evolution over time. Similar behaviour has been shown in the literature for pure Mg [8]. Again, this information would be difficult to ascertain using only ML tests.

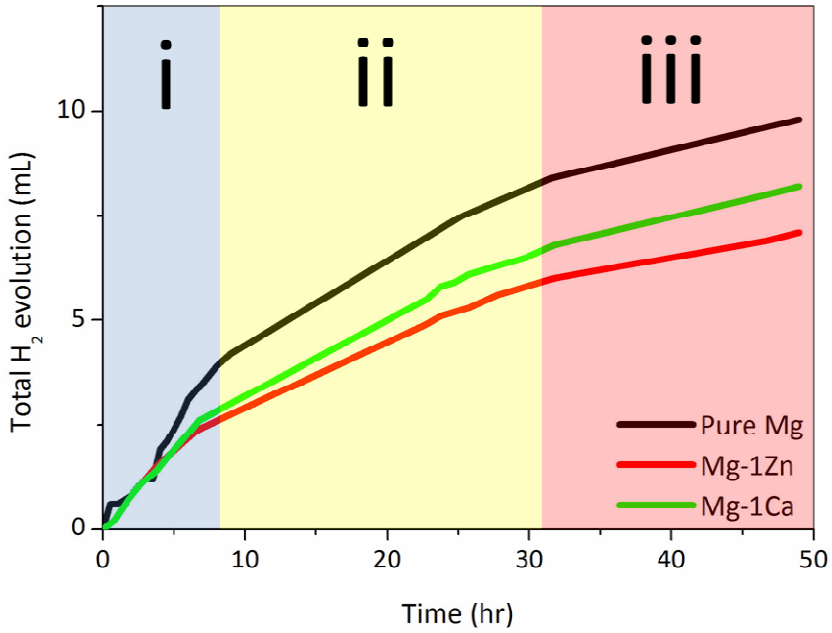

Figure 5-3 : H_2 evolution over 48 hrs for pure Mg. Different rates of evolution are indicated (i, ii, iii). (HBSS, T_{phy}, 7.4)

This test is also useful in that the degree of alkalisation can be determined based on the volume of hydrogen evolved if it is assumed that 2 mol of OH^- are released for every 1 mol of Mg that is oxidised (Equation 5-1).

$$Mg + 2H_2O = Mg^{2+} + 2OH^- + H_2 \qquad \text{Equation 5-1}$$

It is important to note that H_2 evolution has been shown to be a problem *in vivo*, and can potentially lead to implant failure [2, 9]. Thus, measuring of the gas evolution rate *in vitro* may provide additional information on whether the tissue surrounding the implant is likely to experience gas accumulation.

5.2.2.1. Limitations of the H_2^{evo} technique

Similar to ML experiments, the H_2^{evo} technique itself does not reveal information on most of the corrosion mechanisms that are occurring at the sample surface. Although time varying data is provided, the reasons for the changes in evolution rate are not indicated by the test. This is a limitation of any non-electrochemical experiment. Furthermore, only after significant corrosion has occurred does a sufficient volume of gas exist that it can be accurately and reproducibly measured. This means that H_2^{evo} is typically not a suitable

method for the study of corrosion in the early stages (<1 hr) of immersion, or for very corrosion resistant alloys.

The investigation of flow rates on Mg corrosion is also not possible using the H_2^{evo} technique, as the evolved H_2 would be very difficult to capture unless the corrosion cell was entirely sealed. Concurrent electrochemical tests are also more difficult to set up than in ML experiments, due to the additional glassware (burette, funnel) that make electrode placement problematic.

5.2.2.2. Minor experimental considerations for H_2^{evo} tests

The solubility of hydrogen gas in H_2O at 37 °C is 0.0014 g/kg [10]; its density at this temperature is approximately 9 x 10^{-5} g/mL [11]. For an average experiment with 250 mL (0.25 kg) of water (or SBF with a similar H_2 solubility), a total of (0.25 x 0.0014) = 0.00035 g of H_2 can be absorbed by the solution. This is equivalent to (9 x 10^{-5} / 0.00035) = 0.26 mL of H_2. Given the precision of most H_2^{evo} setups of 0.1 mL, this results in only a small amount of error for most long-term experiments. However, this solubility may be more important in short-term experiments or where a large solution-to-sample ratio is used.

As the temperature of a solution rises (such as from room temperature to 37 °C), the gas solubility of the solution falls and bubbles will start to precipitate. For example, a total of 2.14 mL and 4 mL of O_2 and N_2 could potentially be released from 1 L of solution due to the increase in temperature from T_{rm} to T_{phy} (Table 5-1). However, these measurements are for a solution with quadruple the volume of a typical test (250 mL) and assume that all the released gas is captured by the apparatus. Thus it is unlikely that this gas release would have a considerable effect on the overall recorded H_2.

Table 5-1 : Change in solubility of O_2 and N_2 and potential release of gas for 1 L of H_20 at pH 7.0 at 1 atm.

Gas	Solubility at 20 °C (mg/L)	Solubility at 37 °C (mg/L)	Gas Density (mg/mL)	Release of gas (mL)
O_2	9	6.2	1.31	2.14
N_2	18	13	1.25	4

Data from [12]

It was observed in the course of this work that unknown gas bubbles often nucleate on the surface of the funnel and in the area surrounding the sample when performing H_2^{evo} experiments, even when the temperature was held constant (Figure 5-4). Although this could potentially add to the overall volume measured, controlled trials found the contribution of these bubbles to be less than 0.1 mL on a 10 cm^2 surface over 72 hours at both 20 °C and 37 °C, which is effectively negligible.

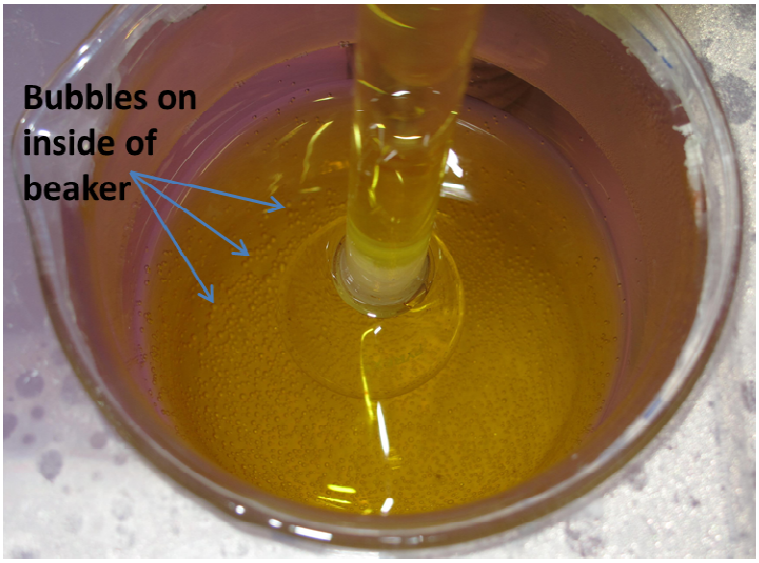

Figure 5-4 : Bubble formation in H_2^{evo} test.

5.2.2.3. Important considerations when performing H_2^{evo} tests

Hydrogen evolution is solely a measurement of the cathodic reaction that is occurring. Thus it will not reflect processes such as dealloying, where certain particles of the secondary phase(s) may break away from the sample. This would result in additional mass loss to the sample but would not be detected by the H_2^{evo} technique. This may lead to considerable error in heavily alloyed Mg.

Hydrogen is also known to be permeable through many polymeric materials [13]. Hydrogen diffusion therefore needs to be considered when designing a suitable test setup, as the choice of inappropriate materials may alter results. It has been found that H_2 leaks quickly when stored in plastic bottles and was completely gone after 2 weeks [14]. Consequently it is recommended that all equipment used to capture the released gas should be made of glass to minimise any potential leaks.

The ideal gas law, which governs the volume of gas produced per mol of H_2, is given by:

$$PV = nRT \qquad \text{Equation 5-2}$$

where P is the pressure, V is the volume, n is the amount of the gas in moles, R is the ideal gas constant, and T is the temperature.

With n, R and T constant in a given experimental setup, the volume of the evolved hydrogen is solely related to the surrounding atmospheric pressure. The variance caused by these differences in atmospheric pressure may be significant; for example, an experiment performed at 2,000 m would evolve almost 30% more volume of H_2 than that performed at sea level. Thus, experiments should take atmospheric pressure into account by utilising:

$$\Delta W = 1.085 V_H / P_{ATM} \qquad \text{Equation 5-3}$$

where ΔW is the change in mass (mg), V_H is the volume of hydrogen that has evolved (ml) and P_{ATM} is the atmospheric pressure (atm).

There are also experimental errors that can be introduced in setting up an H_2^{evo} test. A common error is placing the inverted funnel directly over the Mg sample such that the mouth of the funnel contacts the base of the beaker. This type of "closed" system such as this will limit the amount of corrosive medium that is in contact with the sample solely to the volume that is solely contained within the funnel, and this inadvertent increase in the ratio of surface area to volume of medium may significantly increase the pH. This was found for pure Mg samples over 24 hours in HBSS (Figure 5-5). The setup of both tests was identical except in one funnel, with approximately 50 mL of solution, which was placed so it completely covered the 5 cm^2 sample. Recordings of pH approximately 1 cm from the sample over time clearly show that the reduced solution volume caused a considerable increase in pH.

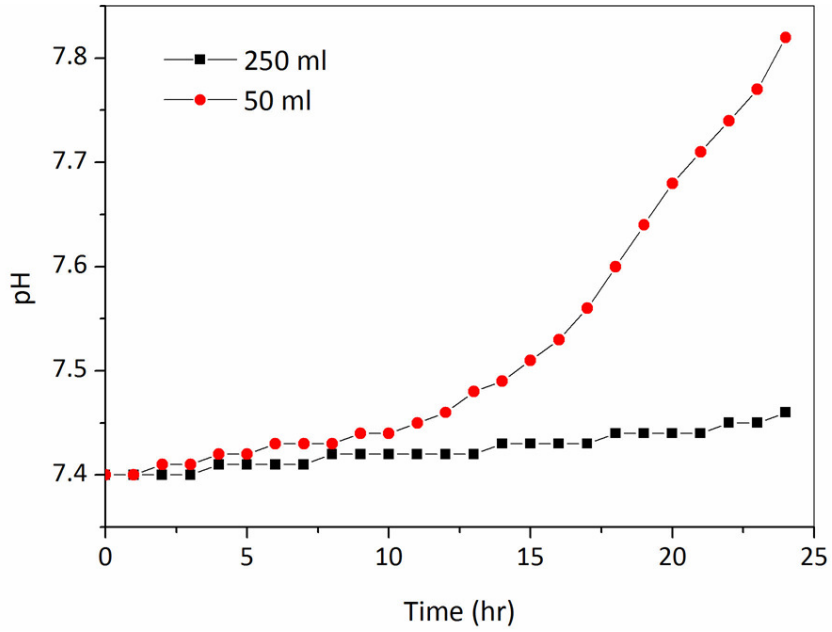

Figure 5-5 : Comparison of pH over time for pure Mg with H_2^{evo} funnel placement altered. (HBSS, T_{phy})

No study that has performed H_2^{evo} experiments has reported whether the side of the sample in contact with the bottom of the beaker was coated to stop corrosion. This is an important detail, as this work found that, if left bare, this surface would always partially corrode, releasing H_2 (Figure 5-6). This could affect calculations of the evolution rate which is based on a known surface area. Hence, any surfaces that are not to be included in the measurements require a sealant to prevent their unintended degradation.

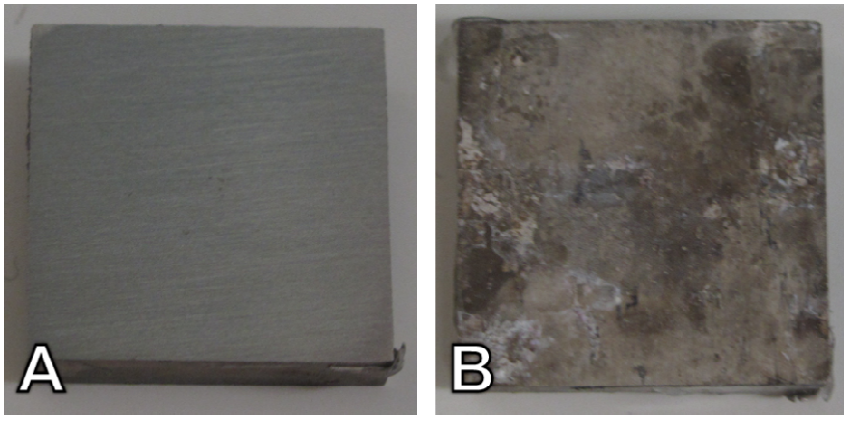

Figure 5-6 : Photographs (2 ×) of the bottom surface of pure Mg samples (A) before and (B) after immersion for 72 hrs. (HBSS, T_{phy}, 7.4)

The majority of the studies in the bio-Mg literature that have compared H_2^{evo} (converted to equivalent mass loss) with actual mass loss have not found the ideal 1:1 ratio (Table 5-2). Some studies found this ratio to vary between 0.22-0.323 [15-17], while others have determined it to vary between 0.89-1.31 [7, 18-20]. This apparent disparity between the ideal and actual results was also established in this work, with the ratio typically within the range of 0.6 ± 0.08. The reasons for this variation are not clear, but indicate that either more complex reactions are affecting the evolution rate or experimental setups are crucially impaired in some way. Consequently ML experiments must be performed in conjunction with H_2^{evo} in order to confirm obtained results.

Table 5-2 : Studies of Mg where H_2^{evo} and ML experiments have been concurrently performed.

Alloy	Solution	Temp / pH	Test Period (hr)	Measured Mass Loss (mg/cm^2/d)	H_2 Equivalent Mass Loss (mg/cm^2/d)	Ratio (H_2 : ML)	Ref.
Pure Mg	1M NaCl	Rm / N/S	48	0.43	0.44	**1.023**	[21]
AZ91 (D)	1M NaCl	Rm / N/S	48	3.0	3.1	**1.03**	[21]
ZE41	1M NaCl	Rm / N/S	48	5.7	5.9	**1.03**	[21]
Mg-0.8Ca	0.9% NaCl	N/S / N/S	360	0.31	0.10	**0.323**	[15]
Mg-2Gd	1% NaCl	21.5 / 6.5	N/S	6.4	6.4	**1**	[7]
Mg-5Gd	1% NaCl	21.5 / 6.5	N/S	1.78	1.97	**1.11**	[7]
Mg-10Gd	1% NaCl	21.5 / 6.5	N/S	0.54	0.49	**0.91**	[7]
Mg-15Gd	1% NaCl	21.5 / 6.5	N/S	8.38	10.95	**1.31**	[7]
AZ31B	HBSS	37 / 7.5	720	0.14	0.038	**0.27**	[16]
Pure Mg	HBSS	37 / 7.5	168	0.094	0.021	**0.22**	[17]
MEZr	5% NaCl	N/S / N/S	24	28	25	**0.89**	[20]
99.96 Mg	1M NaCl	N/S / 6	N/S	47	50*	**1.06**	[18]
99.96 Mg	1M NaCl	N/S / 11	N/S	19.5	20*	**1.03**	[18]
99.96 Mg	1M NaOH	N/S / N/S	N/S	0.07	0.07*	**1**	[18]
99.96 Mg	1M HCl	N/S / N/S	N/S	~70000	~70000*	**1**	[18]
99.96 Mg	5% NaCl	Rm / N/S	N/S	20	20*	**1**	[18]
A6	1M NaCl	N/S / N/S	N/S	37	35*	**0.95**	[18]
AZ21	1M NaCl	N/S / N/S	N/S	0.47	0.50*	**1.06**	[18]
AZ91D	1M NaCl	N/S / N/S	N/S	0.205	0.2*	**0.98**	[18]
AZ91D	5% NaCl	N/S / N/S	N/S	0.21	0.21*	**1**	[18]
AZ91	SBF	N/S / N/S	168	0.47	0.43*	**0.915**	[19]

Alloy	Solution	Temp / pH	Test Period (hr)	Measured Mass Loss ($mg/cm^2/d$)	H_2 Equivalent Mass Loss ($mg/cm^2/d$)	Ratio (H_2 : ML)	Ref.
Selected data from this work							
Pure Mg	HBSS	37 / 7.4	72	9.1	5.47	**0.601**	
Mg-1Ca	HBSS	37 / 7.4	72	8.3	5.40	**0.651**	
Mg-1Zn	HBSS	37 / 7.4	72	6.2	3.35	**0.540**	

N/S indicates that the value was not stated, Rm indicates room temperature
* these values were converted from the provided data to $mg/cm^2/day$ or was obtained from graphs.
Data presented for this work is average of 3 samples for each data point.

5.3. Electrochemical tests

5.3.1. pH monitoring

As Mg corrodes, OH^- is released which results in an increase in the pH of the solution (see Equation 5-1). This half reaction equation may be used to determine how much corrosion is taking place based on measurement of the rise in pH. This has been used widely in the Mg biomaterial literature, although normally only to provide qualitative results [4, 17, 22-33].

However, the use of pH monitoring to determine corrosion rate for Mg alloys in SBF is critically flawed. The primary requirement for a change in pH needed to provide a measurement means that the pH will typically exceed the physiological range (7.4-7.6) before any significant information is provided. This creates a non-realistic environment, and has been shown in this work (Chapter 6.3) to have a significant impact on the corrosion rate and any $Mg(OH)_2$ or CaP layers that form on the surface. This limits the use of this testing method, as a measureable pH change is only possible in an environment that is inappropriate for predicting physiological corrosion of Mg. Hence, pH monitoring should only be used to help maintain a controlled level in the solution rather than providing a measure of the corrosion rate.

5.3.2. *Potentiodynamic polarisation – Elucidating the mechanistic behaviour of electrochemical reactions*

In the Mg literature, over 70 studies have used the potentiodynamic polarisation (PDP) technique to analyse alloy corrosion *in vitro*. PDP provides instantaneous data on the overall rate at which current flow (and hence corrosion) is taking place at a single point in time. Sample preparation is straightforward, and a single PDP scan typically takes less than 5 min to complete. A single sample may be tested as many times as required when using a flat corrosion cell. This minimises any variances between samples that may be encountered in ML or H_2^{evo} experiments.

PDP may also be used to evaluate thermodynamic variances that occur when changing a variable in a given experiment. For example, it can be used to determine the effect that different alloys or solutions have on shifts in the corrosion potential (E_{corr}) and current density (i_{corr}). This may then help explain the differences in absolute corrosion rates. For example, when comparing pure Mg in HBSS and EBSS, it can be seen that the small rise in E_{corr} for the latter solution is due to an anodic shift (Figure 5-7).

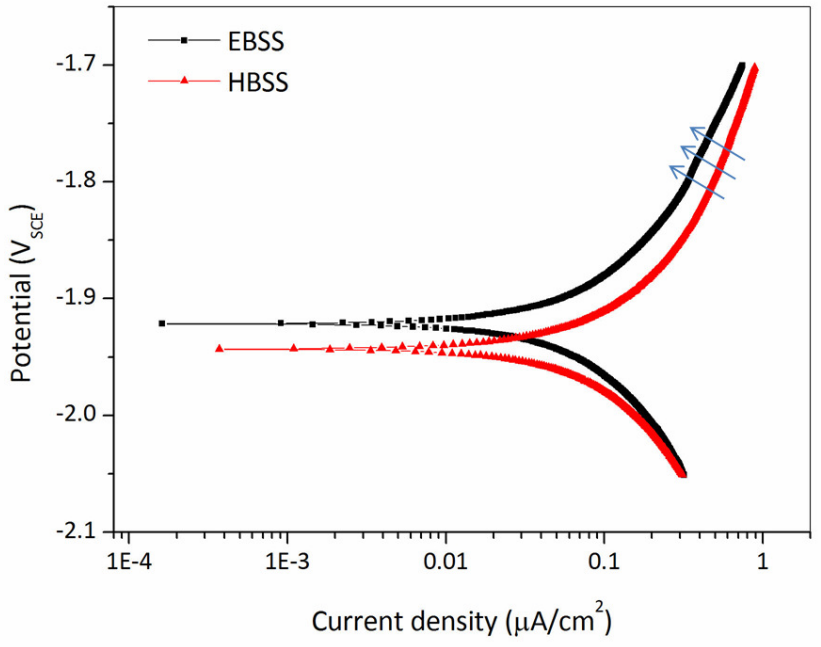

Figure 5-7: Polarisation curves of pure Mg in HBSS and EBSS. Anodic shift is indicated by arrows. (T_{phy}, 7.4)

The single biggest benefit of the PDP technique is that it allows quantification of the relative rates of the anodic and cathodic reaction over a range of potentials. This is vital when attempting to unravel the mechanistic aspects of Mg alloy biocorrosion. For example, two alloys with similar i_{corr} values may display significantly different anodic and cathodic kinetics. This is shown clearly for pure Mg and Mg-2Zr in MEM+FBS (Figure 5-8). Both samples resulted in a very similar i_{corr} yet displayed significantly different E_{corr} values due to a large shift in cathodic kinetics.

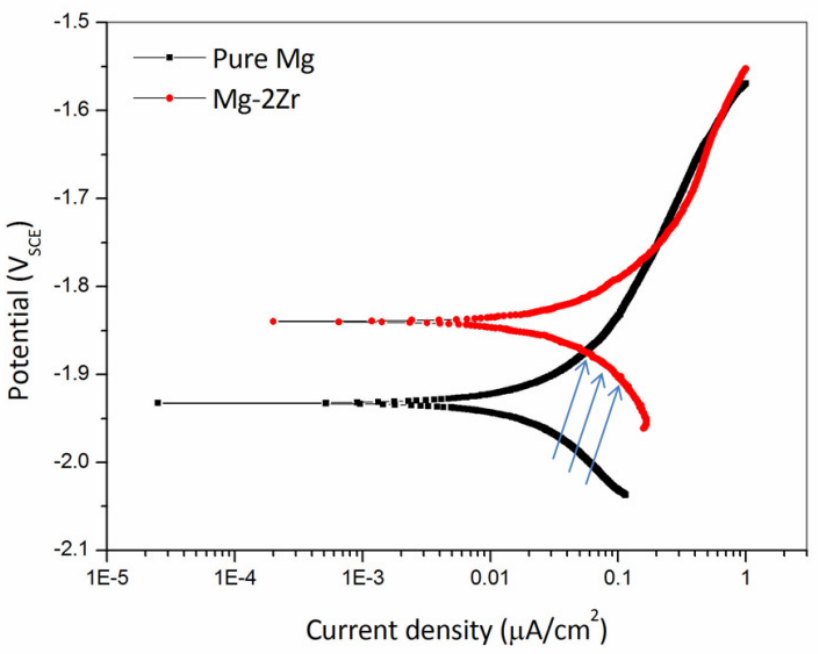

Figure 5-8 : Polarisation curves for pure Mg and Mg-2Zr. Arrows indicate cathodic shift. (MEM+FBS, T_{phy}, 7.4)

When utilised in a microelectrochemical setup, PDP may be used to explicate the microstructural effects of multi-phase alloys on the biocorrosion of Mg alloys in SBF (see Chapter 7). It may therefore be used to determine the individual contributions of each phase to the overall corrosion mechanisms of an alloy, which in turn may be used to tailor alloy microstructure for different corrosion rates and applications. PDP can furthermore be used to determine the effect of organic components (***e.g.*** proteins, amino acids) on individual phases, allowing optimisation of alloy microstructure for the biological environment.

5.3.2.1. Limitations and considerations when performing PDP tests

Due to the nature of the PDP test, the surface of a Mg sample will experience significant perturbation during the experiment owing to the excessive currents achieved. This means that only a single scan may be performed on a sample before it must be removed and re-polished. This also limits the surface analysis (*e.g.* SEM) that may be performed on the corroded surface as the reactions are artificially accelerated during the test.

Cyclic voltammetry, a potentiodynamic polarisation technique widely used to analyse layer formation [34], is not suitable for Mg alloys in SBFs due to their rapid corrosion and subsequent changes of the sample surface during scanning. Consequently PDP cannot typically be used to reveal the individual contributions of any layers that form on the surface of Mg other than their overall effect on i_{corr} and shift in E_{corr}.

It should be noted that the majority of uncoated Mg alloys corrode non-uniformly. The conversion of i_{corr} to a corrosion rate assumes that general (uniform) corrosion takes place [35]. Thus, PDP results do not typically yield an absolute corrosion rate for Mg, but rather are indicative of the severity of the corrosion that is occurring at a specific point in time.

One of the most important considerations when performing PDP experiments is the choice of the time at which to commence the scan. When a metal is initially exposed to an electrolyte, it takes a finite amount of time to transform an air-formed oxide film into an electrical double layer (EDL) (see Chapter 4.3.5.) [36]. Performing scans before the EDL is allowed to form results in wide inconsistencies in the current required to alter the potential and will not accurately reflect the electrode reactions [37]. This is shown in an investigation on pure Mg with varying OCP settling times of 0-20 min (Figure 5-9). It can be seen that the 0 and 3 min samples displayed different reaction rates resulting in more negative E_{corr}, larger i_{corr}, and increased “noise” in the recorded anodic points. The curves of the 15 and 20 minute settling times, on the other hand, are virtually identical, indicating the EDL had fully formed. For the sake of comparison between alloys or solutions, all PDP scans in this work were performed after a ~15 min period during which the OCP was found to stabilise.

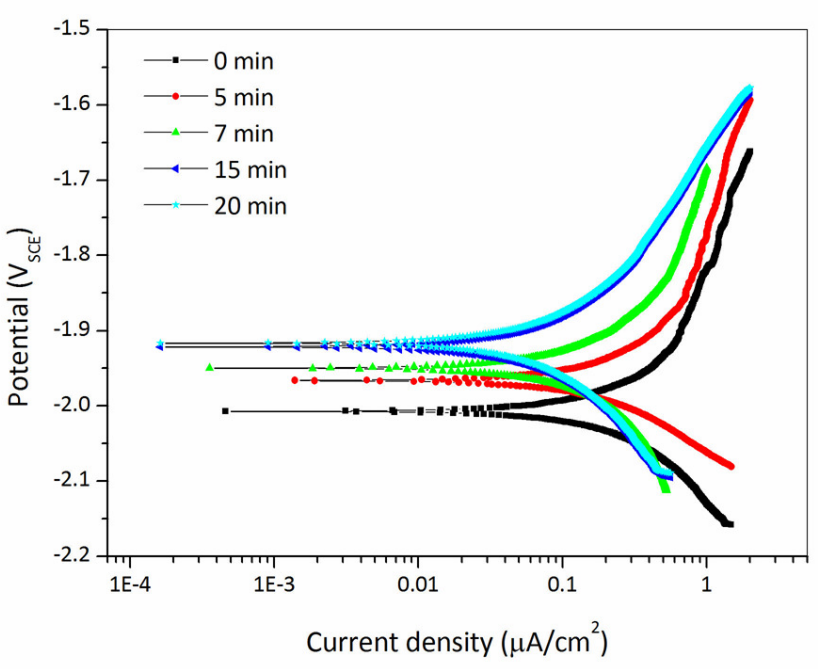

Figure 5-9 : Polarisation curves of pure Mg with varying OCP settling times before scan commencement. (HBSS, T_{phy}, 7.4)

However, results obtained at this early time point may vary significantly with those taken at later stages. This is displayed clearly in Figure 5-10, where the measured i_{corr} rapidly decreases during the first 10 hrs, after which it appears to stabilise. The variation in i_{corr} is likely due to formation of layers on Mg and variations in surface morphology; it appears that the i_{corr} after these changes have occurred, i_{corr} appears to be more representative of the long-term corrosion behaviour. Yamamoto ***et al.*** indicated that PDP testing performed in the early stages of immersion (< 1 hr) may not accurately represent the corrosion process present for the majority of the life of the implant [1].

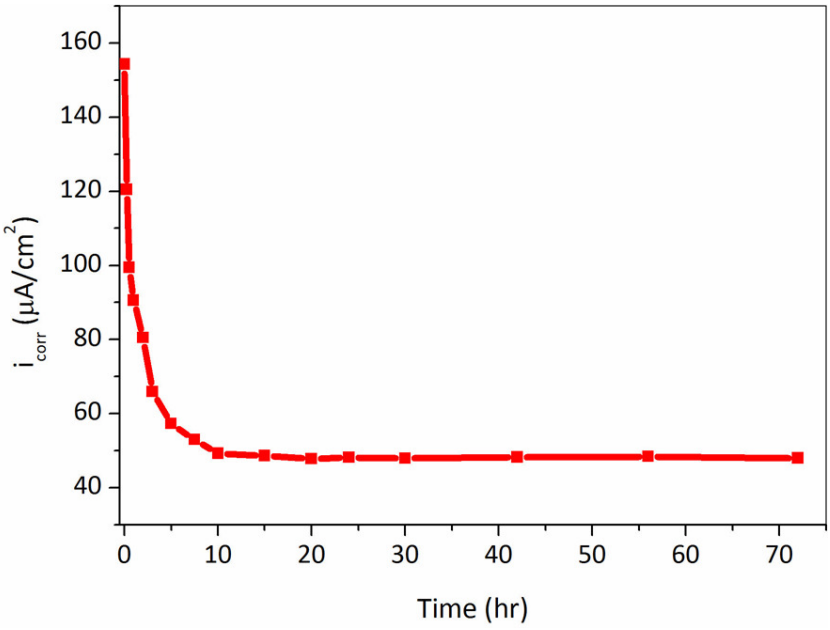

Figure 5-10 : Current density measurements from PDP testing performed over 72 hrs for pure Mg. (HBSS, T_{phy}, 7.4)

Unfortunately, it is not known to what extent the surface area may have altered by this point, making the selection of an ideal starting time difficult at this stage. PDP is an instantaneous test, and as such represents only a snapshot of the corrosion at the time it is performed. This is analogous to measuring the temperature at one time point compared with the average temperature over a day. Thus, although it is clear the i_{corr} at earlier stages is not necessarily representative of all time points, the results are still indicative of the corrosion mechanisms that are taking place and provides a useful tool for comparing multiple variables (*e.g.* changing temperature or alloys).

The potential range over which a PDP scan is performed is another consideration that is especially relevant to rapidly corroding Mg in SBF. Normally this range should provide just enough data to allow a Tafel-type analysis. Polarising a Mg sample further away from its open circuit potential (OCP) can cause increasingly rapid corrosion to occur while the scan is running, impacting obtained results. This is shown when comparing the polarisation curves of pure Mg samples with different scan ranges (-150 mV and -500 mV below OCP) (Figure 5-11). The curve for the -500 mV sample was much more “noisy” than for the -150 mV sample. This is indicative that the increased polarisation away from OCP resulted in perturbations of the sample surface before the scan could complete. For the alloys

investigated in this work, a range of 150 mV below the OCP to 500 mV above was found to provide ample data for analysis without noticeably affecting the corrosion process.

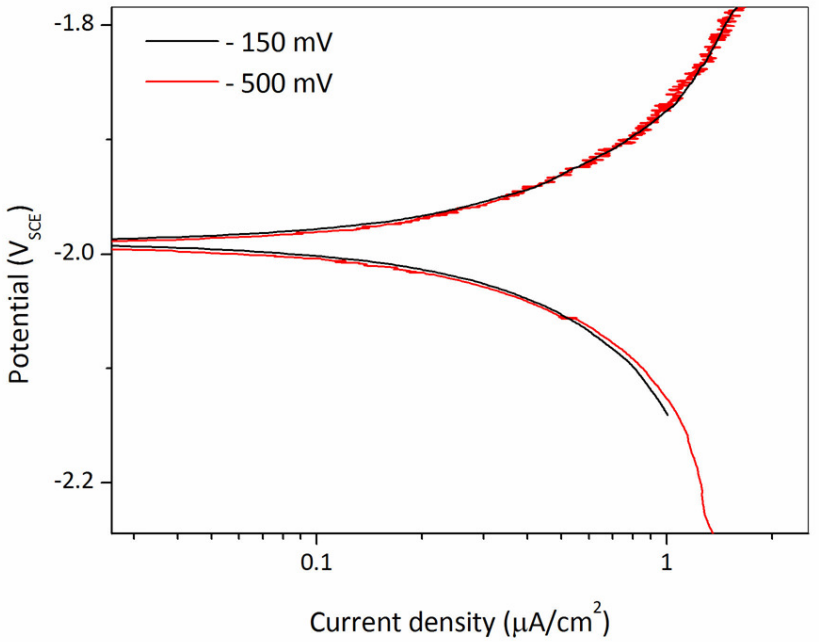

Figure 5-11 : Polarisation curve (close up) of pure Mg scanned over different potential ranges (-150 mV and -500 mV below E_{corr}). (HBSS, T_{phy}, 7.4)

Other important aspects of PDP are the parameters used to perform the Tafel-type analysis. Small changes in the determined Tafel slopes can result in large changes in reported i_{corr}. These changes can often be by more than an order of magnitude due to the logarithmic nature of the current density scale. Consequently, the variation in analysis of the same data between researchers can result in different conclusions (Figure 5-12). It is widely accepted that analysis should not be performed within 50 mV of E_{corr}, as each of the individual reactions in this region is affected by the other [36]. However, it is difficult to set absolute parameters for analysis due to variation between different alloys and solutions. For example, some alloys may corrode so rapidly during the forced oxidation reaction that only the cathodic slope may be analysed effectively. Hence, the report of Tafel-type analysis in published works needs to be accompanied by a description of the voltage range over which the analysis was carried out, and the software and method used to execute the determination

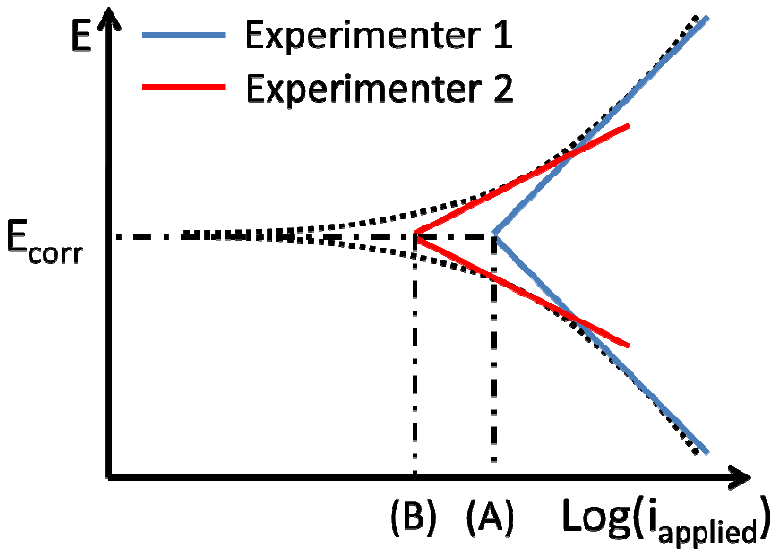

Figure 5-12 : Example of Tafel-type analysis of a set of data where slopes determined by different users result in different current densities (A and B).

Other factors that can affect PDP results include the potential scan rate, which is known to have a significant effect on the amount of current that is produced [38]. This experimental parameter must be determined by the user before starting experiments. Scan rates that are too slow allow the corrosion to change the surface area while the scan is being performed, especially for highly reactive materials like Mg. Scan rates that are too rapid do not allow sufficient time for the system to respond to the changing potential and to get an accurate reading of current density for each potential step. A number of different scan rates were studied for pure Mg to highlight the effect this parameter can have on the resulting polarisation curves (Figure 5-13). It can be seen that for the fast scan rates E_{corr} is not as clearly defined, there are fewer points on which to base Tafel-type analysis, and the current densities are very high (Figure 5-13B). The slower scan rates, 10 mV/s and 1 mV/s, resulted in relatively similar curves (Figure 5-13A). However, in this work 10 mV/s was found to be unsuitable for faster corroding alloys as it resulted in significantly more variation between different scans of the same sample. The slowest scan rate, 0.1 mV/s, was found to show signs of “noise”, especially for the anodic curve. This is likely because the potential is being forced away from the OCP for extended periods, allowing corrosion to occur.

Ultimately, a scan rate of 1 mV/s was chosen for Mg alloys in this study because: (i) it is widely used to investigate Mg alloys in SBFs and similar solutions in the literature [39-42],

(ii) it was found in this work to provide consistent, repeatable results for all alloys, and (iii) using a single, suitable scan rate for all tests allowed for greater comparison of data.

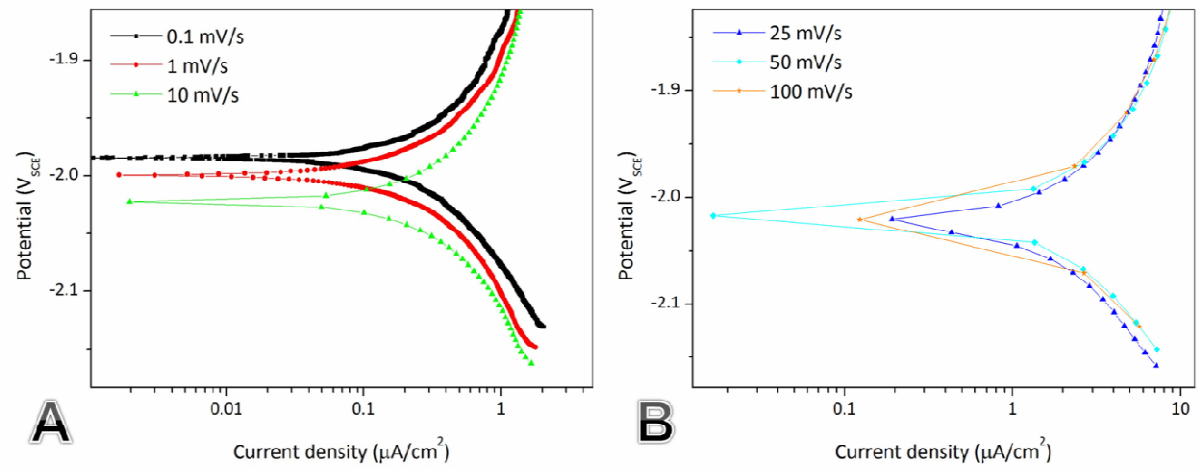

Figure 5-13 : Polarisation curves of pure Mg using a range of scan rates from 0.1-100 mV/s. (HBSS, T_{phy}, 7.4)

The effect of solution resistance also needs to be considered. However, this is usually minimised by the use of a Luggin capillary, which connects the reference electrode directly to the surface of the sample. This was the case for the corrosion cell used for this work.

5.3.3. Electrochemical impedance spectroscopy – Determination of corrosion layer behaviour

Electrochemical impedance spectroscopy (EIS) is a fairly recent technique that may be used to characterise surfaces of a sample using the frequency response of AC polarisation [43, 44]. In recent years, this technique has grown in popularity in the field of Mg corrosion. Since its development, over 50 publications have used EIS to study the corrosion of Mg alloys for biomedical applications. EIS can provide instantaneous data on the impedance reaction of a surface due to polarization [45]. This is intrinsically tied to the corrosion resistance, and it can be used to determine the likelihood of corrosion occurring [44]. Unlike PDP, EIS is a non-destructive technique for Mg in SBF. This allows for multiple recordings of the same sample without having to re-polish the sample surface after each scan.

One of the most beneficial uses of EIS is its ability to detect individual layers on the surface of the Mg [46]. Used over longer periods it can detect the formation of a corrosion layer, such

as CaP, on the Mg and determine how much this layer is contributing to the protection of the underlying Mg surface. This can be seen when pure Mg is investigated in different media, as the Nyquist plot shows a clear secondary time constant, and hence layer, in HBSS but not in NaCl (Figure 5-14). This behaviour can be confirmed using Bode diagrams. EIS can also be used to determine the protection offered by coatings placed on the Mg prior to corrosion, and to pinpoint when these layers start to break down [44]. This is crucial to the study of Mg in SBF because the CaP layers that form provide the majority of the protection to the Mg subsurface, and consequently understanding their behaviour is imperative.

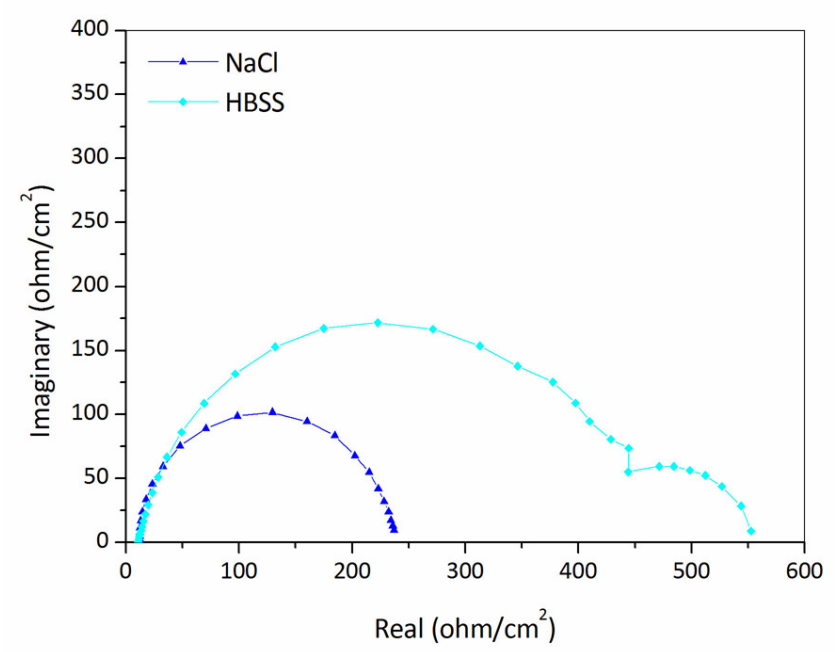

Figure 5-14 : Nyquist plot of pure Mg in NaCl and HBSS after 2 hrs immersion. Second semi-circle is indicative of layer formation on surface. (T_{phy}, 7.4)

In addition, if the slopes of the individual reactions from the PDP data are known for a given setup, it is possible to apply the Stern-Geary equation to obtain an approximate corrosion current density (i_{corr}) from EIS data (Equation 5-4) [47].

$$i_{corr} = B/R_P \quad [B = (b_a \times b_c)/(2.3(b_a+b_c))] \qquad \text{Equation 5-4}$$

Where R_P is the polarisation resistance, B is the proportionality constant as determined by b_a and b_c, the anodic and cathodic Tafel slopes, respectively. However, this method relies on an accurate determination or assumption of the Tafel slopes, which in turn requires correct

analysis of polarisation data. For Mg in SBF this can be difficult as measurements of the anodic and cathodic slopes change when significant corrosion occurs.

5.3.3.1. Limitations and considerations for EIS in analysis of Mg in SBF

Consideration should be given to the fact that EIS only provides partial information regarding corrosion kinetics. It cannot determine shifts in E_{corr} caused by different alloys or solutions. This makes the study of individual contributions due to microstructural features (*e.g.* secondary phases) more difficult.

EIS also does not directly yield a corrosion rate, and is susceptible to degradation that occurs while the scan is running. This degradation can make low frequency measurements difficult, as the active reactions continue while the impedance/resistance is recorded (*e.g.* Figure 5-15). This low frequency "drift" behaviour is especially apparent for Mg in SBF due to its relatively rapid rate of dissolution.

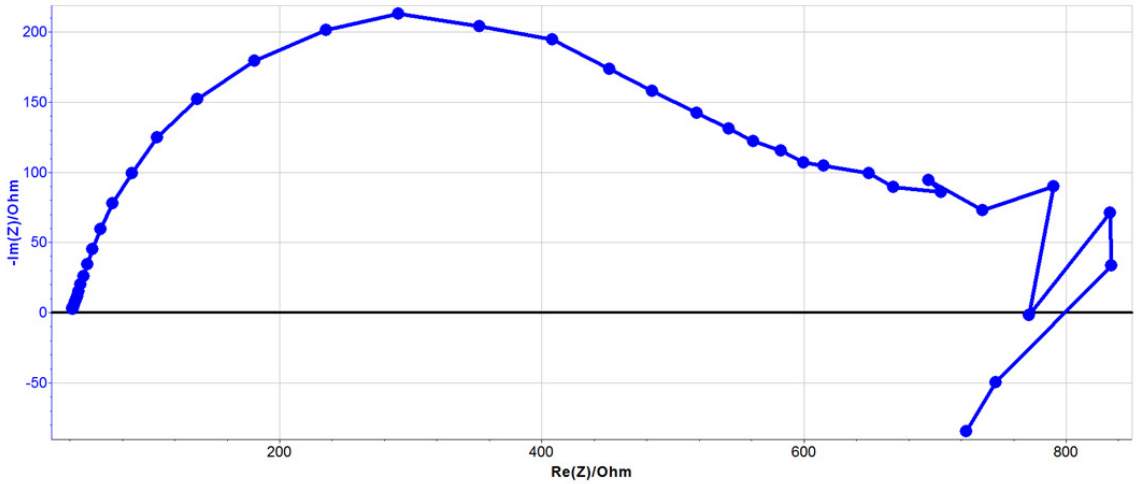

Figure 5-15 : Example of a Nyquist plot of pure Mg where active corrosion interferes with low-frequency behaviour as shown by the large variance to the right. (HBSS, T_{phy}, 7.4)

The electrochemical reactions at the surface must be analysed in terms of an equivalent circuit in order to convert frequency response data to corrosion properties (*e.g.* resistance and impedance). However, problems can arise as often multiple equivalent circuits may fit the same data, which can result in significantly different calculated values, particularly for

resistance (Figure 5-16). Only an equivalent circuit that accurately approximates the actual reactions and layers present at the surface will yield a meaningful interpretation of the data. An understanding of the corrosion mechanisms and potential layers that may be forming is therefore necessary to choose a circuit that accurately represents the surface electrochemistry. Due to the varying nature of the Mg corrosion layers, which depend heavily on *in vitro* variables (*e.g.* media, buffer), the correct choice of circuit can be difficult.

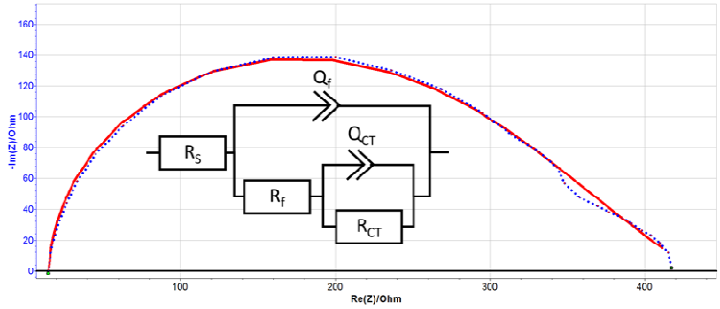

Component	Value (Ω)
R_s	15.23
R_{CT}	292.6
R_f	139.2

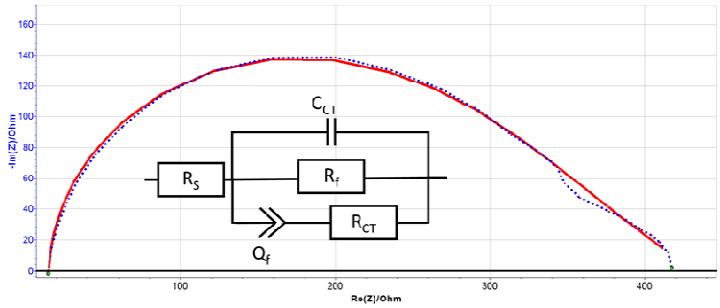

Component	Value (Ω)
R_s	15.34
R_{CT}	434.1
R_f	4.5

Figure 5-16 : Analysis of the same EIS data of pure Mg using two different equivalent circuits. The resulting resistance components are shown to the right. (HBSS, T_{phy}, 7.4)

5.4. Conclusions

Mass loss experiments currently provide the best method of determining the actual amount of corrosion that has occurred for Mg alloys *in vitro*. They are simple to set up and no other test can provide the same accuracy for physical loss measurement. However ML tests do not reveal any of the mechanistic behaviours of Mg alloys. In this work two alloys with a similar total mass loss over 1 week were found to have significantly varied reaction rates (Figure 5-1). It was also found that the sample surface area to solution ratio is crucial to the amount of mass loss that occurs (Figure 5-2). Experiments should be designed to ensure this ratio is appropriate for experimental parameters such as the frequency of solution refreshment. ML

experiments are also liable for greater discrepancy in results due to variation between samples, and sample preparation protocols should therefore be carefully followed.

Hydrogen evolution experiments are effectively a more advanced ML test where the amount of corrosion that has occurred may be determined at any specific point in time. However, many considerations must be taken into account when performing H_2^{evo} tests. For example, other gases may form during tests that can affect the recorded H_2 collection (Figure 5-4). The H_2^{evo} technique also may not accurately identify the physical corrosion of many alloys, as dealloying may lead to undetected mass loss. Experimental conditions such as the atmospheric pressure, funnel placement (Figure 5-5), and samples preparation (Figure 5-6) may also influence results. Most importantly, the majority of the bio-Mg literature has not achieved the theoretical 1:1 ratio of hydrogen evolved to actual mass loss (Table 5-2). This is perhaps the most crucial finding, and highlights the importance of making mass loss measurements at the end of H_2^{evo} experiments to confirm results.

Potentiodynamic polarisation is a dynamic electrochemical technique that is crucial for determining and quantifying the mechanistic corrosion of Mg alloys in SBF. It clarifies which reaction is controlling the overall corrosion rate and provides information on the kinetic and thermodynamic differences between various alloys and solutions (Figure 5-7, Figure 5-8). Using a microcell it is also possible to use PDP to determine not only the effect that individual phases may have on the corrosion mechanisms of the alloys themselves, but also the individual effects of organic components on the microstructure. However, PDP remains a single-time point test, destroys the sample surface, and for Mg in SBF cannot accurately be converted to a corrosion rate. It also does not allow in-depth analysis of the corrosion layers that form due to the rapid dissolution of Mg in the bio-electrolytes. Factors such as OCP settling time (Figure 5-9), potential scan range (Figure 5-11) and scan rate (Figure 5-13) can all influence the results and should be carefully selected by the experimenter.

The primary benefit of electrochemical impedance spectroscopy on Mg alloys in SBF is that it discloses the behaviour of the corrosion layers that form on the sample (Figure 5-14). EIS is capable of determining the time-dependent formation and dissolution of any layer at the Mg surface, and can provide quantitative analysis of the protection a given layer provides. However, at low frequencies EIS results can be affected by the continuing Mg dissolution, causing shifts and inaccuracies in the recorded data (Figure 5-15). The choice of equivalent

electrical circuit can also play a significant role in the results obtained (Figure 5-16). Consequently, correct use of EIS requires a thorough understanding of the corrosion processes and of how they might be represented in the gathered data.

All the techniques discussed in this chapter, with the exception of pH monitoring, are complimentary to each other in the quest to understand Mg biocorrosion. No single experiment provides all the information required to fully understand the corrosion behaviour of Mg and its alloys in SBF. Each offers unique benefits unobtainable through the other testing methods. Clearly, care must be taken when basing conclusions on just one or two types of test, especially when using only short term data.

Although further work is required to determine the correlation between Mg corrosion *in vitro* and *in vivo*, it is first important that the benefits and limitations of the various *in vitro* methods are understood. All relevant experimental parameters must be carefully defined, controlled, and reported in any published work to make these experiments repeatable. Unfortunately, in over 100 published studies, less than 10% contain reproducible work. This is a significant problem, as the number of variables and therefore potential mistakes that can be made greatly hinders the collective use of this data.

It is important in future work that stricter guidelines and clarity of reporting be adopted by the bio-Mg community; this will improve the general understanding of the *in vitro* corrosion behaviour of Mg and allow rapid progress to be made.

5.5. References

[1] Yamamoto, A., S. Hiromoto. *Effect of Inorganic Salts, Amino Acids and Proteins on the Degradation of Pure Magnesium in Vitro*. Materials Science and Engineering: C 2009;29:1559.

[2] Witte, F., J. Nellesen, H.-A. Crostack, V. Kaese, A. Pisch, F. Beckmann, H. Windhagen. *In Vitro and in Vivo Corrosion Measurements of Magnesium Alloys*. Biomaterials 2006;27:1013.

[3] ASTM International. Astm Standard G31-72, "Standard Practice for Laboratory Immersion Corrosion Testing of Metals". West Conshohocken, PA: ASTM International, 2004.

[4] Li, L., J. Gao, Y. Wang. *Evaluation of Cyto-Toxicity and Corrosion Behavior of Alkali-Heat-Treated Magnesium in Simulated Body Fluid*. Surface and Coatings Technology 2004;185:92.

[5] Wang, H., Z.M. Shi, K. Yang. *Magnesium and Magnesium Alloys as Degradable Metallic Biomaterials*. Advanced Materials Research 2008;32:207.

[6] Vojtěch, D., H. Čížová, K. Volenec. *Investigation of Magnesium-Based Alloys for Biomedical Applications*. Kovove Mater 2006:211.

[7] Hort, N., Y. Huang, D. Fechner, M. Störmer, C. Blawert, F. Witte, C. Vogt, H. Drücker, R. Willumeit, K.U. Kainer, F. Feyerabend. *Magnesium Alloys as Implant Materials - Principles of Property Design for Mg-Re Alloys*. Acta Biomaterialia 2010;6:1714.

[8] Gu, X., Y. Zheng, Y. Cheng, S. Zhong, T. Xi. *In Vitro Corrosion and Biocompatibility of Binary Magnesium Alloys*. Biomaterials 2009;30:484.

[9] Staiger, M.P., A.M. Pietak, J. Huadmai, G. Dias. *Magnesium and Its Alloys as Orthopedic Biomaterials: A Review*. Biomaterials 2006;27:1728.

[10] Baranenko, V.I., V.S. Kirov. *Solubility of Hydrogen in Water in a Broad Temperature and Pressure Range*. Atomic Energy 1989;66:30.

[11] Crozier, T.E., S. Yamamoto. *Solubility of Hydrogen in Water, Sea Water, and Sodium Chloride Solutions*. Journal of Chemical & Engineering Data 1974;19:242.

[12] Wilhelm, E., R. Battino, R.J. Wilcock. *Low-Pressure Solubility of Gases in Liquid Water*. *Chemical Reviews* 1977;77:219.

[13] Barton, R.S. *The Permeability of Some Plastic Materials to H2, He, N2, O2, and a,*. Atomic Energy Research Establishment Report 1960.

[14] Piskarev, I., V. Ushkanov, N. Aristova, P. Likhachev, T. Myslivets. *Establishment of the Redox Potential of Water Saturated with Hydrogen*. Biophysics 2010;55:13.

[15] Denkena, B., A. Lucas. *Biocompatible Magnesium Alloys as Absorbable Implant Materials - Adjusted Surface and Subsurface Properties by Machining Processes.* CIRP Annals - Manufacturing Technology 2007;56:113.

[16] Ren, Y., J. Huang, B. Zhang, K. Yang. *Preliminary Study of Biodegradation of Az31b Magnesium Alloy*. Frontiers of Material Science in China 2007;1:401.

[17] Ren, Y., H. Wang, J. Huang, B. Zhang, K. Yang. *Study of Biodegradation of Pure Magnesium*. Key Engineering Materials 2007;342-343:601.

[18] Song, G., A. Atrens, D.H. St. John. *An Hydrogen Evolution Method for the Estimation of the Corrosion Rate of Magnesium Alloys*. In: Hyrn, J.N., editor. Magnesium Technology 2001 Symposium. New Orleans: Minerals, Metals & Materials Society, 2001. p.255.

[19] Xin, Y., C. Liu, X. Zhang, G. Tang, X. Tian, P.K. Chu. *Corrosion Behavior of Biomedical Az91 Magnesium Alloy in Simulated Body Fluids*. Journal of Materials Research 2007;22:2004.

[20] Song, G. Recent Progress in Corrosion and Protection of Magnesium Alloys. Advanced Engineering Materials 2005;7:563.

[21] Shi, Z., M. Liu, A. Atrens. *Measurement of the Corrosion Rate of Magnesium Alloys Using Tafel Extrapolation*. Corrosion Science 2010;52:579.

[22] He, W., E. Zhang, K. Yang. *Effect of Y on the Bio-Corrosion Behavior of Extruded Mg-Zn-Mn Alloy in Hank's Solution*. Materials Science and Engineering: C 2009;30:167.

[23] Liu, C., Y. Xin, G. Tang, P.K. Chu. *Influence of Heat Treatment on Degradation Behavior of Bio-Degradable Die-Cast Az63 Magnesium Alloy in Simulated Body Fluid*. Materials Science and Engineering: A 2007;456:350.

[24] Lopez, H.Y., D.A. Cortes, S. Escobedo, D. Mantovani. *In Vitro Bioactivity Assessment of Metallic Magnesium*. Key Engineering Materials 2006;309-311:453.

[25] Lorenz, C., J.G. Brunner, P. Kollmannsberger, L. Jaafar, B. Fabry, S. Virtanen. *Effect of Surface Pre-Treatments on Biocompatibility of Magnesium.* Acta Biomaterialia 2009;5:2783.

[26] Ng, W.F., K.Y. Chiu, F.T. Cheng. *Effect of Ph on the in Vitro Corrosion Rate of Magnesium Degradable Implant Material*. Materials Science and Engineering: C 2010;30:898.

[27] Song, G., S. Song. *A Possible Biodegradable Magnesium Implant Material*. Advanced Engineering Materials 2007;9:298.

[28] Wang, Y., M. Wei, J. Gao. *Improve Corrosion Resistance of Magnesium in Simulated Body Fluid by Dicalcium Phosphate Dihydrate Coating*. Materials Science and Engineering: C 2009;29:1311.

[29] Wang, Y., M. Wei, J. Gao, J. Hu, Y. Zhang. *Corrosion Process of Pure Magnesium in Simulated Body Fluid*. Materials Letters 2008;62:2185.

[30] Yan, T., L. Tan, D. Xiong, X. Liu, B. Zhang, K. Yang. *Fluoride Treatment and in Vitro Corrosion Behavior of an Az31b Magnesium Alloy*. Materials Science and Engineering: C;In Press, Accepted Manuscript.

[31] Yang, L., E. Zhang. *Biocorrosion Behavior of Magnesium Alloy in Different Simulated Fluids for Biomedical Application*. Materials Science and Engineering: C 2009;29:1691.

[32] Zhao, M.-C., M. Liu, G.-L. Song, A. Atrens. *Influence of Ph and Chloride Ion Concentration on the Corrosion of Mg Alloy Ze41*. Corrosion Science 2008;50:3168.

[33] Zhuang, H., Y. Han, A. Feng. *Preparation, Mechanical Properties and in Vitro Biodegradation of Porous Magnesium Scaffolds*. Materials Science and Engineering: C 2008;28:1462.

[34] Gosser, D.K. *Cyclic Voltammetry: Simulation and Analysis of Reaction Mechanisms*. New York: John Wiley & Sons, Inc., 1993.

[35] ASTM International. Astm Standard G102-89, "Standard Practice for Calculation of Corrosion Rates and Related Information from Electrochemical Measurements". West Conshohocken, PA: ASTM International, 2004.

[36] Tait, W.S. *An Introduction to Electrochemical Corrosion Testing for Practicing Engineers and Scientists*. Racine, Wisconsin: PairODocs Publications, 1994.

[37] Wang, J. *Analytical Electrochemistry (Second Edition)*. New York: Wiley-VCH, 2002.

[38] Zhang, X.L., Z.H. Jiang, Z.P. Yao, Y. Song, Z.D. Wu. *Effects of Scan Rate on the Potentiodynamic Polarization Curve Obtained to Determine the Tafel Slopes and Corrosion Current Density*. Corrosion Science 2009;51:581.

[39] Fekry, A.M., R.M. El-Sherif. *Electrochemical Corrosion Behavior of Magnesium and Titanium Alloys in Simulated Body Fluid*. Electrochimica Acta 2009;54:7280.

[40] Op't Hoog, C., N. Birbilis, M.-X. Zhang, Y. Estrin. *Surface Grain Size Effects on the Corrosion of Magnesium*. Key Engineering Materials 2008;384:229.

[41] Birbilis, N., C. op't Hoog, Y. Estrin. *Corrosion of Pure Mg as a Function of Grain Size and Processing Route*. Advanced Engineering Materials 2008;10:579.

[42] Bender, S., J. Goellner, A. Heyn, E. Boese. *Corrosion and Corrosion Testing of Magnesium Alloys*. Materials and Corrosion 2007;58:977.

[43] Macdonald, J.R., E. Barsoukov, editors. *Impedance Spectroscopy: Theory, Experiment, and Applications*. New York: Wiley-Interscience, 2005.

[44] Ghali, E. *Conventional and Electrochemical Methods of Investigation. Corrosion Resistance of Aluminium and Magnesium Alloys : Understanding, Performance and Testing*. Hoboken, NJ, USA: John Wiley & Sons, Inc., 2010.

[45] MacDonald, D.D., M.C.H. McKubre. *Impedance Measurement Techniques*. In: Macdonald, J.R., editor. Impedance Spectroscopy: Emphasizing Solid Materials and Systems. New York: Wiley-Interscience, 1987. p.133.

[46] Lasia, A. *Electrochemical Impedance Spectroscopy and Its Applications*. In: Conway, B.E., Bockris, J., White, R.E., editors. Modern Aspects of Electrochemistry, vol. 32. New York, 1999. p.143.

[47] Stern, M., A.L. Geary. *Electrochemical Polarization: A Theoretical Analysis of the Shape of Polarization Curves*. Journal of the Electrochemical Society 1957;104:56.

CHAPTER 6: Influence of Experimental Variables on the *In Vitro* Performance of Magnesium Alloys

6.1. Introduction

A survey of the available literature reveals that over 75% of *in vitro* biodegradation studies of Mg alloys either failed to mention or to properly control variables that significantly influenced the results. For example, some investigations used unphysiological temperatures [1, 2], extremely basic media [3, 4], or have not adjusted or controlled the pH values to within the body's natural range [5, 6]. Others did not mention one or more of these values, making it impossible to determine what was and wasn't controlled [7, 8]. Essentially this affects the usefulness of any results and may invalidate the conclusions drawn.

The most important variables identified for a range of experiments based on the findings in this work are outlined below. Most apply to all corrosion and toxicity experiments that are carried out on Mg. Some variables, such as temperature, are simple to control and an ideal value can be provided. However for others, including choice of medium and buffering system, a greater understanding of the specific effects on degradation mechanisms is required to make an appropriate selection during experimental design.

6.2. Temperature

6.2.1. Introduction

It is vital to consider the temperature at which an experiment is performed given that electrochemical reactions are thermally activated. Given the already rapid corrosion rate of Mg alloys in mildly aggressive environments it is certainly possible that the difference of 12-17°C between room and physiological conditions can significantly affect results obtained from corrosion tests, and potentially the conclusions that are subsequently drawn. Of 92 papers on bio-Mg where the temperatures have been stated, 36 have performed experiments at room temperature or between 20 °C and 25 °C. This represents a significant portion of the

literature, over a third, where physiological temperature has not been fully considered. In addition, many other studies have either not controlled or monitored temperature, which presents a significant amount of work that is neither easily compared nor where the potential impact of physiological temperature has been considered. Further investigation is warranted into the effect this temperature difference may have on bio-Mg performance.

The aim of this work is to determine the effect the relatively small change between room and physiological temperature can have on the biocorrosion of Mg alloys. A number of media are investigated and both immersion and electrochemical methods are utilised to provide a more complete understanding of both the physical rates of corrosion and the underlying electrochemical reasons.

6.2.2. Experimental methods

6.2.2.1. Potentiodynamic polarisation

PDP experiments were carried out in a standard setup and conditions as described in Chapter 4.3.3. Experiments performed at room temperature (T_{rm}, 20 °C) and physiological temperature (T_{phy}, 37 °C) with a variance of ± 0.5 °C and pH was maintained at 7.4 ± 0.05.

A range of Mg alloys were analysed by PDP including Mg-0.4Ca, Mg-10Ca, Mg-1Zn, Mg-10Zn, Mg-1Mn, Mg-5Mn, Mg-0.57Zr, Mg-2Zr, Mg-0.4Ca-3Zn, Mg-5Ca-6.2Zn, AZ31, AZ91, and pure Mg. Apart from the AZ-series, the alloys were prepared using the casting method described in Chapter 4.1.2. These alloys were chosen because they represented a wide range of alloying additions both under and above their respective solid solubility in Mg, resulting in single, dual or multi-phase microstructures. The alloys were tested in HBSS as well as MEM+FBS.

6.2.2.2. Hydrogen evolution

Hydrogen evolution was measured using the experimental setup as described in Chapter 4.2.2. Temperature was controlled to T_{rm} and T_{phy} with a variance of ± 1°C. Measurements of evolved hydrogen were taken every 30-60 min during normal working hours over the course of 72 hrs. The medium was stirred and pH/temperature was recorded at each measurement time point, while the pH was corrected to maintain 7.4 ± 0.05.

6.2.2.3. Microstructural characterisation

Samples were prepared to characterise the surface morphology of pure Mg after 24 hrs of immersion for both T_{rm} and T_{phy}. These were optically inspected after the experiment using an Olympus B061 upright optical microscope. Selected samples were examined using a SEM.

6.2.3. Results and discussion

6.2.3.1. Shifts in corrosion potential due to increase in temperature

The change in corrosion potential (ΔE_{corr}) of the Mg alloys was determined from PDP measurements in HBSS and MEM+FBS at T_{rm} and T_{phy} (Figure 6-1). Overall a general trend towards a more electronegative potential was observed due to an increase in temperature. This would indicate that reactions were more likely to happen, as the processes would be more thermodynamically favourable. However, the trend is neither significant nor clear and with an average standard deviation of nominally ± 2%, many changes are within this range of uncertainty.

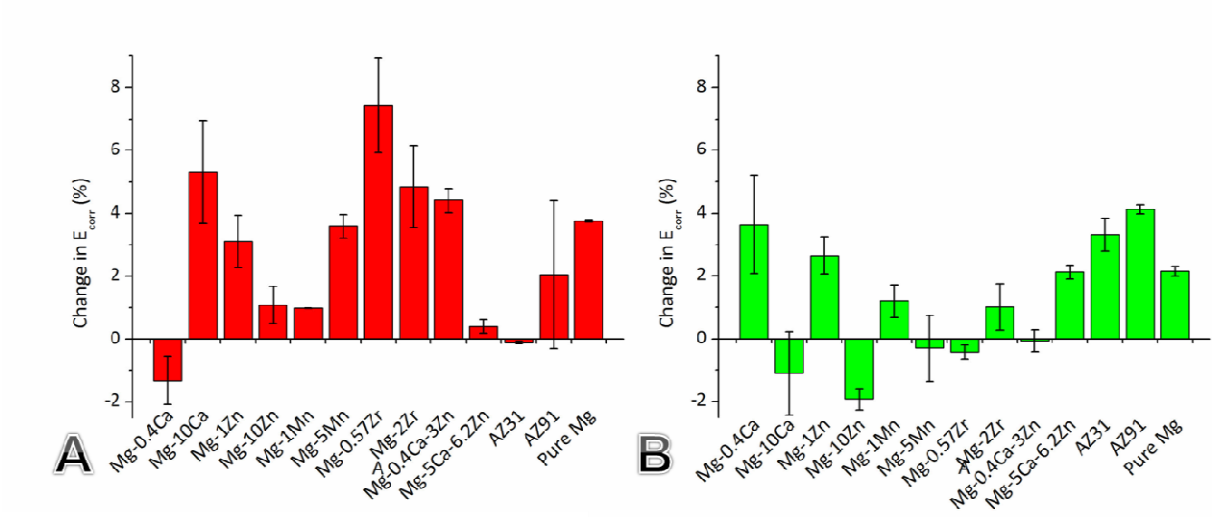

Figure 6-1 : ΔE_{corr} due to an increase in temperature from 20°C to 37°C for (A) HBSS and (B) MEM+FBS. Positive values indicate a more electronegative value. (7.4)

For alloys where the corrosion potential became more negative as the temperature increased, the process was likely controlled by the anodic reaction, meaning there were ample cathodic sites for hydrogen evolution to occur but the magnesium disassociation was restrained. This occurred for the majority of the alloys, as shown for Mg-10Ca and Mg-10Zn in HBSS

(Figure 6-2). Here it can be clearly seen that there is a significant shift in the anodic branch while the cathodic branch remains relatively constant. This indicates that the increased rate of oxidation of Mg is allowing for an increase in overall corrosion rate, and the processes are not cathodically limited.

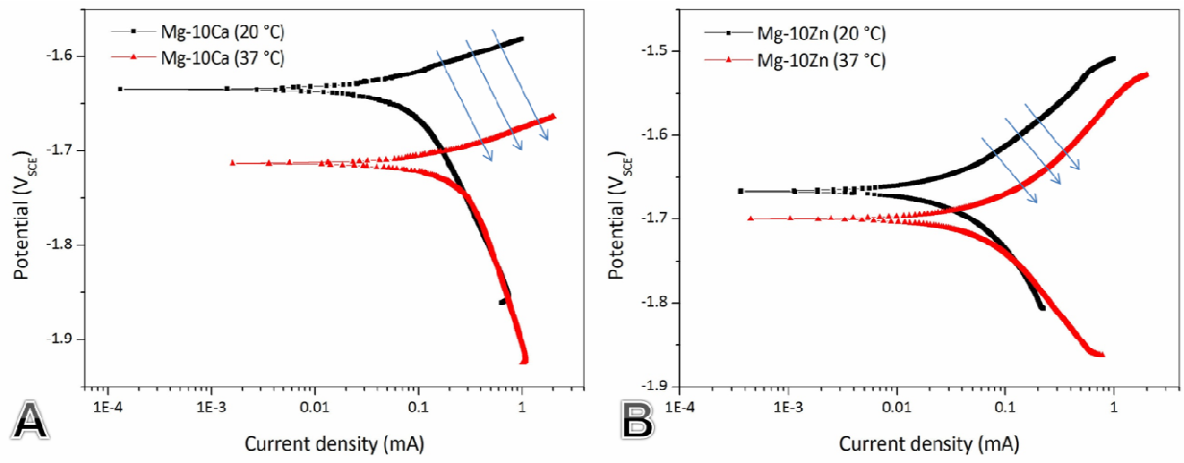

Figure 6-2 : Polarisation curves for (A) Mg-10Ca and (B) Mg-10Zn at 20 °C and 37 °C. Anodic shift is indicated by arrows. (HBSS, 7.4)

In a study of two alloys (WE43, AZ31), Zeng *et al.* found no obvious changes in E_{corr} between 20°C and 37°C in either a NaCl solution or HBSS, with a maximum variation of 5% [9]. They did not comment on the values except to say that the differences could be down to small changes in the microstructure or the stress on the surface. This may be partially responsible for the variation in results shown in this work, as differences are possible even if preparation steps are tightly controlled.

6.2.3.2. Increase in corrosion current density

Every alloy displayed a significant increase in i_{corr} due to the rise in temperature from T_{rm} to T_{phy} (Figure 6-3). For the cast alloys the i_{corr} increased from 64%-359% in HBSS and 14%-94% in MEM+FBS. Although AZ31 and AZ91 displayed the lowest corrosion rates at 20°C in both solutions they displayed the largest increase in i_{corr} due to the higher temperature, rising 211% and 840% in HBSS and 437% and 376% in MEM+FBS, respectively.

It is possible that the acceleration in corrosion may be due to a number of factors. Firstly, there will be an increase in reaction kinetics of both the cathodic and anodic processes due to

the increased energy in the solution. Molecules at higher temperatures have more thermal energy, which increases not only the collision frequency but also the proportion of reactant molecules with sufficient energy to exceed the activation energy (and react). For most alloys, this was shown to be anodically controlled (Figure 6-2).

Secondly, a rise in the diffusion of hydrogen ions due to the rise in temperature could increase the corrosion rate as the H_2 gas would diffuse away from the surface more quickly. It has been proposed that, in mildly acidic solutions, the entire process of magnesium corrosion is primarily controlled by the transport rate of hydrogen on the surface (cathodically limited) and thus the increase in diffusion of hydrogen is the main factor for increasing corrosion [10]. However, this would indicate cathodic control, which did not appear to be the case for the majority of the alloys. Finally, the additional energy in the system would cause the chloride ions to have a significantly amplified reaction rate with the Mg, further reducing its resistance [11].

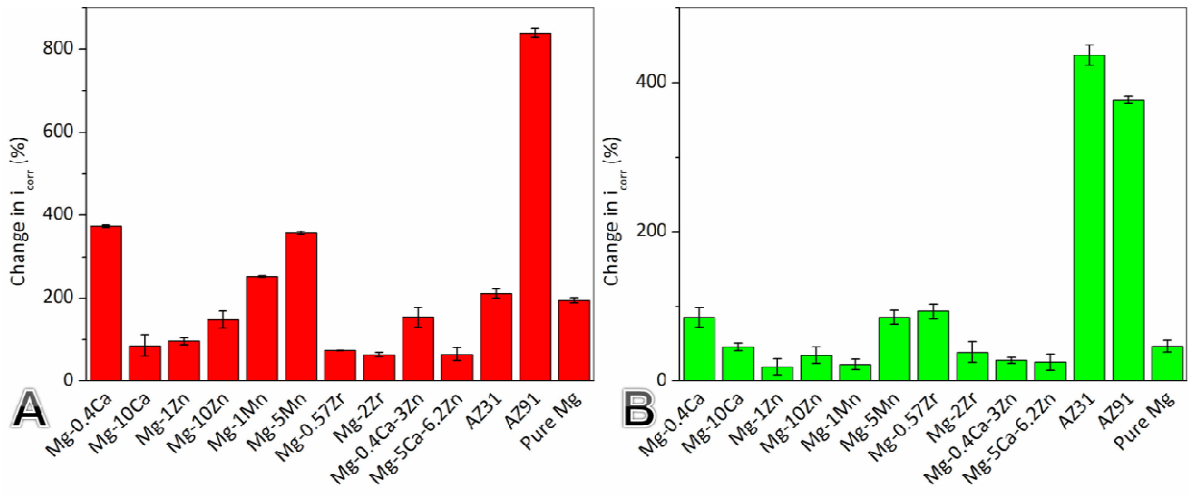

Figure 6-3 : Δi_{corr} due to increase in temperature from 20°C to 37°C for (A) HBSS and (B) MEM+FBS. (7.4)

One key finding from this work is that both the alloy itself and the solution can have a significant effect on the perceived change in corrosion at different temperatures. It is not acceptable to test one alloy and assume others will display a similar behaviour, as shown by the differences between the Mg-Ca and Mg-Zn alloying systems due to the change from T_{rm} to T_{phy} (Figure 6-3). Similar work for a range of metals in an acidic solution found a significant effect and variation in corrosion rates due to temperature change [12]. However, the solution itself can cause these mechanisms to vary and either amplify or reverse the

changes in i_{corr}. For example, i_{corr} of pure Mg increased by 200% in HBSS, while i_{corr} increased by 50% in MEM+FBS (Figure 6-3).

Zeng *et al.* found increased i_{corr} for WE43 and AZ31 of 363% and 290%, respectively, as the temperature increased from 20°C to 37°C in 0.9% NaCl [9]. However, the authors found that i_{corr} in HBSS actually decreased by 20% and 50%, respectively. This result contradicts the data for all alloys tested in this study. It is possible that the decreased i_{corr} result may be due to an amplified rate of CaP formation on the surface of the Mg immediately following immersion in the solution. If the PDP experiment is started right away, or before the OCP is allowed to settle, then this layer may have formed more quickly at the higher temperature and thus shown increased corrosion protection at 37°C than 20°C. However, this is unlikely as the reaction rates of the Cl^- ions with the Mg would also have increased. It is important to note that Zeng *et al.* performed the study on only two alloys and did not report the number of repetitions or Tafel-type analysis conditions used to obtain their results [9]. They also performed the PDP scan from 300 mV below the OCP. This is a range typically wider than required to obtain sufficient points to perform Tafel-type analysis, and presents a problem as it causes significantly more cathodic polarisation and may result in a potentially altered surface, negatively impacting the accuracy of their results.

6.2.3.3. Evolution of H_2 over 72 hrs for Mg alloys at T_{rm} and T_{phy}

Analysis of the H_2 evolution rate over time elucidates several important aspects of the corrosion of the alloys at the two temperatures (Figure 6-4). First, it can clearly be seen for both T_{rm} and T_{phy} that the evolution of hydrogen is much higher in the initial several hours than the rest of the experiment. After 24 hours the rate is approximately half its initial peak and is between 15-40% of the peak after 72 hours. This is important, as it is clear that considerably more corrosion occurs in this initial stage. It can also be seen that both temperatures displayed a levelling of the evolution rate after 1-2 days of immersion. Although this rate remained nearly constant for the last 20 hours of the experiment, the absolute values were over 100% greater in T_{phy} than T_{rm} for all alloys. This reinforces the electrochemical data indicating the significant effect the temperature can have on the corrosion rate

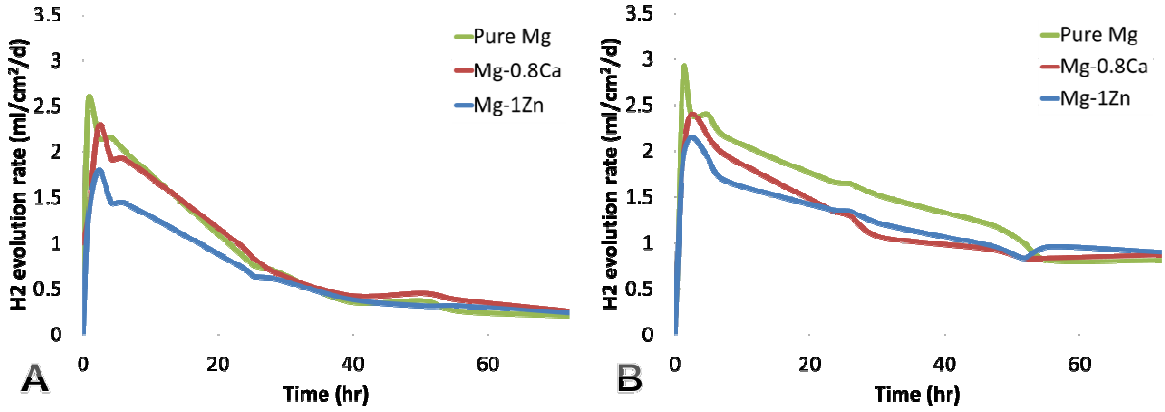

Figure 6-4 : H_2 evolution rate for alloys at (A) 20 °C and (B) 37 °C. (HBSS, 7.4)

The volume of hydrogen collected was converted into mass loss using the equation ML = $1.085V_H$ (see Chapter 4.2.2.), which was then converted into an average mass loss rate based on the time period (Figure 6-5).

The rise in temperature was found to result in a significant increase on the amount of hydrogen evolved and consequently the effective mass loss. Pure Mg displayed a 130% increase in corrosion rate, while Mg-0.8 and Mg-1Zn corroded 99% and 129% faster, respectively. Although the equivalent increase in corrosion rate for pure Mg was lower than that found using the electrochemical techniques, Mg-1Zn displayed a very similar corrosion increase to that found using PDP (Figure 6-3).

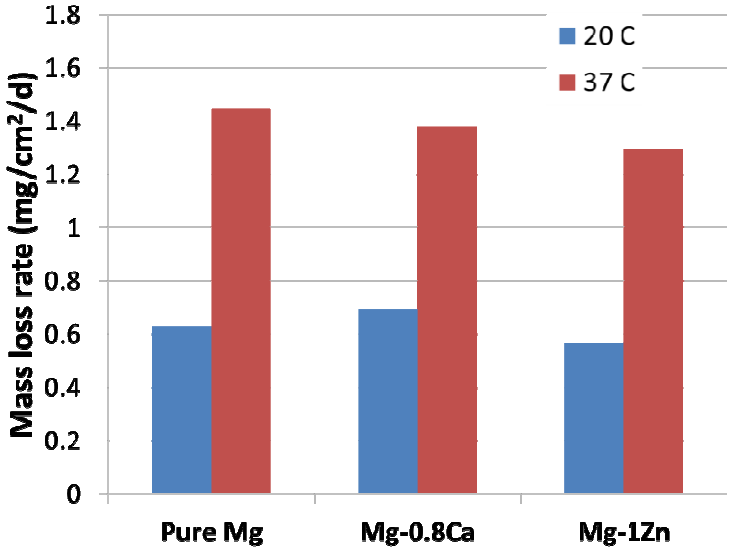

Figure 6-5 : Mass loss rate of alloys tested at 20°C and 37°C. (HBSS, T_{phy}, 7.4)

6.2.3.4. Limited variation in surface morphology of pure Mg

Analysis of the surfaces of the pure Mg at different time points and temperatures did not elucidate any clear differences. Electron micrographs of the corrosion morphologies at T_{rm} and T_{phy} were very similar at corresponding time points (Figure 6-6). This indicates that the corrosion mechanisms were comparable at both temperatures, and the increase in i_{corr} may have been due primarily to an increase in reaction rates, not changes in surface morphology.

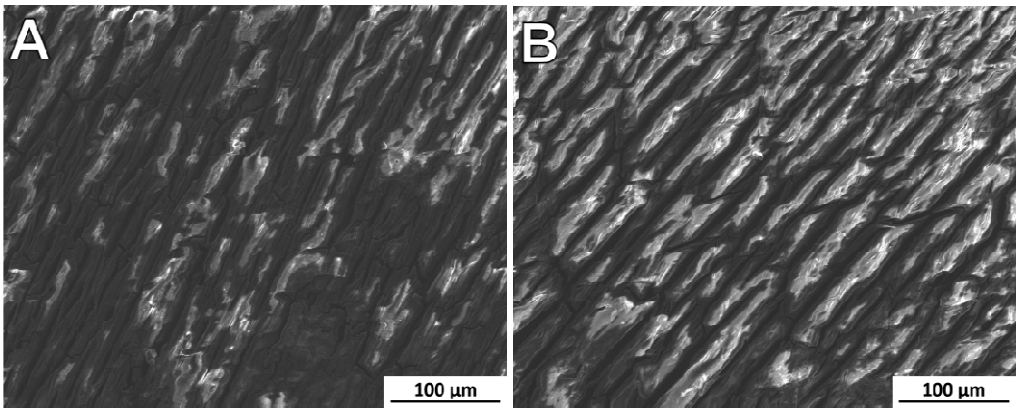

Figure 6-6 : Scanning electron micrograph of surface of pure Mg sample after 24 hours at (A) 20°C and (B) 37°C. (HBSS, 7.4)

6.2.4. Summary

It is clear that the temperature has a significant effect on the corrosion rate for a wide range of Mg alloys. A rise of just 17 °C resulted in an increased i_{corr} of up to 840% (Figure 6-3A) and a rise in evolved H_2 of up to 130% (Figure 6-4). This highlights the effect that such a relatively small increase in temperature can have on the degradation of Mg alloys. It was also found that the magnitude of this influence was heavily dependent on the alloy and the chosen solution. This makes it difficult to determine the exact relationship between temperature changes and the resultant corrosion performance for any alloy/solution combination without testing it.

In general, it was noticed that most recent *in vitro* bio-Mg studies have used physiological temperatures, perhaps as the authors have realised its importance. However, several recent papers have utilised room temperatures [13, 14] or have not stated the temperature that was

employed [6, 15]. When testing Mg alloys for biomedical purposes, the significance of using a physiological temperature cannot be understated.

6.3. Effect of solution pH on Mg biocorrosion

6.3.1. Introduction

It is well understood that the pH value of a solution has a significant effect on the corrosion of Mg and its alloys [16, 17]. A higher pH has also been known to cause increased and thicker formation of CaP compounds *in vitro* and *in vivo* [18, 19]. These layers are commonly found on Mg alloys in more realistic SBFs that contain the necessary Ca^{2+} and PO_4^{3-} not found in NaCl solutions [1, 20, 21]. pH also plays a significant role in the absorption of proteins [22]. The pH of the body is normally regulated between 7.4-7.6.

The design of the experiment may also play a role in the magnitude of the pH effect. For instance, if the ratio of surface area to solution is too large this can influence the local pH (at the metal surface) resulting in unrealistic corrosion conditions. This was found for AZ63 in Tyrode's medium where the pH rose to more than 10 within the first 24 hrs of measurement, failing to replicate the *in vivo* environment of an implant under normal conditions [23]. An artificially elevated pH leads to significantly decreased corrosion rates due to the formation of a more stable $Mg(OH)_2$ layer. Some studies have attempted to use the change in pH to determine how much corrosion has occurred [5, 23-25]. This method, discussed in more detail in Chapter 5.3.1. , is extremely limited in its utility and also allows the existence of non-physiological conditions.

Unfortunately, the majority of the Mg biocorrosion literature does not appear to consider the fact that the pH of the body is efficiently controlled when setting up experiments. Only 30 studies in the bio-Mg literature both adjusted the pH to the physiological range and maintained it in longer term experiments, either through buffering, changing of medium or the use of a large volume. A further 19 studies adjusted the pH, but did not maintain it. However, 58 studies did not adjust pH to physiological levels at all or maintain the chosen level. This severely limits the use of the data they have reported.

It is clear that an investigation is needed to examine the effect that pH can have on the degradation rates and mechanisms of Mg. A recent study by Ng *et al.* attempted this by investigating pure Mg in HBSS with pH values between 5.5 and 8 [26]. However the study performed only basic electrochemical analysis and, although it provided some information

towards the understanding of the role of pH in corrosion of Mg, it left significant gaps in knowledge that still need to be filled. The aim of this study was to further the understanding of how pH can affect not only the corrosion rate of Mg but also the morphology of corrosion layers that form on its surface.

6.3.2. Experimental Methods

6.3.2.1. pH measurement of multiple solutions

The measurement of the initial pH of the solution was performed with a SevenEasy® S20 pH/Temperature meter (Mettler-Toledo Inc.), which was calibrated before each reading. This meter was also used to determine the precise amount of 1 M NaOH/HCl buffer required to maintain the pH at with an accuracy of ± 0.02.

6.3.2.2. Electrochemical impedance spectroscopy

Scans were carried out at 30 min intervals during 24 hrs. EIS was also performed in HBSS of varying pH levels of 7.0, 7.2, 7.4, 7.6, and 7.8 to ±0.02. Experiments were carried out using the standard setup (see Chapter 4.3.5.). As the temperature, pH, area of the electrodes and distance between them were controlled in the tests, the solution resistance did not change for each sample set. This was approximately 15 ± 5 Ω for all pH values.

6.3.2.3. Potentiodynamic polarisation

PDP experiments were carried out at T_{phy} in the standard corrosion cell setup as described in Chapter 4.3.3. . pH was controlled in HBSS to the desired value of 7, 7.2, 7.4, 7.6 or 7.8 throughout the test to within ± 0.02.

6.3.2.4. Microstructural characterisation

Samples were inspected after each experiment using an Olympus B061 upright optical microscope. EIS samples were carbon coated and examined with a SEM following testing in the different solutions. Images were recorded across a range of magnifications, and EDS was performed to determine a quantitative chemical composition of the corrosion products.

6.3.3. Results and discussion

6.3.3.1. Corrosion media - pH values before adjustment

All of the pH values for the various solutions that were prepared over the course of this work are collated in Table 6-1. Due to differences in composition, the initial pH of the solutions varied considerably following their preparation. For the solutions investigated, this ranged from 5.11 to 6.54, depending on the temperature. The importance of this variation is highlighted by the fact that a wide range of studies either did not adjust or mention the pH value of the chosen medium, such as for NaCl solutions [27, 28], HBSS [29-31], MEM [32, 33], and MEM+BSA/FBS [32]. Others did not even mention the composition of the chosen medium [34].

Depending on the chosen solution the pH can be from 0.9 to 1.6 lower than that of normal physiological levels (nominally 7.4). This effectively means that all studies in which the solutions have not been adjusted have likely reported higher than normal corrosion, at least in the initial stages. The pH difference could also alter or completely stop the formation of $Mg(OH)_2$ or CaP corrosion layers.

It can also be seen in Table 6-1 that there is typically a drop in the measured pH between 20°C and 37°C. This is expected due to the nature of pH dependence on temperature through the Nernst equation. This highlights the importance of adjusting the pH to the desired value when the solution has reached the temperature at which the experiment will take place. Between T_{rm} and T_{phy} the pH values may vary up to 0.1. If not re-adjusted at the test temperature this may impact the results, as discussed in Chapter 6.3.3.2. For example, a quick trial found that adjusting the pH of HBSS to 7.40 at T_{rm} would result in a pH value of approximately 7.31 at T_{phy}.

Table 6-1 : Solution pH values of various media as prepared at different temperatures.

Solution	pH at 20 °C (±0.02)	pH at 37 °C (±0.02)
Distilled Water	6.49	6.5
8 g/L NaCl	5.87	5.85
NaCl + HEPES	5.28	5.17
HBSS	6.54	6.45
HBSS + HEPES	5.63	5.45
HBSS + SB	7.8	7.72
EBSS	5.08	4.94
EBSS + HEPES	5.14	5.11
EBSS + SB	7.54	7.45
PBS	7.41	7.37
PBS + HEPES	6.63	6.56
PBS + SB	7.63	7.58
MEM	4.97	4.90
MEM + HEPES	5.27	5.20
MEM + SB	7.53	7.43
MEM + BSA + HEPES	6.01	5.88
MEM + BSA + SB	8.05	7.95

6.3.3.2. Corrosion resistance of Mg at near-physiological pH

Several features can be seen upon analysis of the total resistance (R_{tot}) of pure Mg in HBSS adjusted to different pH values (Figure 6-7). Firstly, all solutions displayed an initial peak in the rise of resistance after 3-4 hrs. In general, a steady, more gradual rise was observed after this, with R_{tot} continuing to grow slowly at a rate of approximately 25 Ω/cm^2/hr. For pH levels of 7.2, 7.4 and 7.6, R_{tot} eventually reached between 900-1100 Ω/cm^2 after 24 hrs. A higher pH value resulted in a slightly greater R_{tot}, indicating the pH was still having a positive correlation with resistance, albeit a minor one. The average rate of increase in R_{tot} at a pH of 7.0 was observed to be approximately 17 Ω/cm^2/hr after the initial period. After 24 hours the total resistance was 745 Ω/cm^2, which was lower than pH 7.2, 7.4 and 7.6 by 24%, 43% and 57%, respectively.

The sample in the solution with a pH of 7.8 displayed the most dramatic difference. With significantly greater initial resistance, the R_{tot} continued to increase after the first 3 hrs at a rate of 40 Ω/cm^2/hr, roughly double that of the 3 middle pH solutions (Figure 6-7). With a final R_{tot} of 1700 Ω/cm^2, it was also approximately 70% higher than the middle pH solutions and this gap would likely increase based on the steeper slope.

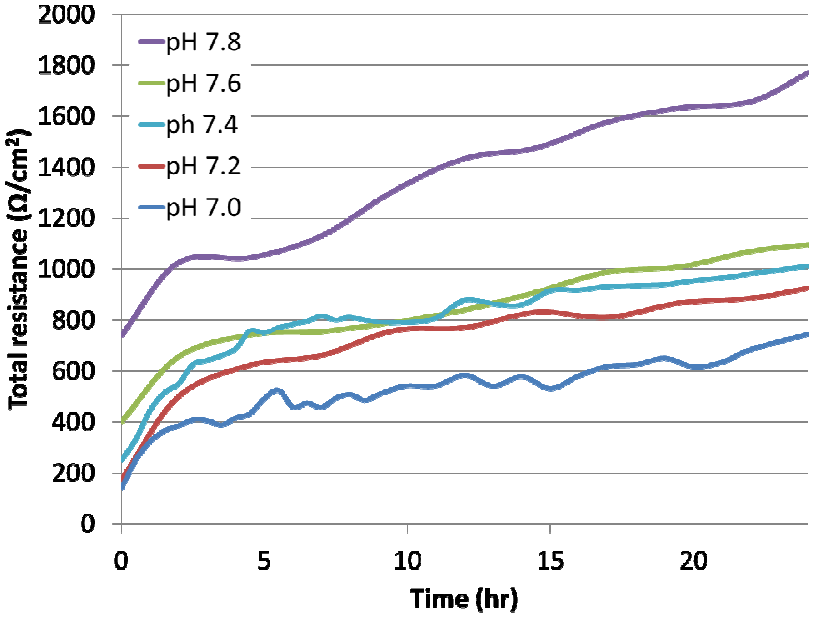

Figure 6-7 : R_{tot} of pure Mg with pH values between 7 and 7.8 over 24 hrs. (HBSS, T_{phy})

It is necessary to elucidate the contributions of the individual resistance components of the Mg surface and any films that might form to better understand the behaviour of the total resistance values at the different pH values (Figure 6-8). The resistance to charge transfer (R_{CT}) represents primarily the resistance across the EDL or of that between any coating and the Mg base layer. This was found to stabilize somewhat after 14 hrs of immersion (Figure 6-8A). After this, the values continued to rise slowly, at a rate of approximately 10 Ω/cm^2/hr. All R_{CT} values were within 200 Ω/cm^2 of each other, indicating that pH has a relatively weak influence on this parameter.

However, the same is not found for the film resistance (R_f), representing any significant layer that forms between the Mg and the solution. The three middle pH solutions quickly stabilized to a fairly linear R_f between 500-600 Ω/cm^2 (Figure 6-8B). This indicated that although a layer was forming on the surface, it was likely not becoming significantly thicker, denser, or providing greater coverage of the bare Mg. A pH of 7.0 resulted in lower R_f of ~400 Ω/cm^2.

For the sample at a pH of 7.8, the R_f was consistently higher than the other solutions and was found to grow steadily after 5 hrs at a rate of ~30 Ω/cm^2/hour. Comparisons with the corresponding R_{CT} suggest that a more protective coating is the main contributor to the steady increase in total resistance at a pH of 7.8.

Song *et al.* suggested that a higher concentration of OH^- groups near the surface at higher pH values will decrease the competition from Cl^- ions for adsorbing onto the surface by electrical repulsion of the Cl^- from the solution/surface interface [17]. Consequently, the effect of Cl^- on corrosion rate is reduced in an OH^- rich solution. Although the experiments performed to test this theory were at higher pH values and in different solutions than those used in the results reported here, it is possible that the same reactions are occurring.

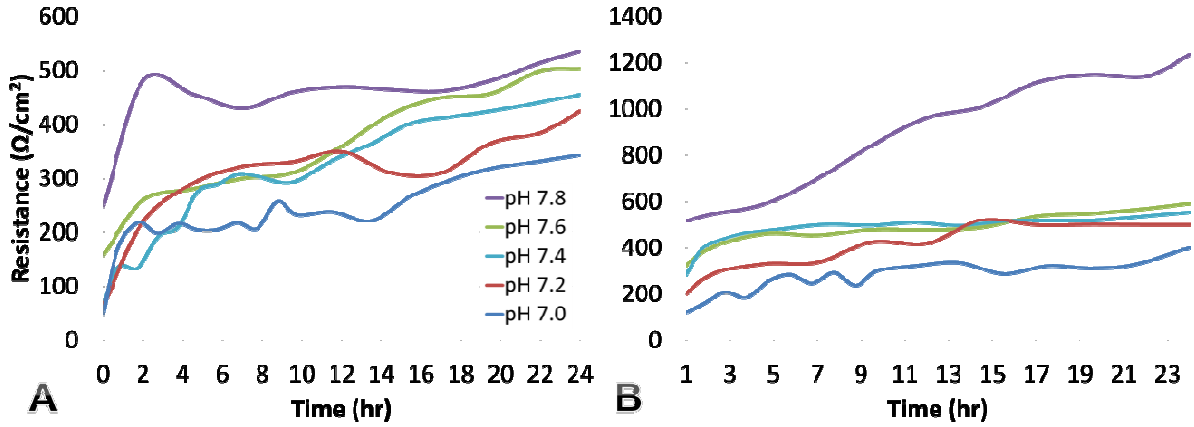

Figure 6-8 : (A) R_{CT} and (B) R_f obtained for different pH solutions (7.0-7.8) over 24 hrs. (HBSS, T_{phy})

6.3.3.3. Polarisation behaviour due to pH variance

The corrosion potential (E_{corr}) initially became more electronegative from 7.0 to 7.2, and then rose to become more positive as the pH increased. However, this trend was minimal and all values were within 40 mV of each other. Analysis of the different pH solutions on the Evans diagram indicated that a shift was occurring as the pH rose (Figure 6-9). The changing pH appeared to most affect the anodic reactions, causing an overall shift which resulted in reduced kinetics as the pH rose. This was most evident for the 7.8 solution, in which a significant shift in the anodic slope results can be seen.

The cathodic branch also appeared to display a small positive shift for the pH 7.0 solution. This may be due to an increase in the rate of water reduction that occurs with decreasing pH [35]. Consequently, the faster that water can be reduced, allowing H_2 to evolve at the Mg surface, the faster the cathodic reaction will take place.

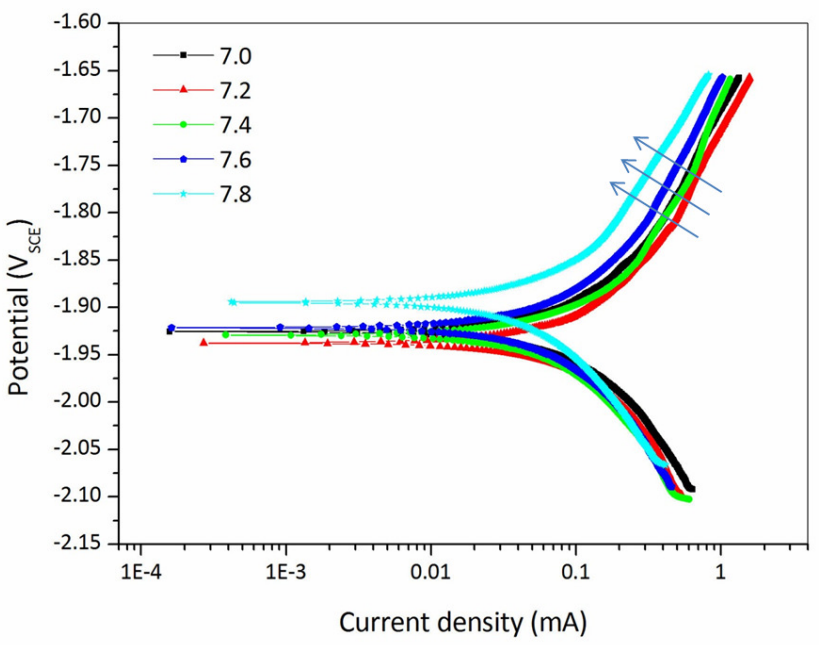

Figure 6-9 : Polarisation curves for pure Mg buffered to different pH values (7.0-7.8). (HBSS, T_{phy})

Corrosion current density (i_{corr}) results displayed a consistent trend with approximately 75% more corrosion occurring at a pH of 7.0 than in the 7.2 to 7.6 range (Figure 6-10). Between 7.2 and 7.6 the i_{corr} decreased by 6%, which was within one standard deviation. The average i_{corr} was 49 µA/cm^2 at a pH of 7.8 – 40% less than that observed at a pH of 7.6.

Overall, the PDP results followed a similar trend to the EIS, with the 7.2-7.6 pH range displaying similar corrosion properties. Samples analysed in solutions with a pH of 7.0 corroded faster and formed a weaker R_f to attack, while a pH of 7.8 resulted in significantly decreased i_{corr} and a more resistive film.

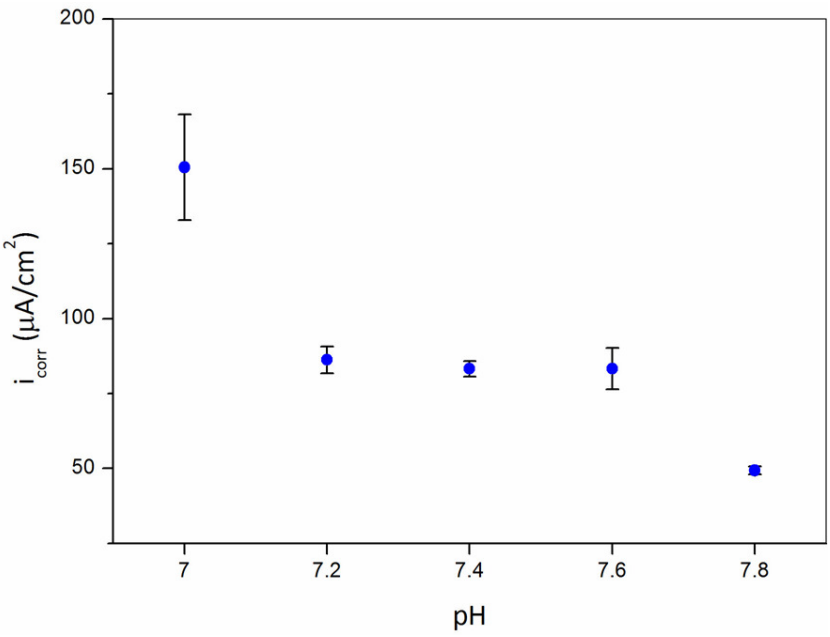

Figure 6-10 : i_{corr} of pure Mg as a function of pH. (HBSS, T_{phy})

6.3.3.4. Effect of pH on surface microstructure

SEM and EDS analysis of the different samples displayed several factors common to all (Figure 6-11 & Figure 6-12). The base layer was found to be composed primarily of Mg and oxygen (O). Resembling dry, cracked earth or clay, this was indicative of the $Mg(OH)_2$ layer that forms on Mg when placed in aqueous solutions. On top of this all samples also displayed some form of secondary layer comprised primarily of Mg with an increasing amount of Ca, phosphorus (P) and O as the pH increased. This is suggestive of the formation of calcium phosphates (CaP), which are known to preferentially nucleate on $Mg(OH)_2$ [36]. However the makeup of the layers in the lower four pH solutions were a mix of CaP and Mg, likely stemming from a thinner CaP layer and/or combination of CaP and $Mg(OH)_2$. Large “flakes” comprised entirely of Ca, P and O were found on all surfaces except the pH 7.8 samples. The flakes were crystalline in appearance, ranged from 40-100 µm and had poor coverage of the surface below. The surfaces of the pH 7.8 samples were found to be entirely covered in a dry-earth like CaP coating, with Mg only detected in the cracks between the coating.

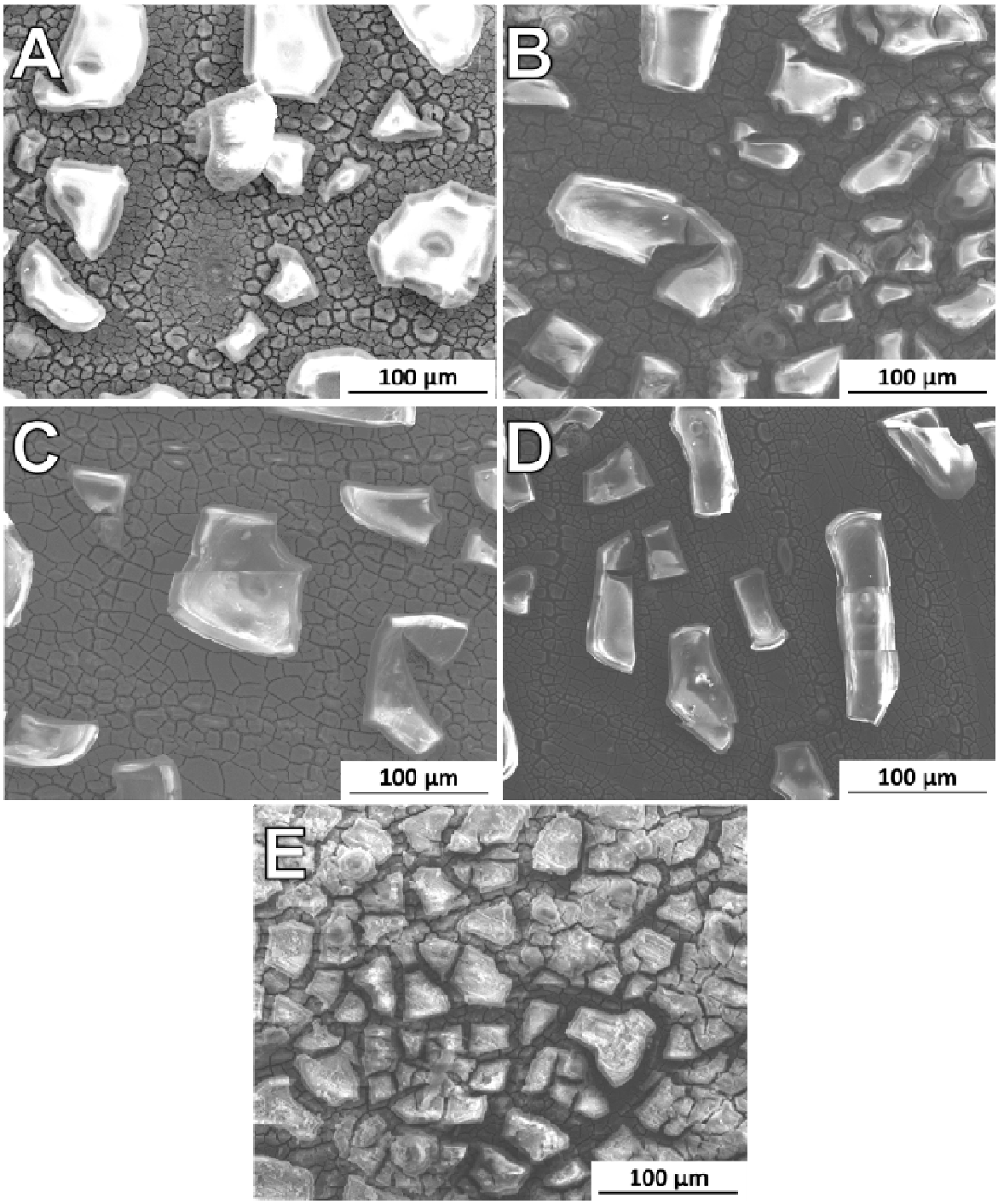

Figure 6-11 : Scanning electron micrographs of the surface of pure Mg samples after 24 hrs immersion at pH (A) 7.0, (B) 7.2, (C) 7.4, (D) 7.6, and (E) 7.8. (HBSS, T_{phy})

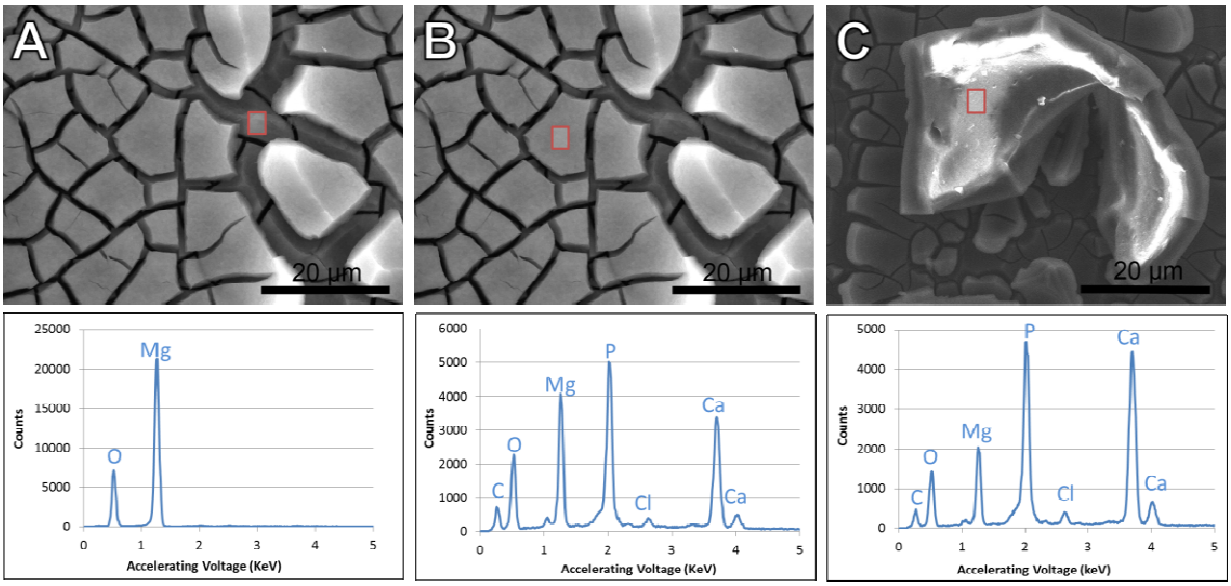

Figure 6-12 : Scanning electron micrographs and EDS analysis of typical surfaces on pure Mg at pH 7.0-7.6 showing: (A) $Mg(OH)_2$ underlayer, (B) $Mg(OH)_2$ / CaP mix layer, and (C) CaP flake. (HBSS, T_{phy})

The difference in surface film between the pH 7.8 solution and the others may be attributed to providing the majority of the added resistance to corrosion for the samples. pH 7.0-7.6 displays a mix of $Mg(OH)_2$ and CaP on the surface, while 7.8 had a thick CaP-only coating. What is evident is the importance of controlling the pH value of any test solution to within a very small range of the desired value. As the normal body pH varies between 7.4-7.6, it is important that experiments be conducted within this range as even a small deviation, as shown by the 7.8 experiments, can have a huge impact on the corrosion layers that form and subsequent corrosion process.

To more fully investigate this effect a chemical equilibrium software package, Medusa (Ignasi Puigdomenech, Royal Institute of Technology, Sweden), was used to determine the idealised formation conditions for CaP across a wide range of pH values. The program allowed the temperature to be adjusted to T_{phy} and the concentrations of Ca^{2+} and PO_4^{3-} were changed to be the same as those found in HBSS. A diagram of the fraction of CaP formation against pH was then created (Figure 6-13).

The CaP formed according to the fraction equilibrium diagram should be primarily one of two forms; calcium-deficient apatite (CDA, Ca^{2+}/PO_4^{3-} ratio 1.33-1.66) or hydroxyapatite

(HA, Ca^{2+}/PO_4^{3-} ratio 1.67) [19]. Both of these forms have Ca^{2+}/PO_4^{3-} ratio close to that of the amount dissolved in HBSS (1.625).

It is clear that the pH range near physiological levels is crucial in the formation of CDA/HA, where a small change in pH can result in a large shift in the amount of CaP that is able to form (Figure 6-13). However, the equilibrium equations assume perfect mixing and an infinite time, which likely explains why the differences in corrosion values (and assumed formation of CaP layers on the surface) do not match numerically with the fraction of CaP that would ideally be formed at each pH. In addition, other CaP compounds may also have formed in the pH experiments, as the solution would not have provided an entirely ideal environment. Rettig and Virtanen found Mg could substitute for Ca in certain situations, and corrosion layers on WE43 in a similar solution to HBSS to be composed of a carbonated calcium phosphate layer [37].

Overall, it is evident that the pH region around physiological levels is critical to the formation of CaP compounds, especially at the Ca^{2+} and PO_4^{3-} levels in the body (and most SBFs). This further highlights the importance of proper pH control during any biological test, not just with Mg but with all biomaterials.

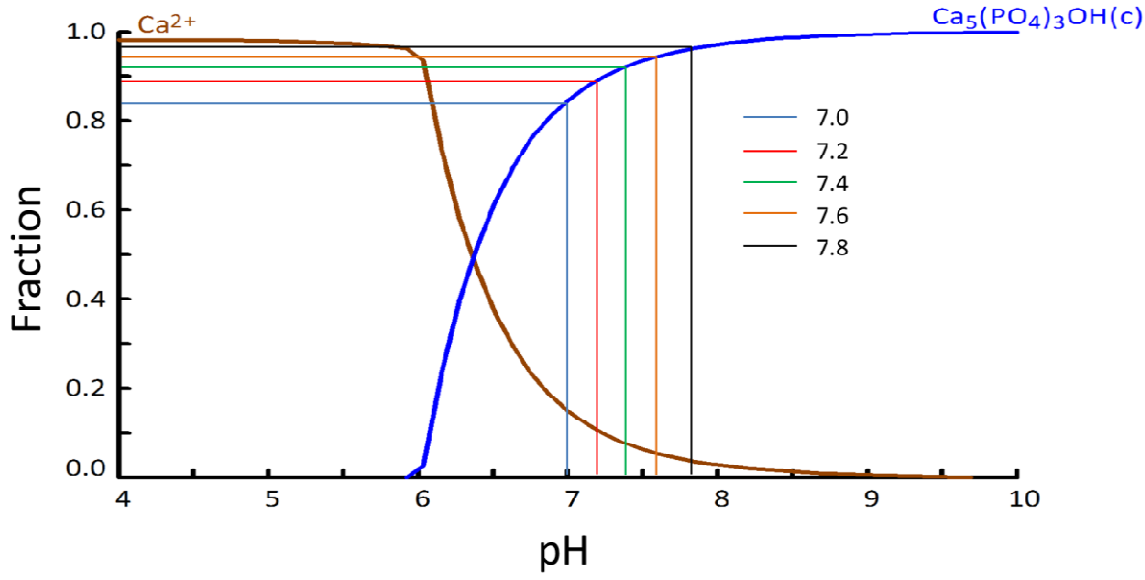

Figure 6-13 : Calcium phosphate formation according to ideal chemical equilibrium reactions over a pH range of 4-10 in a HBSS-equivalent solution.

6.3.4. Summary

The pH value of a solution used to test the performance of any material may play a considerable role in the end result. It is especially critical for Mg alloys as the effect it can have on corrosion performance cannot be underestimated. The difference in corrosion rates and resistance between a solution of 7.2 and 7.8 in this work was found to be over 300% from PDP results (Figure 6-10) and 220% from EIS (Figure 6-7). The electrochemical reason for this difference was found to be due to a decrease in the rate of anodic reactions at higher pH values (Figure 6-9). Analysis of the surface showed significantly different morphologies (Figure 6-11), especially at 7.8, with a denser, consistent coating of CaP (Figure 6-12). The physiological pH has also been shown to be in a critical range for the formation of CaP according to the idealised thermodynamic reactions (Figure 6-13).

Some suggest that pH can vary due to surgery and during the healing process [26]. However, significant change is usually only very temporary [38]. Thus, although an implant material may experience short periods of contact with different pH values, the vast majority of the time the pH will be closely controlled by the body to within the physiological range.

6.4. Buffering systems

6.4.1. Introduction

A buffer's primary role is to maintain the pH value within a specified range. The human body uses a buffering system that relies on bicarbonate ions, carbon dioxide and carbonic acid. These components each work together to neutralize hydroxide and hydrogen ions that act to alter the pH [39]. This control is vital to the normal function of proteins and cells, and the body is normally effective at maintaining a suitable range [40].

In the Mg biocorrosion literature over 75% of studies have either not used or not reported the use of a buffer. This presents an issue, especially in the case of the longer-term studies. Although a buffer may not be necessary for short-term electrochemical tests, it can play a significant role in multi-day or week experiments. Even if the test medium is changed at regular intervals, it is still possible (and relatively common) for the pH to rise significantly in-between these changes, creating unphysiological conditions. Of the works that have used a buffer, the most common by far was HEPES (14) followed by TRIS (5), borate buffer (2) and a citric acid buffer (1). Only a limited number of Mg corrosion studies were carried out using sodium bicarbonate [32, 41, 42].

Presently, it is not clear from the literature how a buffer may influence the corrosion behaviour of Mg alloys. To date no published work has looked specifically at this in detail, and many new studies continue to disregard this potentially important component [33, 43]. The aim of this study was to elucidate the differences between the most common (HEPES) and more realistic (SB/CO_2) buffering systems, determining their importance and role in the corrosion of Mg.

6.4.2. Experimental methods

6.4.2.1. Immersion tests

Mass loss tests were carried out over one week for pure Mg samples. The samples were placed into vented containers containing 20 mL of solution per cm^2 of surface area. This volume was chosen as it represented a ratio similar to the approximate amount of blood plasma the body contains (2.75 L) relative to the approximate surface area of typical bone

fixation devices (140 cm^2) [44]. 45% of the solution was replaced each day, based on daily urinary excretion (1.5 L) versus the total volume of human blood plasma [42]. These approximations do not exactly replicate the actual environment a specific implant would experience in the body although the aforementioned assumptions help to justify the selected solution to surface area ratio.

In the initial experiment, HBSS, EBSS, MEM and MEM with 40 g/L of BSA (MEM+BSA) were investigated. For each solution HEPES was used for tests performed in a water bath and SB/CO_2 was used for tests in an incubator. In both situations temperature was controlled at T_{phy} ± 1°C and pH was monitored and controlled to 7.4 ± 0.05. In addition, a hybrid solution of both HEPES and SB was also investigated, based on a commonly available dual-buffer system known as the "Dutch Modification" [45]. Samples were immersed for 1 week, after which they were removed and cleaned with chromic acid.

An experiment was also carried out to determine the effect that HEPES itself might have on the corrosion rate of Mg. Hydrogen evolution was used to measure the corrosion rate of pure Mg samples in distilled water and HBSS both with and without HEPES.

6.4.2.2. Microstructural characterisation

Samples of pure Mg were prepared and immersed by the above methods for 3 hrs for microscopy analysis. After removal from solution the samples were dried and sputter coated with carbon. Samples were analysed using a SEM and EDS to determine the elemental composition of the surface layer.

Samples from different buffered solutions were also analysed by FTIR. Standard scan conditions were used, as discussed in Chapter 4.5.4.

6.4.3. Results and discussion

6.4.3.1. Effect of buffering system on mass loss of pure Mg

Mass loss data displayed a significant increase in corrosion in all solutions when the buffering system was changed from SB/CO_2 to HEPES (Figure 6-14). The amount of mass loss that occurred was 100-350% greater in the HEPES-buffered solutions. This was further

increased when both buffers were used in combination, with a 300-620% increase in corrosion over the SB/CO_2 buffered solutions.

It is clear that the choice of buffer has a significant role in the corrosion of pure Mg in the investigated SBFs. All media buffered with SB/CO_2 displayed very similar mass loss of 1.55 ± 0.16%, excluding the protein-containing solution. For the HEPES-buffered media this range was slightly larger at 6.86 ± 1.04%. Overall there was an average increase in mass loss of 350% for samples in HEPES when compared with SB/CO_2.

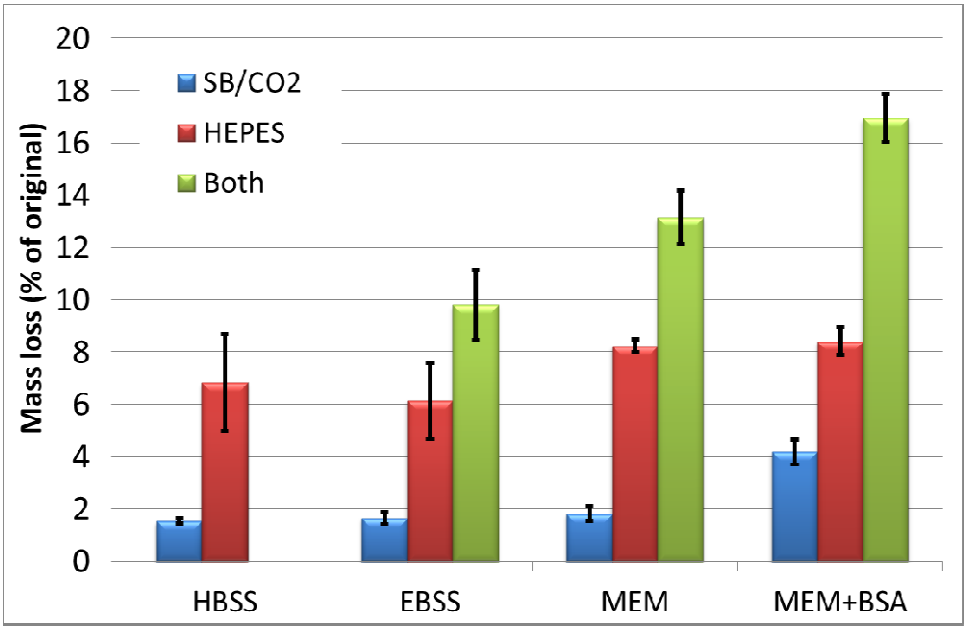

Figure 6-14 : Mass loss of pure Mg samples after 1 week immersion in solutions with different buffers. (T_{phy}, 7.4)

6.4.3.2. Variance in corrosion layer formation due to buffering system

SEM images of the Mg samples after 3 hrs immersion indicated that comparable layers were forming in both buffers (Figure 6-15). All samples displayed the characteristic cracked-earth-like formation that is commonly found in the literature for Mg corrosion layers [1, 46, 47]. For the samples buffered in HEPES, this surface was almost entirely composed of Mg and O, indicative of the $Mg(OH)_2$ that forms on pure Mg. However, the surfaces of samples buffered with SB/CO_2 displayed a denser layer containing ~10 at. % Ca and P. A sub-layer composed almost entirely of Mg and O was visible in the larger cracks of this layer. This indicates that at relatively early stages of immersion a CaP layer is rapidly formed in SB/CO_2 buffered

media. A CaP layer may provide significant protection from corrosion in this early period [48].

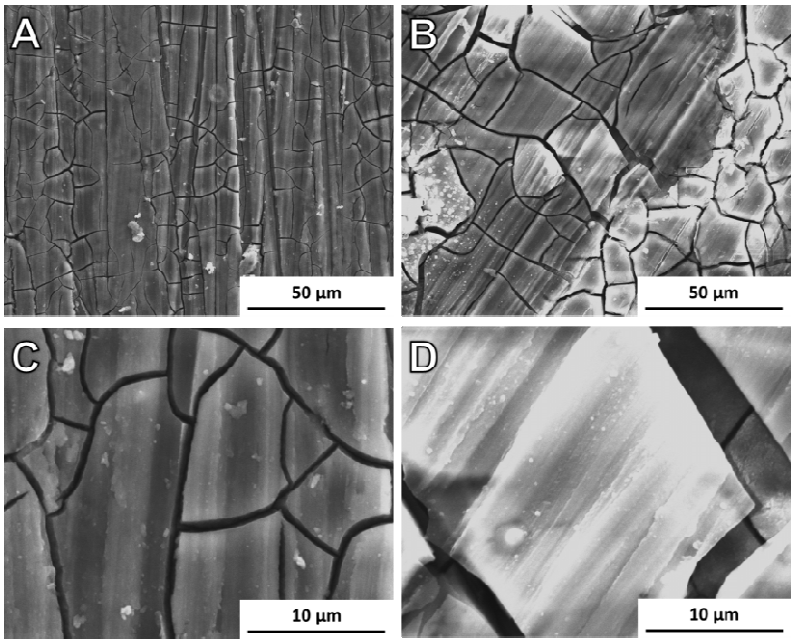

Figure 6-15 : Scanning electron micrographs of pure Mg corroded for 3 hrs with HEPES (A,C) and SB/CO_2 (B,D). Images in the top row are at 1000 × magnification; second row at 5000 ×. (HBSS, T_{phy}, 7.4)

Calcium/magnesium carbonate formation

A potential reason for the decreased corrosion in SB/CO_2 buffered solutions is the formation of a calcium carbonate ($CaCO_3$) or magnesium carbonate ($MgCO_3$) layer on the surface. Calcium salts, such as $CaCO_3$ and CaP, are known to be cathodic inhibitors of corrosion for metals [49]. $MgCO_3$ has also been shown to provide protection to pure Mg in a bicarbonate-buffered SBF [42]. Consequently it appears that carbonates may play a role in the difference in corrosion that is observed between the HEPES and SB/CO_2 buffering systems.

FTIR graphs of the corrosion product of samples immersed in HBSS with HEPES and SB/CO_2 buffering systems provided further evidence of $CaCO_3$ or $MgCO_3$ forming on the surface (Figure 6-16). Carbonate typically displays absorbance peaks at 875-878 [50, 51] and 1415 [52], 1420, and 1460 cm^{-1} [53]. In this work samples immersed in the SB/CO_2 buffer system displayed peaks at 875, 1416 and 1460, which confirms the presence of CO_3^{2-}. The same peaks were not visible in the corrosion product from samples buffered in HEPES. This

strengthens the argument that carbonate may be providing some of the corrosion protection in the SB/CO_2 buffer system.

In the literature, carbonate compounds have been shown to form on Mg surfaces. Xin ***et al.*** found rapid precipitation of $MgCO_3$ on the surface of AZ91 in a SBF similar to HBSS [54]. Yamamoto ***et al.*** discovered that $MgCO_3$ was even more likely to form than $Mg(OH)_2$ in a SB/CO_2 buffered NaCl solution in the pH range of 7-8 [42]. In a comprehensive study of the corrosion behaviour of WE43, Rettig and Virtanen observed the corrosion layer formed in m-SBF to be primarily an amorphous carbonated calcium-magnesium-apatite ($(Mg,Ca)_x(PO_4)_y(CO_3)_z(OH)_i$) [37].

Lin ***et al.*** studied the corrosion behaviour of AZ91 in a salt-spray test in a 1% CO_2 atmosphere [55]. 300% less corrosion product formed in a CO_2 environment after 30 days. The corrosion layer on AZ91 was also more homogenous in the presence of CO_2. Similar results were also found by Lindstrom ***et al.*** for AM20, AM60, and AZ91, where a layer of hydrated magnesium hydroxyl carbonate ($Mg_5(CO_3)_4(OH)_2.5H_2O$) formed [56]. Both studies concluded that the NaCl-induced corrosion was being inhibited by a slightly soluble layer containing hydroxyl carbonates and hydroxyl chlorides in the presence of CO_2.

It has also been found that proteins can inhibit the formation of $CaCO_3$ ***in vitro*** [57]. This may explain why the HEPES-buffered MEM+BSA and MEM displayed very similar results, but MEM+BSA buffered with SB/CO_2 displayed 2 ***x*** the mass loss as SB/CO_2 buffered MEM.

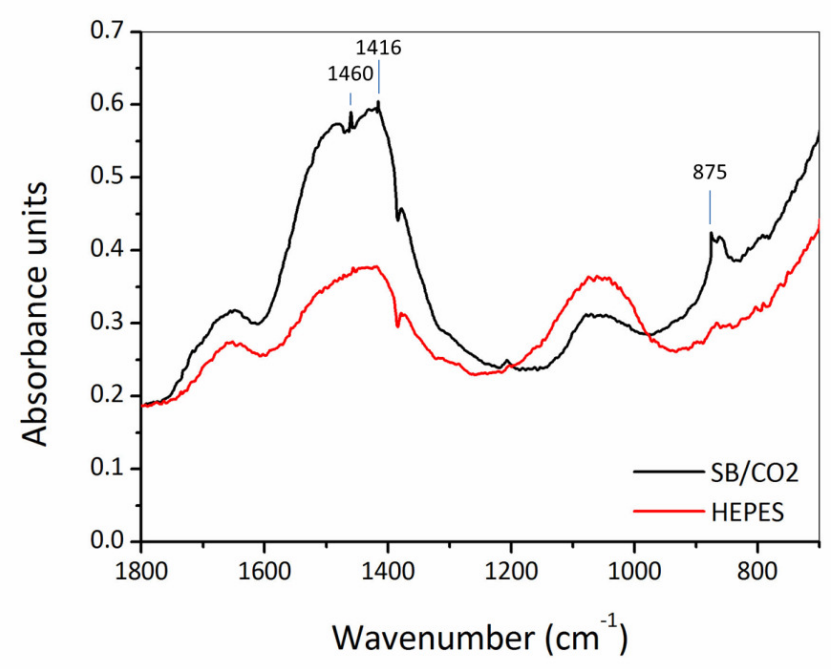

Figure 6-16 : FTIR absorbance graph of pure Mg samples immersed with different buffers. Typical carbonate peaks are indicated. (HBSS, T_{phy}, 7.4)

CaP precipitation dependency on solution composition

A further study with similar amounts of Ca and P to the SBFs as used in the present work reports that CaP precipitation varies as a function of bicarbonate level [58]. CaP precipitation was observed to be enhanced by increasing the bicarbonate level in solution, suggesting that more CaP can form on the surface of the Mg in an SB/CO_2 system, offering further protection from corrosion.

6.4.3.3. Effect of Mg-buffer interactions on the corrosion rate of Mg

Hydrogen evolution data on pure Mg in distilled water and HBSS, both with and without HEPES, displayed just how strongly the buffer can affect the corrosion (Figure 6-17). It is immediately obvious that the buffer is affecting the corrosion rate of Mg, rapidly increasing it from the very beginning. In HBSS, this increase was more than 900% due to the addition of HEPES, and in distilled water it was 1250%. It is important to note that HEPES could be reducing the CaP formation in HBSS thereby increasing the corrosion rate. However, CaP layers will not form in distilled water. It appears that the increase in corrosion in distilled water is related to the presence of HEPES that is presumed to react with some component of the Mg substrate.

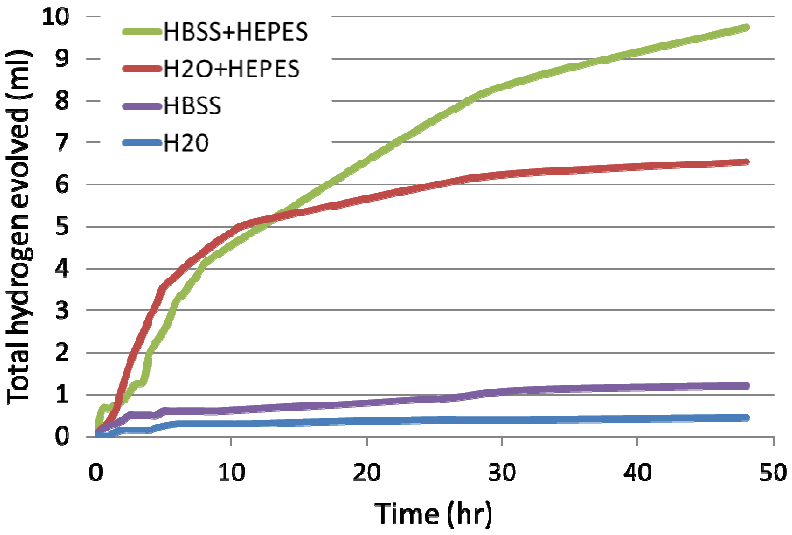

Figure 6-17 : H_2 evolved over 48 hrs from pure Mg in distilled water and HBSS with and without the addition of HEPES. (T_{phy}, 7.4)

It is possible that the chemical structure of HEPES itself is leading to increased corrosion when compared with SB/CO_2 or no buffer at all. A recent study by Xin *et al.* investigated the effect of a TRIS buffer on the corrosion of pure Mg [59]. They found that the Tris-HCL compound that formed during the buffering process lowered the corrosion potential slightly but increased the corrosion rate. It was suggested that Tris-HCL consumes the OH^- generated by the corrosion process, accelerating the oxidation of Mg to Mg^{2+}. They also found increased pitting corrosion in the early stages in the presence of the buffer [59].

Rettig and Virtanen suggested that the buffer acts to neutralize the OH^- as it is released by the Mg, maintaining pH neutrality in the vicinity of the surface [60]. Hence, it is hypothesised that a high local pH level that would act to passivate the surface will not develop. Xin *et al.* suggested that a rapid reaction between the buffer and OH^- dramatically promotes transformation of Mg to Mg^{2+} [61]. The evolution of the pH level at the Mg substrate is likely to play a significant role in its corrosion rate.

It is hypothesised that part of the HEPES structure is able to react with the OH^- group in the $Mg(OH)_2$ layer decreasing the effectiveness of the $Mg(OH)_2$ layer in hindering corrosion and presenting the bare Mg substrate to the solution. Further work is required to determine the exact nature of these interactions.

6.4.3.4. Effect of HCl/NaOH additions to balance pH levels

It is important to consider the additional components that are being added when adjusting buffered solutions to an appropriate pH. When HEPES is added to an SBF it typically reduces the pH level (see Table 6-1). Although it is common to use 1 M NaOH to raise the pH to a physiological level, the amount that is added has never been reported for any study in the bio-Mg literature. The volume of 1 M NaOH required to buffer a range of solutions to 7.4 can vary between different solutions (Table 6-2). For most solutions this effectively adds around 10-14% more Na. However, this is not necessarily an issue as Na is a spectator ion, is not typically associated with any corrosion mechanism for Mg alloys, and has not been found to have a significant effect on the corrosion of Mg alloys [62, 63]. The Na levels of all solutions were within ± 12% of those in human plasma, and as such are not significant.

When the pH of a solution rises, 1 M HCl is commonly added to lower it [64, 65]. This is a concern as Cl^- ions are released into the solution, which are known to cause an increase in corrosion [66]. During longer-term experiments the amount of 1 M HCl that was added to maintain pH levels was recorded in this work. It was found that for a typical solution amount of 400 ml and sample with 5 cm^2 of surface area, between 0.3-0.5 mL of 1M HCl was added to the solutions each day. This is equivalent to the addition of 0.5-1% Cl^- per day to the original composition of the NaCl, HBSS, EBSS and MEM solutions. Although not an issue for short-term experiments, the sole use of this method for pH balance could result in a significant increase in Cl^- anions in multi-week tests.

Table 6-2 : Amount of 1 M NaOH required to buffer different solutions to 7.4 at 37 °C.

Solution	1 M NaOH Required (ml / L)
NaCl + HEPES	13.5 ± 0.25
HBSS + HEPES	14.25 ± 0.25
EBSS + HEPES	12.5 ± 0.5
PBS + HEPES	12.5 ± 0.5
MEM + HEPES	14.5 ± 0.25
MEM + BSA + HEPES	18.5 ± 0.5

6.4.4. Discussion

A buffering system may be considered a necessary part of any *in vitro* experiment to minimise variations in pH. The OH^- release due to Mg corrosion is rapid, and can quickly change the pH of a solution to un-physiological values [59]. Even experiments utilising a large solution volume to surface area ratio with no buffer have shown a rapid rise in pH levels [67]. A frequent replacement/refreshment of media or extremely large solution volume to surface area ratio would be required for an unbuffered media to maintain pH balance during Mg immersion experiments. In many cases this may not be feasible, necessitating the use of a buffering system.

If not carefully controlled the refreshment of medium could itself introduce issues such as the creation of dynamic conditions as the medium is mixed and changed. However, the sole use of HCl additions for long-term experiments (> 3 week) presents the concern of increased Cl^- concentration (see Chapter 6.5.4.1). A careful balance of both solutions may provide the most ideal situation, where medium refreshments are not frequent enough to create a dynamic environment and HCl is added in small quantities.

A SB/CO_2 buffering system possesses several benefits over chemical buffers. It has been shown to have slower rates of corrosion (Figure 6-14). This can be attributed to a $CaCO_3$ / $MgCO_3$ which forms on Mg in SBF (Figure 6-15, Figure 6-16). Carbonates are known to commonly form on implants *in vivo* [51, 57], suggesting that the SB/CO_2 buffer provides results more comparable to a physiological surface layer on Mg alloys. However, there are also some disadvantages to using SB/CO_2. The prerequisite of a high CO_2 atmosphere means specialised equipment is required to provide the necessary environment. All media must be handled and kept in this environment, as the pH and temperature will quickly change if they are removed. In addition, electrochemical experiments can be difficult to perform in a standard CO_2 incubator due to: (i) electrical noise that interferes with corrosion current signals [68], (ii) difficulty in physically setting up hydrogen evolution experiments due to space constraints, and (iii) complications with frequent monitoring that necessitates opening of the unit, causing fluctuations in CO_2 levels.

However, the effects of chemical buffers must also be taken into account. The lack of bicarbonate buffer leads to little formation of Mg and Ca carbonates (Figure 6-16),

compounds known to provide protection to the bare Mg. It also appears that faster corrosion occurs when HEPES is present in the solution, further increasing corrosion via processes that are unlikely to occur in the body (Figure 6-17). HEPES and TRIS have also been shown to affect cell growth [69] and inhibit enzymes [70], and thus care must be taken when studying Mg in media containing these organic additions. However, experiments with HEPES and many other chemical buffers may be performed in air, permitting a relatively straightforward experimental set up for all types of corrosion tests.

6.5. Choice of simulated body fluid

6.5.1. Introduction

Although many different solutions have been used to investigate Mg biocorrosion, only a few studies have compared the effects of multiple media. A review of the most pertinent studies in the literature revealed that a piece-wise understanding of how different media affect Mg corrosion is evident, although the papers are restricted to a small number of Mg alloys (Table 6-3). Moreover, the available literature suffers from a number of issues that limits its utility. For example, Gu *et al.* based their observations of corrosion rate on a single PDP scan and examined the corroded surfaces only after PDP, a technique that forces accelerated corrosion and consequently dramatically alters the surface [71]. Liu *et al.* had little discussion of the effects BSA had on surface protection, other than claiming the protein provided a "blocking effect" [72]. Xin *et al.* did not control the pH during testing, which would have created an unphysiological environment and resulted in much less corrosion occurring [61]. Yamamoto and Hiromoto recorded the concentration of Mg^{2+} ions in solution as a measure of corrosion rate [42]. However, selective ionic measurement can be prone to errors such as interference from other ions in the solution and potential drift [73]. It also does not take into account the Mg that has been changed into $Mg(OH)_2$ or $MgCO_3$ on the surface. A number of other studies have also compared one or two media, but most have suffered from similar issues to those mentioned above [23, 74, 75].

The aim of the present work was to provide a comprehensive investigation of Mg biodegradation in a range of media using different corrosion testing techniques to elucidate the effect each solution may have on the corrosion mechanism and rates of Mg alloys. However, it was first necessary to examine the potential media in light of what is perhaps the most important component affecting Mg corrosion, Cl^-.

Table 6-3 : Summary of studies of the biodegradation of Mg and its alloys as a function of the corrosive media.

Author	Alloys	Solutions	Time	Tests	Main Findings
Gu **[71]**	Mg-1Ca, AZ31, AZ91	HBSS, DMEM ±10% FBS	7 days	PDP EIS OCP	• DMEM caused less corrosion than HBSS. • Mg-1Ca corroded faster in FBS, AZ91 was slower, AZ31 was initially faster and then slower after 3 d. Effect of proteins on AZ was attributed to better attachment to Al_2O_3 layer [72]. • After the initial few hours the corrosion rate levelled out and did not vary significantly • Analysis of surfaces after 7 d presented surface film with significant cracking/pits • Severe corrosion attack was seen for all alloys in HBSS.
Rettig **[60]**	WE43	NaCl (± $CaCl_2$ / K_2HPO_4) m-SBF (±40 g/L BSA)	5 days	PDP EIS OCP	• Except for NaCl, all electrolytes displayed linear polarisation resistance to increase over time. • Radically different corrosion behaviour in first hours for samples in m-SBF with and without BSA. Potentially due to adsorption onto surface. • Buffering lead to more homogenous, less complex conditions at surface and fewer fluctuations. • Buffering prevents surface alkalization, no partial passivation of Mg takes place in buffered solutions. • Corrosion occurred faster in m-SBF than NaCl.
Liu **[72]**	AZ91	SBF ±0.01/1 g/L BSA	7 days	ML PDP EIS OCP	• Proteins made OCP more positive. • Protein amount had little effect on corrosion over 7 d, but significant effect on short term PDP. • “Blocking effect” of anodic reaction described as reason for protein protection.
Xin **[61]**	AZ91	0.9% NaCl PBS c-SBF HBSS DMEM	4 days	OCP H_2Evo PDP	• Initially DMEM and c-SBF degrade slower, then increase to 10x those of HBSS, NaCl, and PBS. • In NaCl and c-SBF sample was more prone to pitting. • 0.9% NaCl is not a suitable solution due to lack of components. • DMEM is most suitable medium for future tests.
Yamamoto **[42]**	Pure Mg	NaCl EBSS MEM (±10% FBS)	14 days	Mg^{2+} Ion	• Maximum corrosion occurred during first day, decreased until day 5-8, then remained constant. • For corrosion rate, NaCl > MEM > EBSS > MEM+FBS. • CaP layer protected balanced salt solutions, proteins helped form insoluble salt layer.

6.5.2. High Cl^- content of current SBF

One component that has been virtually overlooked by the entire Mg biocorrosion community is the Cl^- content of the SBFs that are used. HBSS, EBSS, and MEM all contain significantly more Cl^- than human plasma (Table 6-4) due to the original purpose for which the media were designed. Almost all the solutions that have been used in the literature on Mg biocorrosion were intended to be used for cell culture. The role of the salts in this culture media is to provide a physiological ionic environment for cell metabolism [69]. However, certain ions are more important than others. Sodium (Na) and potassium (K), for example, are essential for pump functions across the cell membrane [69]. This is crucial for cell survival and growth and therefore, in cell culture experiments, levels of these ions are kept as closely as possible to the body's conditions.

Table 6-4 : Chloride content of different SBF media.

Media	**Cl^- Content (mmol/L)**
Human Plasma	100-103
8 g/L NaCl	136.9
PBS	140
HBSS	144.6
EBSS	135
MEM	123.5

The primary reagent for all the SBFs is NaCl. It provides the bulk of the Na^+ and Cl^- to the solution, which are the two primary ionic salts. The amount of Cl^-, however, does not appear to be as crucial to cell viability as Na^+ [69]. Na^+ is also often added to media as the compound Na_2HPO_4, but this amounts to less than 2% of the total, due to limits on the amount of HPO_4 that is required. Thus 7.5-8 g/L NaCl is normally added to obtain the correct Na^+ concentration. This results in 136.9 mmol/L of Cl^-, almost 40% more than that found in human plasma. Given the active role Cl^- plays in accelerating the corrosion of Mg alloys, this difference is likely part of the reason why *in vitro* tests consistently report higher corrosion rates than *in vivo* [76].

6.5.2.1. Design of a biocorrosion medium with physiologically-correct Cl^- levels

This variance in Cl^- content highlights the fact that the majority of SBFs used in the bio-Mg literature were not designed specifically for corrosion experiments. Kokubo [77, 78], Oyane [79] and Takadama [80] have recently created revised versions of a generic SBF that contain similar Cl^- concentrations to human plasma. However, these solutions contain less than 20% (4.2 mmol/L) of the physiological level of HCO_3^-. The reason for this reduction was that physiological levels of HCO_3^- resulted in the deposition of calcite onto some biomaterials due to the release of Ca^{2+} ions [80]. However, this occurs primarily on Ca-rich biomaterials [80]. It is understood that a minimum of 25 mmol/L of bicarbonate is necessary to buffer an SBF to 7.4 according to the Henderson-Hasselbalch equation [69]. This means that the generic SBFs would always require the use of a chemical buffer.

In an attempt to rectify the high Cl^- concentration issue of most BSS and allow for choice of buffer, a newly modified SBF was created in this work (Table 6-5). For lack of a better name, this solution was called Kirkland's biocorrosion medium (KBM). The preparation steps for this medium may be found in Appendix E. It should be noted that in this work KBM was used primarily for comparison, as the majority of experiments had already been performed in other BSS, such as HBSS.

Table 6-5 : Component comparison of human plasma and KBM (mmol/L).

Component	Human plasma	KBM
Na^+	142	120.305
Cl^-	103	102.541
K^+	5.0	5.097
Ca^{2+}	2.5	2.523
Mg^{2+}	1.5	1.498
HPO_4^{2-}	1.0	0.859
SO_4^{2-}	0.5	0.498
D-Glucose	5	4.996
Bicarbonate (HCO_3)	22-30	± 26.187
HEPES	-	± 25.010
Phenol Red	-	0.031

6.5.3. Experimental methods

6.5.3.1. Immersion testing

Mass loss experiments were performed on pure Mg to compare the effect of Cl^- content by using KBM and HBSS. Immersion tests were carried out for 1 and 3 week periods using either HEPES or a SB/CO_2 buffering system following Chapter 4.2.1. . Samples were weighed before immersion and after cleaning of the corrosion layer with chromic acid.

6.5.3.2. Electrochemical testing

Unless otherwise stated all experiments were carried out in solutions buffered with HEPES at T_{phy} ± 0.5 °C and a pH of 7.4 ± 0.05. All experiments with MEM were performed in sterile conditions in a laminar flow hood to minimise the possibility of contamination.

PDP experiments were carried out on pure Mg and a total of 28 different Mg alloys. The polarisation scans were done following the normal conditions outlined in Chapter 4.3.3. . Tests were performed in MEM with and without 10% FBS for all 29 alloys. At the time of the present experiments, a MEM+FBS solution was the most physiologically-correct *in vitro* medium that had been investigated in the literature. A further 13 alloys were tested in a solution of PBS and 50 vol.% human plasma (PBS+HP). This is the first time in the literature that a solution containing human body fluid has been used to investigate Mg alloys. Human plasma was handled in a physical containment 2 (PC2) lab as it is considered a biohazard. All proper procedures were followed to fully sterilize the electrochemical cell before and after the experiments, including spraying with a 70% ethanol solution and gamma irradiation. Human plasma and facilities were supplied by the School of Biological Sciences at University of Canterbury.

PDP was also carried out on pure Mg using the various media that had been used in the literature including 0.8% NaCl, KBM, HBSS, EBSS, PBS and MEM ± 20/40/60 g/L BSA.

EIS was performed on pure Mg using the standard setup described in Chapter 4.3.5. . Tests were performed over 72 hrs in 0.8% NaCl, KBM, HBSS, EBSS, PBS and MEM ± 20/40/60 g/L BSA.

6.5.3.3. Microstructural characterisation

Following the 72 hrs immersion in the various media pure Mg samples were dried and analysed using a SEM. The elemental composition of the corrosion layer was analysed with EDS.

6.5.3.4. Protein adsorption tests

Protein staining, a solute-depletion method, and QCM were carried out to determine the level and amount of protein that had attached to pure Mg surfaces. A detailed description of the various setups is described in Chapter 4.6.

6.5.4. Results and discussion

6.5.4.1. Effect of media Cl^- content on the mass loss of pure Mg over 3 weeks

To determine the effect the reduced Cl^- content of KBM may have on the corrosion rate of pure Mg, immersion tests were performed in both HBSS and KBM buffered with either HEPES or SB/CO_2. Considering the similarity between the two media, the Cl^- concentration appears to make a considerable difference to the total mass loss (Figure 6-18). In both buffering environments less corrosion occurred in KBM, with the biggest difference being a 36% decrease in mass loss after 1 week in HEPES-buffered media. The difference was much smaller for samples buffered with SB, resulting in 21% and 13% drop at 1 and 3 weeks, respectively. The difference in reduction in corrosion rate due to the buffering environment may be due to a Mg carbonate layer forming on the surface in the SB/CO_2 environment (see Chapter 6.4).

Overall it is clear that the Cl^- concentration at the investigated levels plays an important role in the measured corrosion rate, regardless of buffering system. This highlights the importance of developing and utilising media similar to KBM in future experiments in order to most closely mimic the ionic environment of the body.

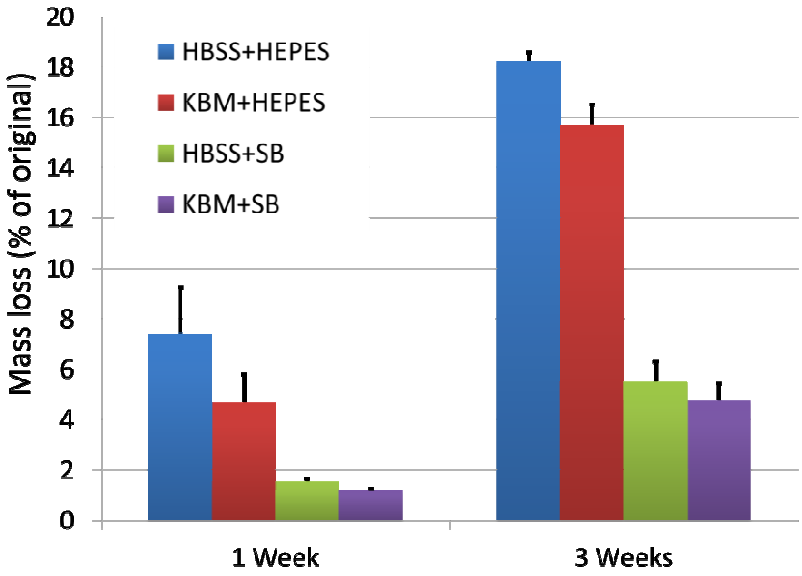

Figure 6-18 : Mass loss of pure Mg in KBM and HBSS over 3 weeks. (T_{phy}, 7.4)

6.5.4.2. Mg alloy degradation as a function of organic components in biocorrosion media

The addition of proteins displayed an inhibitory effect on the i_{corr} of each of 29 alloys investigated (Figure 6-19). There was also much less variation when performing repeat tests in MEM+FBS than in MEM. This could be indicative of a more uniform layer on the surface due in part to rapid protein adsorption as has been suggested elsewhere [72]. Excluding Mg-16.2Ca, the average i_{corr} for alloys tested in MEM was 145 µA/cm^2, whereas the average for the MEM+FBS alloys was 52 µA/cm^2. This would indicate that at this time point the alloys in MEM+FBS were corroding, on average, 3 × slower than those in MEM. A reduction in i_{corr} for Mg alloys due to proteins has also been reported in the literature [42, 72, 81, 82]. Suggested reasons for this reduction include the possibility that proteins: (i) thicken the $Mg(OH)_2$/CaP corrosion layer [42], (ii) provide a "blocking effect" [72], (iii) react rapidly with divalent ions, speeding the formation of a $Mg(OH)_2$/CaP corrosion layer [83], and (iv) block the migration of Cl^- ions to the surface [84, 85]. However, few studies have provided further evidence to back up these theories. It can be said with relative certainty that in general the proteins are having a significant effect on the electrochemical reactions that are taking place, as discussed in Chapter 6.5.4.3.

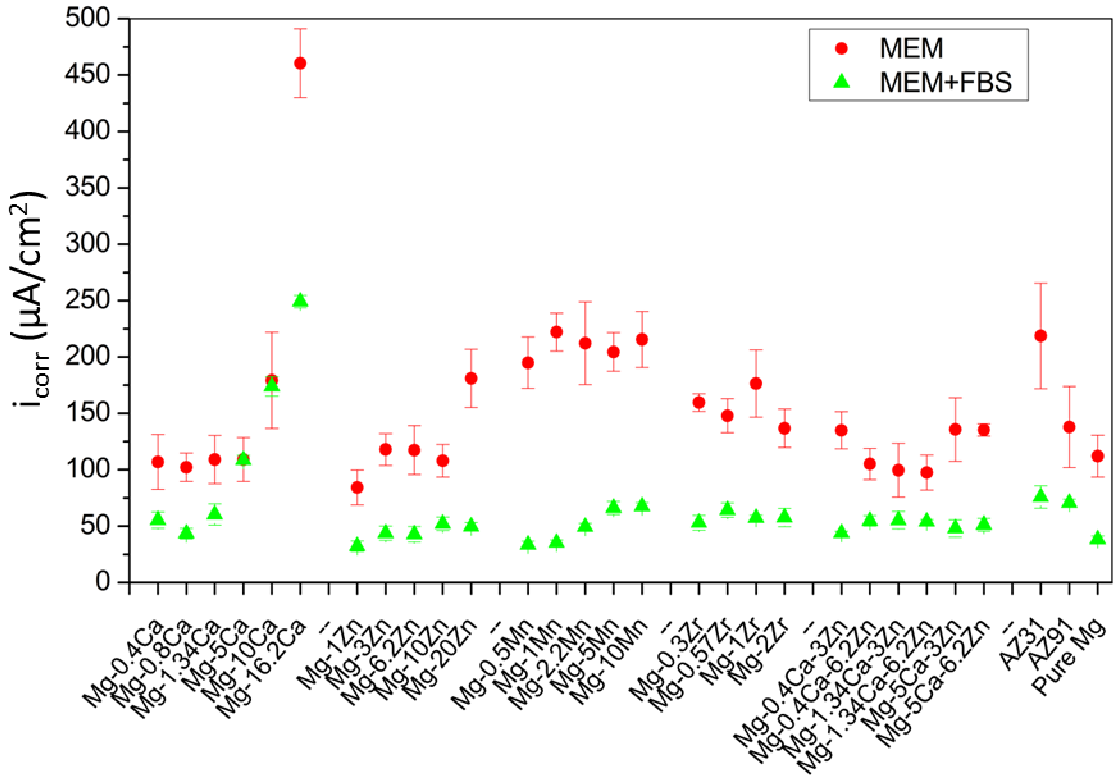

Figure 6-19 : i_{corr} for pure Mg and various binary and ternary alloy systems in MEM with and without 10 vol. % FBS. (T_{phy}, 7.4)

Alloys that displayed some of the lowest and highest i_{corr} were chosen for further investigation in the most realistic *in vitro* solution used to date, PBS with 50% human plasma (Figure 6-20). Although the i_{corr} values in PBS+HP were lower than those in MEM+FBS, most alloys display very similar results in both media. The decrease of between 15-50% may be attributed to a number of factors. Firstly, the MEM+FBS solution contains only an average of 4-6 g/L of proteins, whereas the human plasma has the full complement of 60-80 g/L of proteins found *in vivo*. Thus, the PBS with 50 vol. % HP contained 30-40 g/L of total protein. According to the Langmuir adsorption isotherm, the amount of protein that will adsorb to a surface is heavily dependent on the concentration in the solution [86]. Consequently, the proteins may be adsorbing to the surface of the Mg alloys in PBS+HP in greater amounts given the 5-10 × higher protein concentration compared with MEM+FBS. It is hypothesised here that in PBS+HP the proteins form a thicker, more protective layer against Mg corrosion.

Another reason for the variance in i_{corr} is potential discrepancies in composition of human plasma. The total theoretical inorganic contents of the two solutions were very similar, with a

Cl^- difference of less than 4 wt.%. However, there may have been variance within the HP that was unaccounted for. This was collected from a pool of donors, and as such could be different from the typical levels.

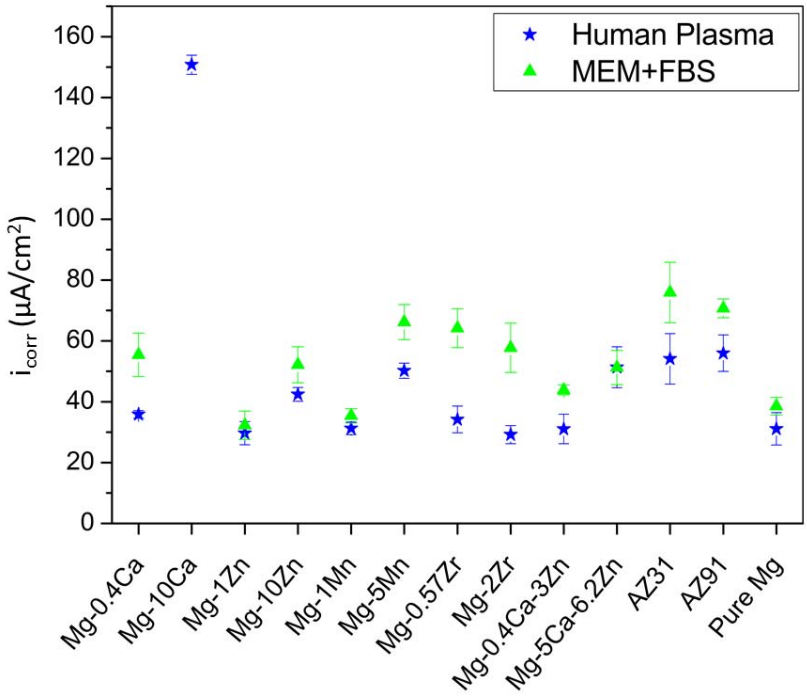

Figure 6-20 : i_{corr} of 13 alloys in PBS with 50 vol. % human plasma. MEM+FBS data is included for comparison. (T_{phy}, 7.4)

This data establishes that the electrochemical performance of a range of alloys in a 50 vol. % human plasma solution is relatively close to that of a similar calf-serum medium. Although more work is necessary to fully elucidate this relationship, it appears that it may not be necessary to utilise potentially dangerous human material in the search for a bio-realistic environment for Mg biodegradation. However, further long-term studies are required to confirm this behaviour.

6.5.4.3. Corrosion behaviour of pure Mg in various *in vitro* media

The benefit of looking at a single alloy for a range of solutions is the reduction of variables that can cause discrepancy in the results. Chemical composition (***e.g.*** multiphase, impurity levels) or microstructure (***e.g.*** grain size, morphology) are two examples of variables that have a great influence on the corrosion behaviour of Mg alloys. In this regard it is advantageous to use pure Mg in ascertaining the influence of medium alone.

The E_{corr} values for pure Mg displayed varied trends when compared between different media (Figure 6-21). KBM displayed the most positive potential (-1900 mV_{SCE}), while HBSS and EBSS were very close at approximately -1925 mV_{SCE}. PBS exhibited slight decrease in E_{corr} to -1940 mV_{SCE}. For the MEM, as the protein concentration increased, E_{corr} became more negative; a similar shift to that found by Mueller ***et al.*** [28].

It should be noted that the E_{corr} values for PBS with human serum are not shown on the graph as they were off the scale with an average of -1,642 ± 8 mV_{SCE}. This is a significant positive shift compared with the other solutions, although the reasons for such a change are not known due to difficulty carrying out further experiments in such a hazardous solution.

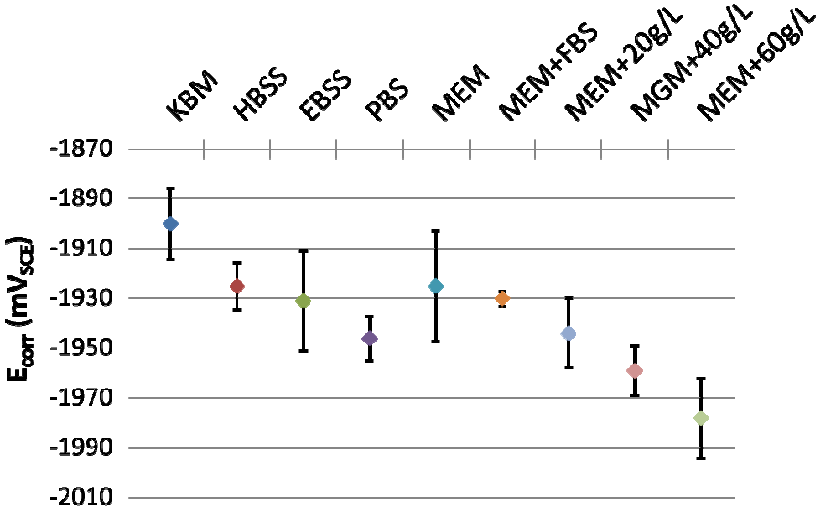

Figure 6-21 : E_{corr} for pure Mg in various ***in vitro*** media. (T_{phy}, 7.4)

Analysis of the polarisation curves reveals the reasons for the shifts in E_{corr} (Figure 6-22). For the BSS, KBM was found to result in a slight decrease in the rate of oxidation, as shown by a shift in the anodic curve (Figure 6-22A). Given the similarity of KBM to the other BSS, this shift is likely due to the decreased Cl^- content. PBS was also seen to result in a small cathodic shift, which caused the slight decrease in E_{corr}. This may be due to the different composition of the media resulting in a different corrosion layer. The morphology and composition of this layer is explored further in Figure 6-28 and Table 6-6.

In MEM, increasing amounts of proteins resulted in a decrease in the reduction reaction, highlighted by the cathodic shift (Figure 6-22B). The addition of just 4 wt. % proteins, from the FBS, resulted in the largest shift. Thereafter increasing the protein concentration made

E_{corr} more electronegative, albeit by a smaller magnitude. It appears that the proteins are acting as mild cathodic inhibitors for pure Mg, decreasing the rate of H_2 evolution and consequently the corrosion rate.

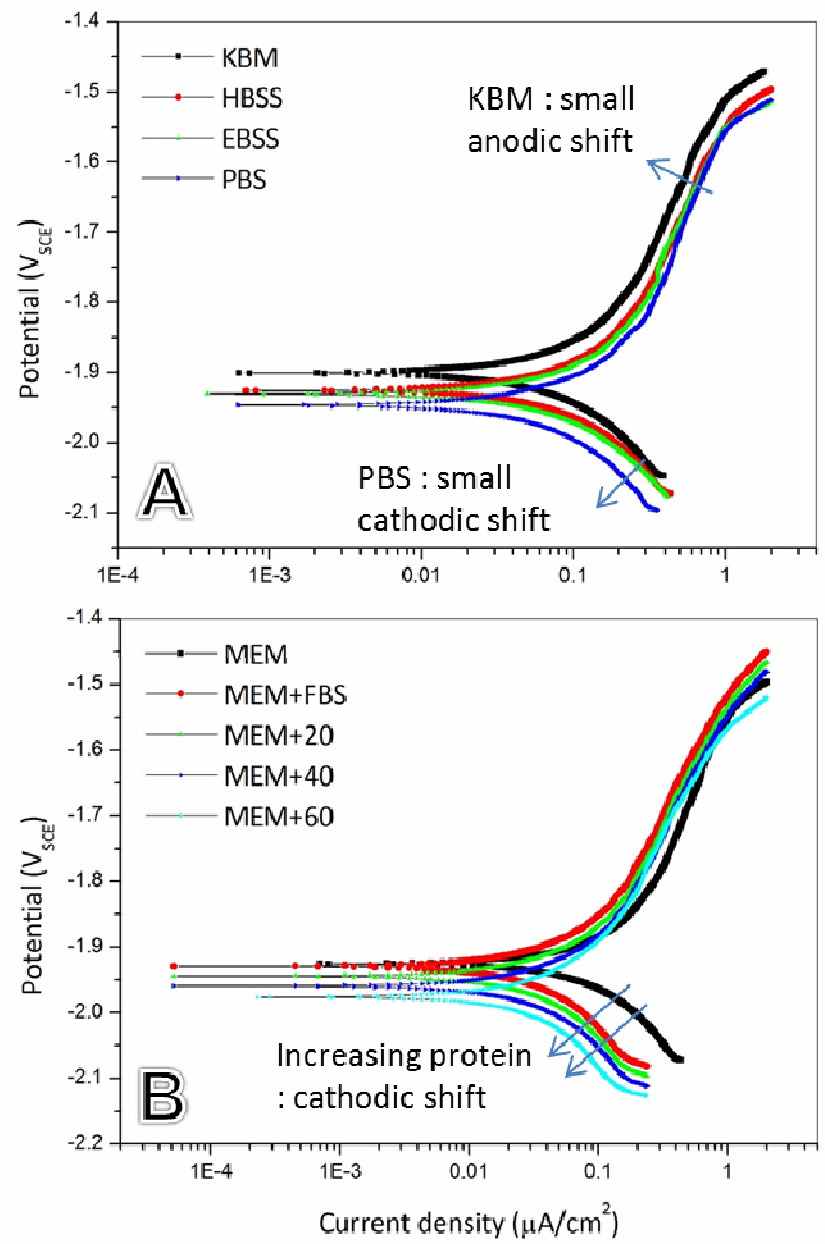

Figure 6-22 : Polarisation curves for pure Mg in (A) BSS and (B) MEM with varying amounts of proteins. (T_{phy}, 7.4)

The i_{corr} of pure Mg in the different media provided comparable information with small but apparent trends in the data (Figure 6-23). Of the BSS, KBM corroded approximately 30% slower than HBSS, EBSS, and PBS. This follows the decrease in the rate of anodic reactions that was seen from the polarisation curves (Figure 6-22A). MEM displayed the greatest

variation in i_{corr}, which indicates that although AA appear to be playing a role in this early corrosion, they might be adhering to the surface inconsistently. Perhaps the most interesting trend is due to the addition of proteins, where initially smaller amounts (such as in MEM with FBS or 20 g/L BSA) resulted in a significant decrease in i_{corr}. Higher concentrations resulted in an increasingly large i_{corr}, although always less than the bare MEM. Combined with the reduction in the rate of cathodic reactions that was observed (Figure 6-22B). This indicates that the proteins must be causing a simultaneous increase in the anodic reaction rate, a trend noted by Mueller *et al.* for WE43 and LAE442 [7]. Therefore, it is evident that the proteins slow the rate of corrosion of pure Mg primarily by limiting the cathodic reactions, while increasing amounts to the physiological range increases the anodic reaction rate.

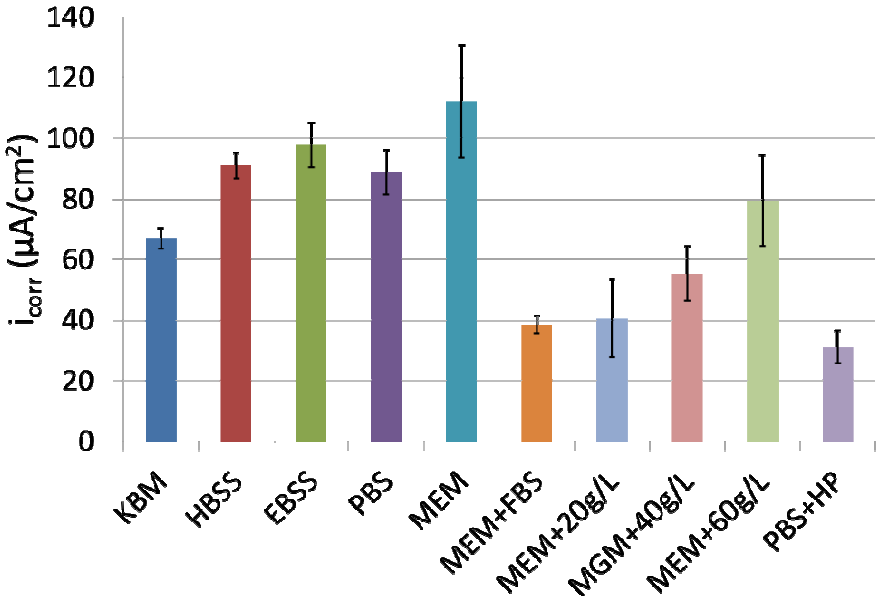

Figure 6-23 : i_{corr} for pure Mg in various *in vitro* media. (T_{phy}, 7.4)

The overall anodic and cathodic shifts due to the various media and their effect on i_{corr} and E_{corr} can be seen in Figure 6-24.

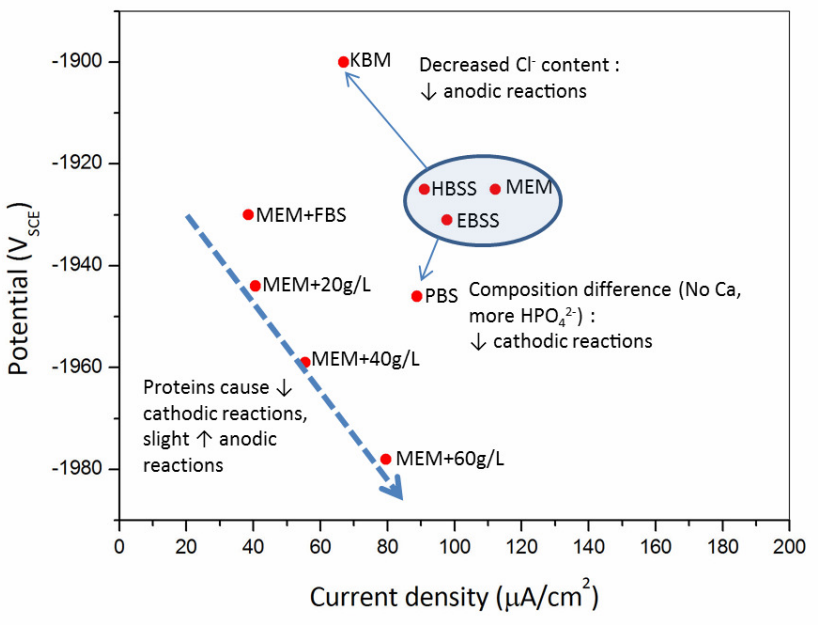

Figure 6-24 : E_{corr} versus i_{corr} for pure Mg a range of media with reaction shifts indicated. (T_{phy}, 7.4)

6.5.4.4. Effect of medium on the polarisation resistance of pure Mg

EIS was carried out on pure Mg samples in all the solutions except for PBS with human plasma (Figure 6-25). KBM, HBSS and EBSS all displayed similar overall behaviour (Figure 6-25A). An initial peak in total resistance (R_{tot}) was found at between 2-4 hrs, however this quickly settled to ~600-800 Ω/cm^2. This peak was due to a rapid increase in the resistance of a layer which had formed on the surface of the Mg, as shown by the concomitant behaviour of the film resistance (R_f) (Figure 6-25C). The peak did not occur in the NaCl or PBS solutions and is indicative of the rapid formation of CaP layer on the surface. This was later confirmed by SEM (Figure 6-26) and EDS analysis of the surface (Table 6-6), verifying the presence of Ca and P in the corrosion layer. After this initial 2-4 hr period the R_f values for the KBM, HBSS and EBSS decreased, eventually becoming relatively constant at 600-700 Ω/cm^2 (Figure 6-25C). KBM displayed the greatest R_{tot} after 72 hrs (1600 Ω/cm^2) while HBSS and EBSS settled to approximately 1300 Ω/cm^2 and 1200 Ω/cm^2, respectively. It is likely that this difference is primarily due to the Cl^- difference between the solutions, affecting the charge transfer resistance (R_{CT}) due to increased attack of the surface *via* the cracks in the CaP coating (Figure 6-26D).

NaCl and PBS solutions displayed a similar R_{tot} trend with no large peak in the first 4 hrs. The samples in NaCl were found to possess only a single time constant throughout the entire 72 hrs, indicating a lack of any significant film or layer on the surface. However, PBS samples were revealed to have two distinct time constants soon after immersion, with R_f rising to approximately 200 Ω/cm^2 within 2 hrs, after which it remained constant for the remainder of the experiment. This layer was found to be composed of significant amounts of phosphorus but only a small quantity of calcium (Table 6-6), which is similar to what has been found on AZ31 in PBS [74].

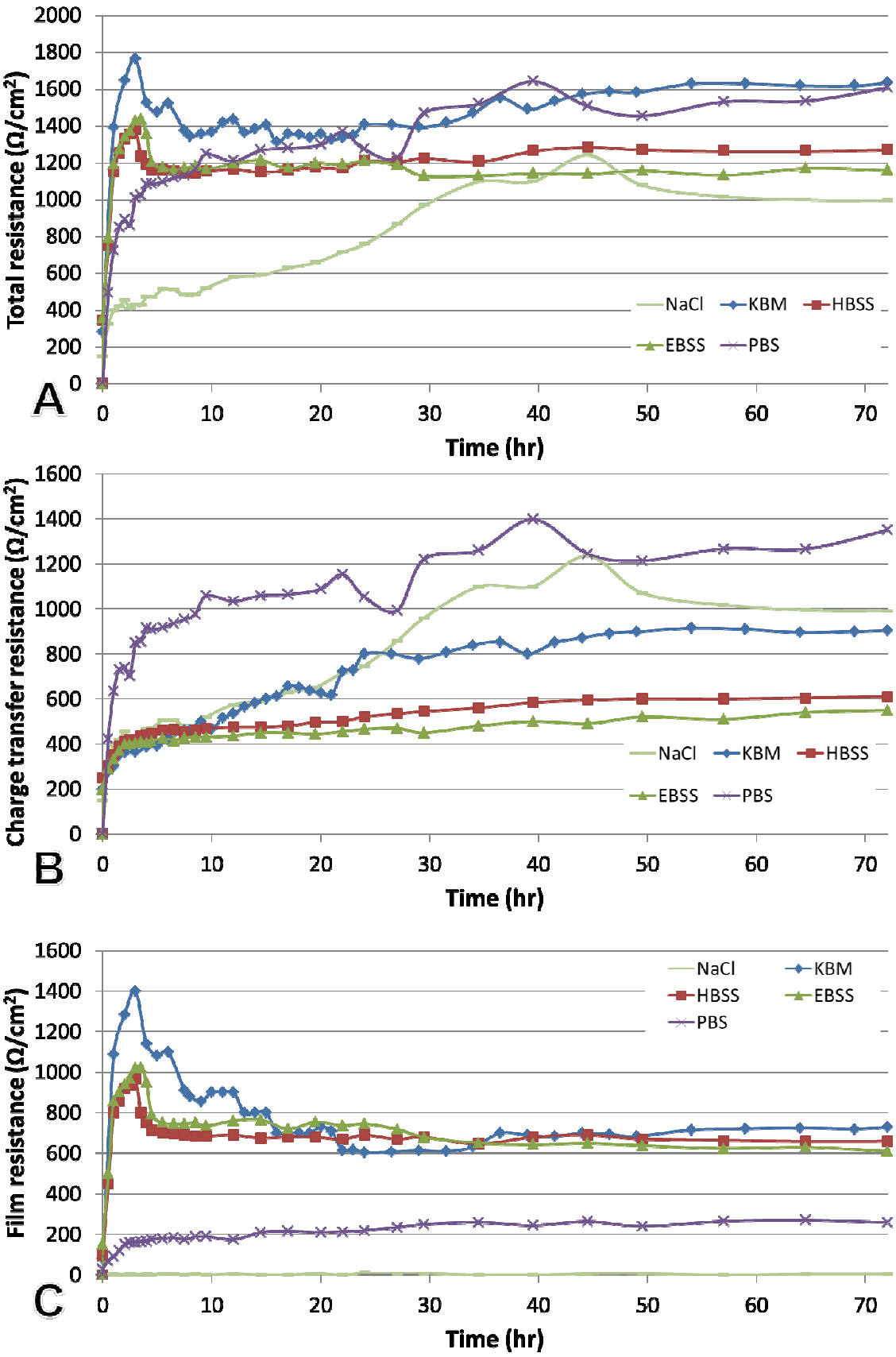

Figure 6-25 : (A) R_{tot}, (B) R_{CT} and (C) R_f for pure Mg in balanced salt solutions over 72 hrs. (T_{phy}, 7.4)

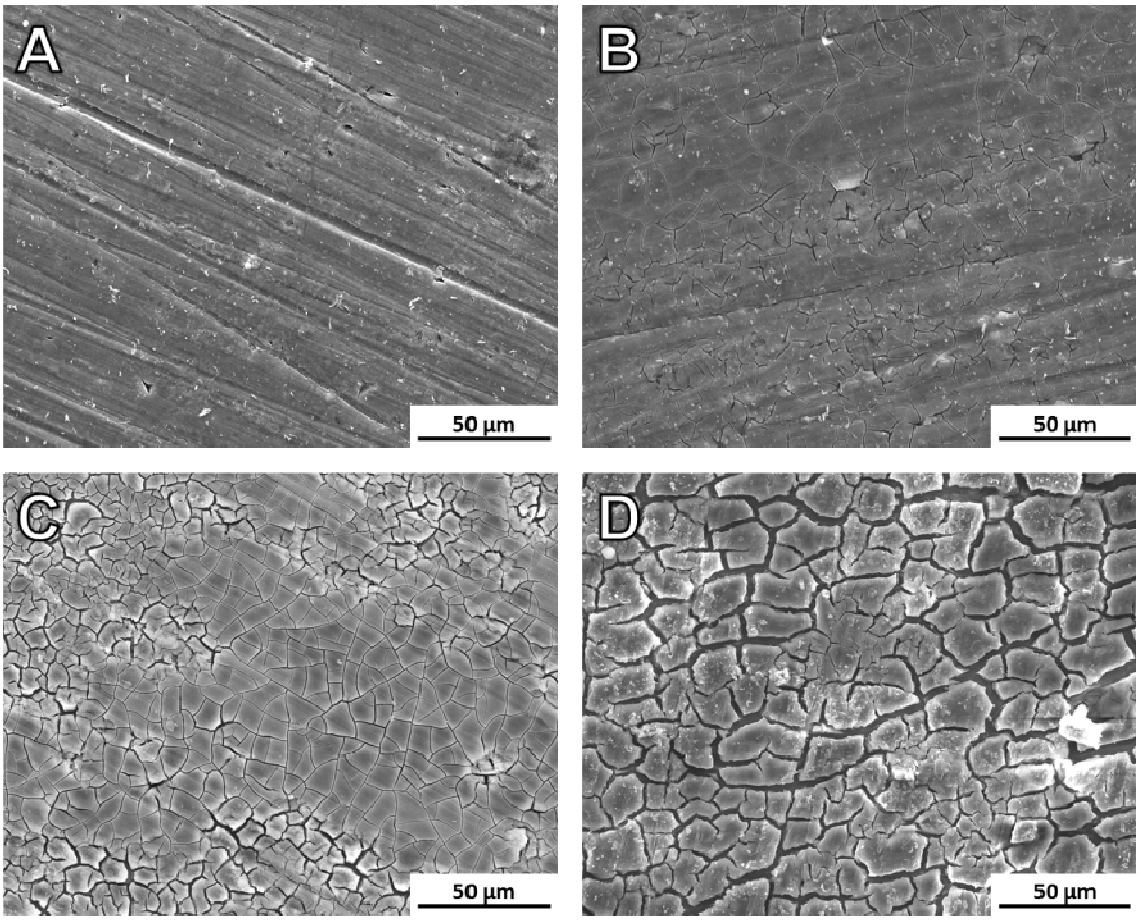

Figure 6-26 : Scanning electron micrographs of pure Mg after immersion for (A) 5, (B) 30, (C) 60, and (D) 180 min. (HBSS, T_{phy}, 7.4)

MEM displayed similar polarisation behaviour to the BSS (Figure 6-27). An initial peak in R_f was observed at 3.5 hrs, after which the values settled to approximately 550 Ω/cm^2 which is comparable to the BSS (except for PBS). However, the R_{CT} was significantly lower than in the BSS. Although MEM contains around 20% less Cl^- than HBSS or EBSS, the inclusion of AA may be the cause of this decrease. A number of reasons have been suggested for their effect (see Chapter 6.5.5.1).

The addition of proteins displayed a number of interesting phenomena. Unlike other media, the addition of BSA resulted in an initial peak in R_{CT} rather than R_f. Although smaller peaks were also visible for the R_f, the R_{CT} dominated the early resistance with all three solutions having approximately 1000 Ω/cm^2 after 1-2 hrs. However, this rise in R_{CT} did not last long and soon dropped to less than 50% of its peak value after just 3 hrs of immersion. The R_{CT} of

the 40 g/L and 60 g/L solutions remained constant at ~400-500 Ω/cm^2 until 30 hrs, then started to slowly decrease. This may be due to significant corrosion having occurred, as shown in Figure 6-28G-I, which would have increased the surface area dramatically, further decreasing the resistance (which was based on a known surface area). The MEM containing 20 g/L BSA displayed slightly different R_{CT} behaviour with a rise between 15 and 30 hrs. This coincided with a decrease in the film resistance, and may be related to a second adsorption layer as the CaP layer breaks down revealing the bare Mg. However this behaviour was not confirmed experimentally.

The surface film that formed in the presence of proteins did not provide significant protection. A R_f was only visible for approximately 12, 20, and 27 hrs for the 60 g/L, 40 g/L and 20 g/L solutions, respectively (Figure 6-27C). The formation of a CaP-containing layer was significantly hindered by the presence of proteins, with higher concentrations resulting in increasingly rapid degradation. EDS analysis confirmed decreased levels of Ca and P on the surfaces of the samples immersed in protein-containing solutions (Table 6-6). A similar behaviour has been found for certain proteins in the literature [57]. After 30 hrs all protein-containing solutions displayed only one time constant, indicating that no protective layer remained. The lack of a semi-protective layer on the surface of the Mg is likely the reason that the corrosion rate increased in the presence of proteins.

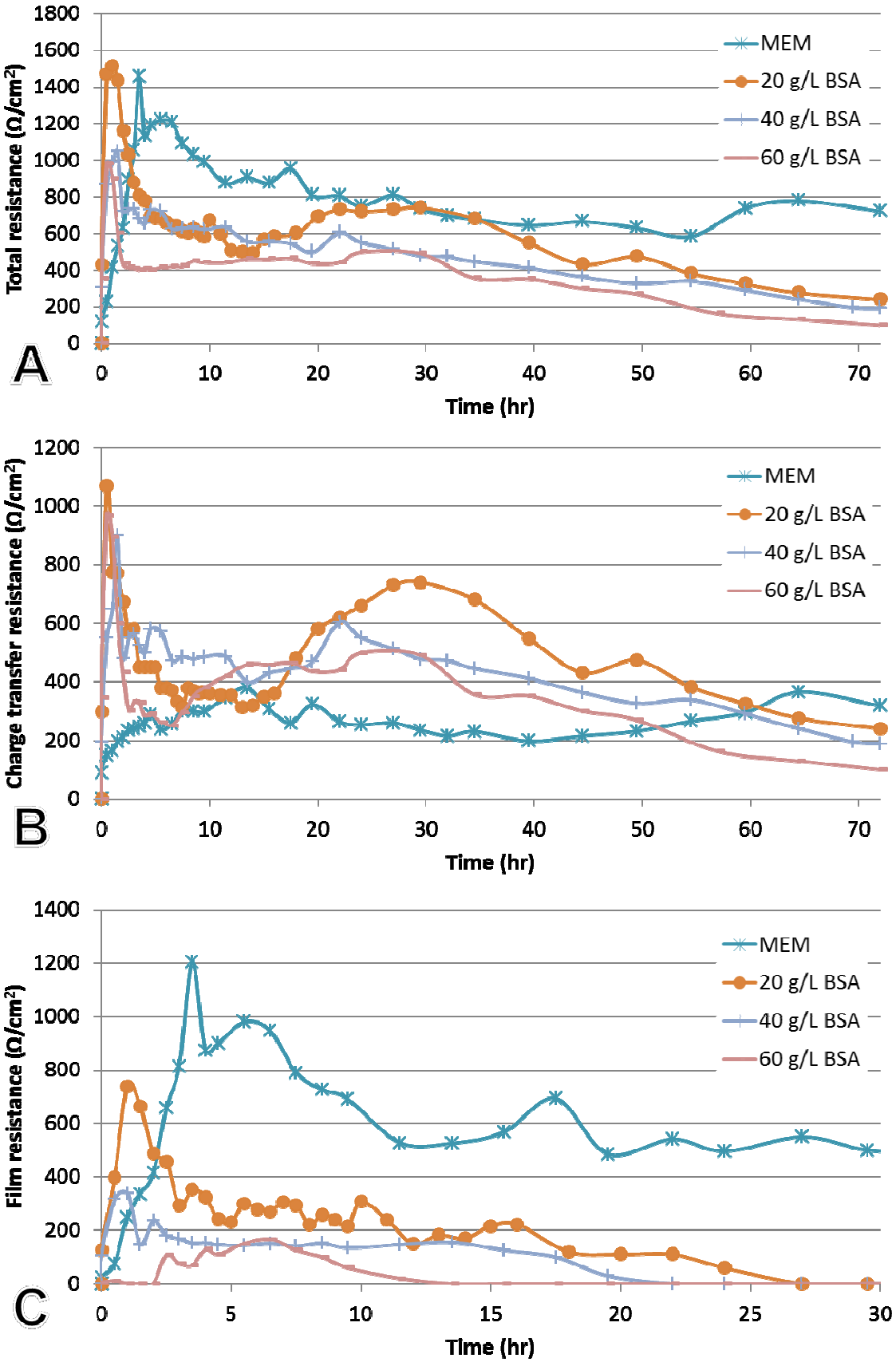

Figure 6-27 : (A) R_{tot}, (B) R_{CT} and (C) R_f of pure Mg in MEM with varying amounts of BSA over 72 hrs. R_f is shown for only the first 30 hrs for clarity. (T_{phy}, 7.4)

Several important observations can be made by examining the behaviour of pure Mg in these different media. It is clear that NaCl and PBS media cause significantly different corrosion mechanisms than the other BSS and MEM. For NaCl no layer forms other than a very weak $Mg(OH)_2$ film. PBS causes a relatively weak magnesium phosphate layer to form which provides minimal protection of the subsurface. In contrast KBM, HBSS, EBSS and MEM all form a significant CaP-containing layer which appears relatively stable and provides some protection from corrosion. KBM, HBSS and EBSS all displayed virtually the same behaviour with any differences likely due to the Cl^- variation in their composition. Amino acids (AA) in MEM appear to have a negative effect on R_{CT}, lowering it below the BSS which contain greater concentrations of Cl^-. AA also result in increased variation in both PDP and EIS measurements. Although the exact reasons are unknown, this behaviour is further explored in Chapter 6.5.5.1.

Proteins appear to be involved in more complex reactions at the Mg surface. PDP experiments found the addition of proteins lowered the i_{corr} of pure Mg in MEM (Figure 6-23). In contrast, longer term EIS scans have established proteins to increase the corrosion rate of pure Mg (Figure 6-27A). Proteins also appear to add corrosion protection in the very early stages (0-2 hrs), likely due to adsorption to the surface. This adsorption results in a decrease in the cathodic reaction rate, but may cause a slight increase in the anodic reaction rate at higher concentrations (Figure 6-22). However, EIS analysis has found increasing protein amounts negatively impact the formation of a CaP layer, allowing further attack of the underlying Mg (Figure 6-27C). The impact of several proteins is explored further in Chapter 6.5.4.6.

6.5.4.5. Morphology and composition of corrosion layers on pure Mg in various SBF

The corrosion morphology formed in a NaCl medium displayed a directionally-cracked surface (Figure 6-28A). The direction of the cracking was found to depend on the orientation of the grains. Pitting was also evident, sporadically covering the entire surface. Samples in KBM, HBSS, EBSS and PBS exhibited similar corrosion morphology (Figure 6-28B-E); a cracked earth-like structure prevailed, similar to that commonly found for Mg in BSS [6, 71, 87, 88]. The layer was made up of varying amounts of Mg, O, Ca, and P, indicating a mixed Ca-Mg-P composition as was suggested by Rettig and Virtanen [37]. Occasional pits were visible on the surface, usually surrounded by an area with no Ca or P. It has been suggested

that the formation of Ca / P rich layers provide the bulk of the corrosive protection for Mg alloys in most BSS [42].

Samples corroded in MEM displayed a more severe corrosion morphology (Figure 6-28F). A comparable corrosion pattern as the BSS could be observed, although the cracks tended to form sharper edges. The BSA-containing MEM solutions also displayed a fractured corrosion layer, but did not show the same crack pattern as the other BSS (Figure 6-28G-I). Gaps in the layers were wider and appeared deeper than in the other media. For the protein-containing solutions, no obvious corrosion layer could be seen on the surface.

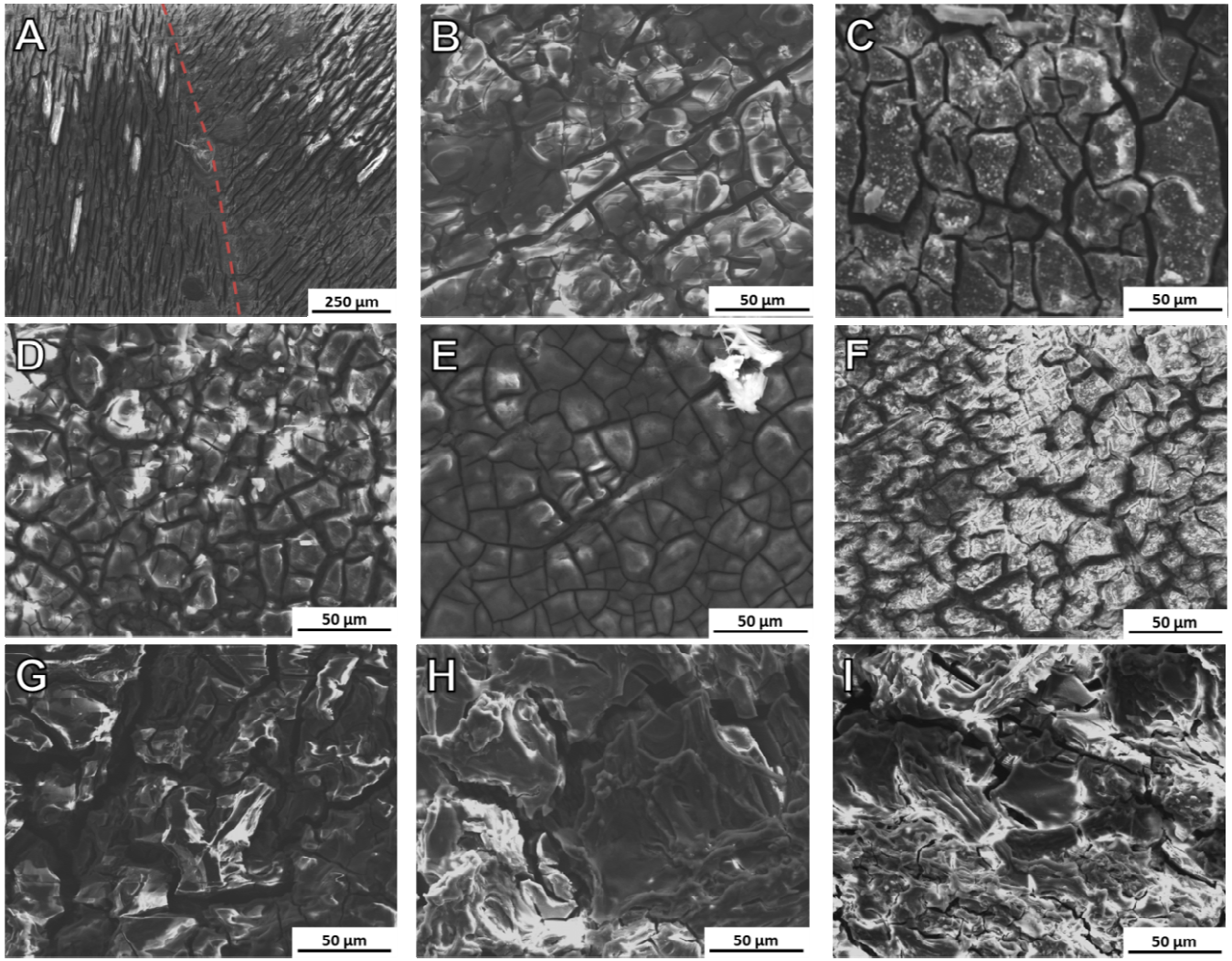

Figure 6-28 : Scanning electron micrographs of the surface of pure Mg samples after 72 hrs immersion in: (A) NaCl, (B) KBM, (C) HBSS, (D) EBSS, (E) PBS, (F) MEM, (G) MEM + 20 g/l BSA, (H) MEM + 40 g/l BSA, and (I) MEM + 60 g/l BSA. Dotted line in (A) indicates the grain boundary. (T_{phy}, 7.4)

EDS analysis of the surface of samples immersed in the NaCl solution found only Mg and O (Table 6-6). This would indicate that a layer of $Mg(OH)_2$ was present, which is typical for Mg in saline solutions [37]. KBM, HBSS and EBSS had comparable quantities of Mg, O, Ca, and P. The elements were distributed evenly across the corrosion layer. The surface of samples immersed in PBS displayed high amounts of P and little Ca. This difference in elemental composition of the corrosion layer is likely a result of two factors. Firstly, PBS does not contain Ca, so there should be very little Ca^{2+} in the solution to form compounds with and precipitate onto the surface [48]. Inaccuracy in the EDS technique may be the reason that any Ca is being picked up on the PBS surface. Secondly, Rettig and Virtanen found that magnesium phosphate tribasic ($Mg_3(PO_4)_2$) will readily form in solutions absent of Ca, whereas Ca will not be deposited on a Mg alloy surface without HPO_4^{2-} [37]. Therefore, it is likely that the surface of the samples in PBS were a combination of $Mg(OH)_2$ and $Mg_3(PO_4)_2$, as indicated by EDS (Table 6-6).

As the concentration of BSA increased in the MEM solutions there was a concomitant decrease in the amount of Ca and P in the corrosion layer. The surface layers of samples immersed in MEM with 60 g/L BSA solution contained less than half the concentration of Ca and P as did the layers of samples immersed in KBM, HBSS and EBSS. Although the thickness of the corrosion layers could not be determined from the micrographs (Figure 6-28), EDS found that they consisted of increasing amounts of Mg as the protein concentration rose. However, the concentration of oxygen on the surface remained relatively stable irrespective of the BSA addition. Therefore it is hypothesised that the increased concentration of Mg may be due to the corrosion layer being thin enough that the EDS detected the pure Mg sub-layer.

Table 6-6 : Elemental composition (at. %) of corrosion layer on pure Mg after testing in various solutions (according to EDS). (T_{phy}, 7.4)

Solution	Mg	O	Ca	P
NaCl	*43.2*	*55.1*	*0*	*0*
KBM	*28.7*	*49.1*	*13.1*	*7.2*
HBSS	*29*	*48.5*	*10.4*	*9.8*
EBSS	*33.1*	*46.8*	*12.5*	*7.4*
PBS	*32.9*	*45*	*0.5*	*17*
MEM	*27*	*50.2*	*9.5*	*5.7*
20 g/L	*36.1*	*50.4*	*5.8*	*4.4*
40 g/L	*40.4*	*50.1*	*4.1*	*3.2*
60 g/L	*42.4*	*47.2*	*4.2*	*3*

Values may not reach 100% due to presence of other elements (Na,Cl) on the surface.

It should be noted that the use of EDS to determine the presence of proteins by detection of C and O is potentially flawed as these elements could come from other sources (***e.g.*** $Mg(OH)_2$, Mg and Ca carbonate). Consequently, although some authors in the bio-Mg literature have used the detection of C and O on the surface to confirm protein attachment, this justification is inappropriate [28]. Others have used EDS analysis to discuss the potential for the existence of organic matter on the surface. Yamamoto ***et al.*** stated that protein additions are responsible for increased Ca and P within surface coatings, although it was acknowledged that the EDS technique was not an accurate measure of protein-substrate binding or adsorption [42]. Rettig and Virtanen suggested it might be possible to detect the nitrogen (N) that is within the amino acid to indirectly measure the presence of proteins [37]. However, the authors were not able to detect any N in the study, and EDS analysis in this work did not find any measurable amount.

6.5.4.6. Adsorption of proteins to pure Mg

Perhaps the most puzzling problem facing the development of appropriate media for Mg corrosion experiments is the role of proteins. As the previous chapters have shown, proteins play a significant role in the degradation of Mg alloys. Although some studies have found protein additions to media decrease the corrosion of Mg alloys [42, 72, 81, 82], others have found proteins to increase degradation rates [28, 89]. Still other studies have found their

effect to be alloy and concentration dependant [7, 71]. The reasons for these differences are currently unclear, and may only be elucidated through better understanding of the mechanics of protein adsorption to the Mg.

Protein adsorption is itself very complex, involving hydrogen bonding, van der Waals forces, hydrophobic and electrostatic interactions [90]. A review of the most common techniques used to study protein adhesion is given in Appendix F. It is well-established in the literature that proteins are likely adsorbing to the surface of Mg. Various experiments were designed in this work with the aim of developing techniques for investigating protein adsorption on Mg.

Surface staining

The protein attachment to pure Mg was investigated using a surface staining technique, as discussed in Chapter 4.6.1. Some staining and a constant blue hue could be seen macroscopically on the surface of samples immersed in PBS with 40 g/L BSA after 15 min (Figure 6-29C). It was thought that this staining was primarily due to protein attachment as little corrosion had occurred (indicated by the visible polishing grooves). The samples in protein-free PBS did not display this colouring, but rather a dulling of the surface as $Mg(OH)_2$ formed (Figure 6-29B). However, significant staining was observed after 30 and 60 min regardless of whether proteins were present (Figure 6-29D). Extended wash times in the distilled water did not remove this stain. The dye also appeared to have bonded to the Mg surface, making it difficult to distinguish whether the observed colour was due to protein attachment or the Mg substrate. Given the incomplete staining of the surfaces it is possible that it is the corrosion layer itself that is being stained.

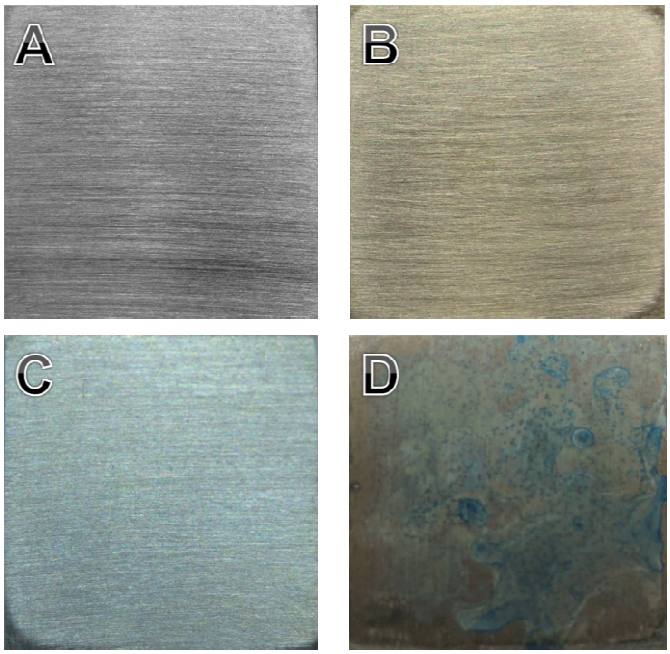

Figure 6-29 : Photographs (2 ×) of protein staining of pure Mg samples. (A) As-polished Mg, (B) 15 min in PBS, (C) 15 min in PBS with 40 g/L BSA, and (D) 60 min in PBS. (T_{phy}, 7.4)

The surface staining method appears to provide information on the success of protein adhesion, at least in the early stages of immersion. Unfortunately the stain is not suitable for longer-term experiments as it may adhere to the corrosion layer. Overall, the method may offer a quick, visual check of protein attachment in the early stages of corrosion. The use of different dyes, along with the potential for determining protein attachment on different microstructures (***e.g.*** phases, surface roughness) means considerable promise remains for future use of this method for Mg alloys.

Solute-depletion method

Solute-depletion provides another potential method for measuring protein attachment to Mg alloys. Initially the Nanodrop spectrophotometer was chosen to investigate the short-term time dependency of the protein adhesion. Both BSA and cytochrome-c (CytoC) proteins displayed a general trend of greater protein depletion percentage with increasing concentrations (Figure 6-30). This agrees with Langmuir's isotherm, which relates the amount absorbed to the concentration in the solution [86]. This relationship was most evident after 20 min for the BSA samples (Figure 6-31).

Solutions containing BSA exhibited a drop in protein levels up until 30 min, with a maximum loss of 18% for the 1 mg/mL of medium (Figure 6-30A). The same trend existed for the CytoC solutions until 40-50 min. However, after 60 min both protein solutions displayed a gain in absorbance at 280 nm. This was unexpected, and repeat tests found the same phenomena. It is known that any non-protein component of the solution that absorbs ultraviolet light will interfere with the assay [91], and it is thought that the corrosion products of the Mg may be introducing this artefact. Aggregates of proteins may also interfere with light transmittance [91]. Moreover, un-spun samples resulted in an increase in absorbance of between 2-4 × the original amount of protein, making this step extremely important for an accurate analysis. Interestingly, samples of corroded Mg in PBS without BSA also displayed absorbance at 280 nm whilst pure PBS did not, further indicating the potential side-effects of Mg corrosion on the test.

The BSA-containing solutions displayed significantly more protein depletion than the CytoC equivalents (Figure 6-30A vs. B). This indicates a stronger affinity for attachment of the BSA to the Mg surface than for CytoC. The differences in protein attachment may be explained in part by considering the electrostatic attraction between the different proteins and Mg surface. It has been found that BSA, with a negative charge at a pH of 7.4, adsorbs better to metal surfaces that have a greater positive charge [92]. MgO has an isoelectric point (pI) of 12-13 [93], which results in a positive charge at 7.4. This would appear to be a plausible explanation for the higher adsorption of BSA compared to CytoC, which has a positive charge at a pH of 7.4. The results from these experiments also highlight the importance of protein selection in designing a realistic *in vitro* experiment for biodegradable Mg.

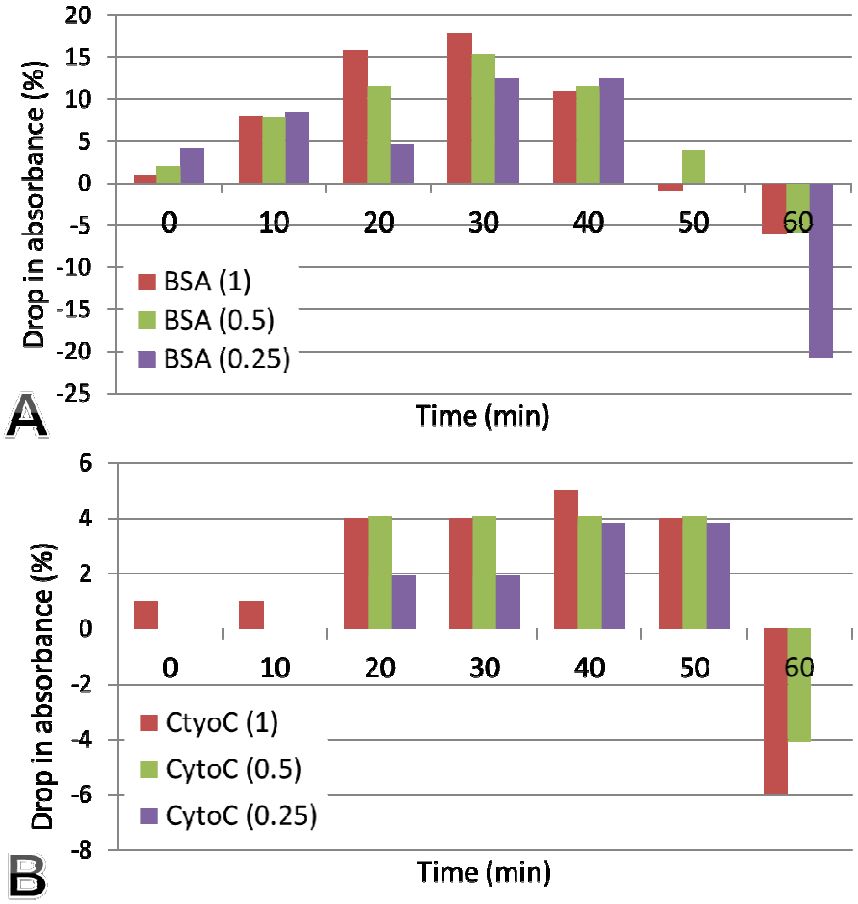

Figure 6-30 : Changes in adsorption over 1 hrs for pure Mg samples in PBS with (A) BSA and (B) CytoC. No change in absorbance was detected where bars are not present. (T_{phy}, 7.4)

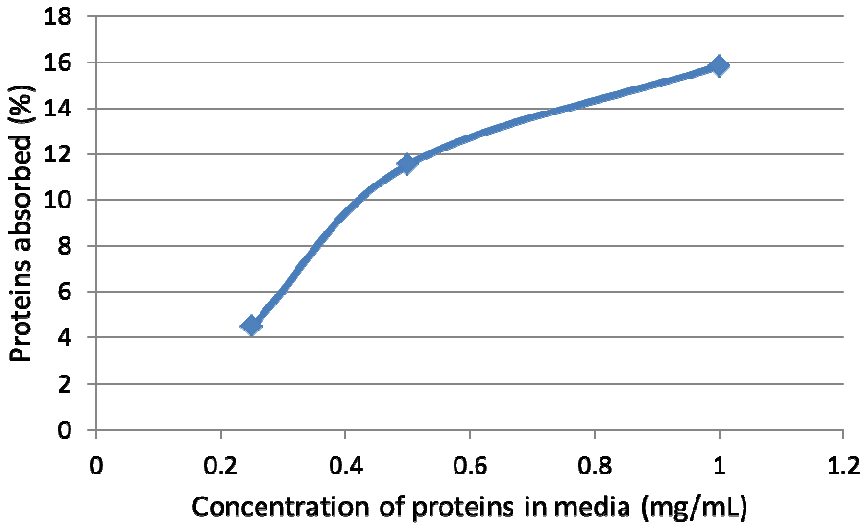

Figure 6-31 : Example of protein adsorption behaviour following Langmuir's isotherm. Data is from 20 min time point of tests in PBS with varying amounts of BSA. (T_{phy}, 7.4)

Following the Nanodrop, longer-term tests were performed in an Ultrospec 2100 pro spectrophotometer which required a 50 × greater volume to analyse. It was thought that the greater volumes involved could minimise or eliminate the extra pickup of absorbance at 280 nm that was occurring around the 1 hr point for the Nanodrop tests. The larger volume and dilution would also allow more accurate readings of the absorbance.

Samples taken at 1 hr supported the trend that was shown by the Nanodrop results, with significantly more loss of BSA occurring than CytoC (Figure 6-32). In addition, the "extra" absorbance at 280 nm did not occur for these experiments. The largest decrease in protein concentration occurred in the 1 mg/mL BSA solution, with the BSA overall showing greater depletion rates at each concentration.

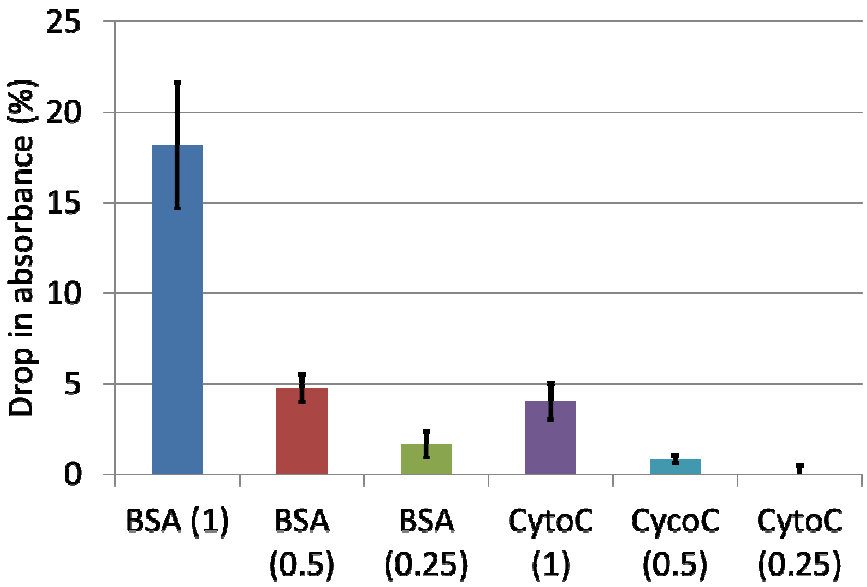

Figure 6-32 : Decrease in adsorption after 1 hr immersion in PBS with different protein concentrations (mg/mL). (T_{phy}, 7.4)

However, data from the 24 hrs samples were not as definitive. The samples displayed extremely varied behaviour with large deviations from sample to sample in the same solution (Figure 6-33). Multiple repetitions of spinning in the centrifuge did not solve this. It appears that the Mg corrosion product that is released over time significantly affects the absorbance of light at 280 nm. This limits the use of this test for longer-term experiments where corrosion products remain in solution.

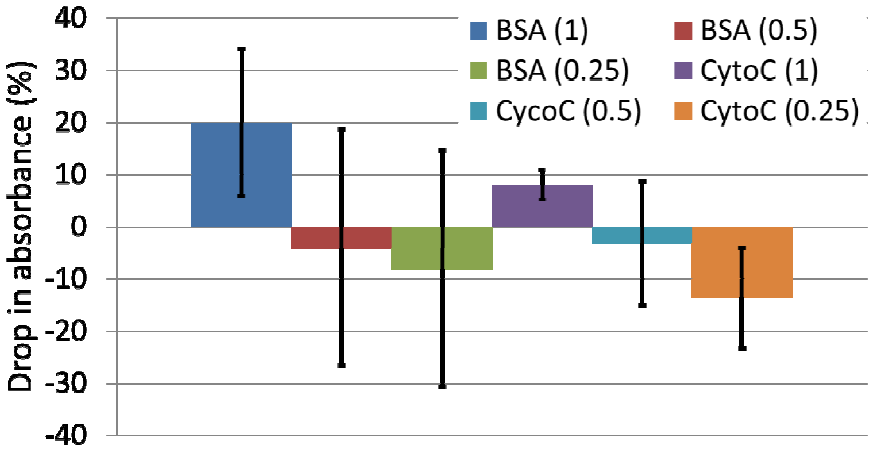

Figure 6-33 : Protein depletion after 24 hrs for PBS with different protein concentrations. (T_{phy}, 7.4)

Overall, the solute-depletion method has shown promise as a powerful technique for detecting the amount of protein that has been absorbed to a Mg surface. In the short term, and using the correct analysis equipment, it is possible to determine the amount of protein that has been adsorbed to a known surface area. However, it appears that the Mg corrosion product also influences the 280 nm absorption profile, creating a problem in longer-term experiments.

It is also possible that the corrosion by-product in solution denatured or aggregated the proteins. This would mean that they would be lost when the media were centrifuged before absorbance measurements. This would account for some of the loss from the solution phase. The difference in adsorption between the two proteins may also be due to their different reactions to this corrosion product. Further investigation of this phenomenon is warranted in order to develop a more robust methodology.

Quartz crystal microbalance

The morphology of the Mg coatings on the crystals resembled hexagonal-shaped "micro-towers" (Figure 6-34). There was an increase in the average size of each micro-tower as the voltage increased, from around 100 nm at 150 V to 400-600 nm at 600 V; this was in line with other studies [94]. The thickness of the coatings was found to be 2.03 ± 0.7 µm, which was close to the value recommended (2 µm) by the manufacturer of the crystals (Q-Sense). Image analysis software (ImageJ) was used to determine the amount of area that was taken up by the micro-towers relative to the gaps in-between. The 600 V samples were found to have

the smallest area occupied by the gaps (21%). Thus, these samples with the lowest surface area were chosen for QCM analysis to minimise the corrosion rate.

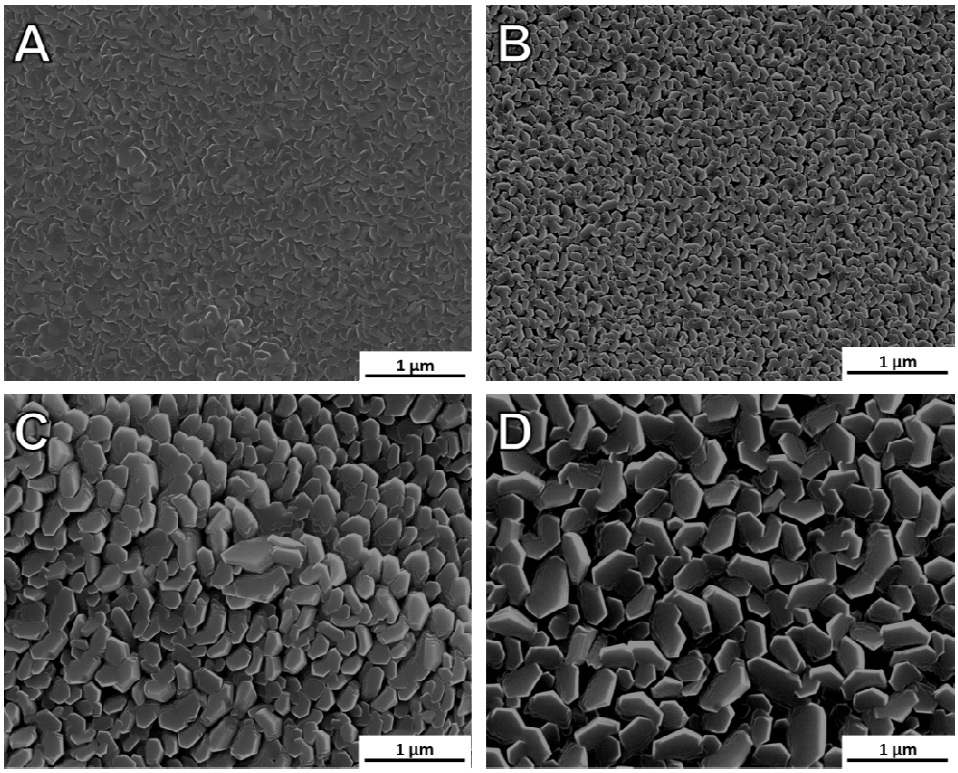

Figure 6-34 : Scanning electron micrographs of sputter coated surfaces using different applied bias voltages: (A) 150 V, (B) 300 V, (C) 450 V and (D) 600 V.

Unfortunately, the results of the QCM experiment displayed a fundamental flaw with the coating of the crystals. The gold-coated reference crystal displayed expected behaviour, with a notable drop in frequency when comparing the MEM after immersion in MEM+BSA to that before (Figure 6-35). This indicated that proteins had adhered to the surface, dampening its frequency response. This was still evident after the ethanol was flowing at the end of the experiment. However, the Mg-coated samples did not perform as was hoped. Soon after immersion in MEM the frequencies started to rise significantly. This was the opposite behaviour to what occurred to the gold samples, indicating a mass loss occurring in the Mg coating. Changing of the medium from MEM+BSA to MEM had a minimal effect on the frequency response compared with mass loss due to Mg degradation on the surface. Several frequencies (not shown) rose by more than 5 orders of magnitude due to this loss. When the samples were removed (after 26 min of immersion) there was no visible trace of the Mg on the surface.

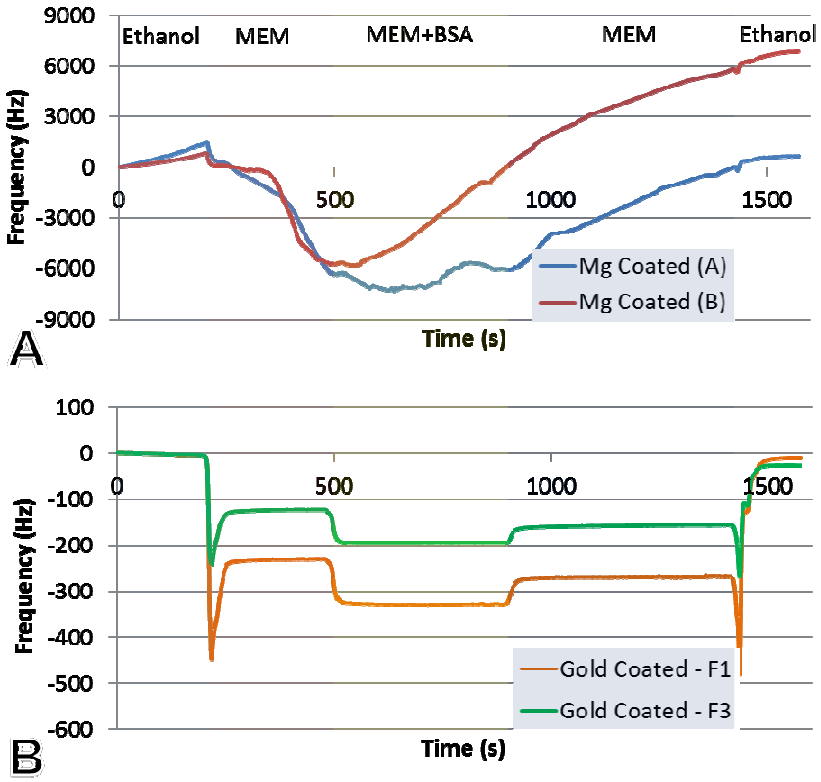

Figure 6-35 : Fundamental frequency responses of Mg sputter coated crystals and a gold-coated reference crystal. Two fundamental frequencies are shown for the gold sample to highlight its stability. (T_{phy}, 7.4)

Although QCM shows significant promise as a relatively easy way to measure protein adsorption over time, the process is currently limited by the coating process for the crystals. It appears that sputter deposition does not provide a suitable surface with sufficient corrosion resistance to measure the protein attachment. This is attributed to the large surface area of the micro-towers that form during sputtering. However, it may be possible that alternative coating techniques will provide a suitably smooth coating with sufficient corrosion resistance. The potential of this technique for studying the impact of proteins on a range of Mg alloys is considerable; provided thin Mg films can be formed on the crystal that closely represent the surface area and microstructure of the bulk alloys.

6.5.5. Further discussion of organic components of SBF

6.5.5.1. Importance of amino acids to Mg biodegradation

AA are a vital component of the body. They are molecules that contain C, H, O, and N, perform many roles that are vital to nutrition, and form the building blocks for proteins [95]. AA are also known to affect corrosion. Several studies on aluminium alloys have found significant corrosion inhibition due to AA [96-98], while others have found similar effects for steel [99] and lead alloys [100]. Recently, some studies have indirectly looked at the effect of AA on the performance of Mg alloys *in vitro*.

Yamamoto *et al.* found the presence of AA in MEM to increase the corrosion rate of pure Mg when compared with AA-free media such as EBSS [42]. The authors suggested that the AA were forming a complex with Mg^{2+} ions, as has been suggested elsewhere [101, 102]. AA may also be involved in inhibiting the formation of the $Mg(OH)_2$/CaP layer on the Mg *via* chelation, where metal ions attach to a large molecule and are removed from the surface [42]. Xin *et al.* also observed an increased corrosion rate in MEM compared with PBS and HBSS, although no explanation was given for this [61].

However, other studies observed AA to result in a decrease in the corrosion rate of Mg alloys. Gu *et al.* reported that, over a period of 7 days, Mg-1.5Ca, AZ31 and AZ91 displayed an increased R_{tot} and reduced i_{corr} in MEM compared with HBSS [71]. However, no experimental evidence was available to support the author's hypothesis that AA adsorb on the Mg surface, acting to decrease the corrosion rate.

In this work it has been found via several methods that solutions containing AA appear to corrode faster than those that do not (Figure 6-23, Figure 6-27). Although the reasons for this variance have not been completely deduced, several theories have been expressed in the literature. Ashassi-Sorkhabi *et al.* found that a wide variety of individually tested AA acted as cathodic inhibitors for aluminium, with increasing concentrations from 0.0001 to 0.1 M providing growing protection [96]. Some AA, such as tryptophan and proline, were more effective at inhibiting corrosion than others, including alanine and valine. They also found that the efficiency of the inhibition increased with concentration, obeying the Langmuir isotherm [96]. Earlier work by the same author found similar results [99], as did another

study on a Pb-Ca-Sn alloy [100]. However, it should be noted that these tests were performed in HCl or H_2SO_4 solutions, so the AA may not behave in the same way in SBFs.

Bereket *et al.* found that AA limited the presence of pitting corrosion on Al [98]. They indicated a shift in the pitting potential due to AA adsorption as the most likely reason for this. A similar effect was found by El-Shafei *et al.,* where a range of AA all resulted in a reduced corrosion rate and a more positive E_{corr} for pure Al [97].

AA have been shown to affect Mg *in vitro* by altering the morphology (Figure 6-28) and elemental composition (Table 6-6) of the corrosion layer. AA also have a considerable effect on the electrochemical corrosion performance of pure Mg, changing both the way in which the surface films form as well as lowering the overall R_{tot} (Figure 6-27). However, it is still unknown how AA affect Mg biodegradation *in vivo* and this area warrants further study.

6.5.5.2. Influence of cellular attachment on Mg biodegradation

Another potential addition to SBFs on the path to biorealistic solutions is the use of cells. Cellular attachment is critical to the success of a Mg implant and may play a considerable role in its corrosion. For example, macrophages and the active oxygen species generated by them are reported to accelerate corrosion of Ti [103]. Although cells were not studied as part of this dissertation work, relevant literature was collected to provide a comparison to the experiments performed.

In the bio Mg literature the vast majority of experiments that have utilised cells have been toxicity studies on different alloys [25, 32, 87, 89, 104-112]. While most have found that the alloys have caused little toxicity with the cells, they generally have not investigated the effect cellular attachment can have on corrosion.

However, recently several studies have made steps to investigate this. Feser *et al.* looked at the concentration of Mg (mmol/L) in cell media for a range of Mg-Ca alloys (0.6-1.2 wt. % Ca) [113]. They found increasing levels of Mg as the Ca content increased. However, little discussion was given on the mechanism or reasons for differences in corrosion. Wong *et al.* compared cell viability with Mg^{2+} ion release over time, but did not directly look at the effect of cells on the corrosion [114]. In perhaps the most relevant study, Gu *et al.* examined the Mg, Ca and Zn concentrations at 1, 3 and 5 days for a range of Mg bulk metallic glasses in

DMEM with and without L929 or MG63 cells [47]. It was found that several alloys corroded around 30-50% slower in media containing cells, however pure Mg remained similar. They also discussed the effect that H_2 evolution, rapid ion release and pH changes may have on cell attachment.

In related work, Hiromoto *et al.* described how cells may slow the interaction of Cl^- ions with the surface of metal implants, slowing corrosion significantly [115]. Witte *et al.* has also reported that giant cells have actually engulfed small amounts of Mg corrosion product, although this was related more to toxicity [116].

It is clear that cellular activity is crucial to the success of a Mg implant *in vivo*. However, what has not been established is the potential role the cells may play in the degradation mechanisms of Mg alloys in both the short- and long-term.

6.5.6. Summary of effect of medium choice on Mg biocorrosion

Correct medium choice is absolutely vital to the biocorrosion of Mg alloys *in vitro*.

At this point in the research of Mg alloys for bio-applications, the use of simple saline solutions is normally inappropriate. It is clear that the corrosion that occurs varies significantly from other BSS, including corrosion rates (Figure 6-25) and the surface morphology (Figure 6-28) and composition of the resultant corrosion layer (Table 6-6). The most crucial of these, a lack of a CaP layer on the surface of the Mg, contributes significantly not only to an increase in corrosion but also to different degradation behaviour.

The BSS that have been used thus far are themselves not perfect. With the vast majority of work performed in HBSS, EBSS, or PBS, the increased Cl^- content over blood plasma (Table 6-4) has been shown in this work to contribute significantly to the corrosion rate in both chemical and carbonate buffering systems (Figure 6-18). The BSS themselves vary somewhat in corrosion rates (Figure 6-23), anodic/cathodic reaction rates (Figure 6-22) and the elemental composition of the corrosion layer (Table 6-6). However, with the exception of PBS, most BSS displayed similar polarisation behaviour over 72 hrs (Figure 6-25) and exhibited comparable corrosion morphology (Figure 6-26). PBS cannot be generally recommended for Mg *in vitro* experiments due to the lack of Ca that is crucial to CaP

formation. While the other BSS may be considered a suitable option, it is recommended that future experiments be performed in SBFs with ionic concentrations as close as possible to physiological conditions, especially for Cl^-, Ca and P (such as KBM).

Proteins and amino acids have also been shown to effect the degradation rates and mechanisms in Mg. Amino acids present in MEM primarily affect the bare Mg surface, causing reduced corrosion resistance (Figure 6-27) and a wider variation in electrochemically recorded values (Figure 6-19). Proteins have a more complex effect, reducing the cathodic reactions of pure Mg (Figure 6-22) and reducing the recorded i_{corr} (Figure 6-23) in the early stages of immersion, likely due to adsorption to the bare Mg surface (Figure 6-30). However, after this period they appear to heavily inhibit the formation of any CaP layer on the surface (Table 6-6) and result in increased overall corrosion (Figure 6-27, Figure 6-28). Although some progress has been made towards greater understanding of the adsorption behaviour of selected proteins to Mg (see Chapter 6.5.4.6), there remain considerable gaps in this knowledge.

Although arbitrarily it might be correct to say the most realistic solution should always be used for *in vitro* tests, this may not currently be the case. Efforts have been made in the literature and this work to understand the effect that proteins have on the degradation performance of Mg alloys. However, much of the time-dependant adsorption behaviour of proteins and the effect they have on long-term corrosion are unknown. Greater comparison of surface corrosion mechanisms and corrosion layer product between *in vitro* and *in vivo* is drastically needed to confirm that the effects of proteins are similar when investigated outside the body. Without this core knowledge it will not be feasible to recommend any single amount of protein addition and claim that it presents a realistic, physiological environment.

6.6. Other *in vitro* variables that affect biodegradation of Mg

6.6.1. Media flow rates

6.6.1.1. Introduction

At any site in the body, an implant material will come into contact with some form of perfusion (*i.e.* flow) of blood and body fluid. This movement of fluid provides cells and nutrients to the implant surface as well as disposing of degradation products [117]. Flow conditions can vary widely, from rates of ~1 m/s in arteries to virtually undetectable perfusion in cortical marrow [118, 119]. These conditions can therefore have an extensive range of effects on the performance of an implant, including its corrosion rate. This was highlighted in a study by Witte *et al.*, which proposed that blood flow around implants *in vivo* increases the corrosion rates of AZ91 and LAE442 alloys [76]. They inferred that flow accelerates Mg mass diffusion, prevents the formation of gas cavities of evolving H_2, and inhibits pH change at the surface [76].

Recently, there has been increasing interest in the effect of flow rate on the biodegradation of Mg alloys. Bender *et al.* performed electrochemical tests on AM and AZ alloys using a rotating disc electrode at 2000 rpm [120]. However, although they found varied corrosion results between the different alloys and rotation speeds, they did not compare the rates to static (no flow) conditions. Chen *et al.* investigated a Mg-Zn alloy of an unstated composition using parallel flow over the sample surface with a flow shear stress of 0.68 Pa for 180 hrs [121]. However the pH was not controlled during the experiment and no comparison was made between dynamic and static conditions.

Hiromoto *et al.* examined pure Mg in 0.6 wt.% NaCl using a rotating electrode at 0, 120, 240, 720 and 1440 rpm [118]. Increasing the rotation speed of the samples significantly increased the corrosion rate in the first few hours. The authors revealed that the chemical dissolution of $Mg(OH)_2$ was accelerated by increasing rotation speeds up to 720 rpm, thereafter faster speeds had no further impact. Furthermore, electrochemically determined i_{corr} results indicated that approximately three times more corrosion was occurring at 720 and 1440 rpm compared with static conditions. It should be noted that this study was based on a simple saline solution (pH = 6.0), which would not allow a CaP layer to form at the Mg surface, limiting extrapolation of the results to a real physiological situation [118]. Hiromoto *et al.*

also investigated the effect of both flow and pH concurrently for pure Mg samples [122]. They found rotation speed to have minimal influence on corrosion at high pH (9.3), highlighting the importance of considering pH conditions in dynamic environments.

The most thorough investigation into the effect of flow on the biocorrosion of Mg was performed by Levenesque ***et al.*** on AM60 in HBSS [65]. A new type of corrosion flow cell was implemented to investigate shear stresses from 0.88 to 8.8 Pa. It was found that under static conditions the alloy surface exhibited pitting and filiform corrosion, while under moderate shear stresses (0.88, 4.4) a more uniform attack occurred. Conversely, higher shear stresses (8.8) were found to cause extremely localised attack after 24 hrs. The authors thus concluded that moderately dynamic conditions inhibit a pH rise at the surface, promoting more uniform corrosion. The moderate shear stresses also reduced the overall mass loss in comparison to static conditions as localised attack appears to be minimised under dynamic conditions [65].

The current literature provides some insight into the effect of physiological flow rates on the overall corrosion rate and corrosion morphology of Mg alloys in SBF. However, an electrochemical time-dependant relationship of flow on corrosion is lacking. Electrochemical impedance spectroscopy is well-suited to determining the consequence of different flow rates on the corrosion mechanisms of Mg in SBF, such as the formation of corrosion layers (***e.g.*** CaP) on the surface of samples over time.

6.6.1.2. Experimental methods

A custom corrosion flow cell was designed to allow for controlled media flow rates in a direction perpendicular to a sample surface (Figure 6-36). An electrochemical corrosion cell was modified to allow the insertion of a thermoplastic PHARMED® tube (Cole-Palmer Inc., Vernon Hills, IL, USA) with a 3 mm inner diameter in order to direct the medium flow. The outlet was positioned 1 cm from the sample surface. The corrosion cell and medium reservoir were then placed in a water bath which was kept at T_{phy} ± 0.5 °C. A Masterflex® L/S® Digital peristaltic pump (Cole-Palmer Inc.) was used to control the flow rate. The pH of the solution was monitored closely and maintained at 7.4 ± 0.05 during testing.

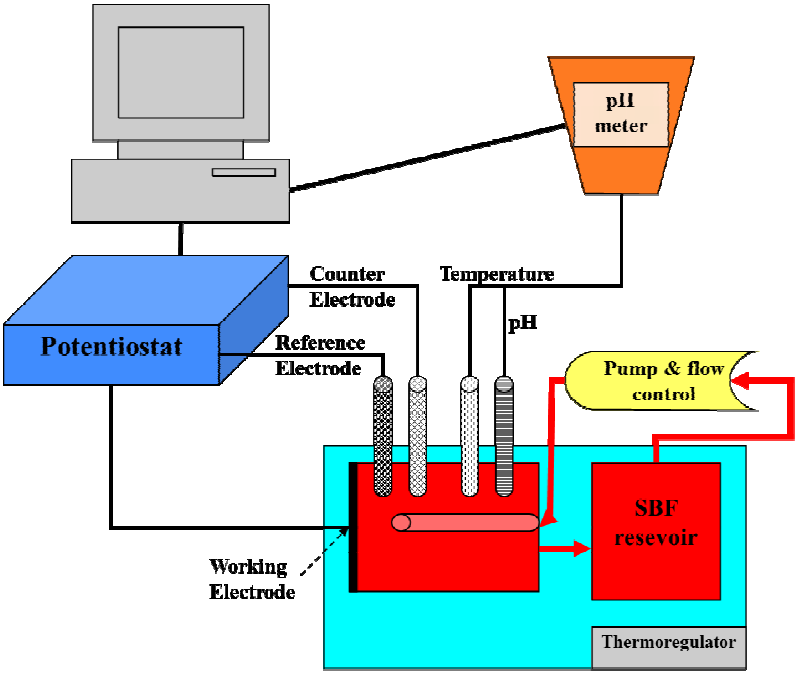

Figure 6-36 : Schematic of flow cell setup.

EIS experiments were performed in the flow cell using standard conditions as outlined in Chapter 4.3.5. Pure Mg was examined in HBSS using flow rates of 0, 5 and 25 mL/min. These rates were chosen as they provide flow close to that of blood through various bone (per 100g) [119], yet were sufficiently different from the bio-Mg literature that focuses primarily on stent applications [65, 118, 122].

6.6.1.3. Results and discussion

Increased corrosion of pure Mg due to faster SBF flow rates

EIS analysis displayed a significant shift in corrosion resistance in differing flow conditions (Figure 6-37, Figure 6-38). Overall the flow resulted in a decrease in R_{tot} of 52% and 66% for the 5 mL/min and 25 ml/min conditions after 72 hrs, respectively (Figure 6-38A). The R_{CT} in the flow conditions was also reduced and more variable compared with static conditions. This indicates that the flow likely prompted a more rapid change in the surface microstructure than that found in non-flow environments. However, both flow conditions displayed a similar behaviour after 24 hrs with an average of ~450 Ω/cm^2.

Unlike in a static environment, a peak in R_f was not evident for either of the investigated flow rates. A flow rate of 5 mL/min resulted in a heavily reduced R_f of 145 Ω/cm^2, 80% lower

than in static conditions (Figure 6-38B). The samples in 25 mL/min conditions did not display any second time constant at all (*i.e.* R_f was zero). This is shown clearly when analysing a Nyquist plot of the data after 30 hrs of immersion, where the 25 mL/min sample displays a single time constant behaviour.

Clearly the investigated flow rates increase the corrosion rate of pure Mg. The flow appears to retard the development of the $Mg(OH)_2$ / CaP layers that are known to form on the surface of Mg in HBSS, with faster flow resulting in a weaker layer. Flow also has an appreciable negative effect on the R_{CT}, further reducing overall resistance.

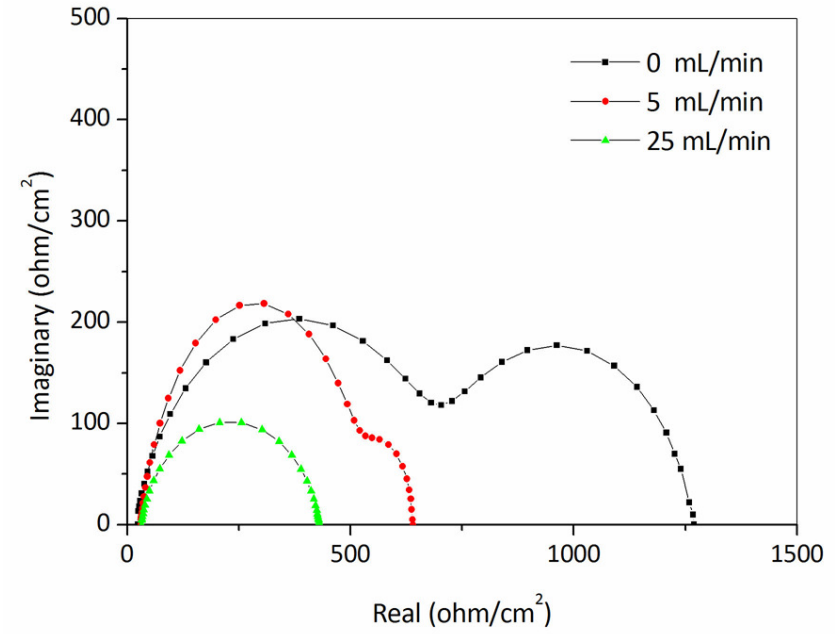

Figure 6-37 : Nyquist plot of pure Mg after 30 hrs immersion with different flow rates (0-25 mL/min). (HBSS, T_{phy}, 7.4)

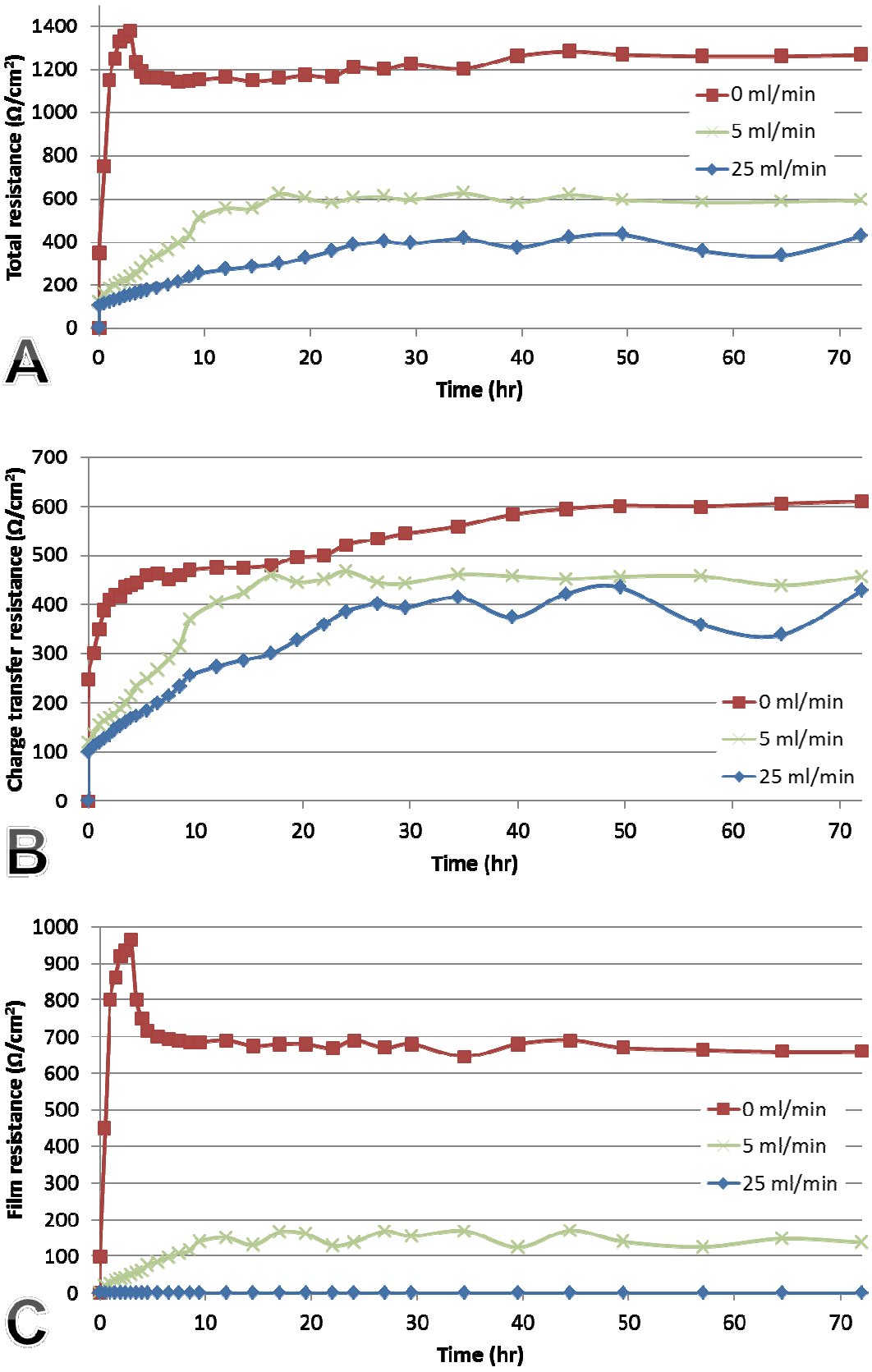

Figure 6-38 : (A) R_{tot}, (B) R_{CT} and (C) R_f of pure Mg for different flow conditions of 0, 5, and 25 mL/min. (HBSS, T_{phy}, 7.4)

6.6.1.4. Summary

Flow rates have been shown to significantly affect the short term corrosion of pure Mg. The effect of flow on degradation rates is likely more important in certain high-flow situations, such as stents, than in environments where fluid is slowly perfused across the surface, such as in orthopaedic applications. Investigation of low-flow environments may require the development of a corrosion cell that simulates the relevant rates, such as those provided by bioreactors used for various biological applications. This could be accomplished by adapting a bioreactor to allow electrochemical measurement, but such a development would likely require significant work. Factors such as shear stress on the surface and the flow type (laminar/turbulent) also need to be considered and maintained as close to *in vivo* conditions as possible.

Although it is not fully understood how flow affects the adhesion of proteins and cells to the Mg surface, a suitable experimental setup must first be developed before this can be fully investigated. This further investigation is required to clarify the effect of flow on the "basic" corrosion mechanisms of Mg in balanced salt solutions. Conditions that simulate different tissues in the body such as soft tissue, bone marrow, and blood vessels must be established. Confirmation of the correlation of the *in vitro* and *in vivo* conditions will also be necessary.

Another important consideration is that, soon after implantation, the surface of many implants become covered in organic matter such as proteins and cells and eventually bone or tissue encapsulation will occur. This may significantly decrease the flow rates the implant is exposed to. Consequently, flow rates in the body may have a negligible effect on the end performance.

6.6.2. Effect of sample preparation (surface roughness)

6.6.2.1. Introduction

Every step taken in the preparation of samples must be considered when comparing results between experiments. Preparation steps that can influence the corrosion rate include:

a. Cutting of samples – may cause subsurface deformation that changes microstructure, leaving residual stresses that may go deep (>50 μm) into the surface [123, 124],

b. Cleaning – contaminants left on the surface of a sample can affect corrosion or biocompatibility,
c. Mounting – it has been suggested [125] that mounting a sample can cause increased crevice corrosion at the interface of the sample and mounting material,
d. Grinding/polishing – differences in roughness and surface topology may affect both corrosion [126] and protein/cell adhesion [127].

Of these parameters, the most crucial and easily controlled is the polishing or grinding of the samples to a desired roughness (R_a). After casting, surface topology may vary widely depending on the location of the sample in the cast mould or ingot. Grinding normalises the surfaces of the samples and may also be used to remove any deep residual stresses due to prior deformation.

However, it should be considered that polishing is effectively a local form of severe plastic deformation and may alter more than just the surface roughness of the material [128]. This could cause local compositions to vary due to redistribution of alloying elements or segregation of impurities, residual strain and/or result in the embedding of foreign particles (such as SiC) [129]. Any change in surface roughness will also change the effective surface area; rougher surfaces with deeper "valleys" have a greater area than smooth surfaces. This in turn can affect both immersion and electrochemical experiments, where surface area must be known to accurately calculate corrosion parameters [130].

The aim of this work was to outline the effect of different polishing grades, and subsequently surface roughness, on the corrosion of pure Mg in HBSS via electrochemical and immersion methods. Roughness is a "bulk" term that does not take into account other microstructural factors that have a significant effect on Mg alloy corrosion, such as grain boundary density, extent of plastic strain, and alloying segregation. The purpose was not to determine the best surface roughness value, but rather to explicate differences between the polishes and highlight the importance of consistency for all experiments.

The roughness of Mg surfaces has been shown to have a significant effect on the corrosion rate both *in vitro* and *in vivo*. Gray-Munro *et al.* found that a rougher, phosphoric acid-etched surface displayed greater corrosion protection than non-etched surfaces, though R_a values were not provided [131]. However, the etching also imparted a thicker $Mg(OH)_2$ and

phosphate layer onto the surface prior to testing, which may have contributed considerably to the corrosion protection.

Denkena *et al.* found Mg-3Ca in 0.9% NaCl to corrode approximately 40% faster with a roughness of 4 µm compared with a 2 µm roughness [3]. The difference was attributed to a sealing of micro-cracks and pores on the smoother sample, which would have helped to prevent the corrosion medium from deeply penetrating the sample. This sealing was in turn a product of the different methods (turning and mechanical deformation) used to obtain the roughness values, indicating the difference in mechanical work on the samples was the primary cause of the corrosion variance [3]. Yoo *et al.* found that oxide-coated AZ91 in 3.5% NaCl corroded an order of magnitude faster for each increase in roughness from a R_a of 0.5 to 1 to 2.5 [132]. Increased pitting was suggested as the main reason for the higher corrosion rate. A similar result was found for AM50 [133] and AZ91 [134]. Alvarez *et al.* performed ML experiments on AE44 in 3.5% NaCl with surface roughness vales of 5.5 and 1 µm [126]. Interesting, although a greater number of deep pits formed on the rougher sample, this study contradicts others in that the smoother surface exhibited greater overall corrosion (2.5 ×) [126].

Only one study was found in the available bio-Mg literature that investigated the effect of surface roughness on biodegradation of Mg in an *in vivo* environment. Von der hoh *et al.* examined the performance of Mg-0.8Ca implants placed into the femora of rabbits over 3 and 6 months [135]. Implants were either “smooth” or sandblasted to produce surfaces with an average roughness of 3.65 and 32.7 µm, respectively. The rougher surfaces were found to cause significantly more H_2 evolution, resulting in multiple gas pockets near the surface of the implants. Therefore, while smooth samples displayed homogenous degradation around the edges of the implants, the sand blasted samples showed substantial structural loss to the cylinder. The extensive H_2 evolution of the sandblasted samples eventually led to failure of the implant [135].

It is well known that the roughness of a surface may also influence cellular adhesion to the substrate [127, 136] and, eventually, bone bonding [137]. The surface roughness can also affect the type of cells that are able to adhere to the substrate [138]. Cells would likely attach to the Mg substrate *via* a protein layer that is adsorbed onto the $Mg(OH)_2$ and CaP layers,

which rapidly form after immersion. This in turn may limit the potential increase in corrosion rate caused by the rougher Mg surface.

6.6.2.2. Experimental methods

Sample preparation

As-cast samples of pure Mg were polished to various surface conditions using SiC paper with grits of 180 (63 µm), 600 (20 µm) and 1200 (9.5 µm). Smoother samples were prepared using a soft polishing pad (Beuhler® Master-Tex 2000) and 9, 3, and 1 µm slurries. A final polish slurry containing 0.02 µm diamond particles (Beuhler® Master-Met 2) was then used on a very soft pad (Beuhler® ChemoMet). After polishing, samples were cleaned by placing them in high purity ethanol (99.8%) in an ultrasonic cleaner for 2 min (to avoid reactions with water).

Actual R_a values were determined using a Dektak 150 stylus profiler (Bruker-AXS, Tuscan, AZ, USA) (Table 6-7). The measured values were found to be different than the theoretical surface roughness, which may be due to "smearing" or other mechanical deformation that occurred during polishing. However, for clarity each sample is discussed with reference to its nominal R_a value in the rest of this work.

Table 6-7 : Theoretical and measured surface roughness of pure Mg polished to various grades.

Nominal Polish	Theoretical Roughness (µm)	Measured Roughness (µm)
180 grit	*63*	*23.105 ± 5.67*
600 grit	*20*	*4.398 ± 1.254*
1200 grit	*9.5*	*2.190 ± 0.211*
1 µm	*1*	*1.242 ± 0.125*
0.02 µm	*0.02*	*0.04 ±0.045*

Electrochemical tests

Pure Mg samples with nominal R_a values of 63, 20, 9.5, 1, and 0.02 µm were investigated in HBSS over 72 hrs at T_{phy} and a pH of 7.4. EIS was carried out using the standard setup described in Chapter 4.3.5.

Hydrogen evolution

H_2^{evo} experiments were performed in HBSS on samples with nominal R_a values of 63, 20, 9.5 and 0.02 µm over 72 hrs at T_{phy} and a pH of 7.4 using the standard setup as described in Chapter 4.2.2.

Microstructural analysis

After EIS experiments the surface topology of each sample was analysed using a SEM and EDS was performed to obtain the elemental composition of the corrosion layers.

6.6.2.3. Results and discussion

Electrochemical corrosion over 72 hrs

EIS over 72 hrs elucidated some interesting behaviour due to the ΔR_a (Figure 6-39). The 0.02 µm sample displayed only one time constant, with no appreciable R_f. The 9.5 µm samples exhibited the characteristic R_f peak after a few hours, as did the 20 µm samples, although to a lesser extent. The 63 µm samples did not display this peak but instead exhibited a slow rise in R_f to 400 Ω/cm^2, almost exactly the same value as the 20 µm samples (Figure 6-39C).

The R_{CT} displayed a similar trend for the four rougher surfaces, although the 1 µm samples exhibited consistently greater resistance values (Figure 6-39B). However, the 0.02 µm samples demonstrated radically different behaviour, rising sharply after 30 hrs to more than double the R_{CT} of the three roughest samples. It was not clear why this occurred at this time point.

All samples other than the 0.02 µm displayed strikingly similar R_{tot}, with values within 100 Ω/cm^2 of each other (Figure 6-39A). This indicates that although the differences in surface preparation resulted in varied corrosion in the initial hours of immersion, the effect was

minimal after 2 days. However, the smoothest surface displayed a significantly different corrosion resistance behaviour and approximately 60% greater R_{tot} over the 72 hrs.

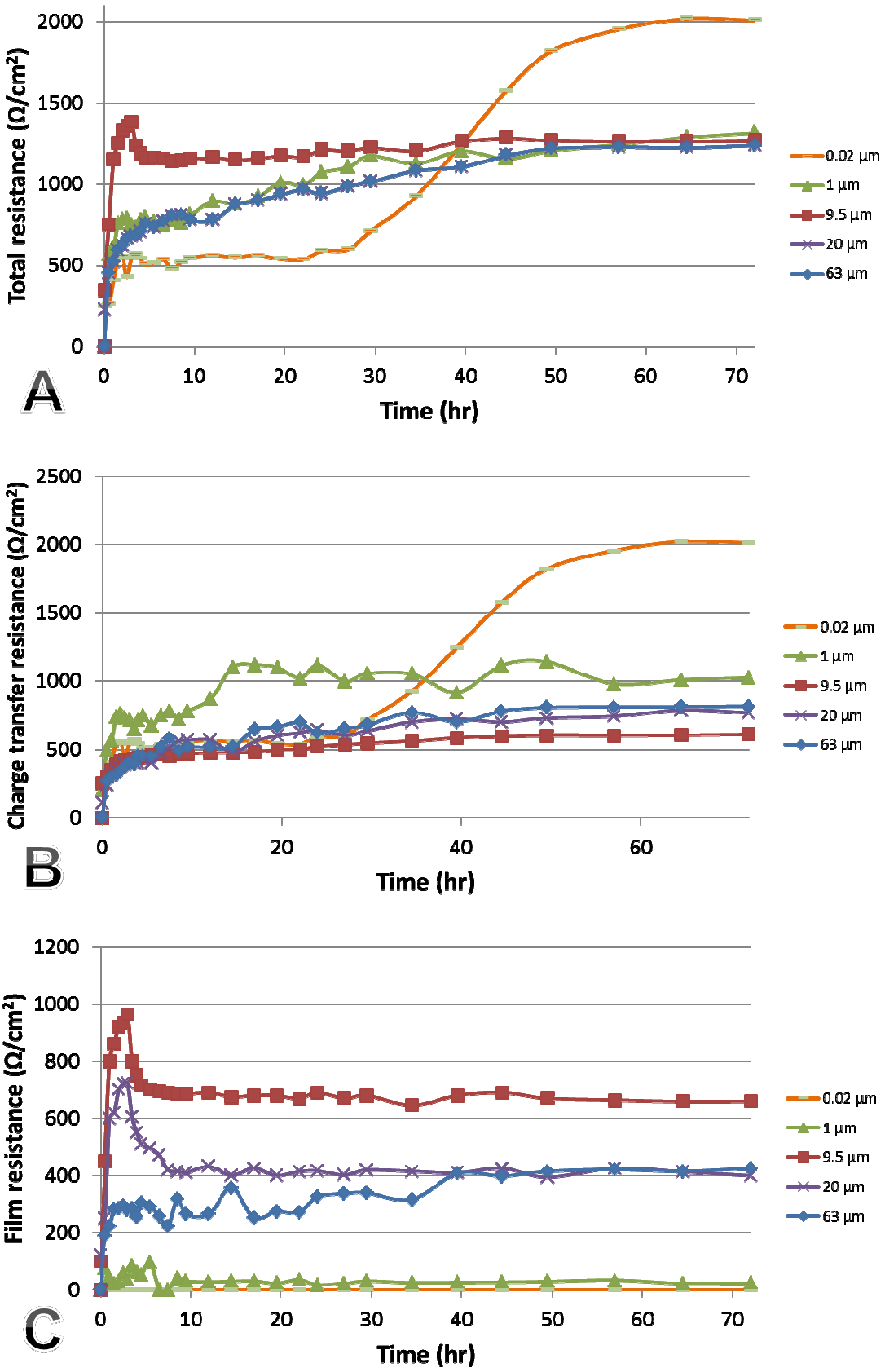

Figure 6-39 : (A) R_{tot}, (B), R_{CT}, (C) R_f of pure Mg as a function of surface roughness over 72 hrs. (HBSS, T_{phy}, 7.4)

Effect of R_a on hydrogen evolution behaviour

H_2^{evo} experiments over a period of 72 hrs did not reveal any substantial differences in H_2 evolution rate as a function of the surface roughness of pure Mg (Figure 6-40). After the first 30 min the three rougher samples had similar evolution rates of approximately 2.5-3 mL/cm^2/d. This rate was maintained for ~5 hrs, thereafter it started to drop. The 0.02 µm sample displayed slightly different behaviour with no noticeable H_2 evolving for the first 1.5 hrs. Between 1.5 and 2.5 hrs a significant amount of corrosion took place – the highest recorded rate. Between 5 and 20 hrs the evolution rates steadily dropped for all samples, although the 63 and 20 µm samples displayed roughly double the rate of the smoother samples. After approximately 30 hrs, the evolution rates of all samples reached a steady state of 0.25-0.5 mL/cm^2/d. After 50 hrs there was no appreciable difference in H_2 evolution rate as a function of surface roughness.

This indicates that although the corrosion rate varies in the first few hours depending on the R_a, the effect is dramatically diminished after just over 24 hrs. This may occur due to rougher samples initially corroding quicker due to an increased surface area, but as a $Mg(OH)_2$ and CaP layer forms the detrimental effects of this increased R_a lessens. The 0.02 µm samples restricted this initial corrosion, but after the degradation attack commenced they actually corroded more rapidly than the other samples.

This behaviour of very slow corrosion in the initial stages of immersion may provide a benefit *in vivo* that has not been investigated here. The lower H_2 evolution and subsequent slower change in pH levels at the surface of the material may be beneficial to protein attachment, which can be easily affected by pH (see Chapter 6.3). This may then be critical for the cascade of events that leads to tissue formation – cell attachment, proliferation, and finally ECM formation. This is an area worth pursuing in future work.

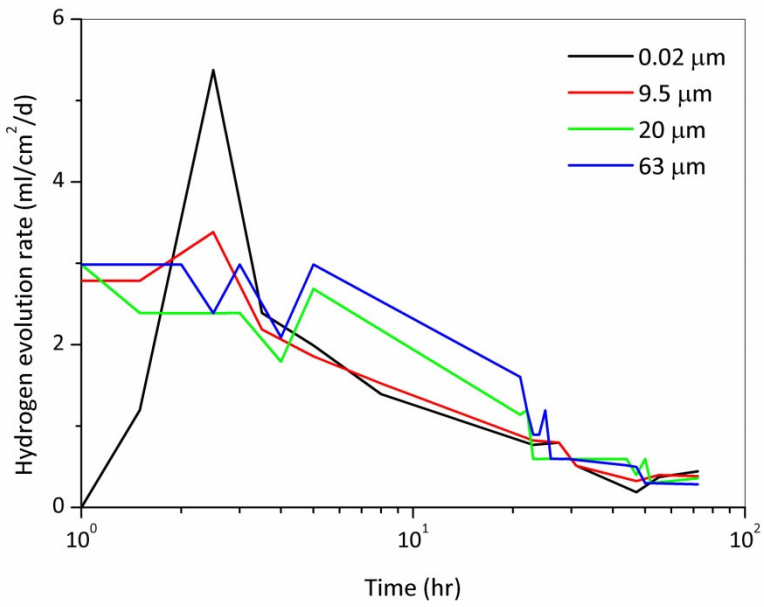

Figure 6-40 : H_2 evolution rates of pure Mg over 72 hrs with R_a values of 0.02, 9.5, 20 and 63 µm. Displayed in log(10) scale to show early evolution rates. (HBSS, T_{phy}, 7.4)

The total H_2 evolved was similar for the pure Mg samples polished to a R_a of 0.02, 9.5, 20 and 63 µm (Figure 6-41). From roughest to smoothest, an average total of 10.3, 9.1, 8.2, and 7.7 mL evolved over the course of 72 hrs. The results indicate that overall the corrosion rates were not drastically different in this period. The small increases in total H_2 evolution that coincide with each increase in R_a may be due to the extra surface area resulting in slightly higher rates of corrosion in the initial stages before the surface becomes coated with a $Mg(OH)_2$ / CaP layer (Figure 6-39).

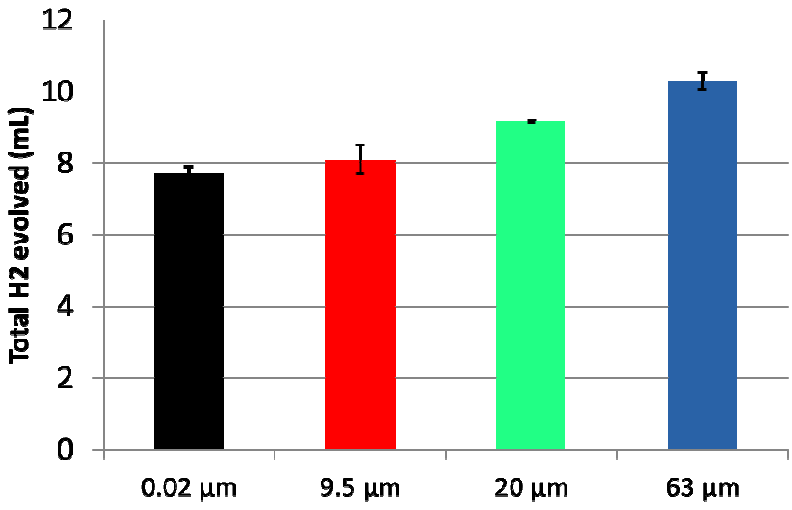

Figure 6-41 : Total H_2 evolved over 72 hrs for pure Mg with Ra values of 0.02, 9.5, 20, and 63 µm. (HBSS, T_{phy}, 7.4)

Analysis of corroded surfaces

The surfaces of the samples provided some indication of how the corrosion proceeded (Figure 6-42). All surface finishes other than the 0.02 µm displayed a similar corrosion layer, with a $Mg(OH)_2$ "cracked-earth" sub-layer and CaP flakes above. This surface morphology is commonly observed for pure Mg in balanced salt media, both in this work and in the bio-Mg literature [6, 71, 87, 88]. However, the 0.02 µm samples displayed an entirely different morphology, with a more amorphous, smooth corrosion layer composed of similar levels of Ca and P as the flakes on the other samples (Figure 6-42A). The coverage of this layer was also far greater than that on the other samples, appearing to envelop the entire surface. The fractures in the layer are likely due to dehydration of the surface during preparation for SEM analysis; the surface would likely be completely covered by this layer during immersion in HBSS. This layer may have caused the significant increase in corrosion protection that was shown in the EIS data (Figure 6-39). In addition the complete coverage and considerable protection that is provided may help explain why the 0.02 µm samples appeared to display only one time constant (Figure 6-39C)

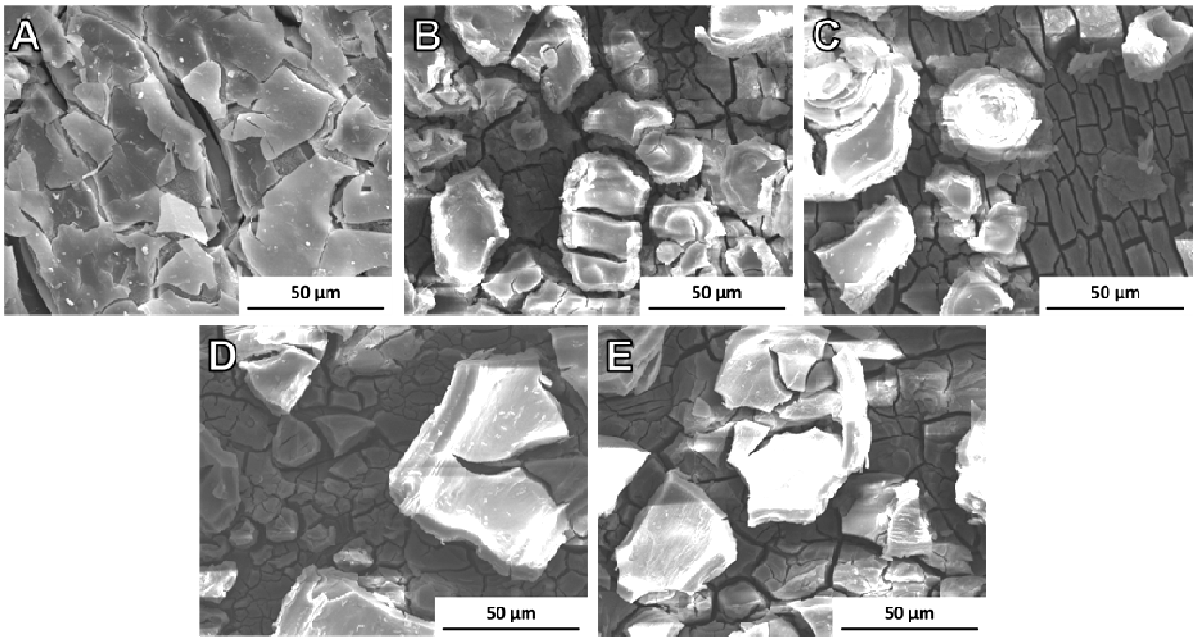

Figure 6-42 : Scanning electron micrographs (1000 ×) of the surface of pure Mg samples after 72 hrs immersion as a function of surface roughness: (A) 0.02 µm, (B) 1 µm, (C) 9.5 µm, (D) 20 µm, and (E) 62 µm. (HBSS, T_{phy}, 7.4)

Summary

In this work is has been empirically shown that the surface roughness of pure Mg can play a role in the corrosion that occurs in HBSS, which is an important finding. However, except for extremely smooth surfaces, the R_{tot} and H_2 evolution rates of all samples values were comparable. This indicates that although differences existed in the initial rate of corrosion due to ΔR_a, the effect became less evident over time. However, it should be considered that the initially slow rate of corrosion that was observed for the 0.02 µm samples may be beneficial to protein and cellular attachment *in vivo*.

Although samples polished to 0.02 µm displayed increased resistance to corrosion, the extra care that must be taken to achieve this polish, requiring 4 polishing steps over 1200 grit paper, limits its feasibility for larger studies. There is also greater potential for the suspension particles to become imbedded in the surface of the sample [139]. Depending on the method used to create a final biomedical device, the 0.02 µm finish is likely to be much smoother than the end implant, and as such may not represent a realistic surface.

A single surface roughness value should be utilised for all tests for the sake of comparison with both literature and between an individual's experiments. A medium/fine R_a, such as that provided by 1200 grit SiC paper (9.5 µm), appears to be ideal as it allows for several rougher steps to remove deep residual stresses from the surface while providing a homogenous surface without large "valleys".

6.7. Summary of effect of *in vitro* variables

- Temperature has an effect on the corrosion rate of a range of Mg alloys, with higher temperature leading to dramatically faster degradation (Figure 6-3, Figure 6-4). The magnitude of the increase is dependent on both the specific alloy and the chosen solution, making it difficult to approximate the exact increase for a given alloy/solution combination without experimentation. Therefore it is crucial that any experiment be carried out at the normal physiological temperature, 37° C, to eliminate any effect a temperature difference may cause.

- The pH of a medium used to test Mg performance critically affects the results that are obtained. A small variation from 7.2 to 7.8 results in a large decrease in corrosion rate (220-300%) (Figure 6-7). Such small changes in pH can also bring the corrosive electrolyte / medium to within the crucial range in the precipitation of calcium phosphate in SBF (Figure 6-13), resulting in radically different corrosion morphologies on the Mg surface (Figure 6-11). pH can also affect other surface interactions, such as amino acid or protein adhesion, that then alter the biodegradation behaviour. Adjustment of the pH to physiological levels (7.4-7.6), and maintenance of this level throughout the experiment should be considered a critical aspect of ***in vitro*** testing.

- Use of a buffering agent is, for all but the shortest experiments, a vital part of corrosion media. If left unbuffered, the rapid release of OH^- during Mg degradation rapidly increases the pH of the solution. This creates an unrealistic environment for corrosion to occur and dramatically alters the degradation process. HEPES and other chemical buffers do not naturally occur in the body although they do provide a method of controlling the pH for ***in vitro*** tests where an incubator and CO_2 environment is not available or feasible. Ideally, biocorrosion testing of Mg should be performed using a physiological amount of sodium bicarbonate in a 5% (or similar) CO_2 atmosphere (***i.e.*** the closest ***in vitro*** condition to the human body).

- The correct choice of an appropriate medium is absolutely vital to obtain valuable data when performing ***in vitro*** tests. NaCl solutions cannot be considered useful in the investigation of Mg biodegradation, as the lack of other inorganic salts results in considerable differences in both corrosion rates and mechanisms (Figure 6-28). Balanced salt solutions provide a more suitable inorganic environment. However, care should be taken to ensure balanced salt solutions have the correct physiological concentration of the elements most significant to the degradation process, including Cl^-, Ca and P (Figure 6-18). Amino acids and proteins increase the physiological relevance of these solutions, but greater understanding of the underlying corrosion mechanisms and their effect on long-term performance is required before they may be confidently and correctly employed ***in vitro***.

- Flow rates are important to the biodegradation of Mg alloys depending on their implant location and intended use. Near-physiological rates have been shown in this work to alter the formation of layers on the Mg surface (Figure 6-37) and increase the corrosion rate of pure Mg (Figure 6-38). However, significantly more work is required to determine appropriate flow rates and pressures for the varied conditions throughout the body. The typical fibrous encapsulation soon after implantation will further change the flow conditions adjacent to the implant over its lifetime and much greater attention is required from researchers to judge the relevance of dynamic conditions during *in vitro* corrosion testing.

- Surface roughness is a variable that needs to be controlled throughout a group of tests to allow for valid comparison between results. Different R_a values can result in varied corrosion rates for pure Mg in HBSS (Figure 6-39, Figure 6-40, Figure 6-41), although the overall degradation mechanism appeared comparable except for very finely polished Mg (Figure 6-42). A finer polish and lower surface roughness does not appear to guarantee slower *in vitro* corrosion. Therefore, there is no specific roughness that can be recommended for testing. However, it appears that a medium grade, such as 1200 grit (9.5 µm), is ideal as it allows for several rougher steps to help remove deep residual stresses from the surface while providing a consistent surface topology.

6.8. References

[1] Lee, J.-Y., G. Han, Y.-C. Kim, J.-Y. Byun, J.-i. Jang, H.-K. Seok, S.-J. Yang. *Effects of Impurities on the Biodegradation Behavior of Pure Magnesium*. Metals and Materials International 2009;15:955.

[2] Peng, Q., Y. Huang, L. Zhou, N. Hort, K.U. Kainer. *Preparation and Properties of High Purity Mg-Y Biomaterials*. Biomaterials 2009;In Press, Corrected Proof.

[3] Denkena, B., A. Lucas. *Biocompatible Magnesium Alloys as Absorbable Implant Materials - Adjusted Surface and Subsurface Properties by Machining Processe*s. CIRP Annals - Manufacturing Technology 2007;56:113.

[4] Hassel, T., F.W. Bach, A.N. Golovko, A. Krause. *Investigation of the Mechanical Properties and the Corosion Behaviour of Low Alloyed Magnesium-Calcium-Alloys for Use as Absorbable Biomaterial in the Implant Technique*. In: Pekguleryuz, M., editor. Conference of Metallurgists : Magnesium Technology in the Global Age. Montreal, Quebec, Canada, 2006. p.359.

[5] Lopez, H.Y., D.A. Cortes, S. Escobedo, D. Mantovani. *In Vitro Bioactivity Assessment of Metallic Magnesium*. Key Engineering Materials 2006;309-311:453.

[6] Yang, L., E. Zhang. *Biocorrosion Behavior of Magnesium Alloy in Different Simulated Fluids for Biomedical Application*. Materials Science and Engineering: C 2009;29:1691.

[7] Mueller, W.D., M. Lucia Nascimento, M.F. Lorenzo de Mele. *Critical Discussion of the Results from Different Corrosion Studies of Mg and Mg Alloys for Biomaterial Applications*. Acta Biomaterialia 2010;6:1749.

[8] Kim, W.-C., J.-G. Kim, J.-Y. Lee, H.-K. Seok. *Influence of Ca on the Corrosion Properties of Magnesium for Biomaterials*. Materials Letters 2008;62:4146.

[9] Zeng, R.C., J. Chen, W. Dietzel, N. Hort, K.U. Kainer. *Electrochemical Behavior of Magnesium Alloys in Simulated Body Fluids*. Transactions of Nonferrous Metals Society of China 2007;17:S166.

[10] Gerasimov, V.V., I.L. Rozenfeld. *Effect of Temperature on the Rate of Corrosion of Metals* Russian Chemical Bulletin 1957;6.

[11] Merino, M.C., A. Pardo, R. Arrabal, S. Merino, P. Casajús, M. Mohedano. *Influence of Chloride Ion Concentration and Temperature on the Corrosion of Mg-Al Alloys in Salt Fog*. Corrosion Science 2010;52:1696.

[12] Shapovalov, É.T. *Temperature Dependence of the Corrosion Rate of Metals, Steels, and Alloys in Concentrated Sulfuric Acid*. Chemical and Petroleum Engineering 1994;30:286.

[13] Hort, N., Y. Huang, D. Fechner, M. Störmer, C. Blawert, F. Witte, C. Vogt, H. Drücker, R. Willumeit, K.U. Kainer, F. Feyerabend. *Magnesium Alloys as Implant Materials - Principles of Property Design for Mg-Re Alloys*. Acta Biomaterialia 2010;6:1714.

[14] Gunde, P., F. Angela, C.H. Anja, S. Patrik, J.U. Peter. *The Influence of Heat Treatment and Plastic Deformation on the Bio-Degradation of a Mg-Y-Re Alloy*. Journal of Biomedical Materials Research Part A 2010;92A:409.

[15] Zberg, B., P.J. Uggowitzer, J.F. Loffler. *Mgznca Glasses without Clinically Observable Hydrogen Evolution for Biodegradable Implants*. Nature Materials 2009;8:887.

[16] Makar, G.L., K. J. *Corrosion of Magensium*. International Material Review 1993;38:138.

[17] Song, G., A. Atrens, D. St John, X. Wu, J. Nairn. *The Anodic Dissolution of Magnesium in Chloride and Sulphate Solutions*. Corrosion Science 1997;39:1981.

[18] Duygulu, O., R.A. Kaya, G. Oktay, A.A. Kaya. *Investigation on the Potential of Magnesium Alloy Az31 as a Bone Implant*. Materials Science Forum 2007;546-549:421.

[19] Layrolle, P., G. Daculsi. *Physiochemistry of Apatite and Its Related Calcium Phosphates*. In: Leon, B., Jansen, J.A., editors. Thin Calcium Phosphate Coatings for Medical Implants. New York: Springer, 2009.

[20] Liang, H., F. Huang, F. He, H.F. Ding, Y.Z. Wan. *Enhanced Calcium Phosphate Precipitation on the Surface of Mg-Ion-Implanted Zr02 Bioceramic*. Surface Review and Letters 2007;14:71.

[21] Lu, X., Y. Leng. *Theoretical Analysis of Calcium Phosphate Precipitation in Simulated Body Fluid*. Biomaterials 2005;26:1097.

[22] Yin, G., Z. Liu, J. Zhan, F. Ding, N. Yuan. *Impacts of the Surface Charge Property on Protein Adsorption on Hydroxyapatite*. Chemical Engineering Journal 2002;87:181.

[23] Liu, C., Y. Xin, G. Tang, P.K. Chu. *Influence of Heat Treatment on Degradation Behavior of Bio-Degradable Die-Cast Az63 Magnesium Alloy in Simulated Body Fluid*. Materials Science and Engineering: A 2007;456:350.

[24] Song, G., S. Song. *A Possible Biodegradable Magnesium Implant Material*. Advanced Engineering Materials 2007;9:298.

[25] Ren, Y., H. Wang, J. Huang, B. Zhang, K. Yang. *Study of Biodegradation of Pure Magnesium*. Key Engineering Materials 2007;342-343:601.

[26] Ng, W.F., K.Y. Chiu, F.T. Cheng. *Effect of Ph on the in Vitro Corrosion Rate of Magnesium Degradable Implant Material*. Materials Science and Engineering: C 2010;30:898.

[27] Zhang, E., L. Xu, K. Yang. *Formation by Ion Plating of Ti-Coating on Pure Mg for Biomedical Applications*. Scripta Materialia 2005;53:523.

[28] Mueller, W.D., M.F.L. de Mele, M.L. Nascimento, M. Zeddies. *Degradation of Magnesium and Its Alloys: Dependence on the Composition of the Synthetic Biological Media*. Journal of Biomedical Materials Research Part A 2009;90A:487.

[29] Kuwahara, H., Y. Al-Abdullat, M. Ohta, S. Tsutsumi, K. Ikeuchi, N. Mazaki, T. Aizawa. *Surface Reaction of Magnesium in Hank's Solutions*. vol. 350-351. Nagaoka City, Japan: Trans Tech Publications, 2000. p.349.

[30] Al-Abdullat, Y., S. Tsutsumi, N. Nakajima, M. Ohta, H. Kuwahara, K. Ikeuchi. *Surface Modification of Magnesium by Nahco3 and Corrosion Behavior in Hank's Solution for New Biomaterial Applications*. Materials Transactions 2001;42:1777.

[31] Brar, H.S., M.O. Platt, M. Sarntinoranont, P.I. Martin, M.V. Manuel. *Magnesium as a Biodegradable and Bioabsorbable Material for Medical Implants*. Jom 2009;61:31.

[32] Pietak, A.M., T. Mahoney, G. Dias, M.P. Staiger. *Bone-Like Matrix Formation on Magnesium and Magnesium Alloys*. Journal of Biomedical Materials Research 2007;19:407.

[33] Zheng, Y.F., X.N. Gu, Y.L. Xi, D.L. Chai. *In Vitro Degradation and Cytotoxicity of Mg/Ca Composites Produced by Powder Metallurgy*. Acta Biomaterialia 2010;6:1783.

[34] Wan, Y.Z., G.Y. Xiong, H.L. Luo, F. He, Y. Huang, Y.L. Wang. *Influence of Zinc Ion Implantation on Surface Nanomechanical Performance and Corrosion Resistance of Biomedical Magnesium-Calcium Alloys*. Applied Surface Science 2008;254:5514.

[35] Miller, D.S., A.J. Bard, G. McLendon, J. Ferguson. *Catalytic Water Reduction at Colloidal Metal "Microelectrodes". 2. Theory and Experiment*. Journal of the American Chemical Society 1981;103:5336.

[36] Yang, J.X., F.Z. Cui, Q.S. Yin, T. Zhang, X.M. Wang. *Characterization and Degradation Study of Calcium Phosphate Coating on Magnesium Alloy Bone Implant in Vitro*. Plasma Science, IEEE Transactions on 2009;37:1161.

[37] Rettig, R., S. Virtanen. *Composition of Corrosion Layers on a Magnesium Rare-Earth Alloy in Simulated Body Fluids*. Journal of Biomedical Materials Research - Part A 2009;88:359.

[38] Waters, J.H., L.R. Miller, S. Clack, J.V. Kim. *Cause of Metabolic Acidosis in Prolonged Surgery*. Critical Care Medicine 1999;27:2142.

[39] Hall, J.E. *Guyton and Hall Textbook of Medical Physiology*. Amsterdam: Elsevier, 2010.

[40] Boron, W.F., E.L. Boulpaep, editors. *Medical Physiology*. New York: Saunders, 2008.

[41] Kirkland, N.T., J. Lespagnol, N. Birbilis, M.P. Staiger. *A Survey of Bio-Corrosion Rates of Magnesium Alloys*. Corrosion Science 2010;52:287.

[42] Yamamoto, A., S. Hiromoto. *Effect of Inorganic Salts, Amino Acids and Proteins on the Degradation of Pure Magnesium in Vitro*. Materials Science and Engineering: C 2009;29:1559.

[43] Zhou, W., T. Shen, N.N. Aung. *Effect of Heat Treatment on Corrosion Behaviour of Magnesium Alloy Az91d in Simulated Body Fluid*. Corrosion Science 2010;52:1035.

[44] Sugawara, M., N. Maeda. *Hemorheology and Blood Flow*. Tokyo: Corona Publishing Co., 2003.

[45] Sigma-Aldrich. *Rpmi-1640 Medium: Dutch Modification*. vol. 2010: Sigma-Aldrich Inc., 2010.

[46] Montemor, M.F., A.M. Simões, M.J. Carmezim. *Characterization of Rare-Earth Conversion Films Formed on the Az31 Magnesium Alloy and Its Relation with Corrosion Protection*. Applied Surface Science 2007;253:6922.

[47] Gu, X., Y. Zheng, S. Zhong, T. Xi, J. Wang, W. Wang. *Corrosion of, and Cellular Responses to Mg-Zn-Ca Bulk Metallic Glasses*. Biomaterials 2010;31:1093.

[48] Leon, B., J.A. Jansen, editors. *Thin Calcium Phosphate Coatings for Medical Implants*. New York: Springer, 2009.

[49] Roberge, P.R. *Handbook of Corrosion Engineering*: McGraw-Hill, 2000.

[50] Regnier, P., A.C. Lasaga, R.A. Berner, O.H. Han, K.W. Zilm. *Mechanism of Co (Super 2-) 3 Substitution in Carbonate-Fluorapatite; Evidence from Ftir Spectroscopy, 13 C Nmr, and Quantum Mechanical Calculations*. American Mineralogist 1994;79:809.

[51] Rey, C., B. Collins, T. Goehl, I. Dickson, M. Glimcher. *The Carbonate Environment in Bone Mineral: A Resolution-Enhanced Fourier Transform Infrared Spectroscopy Study*. Calcified Tissue International 1989;45:157.

[52] Tatzber, M., M. Stemmer, H. Spiegel, C. Katzlberger, G. Haberhauer, M. Gerzabek. *An Alternative Method to Measure Carbonate in Soils by Ft-Ir Spectroscopy*. Environmental Chemistry Letters 2007;5:9.

[53] Doi, Y., Y. Moriwaki, T. Aoba, J. Takahashi, K. Joshin. *Esr and Ir Studies of Carbonate-Containing Hydroxyapatites*. Calcified Tissue International 1982;34:178.

[54] Xin, Y., K. Huo, H. Tao, G. Tang, P.K. Chu. *Influence of Aggressive Ions on the Degradation Behavior of Biomedical Magnesium Alloy in Physiological Environment*. Acta Biomaterialia 2008;4:2008.

[55] Lin, C., X. Li. *Role of Co2 in the Initial Stage of Atmospheric Corrosion of Az91 Magnesium Alloy in the Presence of Nacl*. Rare Metals 2006;25:190.

[56] Lindstrom, R., J.E. Svensson, L.G. Johansson. *The Influence of Carbon Dioxide on the Atmospheric Corrosion of Some Magnesium Alloys in the Presence of Nacl*. Journal of the Electrochemical Society 2002;149:B103.

[57] Burgess, S.K., D.M. Carey, S.L. Oxendine. *Novel Protein Inhibits in Vitro Precipitation of Calcium Carbonate*. Archives of Biochemistry and Biophysics 1992;297:383.

[58] Ferguson, J.F., D. Jenkins, J. Eastman. *Calcium Phosphate Precipitation at Slightly Alkaline Ph Values*. Journal (Water Pollution Control Federation) 1973;45:620.

[59] Xin, Y., P.K. Chu. *Influence of Tris in Simulated Body Fluid on Degradation Behavior of Pure Magnesium.* Materials Chemistry and Physics 2010;124:33.

[60] Rettig, R., S. Virtanen. *Time-Dependent Electrochemical Characterization of the Corrosion of a Magnesium Rare-Earth Alloy in Simulated Body Fluids*. Journal of Biomedical Materials Research Part A 2008;85A:167.

[61] Xin, Y., T. Hu, P.K. Chu. *Influence of Test Solutions on in Vitro Studies of Biomedical Magnesium Alloys*. Journal of the Electrochemical Society 2010;157:C238.

[62] Haynes, W.M., editor *Crc Handbook of Chemistry and Physics*. New York: CRC Press, 2009.

[63] Talbot, D., J. Talbot. *Corrosion Science and Technology*: CRC Press, 1998.

[64] Shi, P., W.F. Ng, M.H. Wong, F.T. Cheng. *Improvement of Corrosion Resistance of Pure Magnesium in Hank's Solution by Microarc Oxidation with Sol-Gel Tio2 Sealing*. Journal of Alloys and Compounds 2007.

[65] Levesque, J., H. Hermawan, D. Dube, D. Mantovani. *Design of a Pseudo-Physiological Test Bench Specific to the Development of Biodegradable Metallic Biomaterials*. Acta Biomaterialia 2008;4:284.

[66] Shaw, B.A. *Corrosion Resistance of Magnesium Alloys*. ASM Handbook 2003;13A Corrosion: Fundamentals, Testing, and Protection.

[67] Wang, Y., M. Wei, J. Gao, J. Hu, Y. Zhang. *Corrosion Process of Pure Magnesium in Simulated Body Fluid*. Materials Letters 2008;62:2185.

[68] Perez, N., editor *Electrochemistry and Corrosion Science*. Dordrecht: Kluwer Academic Press, 2004.

[69] Malda, J., T.B.F. Woodfield, M. Radisic, S. Levenberg, C. Oomens, F.P. Baaijens, P. Svalander, G. Vunjak-Novakovic. *Cell Nutrition : In Vitro and in Vivo.* Tissue Engineering : A Textbook 2008:327.

[70] Desmarais, W.T., D.L. Bienvenue, K.P. Bzymek, R.C. Holz, G.A. Petsko, D. Ringe. The 1.20 *Å Resolution Crystal Structure of the Aminopeptidase from Aeromonas Proteolytica Complexed with Tris: A Tale of Buffer Inhibition.* Structure 2002;10:1063.

[71] Gu, X.N., Y.F. Zheng, L.J. Chen. *Influence of Artificial Biological Fluid Composition on the Biocorrosion of Potential Orthopedic Mg-Ca, Az31, Az91 Alloys*. Biomedical Materials 2009;4:8.

[72] Liu, C., Y. Xin, X. Tian, P.K. Chu. *Degradation Susceptibility of Surgical Magnesium Alloy in Artificial Biological Fluid Containing Albumin*. Journal of Materials Research 2007;22:1806.

[73] Rundle, C.C. *Ion-Selectrive Electrode Measurements*. London: Nico2000 Ltd., 2010.

[74] Alvarez-Lopez, M., M.D. Pereda, J.A. del Valle, M. Fernandez-Lorenzo, M.C. Garcia-Alonso, O.A. Ruano, M.L. Escudero. *Corrosion Behaviour of Az31 Magnesium Alloy with Different Grain Sizes in Simulated Biological Fluids*. Acta Biomaterialia 2009;In Press, Corrected Proof.

[75] Eliezer, A., F. Witte. *Corrosion Behaviour of Magnesium Alloys in Biomedical Environments*. Advanced Materials Research 2010;95:17.

[76] Witte, F., J. Nellesen, H.-A. Crostack, V. Kaese, A. Pisch, F. Beckmann, H. Windhagen. *In Vitro and in Vivo Corrosion Measurements of Magnesium Alloys*. Biomaterials 2006;27:1013.

[77] Kokubo, T., H. Kushitani, S. Sakka, T. Kisugi, T. Yamamuro. *Solutions Able to Reproduce in Vivo Surface-Structure Changes in Bioactive Glass-Ceramic*. Journal of Biomedical Materials Research 1990;24:721.

[78] Kokubo, T., H. Takadama. *How Useful Is Sbf in Predicting in Vivo Bone Bioactivity?* Biomaterials 2006;27:2907.

[79] Oyane, A., H.-M. Kim, T. Furuya, T. Kokubo, T. Miyazaki, T. Nakamura. *Preparation and Assessment of Revised Simulated Body Fluids*. Journal of Biomedical Materials Research Part A 2003;65A:188.

[80] Takadama, H., M. Hashimoto, M. Mizuno, T. Kokubo. *Round-Robin Test of Sbf for in Vitro Measurement of Apatite-Forming Ability of Synthetic Materials*. Phosphorus Research Buletin 2004;17:119.

[81] Liu, C.L., X.M. Zhang, Y.J. Wang, W.J. Huang, R.Z. Zeng, P.K. Chu. *In Vitro Corrosion Degradation Behaviour of Mg-Ca Alloy in the Presence of Albumin*. Corrosion Science 2010;52:3341.

[82] Mueller, W.D., M.L. Nascimento, M. Zeddies, M. Córsico, L.M. Gassa, M.A.F.L. de Mele. *Magnesium and Its Alloys as Degradable Biomaterials*: Corrosion Studies Using Potentiodynamic and Eis Electrochemical Techniques. Materials Research 2007;10:5.

[83] Klinger, A., D. Steinberg, D. Kohavi, M.N. Sela. *Mechanism of Adsorption of Human Albumin to Titanium in Vitro*. Journal of Biomedical Materials Research 1997;36:387.

[84] Vogt, C., K. Bechstein, S. Gruhl, M. Lange, F. Witte. *Investigation of the Degradation of Biodegradable Mg Implant Alloys in Vitro and in Vivo by Analytical Methods*. In: Kainer, K.U., editor. 8th International Conference on Magnesium Alloys and Their Applications. Weimar, Germany: Wiley-VCH, 2008. p.1162.

[85] Padilla, N., A. Bronson. *Electrochemical Characterization of Albumin Protein on Ti-6al-4v Alloy Immersed in a Simulated Plasma Solution*. Journal of Biomedical Materials Research Part A 2007;81A:531.

[86] Langmuir, I. *The Constitution and Fundamental Properties of Solids and Liquids*. Journal of the American Chemical Society 1916;38:2221.

[87] Xu, L., F. Pan, G. Yu, L. Yang, E. Zhang, K. Yang. *In Vitro and in Vivo Evaluation of the Surface Bioactivity of a Calcium Phosphate Coated Magnesium Alloy*. Biomaterials 2009;30:1512.

[88] Gu, X.N., et al. *Microstructure, Biocorrosion and Cytotoxicity Evaluations of Rapid Solidified Mg–3ca Alloy Ribbons as a Biodegradable Material*. Biomedical Materials 2010;5:035013.

[89] Witte, F., F. Feyerabend, P. Maier, J. Fischer, M. Stormer, C. Blawert, W. Dietzel, N. Hort. *Biodegradable Magnesium-Hydroxyapatite Metal Matrix Composites*. Biomaterials 2007;28:2163.

[90] Roach, P., D. Farrar, C. Perry. *Interpretation of Protein Adsorption: Surface-Induced Conformational Changes*. Journal of the American Chemical Society 2005;127:8186.

[91] Aitken, A., M.P. Learmonth. *Protein Determination by Uv Absorption*. In: Walker, J.M., editor. The Protein Protocols Handbook. Humana Press, 2002. p.3.

[92] McDonald, R., J.A. Pask, D.W. Fuerstenau. *Surface Charge of Aluminia and Magnesium in Aqueous Media*. Journal of the American Ceramic Society 1964;47:516.

[93] Kosmulski, M. *Chemical Properties of Material Surfaces*. Basel: Marcel Dekker Inc., 2001.

[94] Wu, G., W. Dai, L. Song, A. Wang. *Surface Microstructurization of a Sputtered Magnesium Thin Film Via a Solution-Immersion Route*. Materials Letters 2010;64:475.

[95] Kohrer, C., U.R. Bhandary. *Protein Engineering*. Berlin: Springer, 2009.

[96] Ashassi-Sorkhabi, H., Z. Ghasemi, D. Seifzadeh. *The Inhibition Effect of Some Amino Acids Towards the Corrosion of Aluminum in 1 m Hcl + 1 m H2so4 Solution*. Applied Surface Science 2005;249:408.

[97] El-Shafei, A.A., M.N.H. Moussa, A.A. El-Far. *Inhibitory Effect of Amino Acids on Al Pitting Corrosion in 0.1m Nacl*. Journal of Applied Electrochemistry 1997;27:1075.

[98] Bereket, G., A. Yurt. *The Inhibition Effect of Amino Acids and Hydroxy Carboxylic Acids on Pitting Corrosion of Aluminum Alloy 7075*. Corrosion Science 2001;43:1179.

[99] Ashassi-Sorkhabi, H., M.R. Majidi, K. Seyyedi. *Investigation of Inhibition Effect of Some Amino Acids against Steel Corrosion in Hcl Solution*. Applied Surface Science 2004;225:176.

[100] Kiani, M.A., M.F. Mousavi, S. Ghasemi, M. Shamsipur, S.H. Kazemi. *Inhibitory Effect of Some Amino Acids on Corrosion of Pb-Ca-Sn Alloy in Sulfuric Acid Solution*. Corrosion Science 2008;50:1035.

[101] William, D.F., R.L. William. *Degradative Effects of the Biological Environment on Metals and Ceramics*. In: Ratner, B.D., Hoffman, A.S., Schoen, F.J., Lemons, J.E., editors. Biomaterials Science: An Introduction to Materials in Medicine. San Diego: Elsevier Academic Press, 2004. p.430.

[102] Bruneel, N., J.A. Helsen. *In Vitro Simulation of Biocompatibility of Ti-Al-V*. Journal of Biomedical Materials Research 1988;22:203.

[103] Mu, Y., T. Kobayashi, M. Sumita, A. Yamamoto, T. Hanawa. *Metal Ion Release from Titanium with Active Oxygen Species Generated by Rat Macrophages in Vitro*. Journal of Biomedical Materials Research 2000;49:238.

[104] Zhang, S., X. Zhang, C. Zhao, J. Li, Y. Song, C. Xie, H. Tao, Y. Zhang, Y. He, Y. Jiang, Y. Bian. *Research of Mg-Zn Alloy as Degradable Biomaterial*. Acta Biomaterialia 2010;6:626.

[105] Zhang, S., J. Li, Y. Song, C. Zhao, X. Zhang, C. Xie, Y. Zhang, H. Tao, Y. He, Y. Jiang, Y. Bian. *In Vitro Degradation, Hemolysis and Mc3t3-E1 Cell Adhesion of Biodegradable Mg-Zn Alloy*. Materials Science and Engineering: C 2009;29:1907.

[106] Zhang, E., D. Yin, L. Xu, L. Yang, K. Yang. *Microstructure, Mechanical and Corrosion Properties and Biocompatibility of Mg-Zn-Mn Alloys for Biomedical Application*. Materials Science and Engineering: C 2009;29:987.

[107] Witte, F., F. Feyerabend, M. Kammal, R. Willumeit. *Unphysiologically High Magnesium Concentrations Support Chondrocyte Proliferation and Redifferentiation*. Tissue Engineering 2006;12:3545.

[108] Lorenz, C., J.G. Brunner, P. Kollmannsberger, L. Jaafar, B. Fabry, S. Virtanen. *Effect of Surface Pre-Treatments on Biocompatibility of Magnesium*. Acta Biomaterialia 2009;5:2783.

[109] Li, Z., X. Gu, S. Lou, Y. Zheng. *The Development of Binary Mg-Ca Alloys for Use as Biodegradable Materials within Bone*. Biomaterials 2008;29:1329.

[110] Gu, X., Y. Zheng, Y. Cheng, S. Zhong, T. Xi. *In Vitro Corrosion and Biocompatibility of Binary Magnesium Alloys*. Biomaterials 2009;30:484.

[111] Feyerabend, F., J. Fischer, J. Holtz, F. Witte, R. Willumeit, H. Drücker, C. Vogt, N. Hort. *Evaluation of Short-Term Effects of Rare Earth and Other Elements Used in Magnesium Alloys on Primary Cells and Cell Lines*. Acta Biomaterialia;In Press, Corrected Proof.

[112] Yun, Y., Z. Dong, D. Yang, M.J. Schulz, V.N. Shanov, S. Yarmolenko, Z. Xu, P. Kumta, C. Sfeir. *Biodegradable Mg Corrosion and Osteoblast Cell Culture Studies*. Materials Science and Engineering: C 2009;29:1814.

[113] Feser, K., M. Kietzmann, W. Baumer, C. Krause, F.W. Bach. *Effects of Degradable Mg-Ca Alloys on Dendritic Cell Function*. J Biomater Appl 2010:0885328209360424.

[114] Wong, H.M., K.W.K. Yeung, K.O. Lam, V. Tam, P.K. Chu, K.D.K. Luk, K.M.C. Cheung. *A Biodegradable Polymer-Based Coating to Control the Performance of Magnesium Alloy Orthopaedic Implants*. Biomaterials 2010;31:2084.

[115] Hiromoto, S. *Corrosion of Metallic Biomaterials in Cell Culture Environments*. The Electrochemical Society Interface 2008:41.

[116] Witte, F., H. Ulrich, M. Rudert, E. Willbold. *Biodegradable Magnesium Scaffolds: Part 1: Appropriate Inflammatory Response*. Journal of Biomedical Materials Research Part A 2007:748.

[117] Marieb, E.N. *Human Anatomy & Physiology*. London: Benjamin Cummings, 2003.

[118] Hiromoto, S., A. Yamamoto, N. Maruyama, H. Somekawa, T. Mukai. *Polarization Behavior of Pure Magnesium under a Controlled Flow in a Nacl Solution*. Materials Transactions 2008;49:1456.

[119] McCarthy, I. *The Physiology of Bone Blood Flow: A Review*. J Bone Joint Surg Am 2006;88:4.

[120] Bender, S., J. Goellner, A. Heyn, E. Boese. *Corrosion and Corrosion Testing of Magnesium Alloys*. Materials and Corrosion 2007;58:977.

[121] Chen, Y., S. Zhang, J. Li, Y. Song, C. Zhao, X. Zhang. *Dynamic Degradation Behavior of Mgzn Alloy in Circulating M-Sbf*. Materials Letters 2010;64.

[122] Hiromoto, S., A. Yamamoto, N. Maruyama, H. Somekawa, T. Mukai. *Influence of Ph and Flow on the Polarisation Behaviour of Pure Magnesium in Borate Buffer Solutions*. Corrosion Science 2008;50:3561.

[123] Love, L.C. *Principles of Metallurgy*. Reston, VA: Reston Publishing Company, 1985.

[124] Doege, E., K. Droder. *Deformation of Magnesium*. In: Kainer, K.U., editor. Magnesium - Alloys and Technologies. Weinheim: Wilkey-VCH Verlag GmbH, 2003.

[125] Shi, Z., A. Atrens. *An Innovative Specimen Configuration for the Study of Mg Corrosion*. Corrosion Science 2011;53:226.

[126] Alvarez, R.B., H.J. Martin, M.F. Horstemeyer, M.Q. Chandler, N. Williams, P.T. Wang, A. Ruiz. *Corrosion Relationships as a Function of Time and Surface Roughness on a Structural Ae44 Magnesium Alloy*. Corrosion Science 2010;52:1635.

[127] Gentile, F., L. Tirinato, E. Battista, F. Causa, C. Liberale, E.M. di Fabrizio, P. Decuzzi. *Cells Preferentially Grow on Rough Substrates*. Biomaterials 2010;31:7205.

[128] Samuels, L.E. *Metallographic Polishing by Mechanicam Methods*. Materials Park, OH: ASM International, 2003.

[129] Gale, W.F., T.C. Totemeir, editors. *Smithells Metals Reference Book*. Oxford: Elsevier Inc., 2004.

[130] Bruckenstein, S., J.W. Sharkey, J.Y. Yip. *Effect of Polishing with Different Size Abrasives on the Current Response at a Rotating Disk Electrode*. Analytical Chemistry 1985;57:368.

[131] Gray-Munro, J.E., C. Seguin, M. Strong. *Influence of Surface Modification on the in Vitro Corrosion Rate of Magnesium Alloy Az31*. Journal of Biomedical Materials Research Part A 2009;91A:221.

[132] Yoo, B., K.R. Shin, D.Y. Hwang, D.H. Lee, D.H. Shin. *Effect of Surface Roughness on Leakage Current and Corrosion Resistance of Oxide Layer on Az91 Mg Alloy Prepared by Plasma Electrolytic Oxidation*. Applied Surface Science 2010;256:6667.

[133] Bala Srinivasan, P., J. Liang, C. Blawert, M. Störmer, W. Dietzel. *Effect of Current Density on the Microstructure and Corrosion Behaviour of Plasma Electrolytic Oxidation Treated Am50 Magnesium Alloy*. Applied Surface Science 2009;255:4212.

[134] Hwang, D.Y., B. Yoo, J.Y. Cho, D.H. Lee, D.H. Shin. *Effect of Surface Roughness on Corrosion Resistance of Oxide Layer on Az91 Mg Alloy Prepared by Plasma Electrolytic Oxidation*. ECS Meeting Abstracts 2008;802:1624.

[135] Von Der Höh, N., D. Bormann, A. Lucas, B. Denkena, C. Hackenbroich, A. Meyer-Lindenberg. *Influence of Different Surface Machining Treatments of Magnesium-Based Resorbable Implants on the Degradation Behavior in Rabbits*. Advanced Engineering Materials 2009;11:B47.

[136] Chen, J., S. Mwenifumbo, C. Langhammer, J.P. McGovern, M. Li, A. Beye, W.O. Soboyejo. *Cell/Surface Interactions and Adhesion on Ti-6ai-4v: Effects of Surface Texture*. Journal of Biomedical Materials Research - Part B Applied Biomaterials 2007;82:360.

[137] Davies, J.E. *Bone Bonding at Natural and Biomaterial Surfaces*. Biomaterials 2007;28:5058.

[138] Chen, C.-C., P.C.-H. Hsieh, G.-M. Wang, W.-C. Chen, M.-L. Yeh. *The Influence of Surface Morphology and Rigidity of the Substrata on Cell Motility*. Materials Letters 2009;63:1872.

[139] Smithells, C.J., E.A. Brandes, G.B. Brook. *Smithells's Metals Reference Book*. London: Butterworths, 1992.

CHAPTER 7: Alloying Effects on Magnesium Biocorrosion

7.1. Introduction

The development of suitable biodegradable implant alloys is a multidisciplinary challenge, since freedom in alloy design must be confined to a range of alloying additions that are biologically nontoxic, whilst still providing the requisite mechanical properties. This leaves a small number of compatible elements that can provide benefits when alloyed with Mg, including Ca and Zn.

To date, although a range of different Mg alloys have been investigated both *in vitro* and *in vivo*, little work has been performed to characterise (electrochemically) the individual phases that form when elements are added in concentrations above Mg solid solubility limits, or to generalise the corrosion morphology in bio-electrolytes. The limited solubility of most elements in Mg typically results in the formation of intermetallic particles (IMP). Typical intermetallics that form include but are not limited to Mg_2Ca, $MgZn_2$, $Mg_{17}Al_{12}$, and Mg_3Al_2. Conversely for elements with low solubility, such as Fe, Mn, Cu, Ni and Zr, it is possible to have a two phase structure consisting of pure Mg and pure X, where X = Fe, Mn, Cu, Ni or Zr. In such instances no IMP forms, but complete insolubility prevails (the ramifications on corrosion being catastrophic).

In this chapter we aim to typify the effects of a specific set of alloying elements upon Mg. This is done by systematically studying binary alloy sets, ternary alloy sets, and using micro-electrochemical testing. Interpretation of IMP electrochemical responses has led to significant developments in the understanding of corrosion, especially for Al alloys [1, 2]. Consequently, an investigation into the corrosion behaviour of any Mg alloy requires an understanding of the relationship between microstructural features/phases, and their influence on overall reaction kinetics.

The microelectrochemical technique

Some of the fundamental localised electrochemical properties of alloys cannot be determined using standard electrochemical setups, such as that outlined in Chapter 4.3. [3]. The contact area is too large (1 cm^2), which does not allow the analysis of the electrochemical behaviour of single phases. Thus a different setup is required to allow analysis of the microstructural characteristics. Microelectrochemical experiments (µCell), also referred to as micro-cell tests, are capable of providing significantly smaller working electrode contact areas for analysis (1 μm^2 – 1000 μm^2). Typical setups have been outlined in [2-4] and reviewed in [5]. The µCell offers a number of benefits over standard electrochemical techniques. For example, due to the small working electrode contact area, current resolution can be drastically improved down to pA, even fA [6]. The small contact area also allows investigation of single areas of interest, such as grain boundaries, inclusions, or precipitates.

The limitations of the µCell technique have been outlined in a review paper by Birbilis ***et al.*** [5]. These include: (i) high impedance (10^{13} – 10^{14} ohm) due to the small working electrode area, (ii) a large ohmic resistance, again due to working electrode surface area, and (iii) need for higher potential scan rates due to potential leakage of solution and blockage of the capillary during anodic cycling. However, the use of a suitable potentiostat with a high-input resistance and low-input current, combined with a selection of appropriate scan rates for the investigated material can minimise the effect these issues can have on results [5].

µCell methods have been used in the literature for ***in vitro*** studies of Ti [7], cobalt-based alloys [8], and a number of pure metals for use in dental applications [9]. For Mg alloys, ***in vitro*** work has almost entirely been performed by Dr. W.-D. Mueller and his associates. In the earliest work, Mueller ***et al.*** used standard and µCell (0.8 mm^2 surface area) electrochemical analysis to investigate pure Mg, LAE442 and AZ31 in 0.9 % NaCl, a SBF similar to HBSS (but without Ca^{2+}), and PBS with and without 0.1, 1, or 10 g/L BSA [10]. Although the study examined the effect of the different solutions and alloys on polarisation performance, it did not investigate the individual phases of each alloy alone. A later study by Mueller ***et al.*** on the same alloys and solutions provided greater insight into the values of i_{corr}, E_{corr}, and R_{tot}, although not in reference to the individual phases of the microstructure. The same issues remain in a recent publication by the same primary author [11].

The separate analysis of individual phases is missing in the bio-Mg literature. Although the interpretation of the electrochemical response of Mg intermetallics was first performed by Lunder *et el.* over 20 years ago [12], no work has been done to characterise this response *in vitro*. This is required from an alloy design perspective for the engineering of alloys with predictable and customized dissolution rates, by helping to understand the composition-microstructure-electrochemistry paradigm of these new biomaterials. Consequently there is a considerable need for a detailed study of the phase-corrosion relationship of common Mg alloys investigated for biomedical purposes.

Investigated alloys and solutions

Calcium is one of the most promising and biocompatible alloying elements for Mg. It is known to be the most abundant mineral in the body [13] and plays a crucial role in the formation of bone [14]. Although several limited studies have investigated Mg-Ca alloys for biomedical applications [15-18], a systematic and primary study of the role of Ca additions upon dissolution of Mg alloys *in vitro* is lacking.

Zn has been commonly used in Mg alloying for biomedical purposes [19-26]. The addition of Zn to Mg results in improved mechanical properties from grain refinement [27], has displayed a reduced corrosion rate compared with pure Mg in HBSS [19, 28], and corroded at a suitable rate *in vivo* [21]. Given its general non-toxicity, wide use and biomedical potential, further investigation of its intermetallic properties is merited.

The addition of Zn to Mg-Ca alloys has been shown to improve the mechanical properties (*e.g.* hardness) significantly [29]. A number of studies have investigated Mg-Ca-Zn alloys *in vitro*, in both cast [30-33] and bulk metallic glass form [34]. The results have normally been promising, and Mg-Ca-Zn alloys have been found to corrode slower than pure Mg *in vitro* [30]. Incorporating two of the most biocompatible elements also minimises any chance of toxicity-related problems when placed *in vivo*. Consequently Mg-Ca-Zn presents an interesting alloy system that requires further examination.

The use of an SBF with a similar composition to *in vivo* conditions combined with a controlled environment has been found in this work to be critical in the evaluation of bioactivity of biomaterials (see Chapter 6.5). The inclusion of proteins, such as albumin, in an

SBF has been shown to dramatically affect the corrosion properties of metallic biomaterials, both in the literature [35, 36] and this work. Recently, this has been further confirmed in a range of tests on pure Mg, as well as Mg alloyed with rare earth elements [37, 38]. Consequently, to greater understand the role of alloying elements on the microstructure/phase differences, an electrochemical study in a variety of electrolyte media is required.

The aim of this study was to use the μCell technique in combination with standard electrochemical methods to analyse a Mg-Ca, Mg-Zn, and Mg-Ca-Zn alloys (and their subsequent secondary phases) to determine their effect on electrochemical biocorrosion. Further analysis was performed on the Mg-Ca alloying system due to its favourable properties *in vivo*. Some of the phases discussed herein have never been studied using the μCell technique nor in combination with an SBF as the corrosive medium.

7.2. Experimental methods

7.2.1. Sample preparation

A range of Mg-*x*Ca alloys (*x* = 0.4-28 wt. %), Mg-*x*Zn (*x* = 1-20 wt. %), and Mg-*x*Ca-*y*Zn (*x* = 0.4-5 wt. %, *y* = 3-6.2 wt. %) were prepared using an induction furnace. Commercial alloys, AZ91, and AZ31 (Magnesium Elektron Ltd., Manchester, UK) were also considered as reference materials such that our results with experimental alloys could be compared to those of standard alloys heavily tested in the literature. Samples were polished to 0.05 μm. Difference phases and grain boundaries were visible optically in the as-polished surfaces without chemical etching.

7.2.2. General corrosion and microelectrochemical testing

For the investigated alloys, experiments were carried out using the normal flat cell with 1 cm^2 of surface area as described in Chapter 4.3.3. PDP was performed in HBSS, MEM and MEM containing 10% FBS. All media were buffered with HEPES.

Electrochemical testing of the intermetallic phases of the Mg-Ca and Mg-Zn alloys was performed using a microelectrochemical cell (μCell) method following the configuration outlined in Chapter 4.3.4. The β-phase of the Mg-Ca-Zn alloys could not be isolated due to

its small size and consequently was not investigated in this study. Tests on the other phases and α-Mg were performed in MEM solution at T_{phy} at a pH of 7.4.

7.2.3. Microstructural characterisation and EBSD

As-polished surfaces of the alloys were analysed using an inverted optical microscope (Leica® DM-IRM). Images were obtained using an attached AxioCam digital camera. Scanning electron microscopy and electron backscatter diffraction (EBSD) were carried out on a Quanta SDFEG with a Hikari EBSD camera.

7.3. Results

7.3.1. Microstructural of Mg-Ca alloys

The phase composition of Mg-Ca binary alloys has been examined in detail previously, where the appearance of a Mg_2Ca intermetallic phase is typical for Mg-Ca alloys to a composition window up to ~45 wt. % Ca [15, 29, 39, 40] as predicted by the phase diagram (Figure 7-1) [41]. This is consistent with the microstructure of Mg-*x*Ca alloys produced for this work, where primary -Mg dendrites and an interdendritic eutectic phase consisting of -Mg and Mg_2Ca was visible (Figure 7-2). The process of relatively slow cooling (~0.1°C/s) from the melt leads to the formation of a dendritic microstructure. There was an increased refinement of the -Mg dendritic structure and Mg_2Ca phase from about 3 to up to 24 vol.% with increasing Ca content from Mg-0.8Ca to Mg-28Ca, respectively.

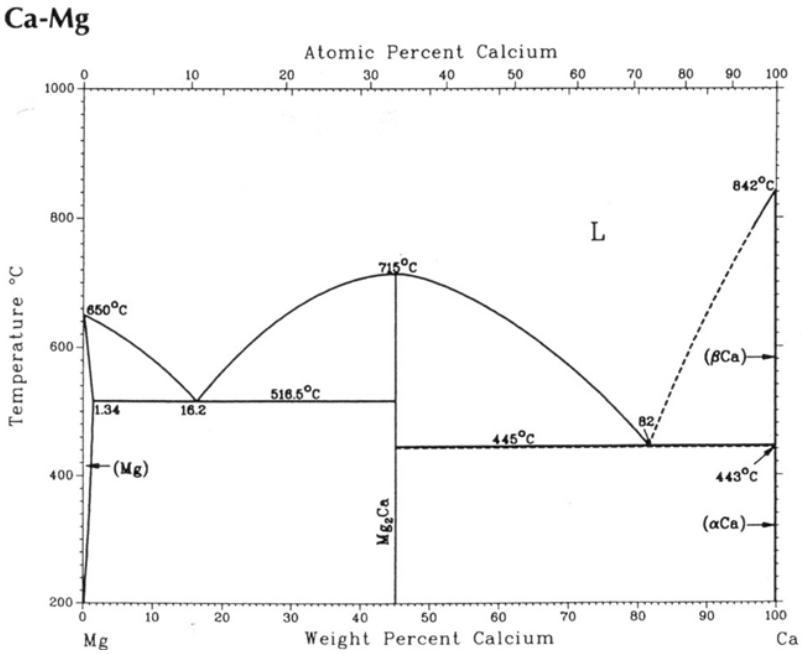

Figure 7-1 : Binary phase diagram of Ca-Mg.

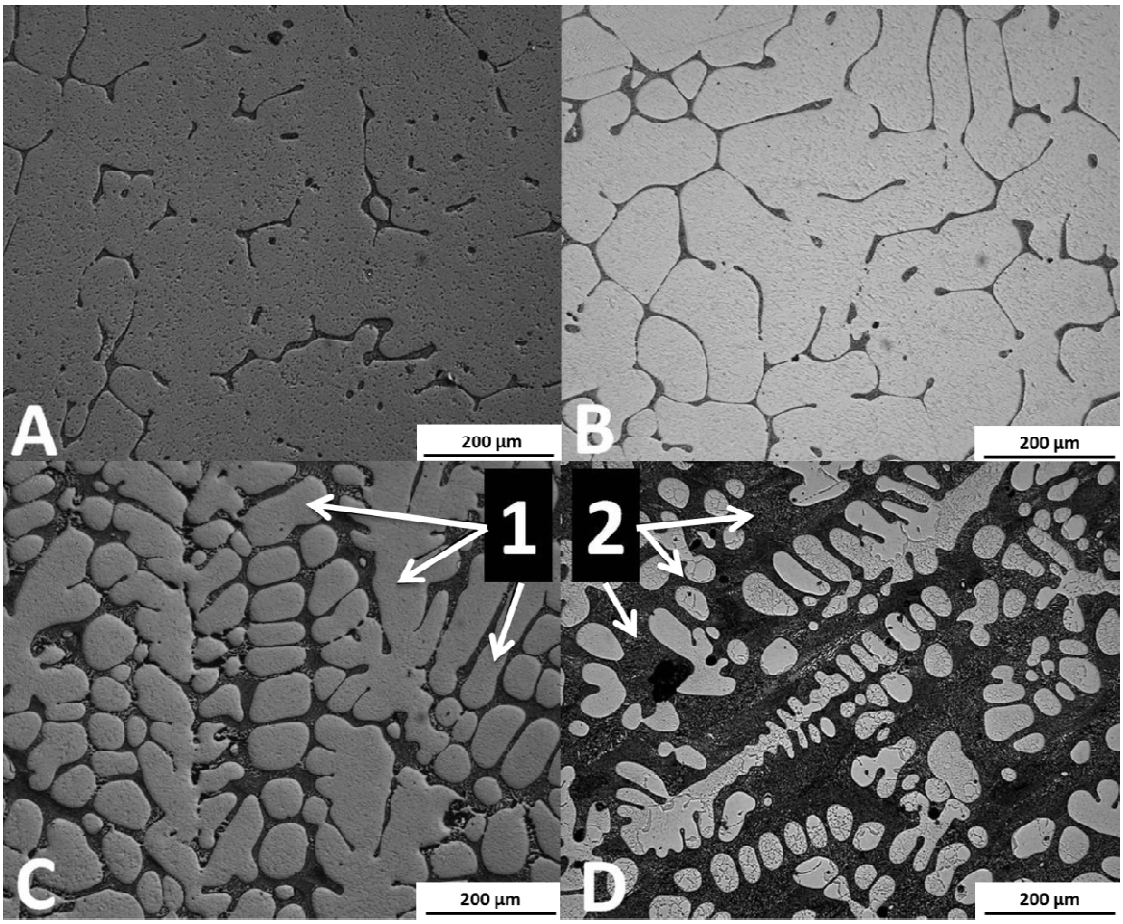

Figure 7-2 : Optical light micrographs of the microstructure of ; (A) Mg-0.8Ca, (B) Mg-1.34Ca, (C) Mg-5Ca, and (D) Mg-10Ca binary alloys. (1) α-Mg and (2) interdendritic eutectic phases are denoted with arrows.

The intermetallic phase is clearly evident in the Mg-28Ca alloy, along with a well-defined divorced eutectic component of the microstructure (Figure 7-3A). Spot EBSD upon the intermetallic phase (Figure 7-3B) reveals that the phase has the crystal structure and lattice characteristics of Mg_2Ca - in accordance with known lattice structures [41]. The Mg_2Ca intermetallic is unique amongst the phases typical of Mg alloys, in that the intermetallic has the same crystal structure (hexagonal) as the Mg itself, and the only difference is that the Mg_2Ca has lattice parameters almost twice as large as the α-Mg.

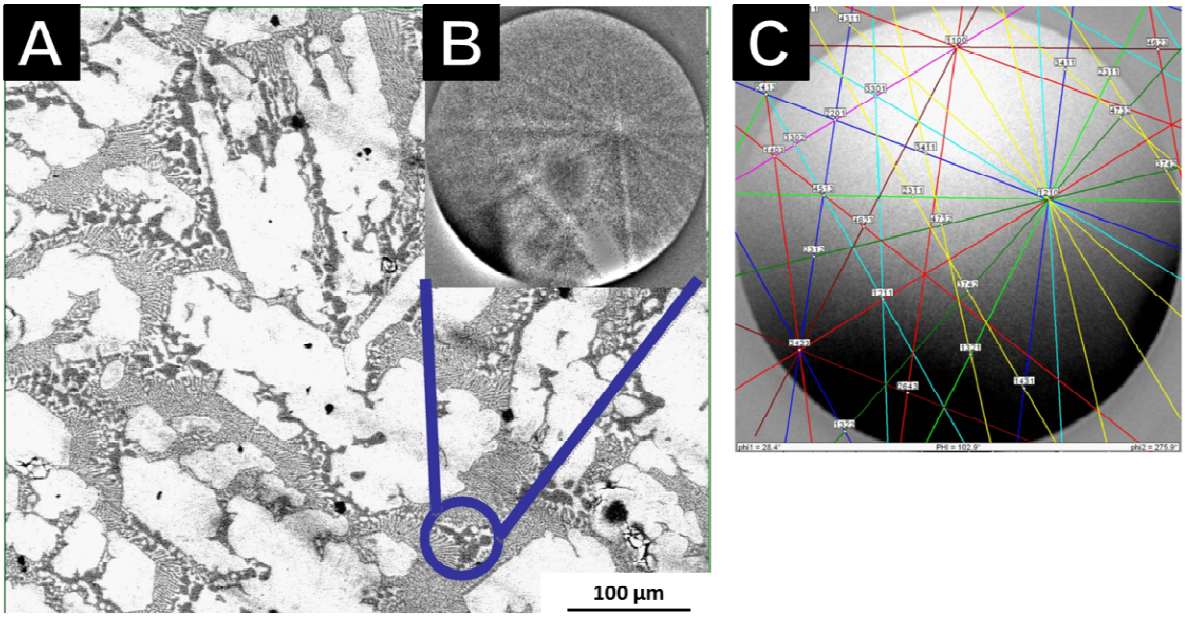

Figure 7-3 : An example of phase analysis performed by EBSD for Mg-28Ca. (A) Scanning electron micrograph of the microstructure. (B) Kikuchi pattern of Mg_2Ca phase as captured by EBSD camera. (C) Virtual Kikuchi pattern of Mg_2Ca phase as calculated by TSL OIM software.

7.3.2. Microstructure of Mg-Zn alloys

The Mg-Zn alloys displayed a typical as-cast dendritic microstructure of primary -Mg dendrites with a MgZn/$MgZn_2$/ -Mg eutectic located between the dendrite arms, based on previous EBSD analysis [2] (Figure 7-5). $MgZn_2$ is not the phase that would traditionally form at the investigated concentrations under ideal conditions according to the Mg-Zn binary phase diagram (Figure 7-4, [42]). However, $MgZn_2$ is commonly found under non-equilibrium cooling conditions [31, 43], and is believed to have formed in this case.

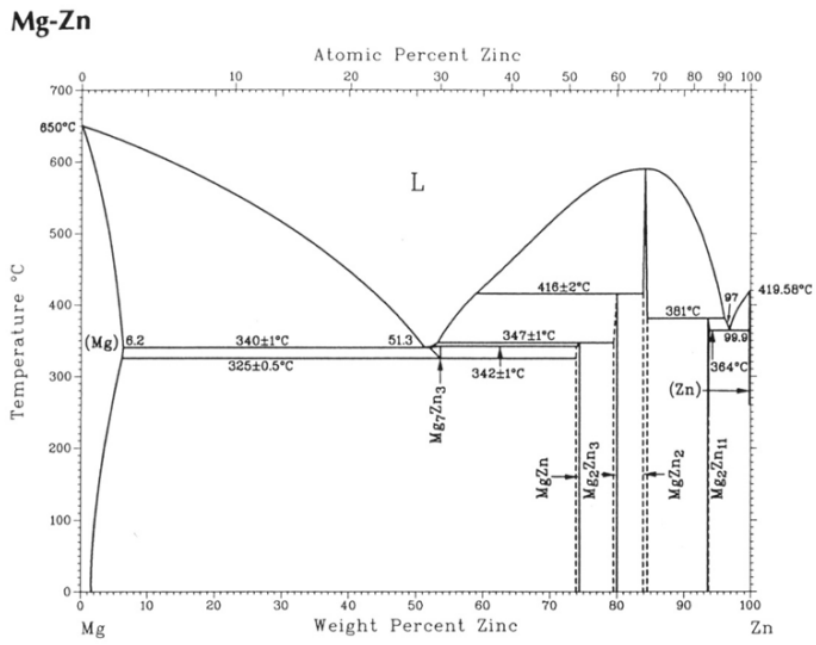

Figure 7-4 : Binary phase diagram of Mg-Zn.

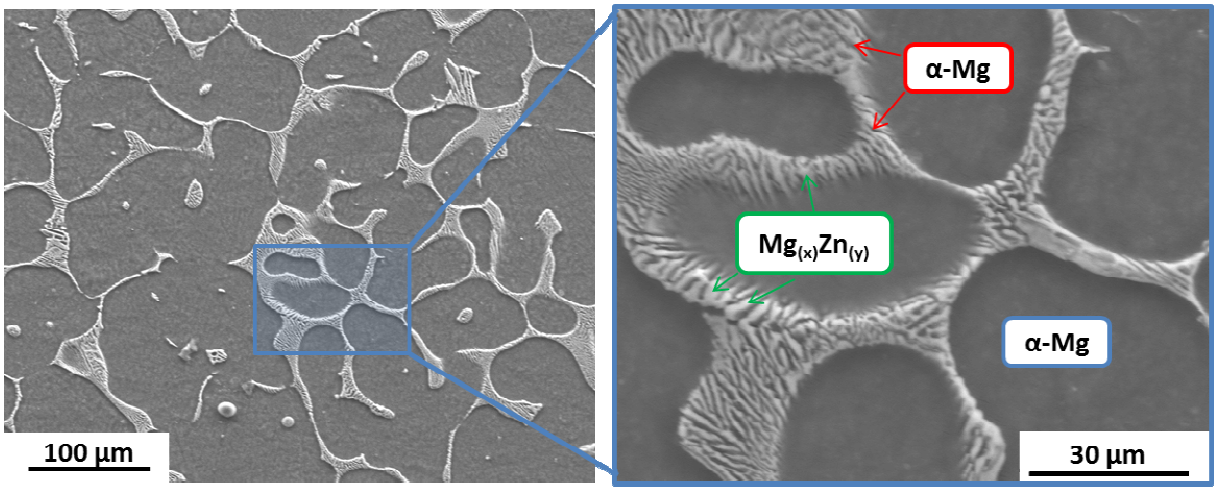

Figure 7-5 : Scanning electron micrographs of Mg-20Zn alloy with and β phases indicated.

7.3.3. Microstructure of Mg-Ca-Zn alloys

The ternary Mg-*x*Ca-*y*Zn alloys were all in the range for the formation of α-Mg and an interdendritic phase of α-Mg + $CaMg_2Zn$, as determined by the phase diagram (YELLOW, Figure 7-6) and scanning electron micrographs (Figure 7-7).

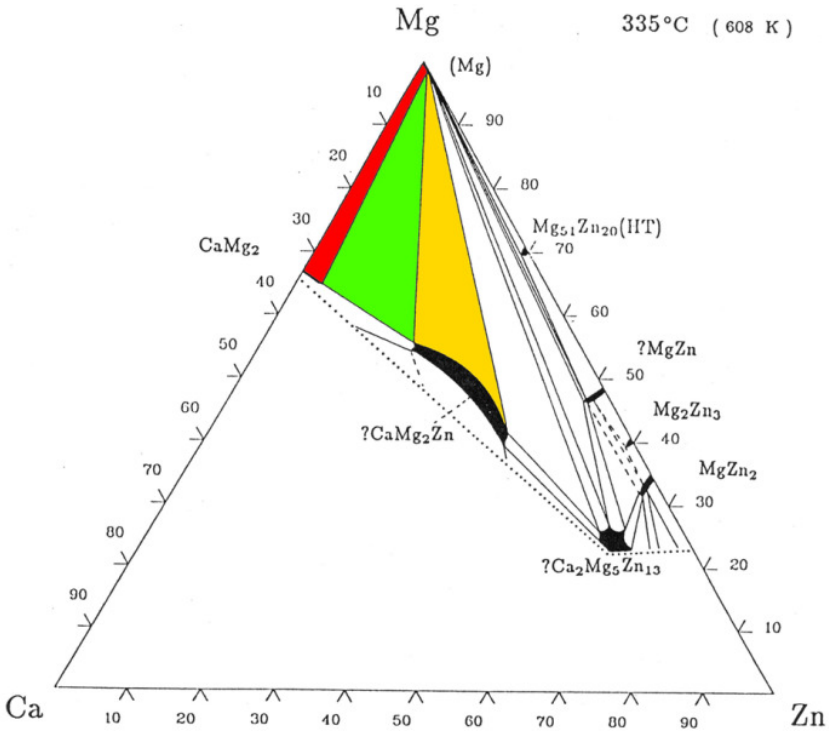

Figure 7-6 : Ternary phase diagram for Mg-Ca-Zn. Colours indicate formation of : (RED) α-Mg + $CaMg_2$, (GREEN) α-Mg + $CaMg_2$ + $CaMg_2Zn$, (YELLOW) α-Mg + $CaMg_2Zn$.

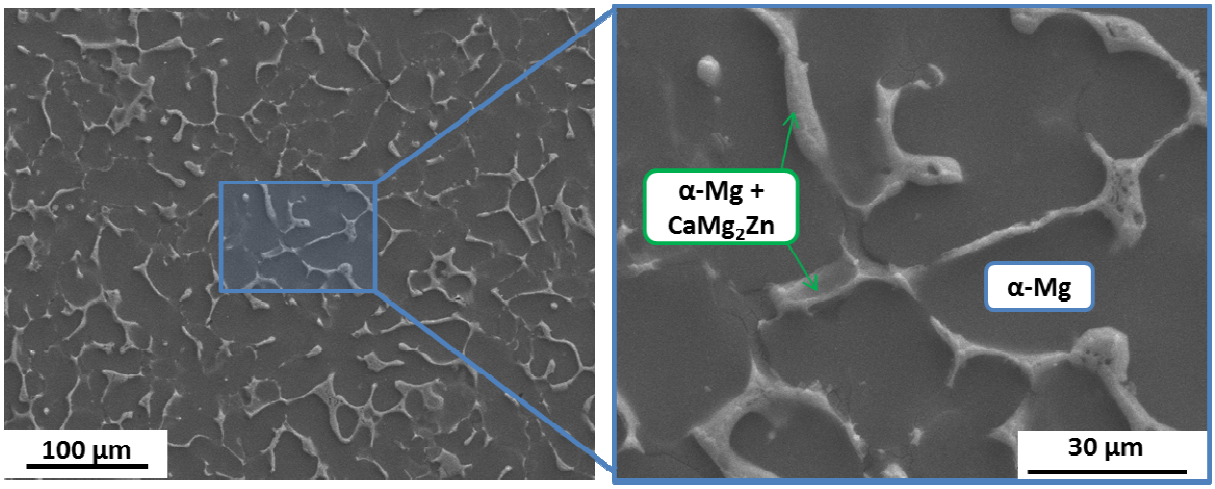

Figure 7-7 : Scanning electron micrograph of Mg-0.4Ca-3Zn alloy with and β phases indicated.

7.3.4. Electrochemical characterisation of Mg-Ca alloys - Effect of alloy concentration and medium composition

For the Mg-Ca alloys it could be readily seen that, with increasing Ca content, the corrosion potential becomes more negative with a concomitant increase in corrosion rate (Figure 7-8). This same overall trend was also observed in HBSS and MEM.

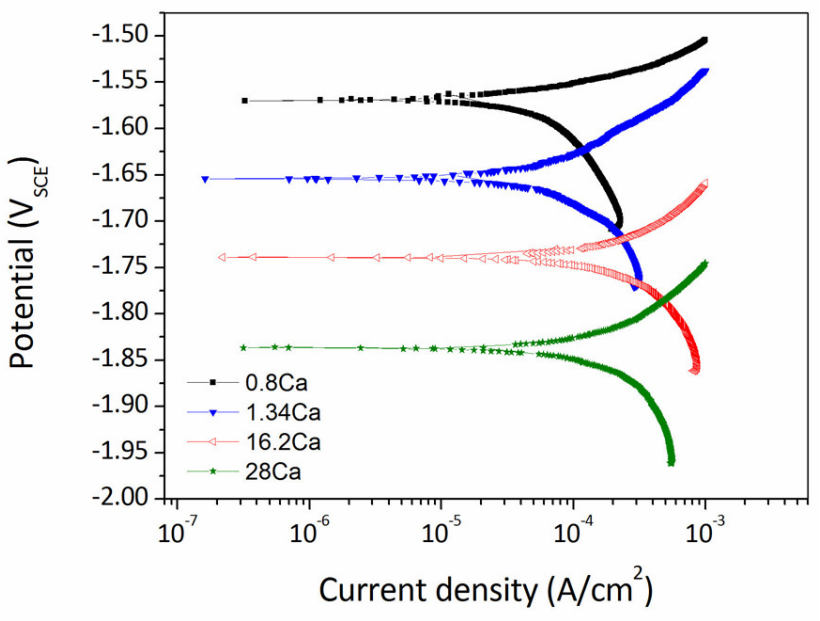

Figure 7-8 : Polarisation curves of selected Mg-*x*Ca alloys in MEM+FBS.

It was observed that all alloys displayed a trend towards reduced corrosion rate as the medium more closely mimicked the *in vivo* environment (Figure 7-9). The addition of FBS to the MEM had a significant effect on the corrosion rate of all the Mg-Ca alloys when compared to the HBSS and standard MEM mediums, with a decrease in the corrosion rate of between 10% - 290%. Furthermore, it was observed that below the solid solubility (C_s) limit of ~1.34 wt.% Ca, the corrosion rate stayed the same or even slightly decreased with increasing Ca additions, while above this limit, corrosion rates increased with increasing Ca content (Figure 7-9A). The corresponding corrosion potential of each of the alloys can be seen in Figure 7-9B.

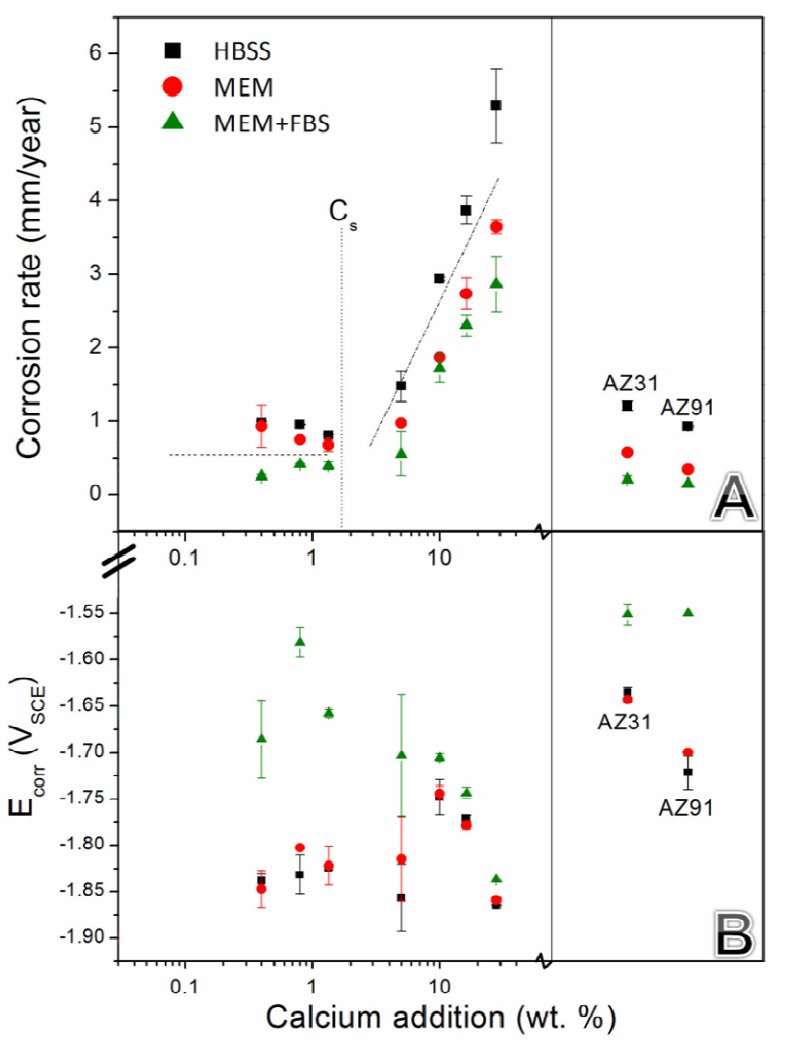

Figure 7-9 : (A) Corrosion rate and (B) potential of Mg-xCa and AZ alloys as a function of the alloy composition and corrosion medium.

Overall, E_{corr} values for all Mg-*x*Ca alloys displayed an ennoblement in MEM+FBS compared to the other media (Figure 7-10). This was due to a shift in the anodic curves.

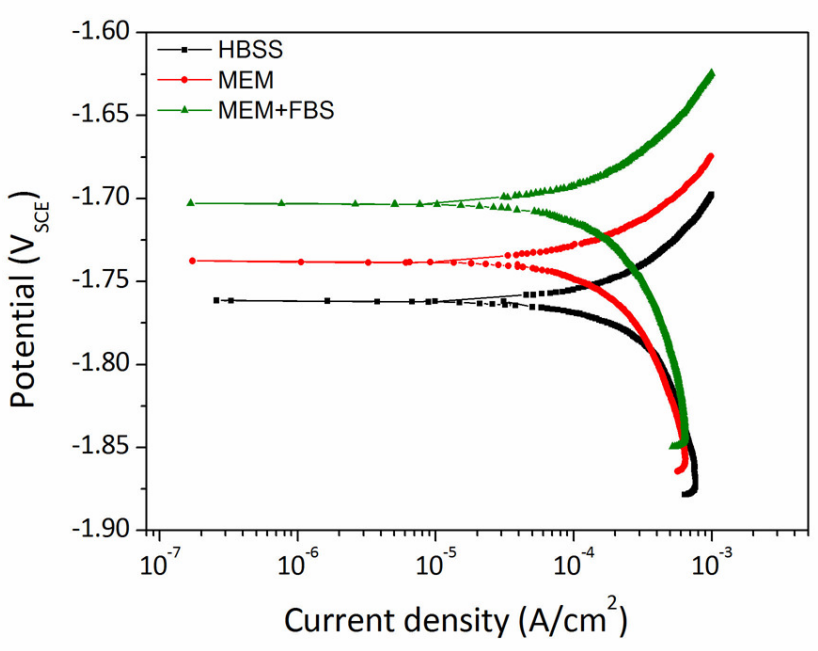

Figure 7-10 : Polarisation curves of Mg-10Ca alloy as a function of the corrosion medium.

7.3.5. Effect of alloying concentration and medium composition on electrochemical response of Mg-Zn alloys

For the Mg-Zn alloys it was found that the corrosion potential becomes more positive with the increasing Zn content (Figure 7-11). This trend, also observed in HBSS and MEM, appeared to be primarily cathodically controlled, as the anodic curves could be seen to start to converge at higher currents.

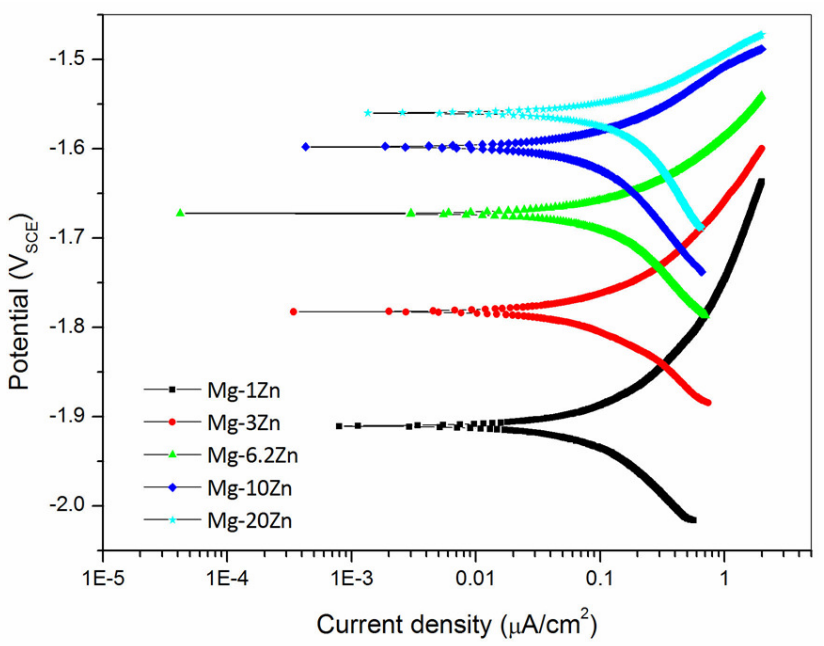

Figure 7-11 : Polarisation curves of Mg-Zn alloys in MEM+FBS.

The Mg-Zn alloys displayed a different behaviour to the Mg-Ca alloys in the various media investigated (Figure 7-12). There was a retardation of the cathodic curve in HBSS relative to the MEM solutions. The addition of FBS resulted in reduced i_{corr} due to a small shift in the anodic curve and larger shift in the cathodic reaction rate.

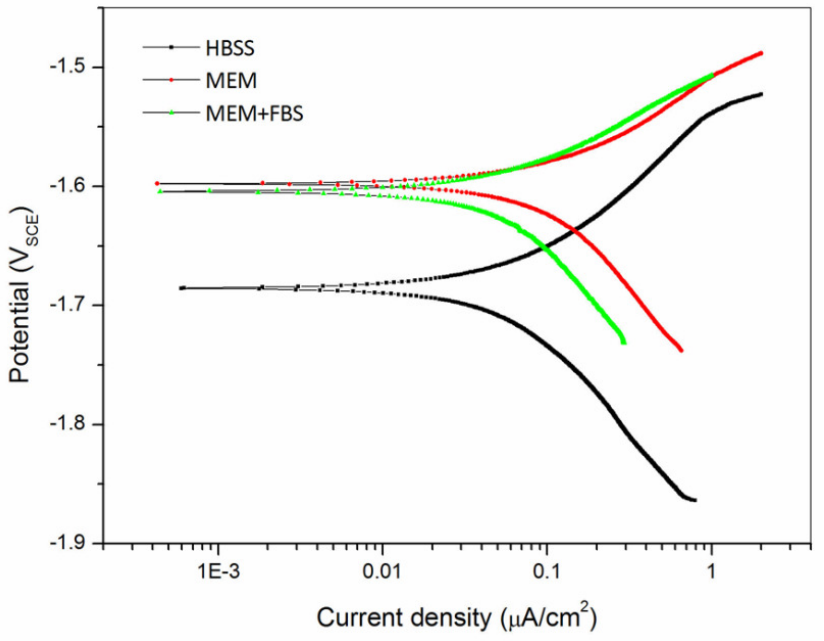

Figure 7-12 : Polarisation curves of Mg-10Zn alloy as a function of the corrosion medium.

7.3.6. Effect of alloying concentration and medium composition on electrochemical response of Mg-Ca-Zn alloys

The polarisation behaviour of the Mg-Ca-Zn alloys was found to be dominated by the Zn concentration (Figure 7-13). In the binary alloys it was found that the Ca content resulted in an increase in the anodic reaction rate (Figure 7-8), however the Mg-Ca-Zn alloys seem to be virtually unaltered due to increasing Ca content. Instead the inclusion of 3 or 6 wt. % Zn appears to control the cathodic reaction rate, with a greater concentration resulting in a more positive E_{corr} and increased i_{corr}.

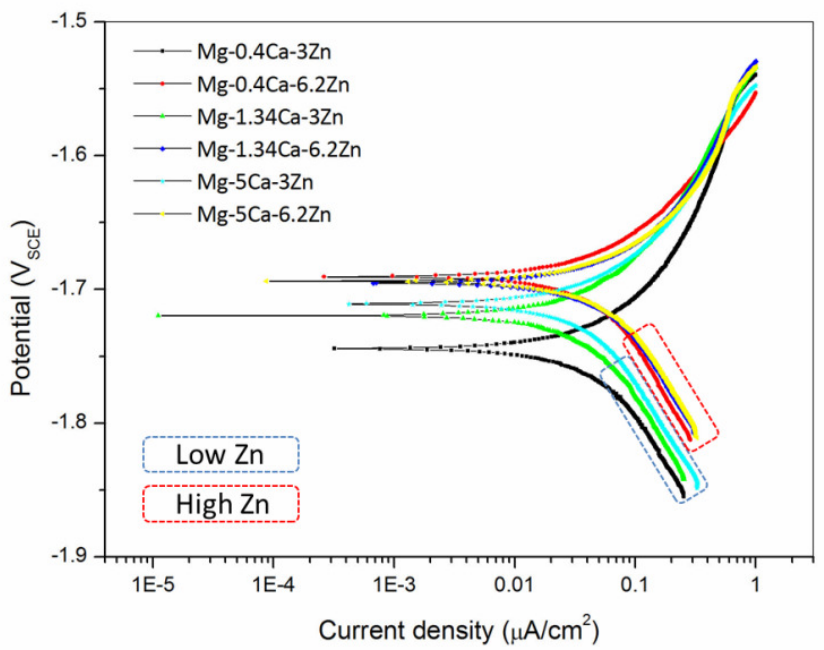

Figure 7-13 : Polarisation curves of Mg-Ca-Zn alloys in MEM + FBS. Low (3 wt. %) and high (6 wt. %) Zn content alloys are indicated.

The ternary alloys all displayed a similar behaviour to Mg-Zn in the different media, with a cathodically controlled rise in E_{corr} occurring between the HBSS and the MEM solutions (Figure 7-14). The addition of FBS reduced both the anodic and cathodic reactions rates.

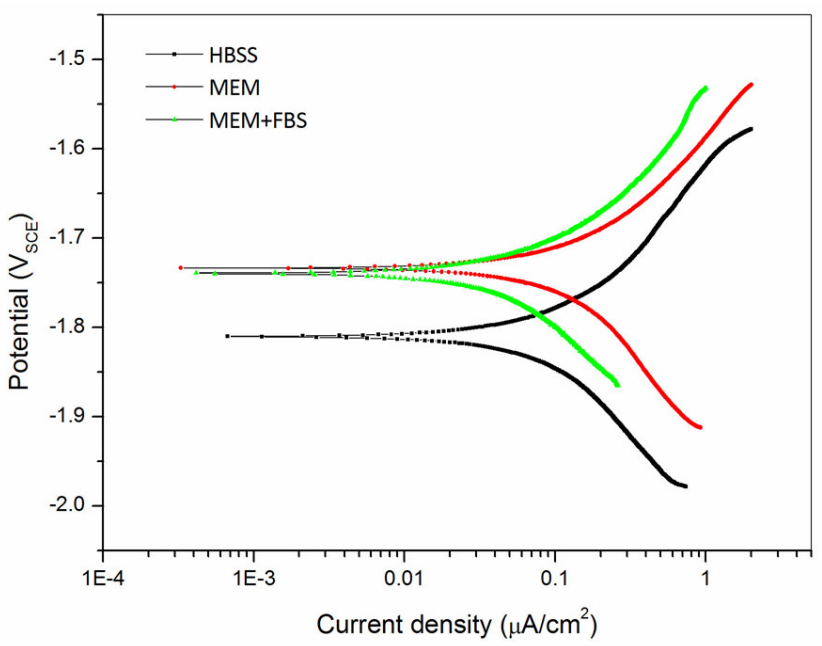

Figure 7-14 : Polarisation curves of Mg-0.4Ca-3Zn as a function of the corrosion medium.

7.3.7. Microelectrochemical investigation of intermetallic phases

The polarisation response of the Mg_2Ca and Mg_xZn_y intermetallic phases displayed starkly different behaviour (Figure 7-15). The Mg_2Ca phase overwhelmingly supports higher rates of reaction in comparison to α-Mg across a wide range of potentials. In contrast the Mg_xZn_y was found to support much faster cathodic reaction rates while slower anodic rates of reaction, resulting in a much more electropositive potential.

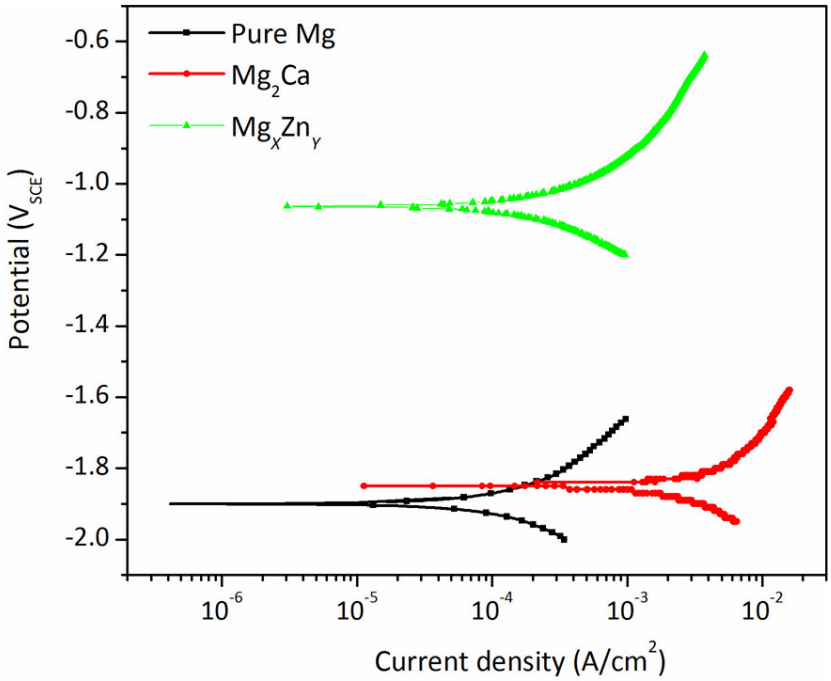

Figure 7-15 : Polarisation curves of pure Mg, Mg_2Ca, and Mg_xZn_y phases from microelectrochemical testing.

7.4. Discussion

7.4.1. Biocorrosion of Mg-Ca, Mg-Zn and Mg-Ca-Zn alloys

Microstructural investigations described herein reveal and confirm that alloying Mg with Ca leads to the formation of the intermetallic phase Mg_2Ca. The presence of this second phase has a significant impact upon the measured anodic kinetics of pure Mg as shown by a shift in the anodic branches of the polarisation curves toward significantly higher currents with increasing Ca additions (Figure 7-8). In contrast, the corresponding cathodic branches are relatively unaffected by Ca additions. If one were to extrapolate the cathodic branch of the polarisation in Figure 7-8 for Mg-0.8Ca towards increasingly negative potentials, the extrapolated curve would overlap the curves of the high Ca containing alloys. This result therefore suggests that Mg_2Ca is a more efficient anode than -Mg.

The notion that Mg_2Ca is more electrochemically active than -Mg is further confirmed by the microelectrochemical testing. It can be seen that the polarisation response of Mg_2Ca clearly reveals very high rates of reaction when compared to other metals or intermetallics in engineering alloys (Figure 7-15). Nominally when intermetallics are present in Mg, the

intermetallic assumes the role of the cathode, since the intermetallic – which is richer in alloying element – cannot nominally support anodic reactions at the rate of Mg, which is itself an active metal. This is not the case with Ca additions.

In part, the genesis of the rapid dissolution of Mg itself is owing to the fact that Mg cannot produce a stable surface oxide of complete coverage, as judged by a Pilling-Bedworth ratio (PBR) < 1 [41]. Thus, the volume of the oxide produced upon Mg is lower than the volume of the metal consumed, indicating that a continuous oxide is not capable of forming in most conditions. There are only very few instances in nature when a PBR < 1 is encountered. The phase identified as Mg_2Ca has the identical crystal structure as Mg but twice the lattice parameter magnitudes (i.e. Mg: a = 0.32093, c = 0.52107, Mg_2Ca: a = 0.623, c = 1.012). Thus the notional expectation is that volume of metal consumed in Mg_2Ca will be greater (for a given number of atoms), and hence the PBR will be even further below unity (i.e. <<1) [41]. This situation – to the author's knowledge – can only occur with Ca additions. It is also noteworthy that Ca itself is amongst the only other elements that can sustain a PBR<1 [44].

Investigations of the Mg-Zn alloys reveal the formation of an intermetallic phase of $MgZn/MgZn_2$ (Mg_xZn_y). This phase has a significant effect on the measured cathodic kinetics of pure Mg, displaying a positive rise in E_{corr} with increasing concentrations of Zn (Figure 7-11). Interestingly the Zn content itself causes a cathodic shift even below its solid solubility in Mg, which is furthered once this limit is reached. The anodic branches appear unaffected by the increased Zn content. Extrapolating the anodic branch of the Mg-xZn alloys towards increasingly positive potentials would eventually cause them to overlap, albeit at relatively high currents. This would suggest the suitability of the Mg_xZn_y phase as a cathode to the -Mg.

This behaviour is confirmed in the analysis of this phase via the µCell technique. The Mg_xZn_y phase can be seen to have an E_{corr} almost 1 V more positive than the -Mg, yet displays a significantly reduced i_{corr} (Figure 7-15). Consequently this Mg_xZn_y phase is acting as a cathode in the alloy, as it cannot support anodic reactions at the rate of the -Mg.

The Mg-Ca-Zn alloys displayed what is believed to be α-Mg and an interdendritic phase of α-Mg + $CaMg_2Zn$ (Figure 7-6). This β-phase, which was visible on all the investigated concentrations, appeared to affect the corrosion of the alloy primarily subject to the Zn

content. The Ca in the alloy appeared to have a negligible effect on the polarisation curves, with no trend apparent (Figure 7-13). However, alloys with a 6 wt. % Zn content displayed a cathodic shift to more positive potentials compared with alloys containing 3 wt. % Zn. This indicated the corrosion of the Mg-Ca-Zn alloys is primarily controlled by the cathode, which in turn is dependent on the Zn concentration.

7.4.2. Influence of electrolyte on biocorrosion of alloys

The type of medium was found to strongly influence the overall dissolution rate of Mg-Ca alloys. Given that experiments were conducted in various media to isolate the impact of materials structure and reveal a general corrosion response, some discussion regarding electrolyte influences is warranted. It was observed that, for a given Mg-*x*Ca alloy composition, the anodic branch was altered, whilst the cathodic branch remained essentially unaffected for media that more closely mimicked the *in vivo* environment (Figure 7-10). This apparent ennoblement of E_{corr} is due to the reduction in anodic reaction kinetics in the presence of serum proteins. In fact, based upon the polarisation data, the presence of proteins appear to act as mild anodic inhibitors, leading to a considerable decrease in i_{corr} by stifling the overall anodic reaction rate (and hence moving the anodic branch towards the left as seen in Figure 7-10). However, work performed in Chapter 6.5 of this thesis shows this effect to be short-term.

Furthermore, the degree of ennoblement of Mg due to changing corrosive medium was not consistent across all alloy compositions. It was observed that disparities in E_{corr}, as measured in the various media, were reduced for Ca additions of 10 wt. % or greater, indicating an apparent decreased ennoblement by the MEM+FBS medium. The underlying mechanism for this is unknown, although there are three possible explanations that exist: (i) the increase in secondary phases with ≥10 wt. % Ca may present a less “attractive” site for protein adsorption, (ii) additional calcium phosphate may form on the surface, conceivably in an amorphous state, altering the corrosion kinetics and protein adsorption [45, 46], and/or (iii) a localised increase in pH at the surface due to rapid degradation (and OH^- evolution) reduces the rate of protein adsorption. For example, Sharpe *et al.* similarly found that a higher pH decreases the rate of protein adsorption on hydroxyapatite surfaces [47]. However, further work is required to better understand the effect of localized pH changes on the surface-protein interaction in Mg alloys.

The Mg-Zn alloys were primarily affected by altering the medium from HBSS to MEM (Figure 7-12). The change in solution resulted in a shift towards a more positive E_{corr}, with a concurrent but minor increase in i_{corr}. The amino acids appeared to slightly inhibit the anodic reaction rate while significantly increasing the cathodic rate. This indicates that they are slowing the dissolution of the α-Mg while speeding the H_2 evolution of the interdendritic β-phase. The addition of FBS to the MEM appeared to result in a minor reduction of the anodic rate while causing a more considerable decrease in the cathodic curve, resulting in a lower i_{corr}. Thus the proteins are having a greater effect on the interdendritic β-phase, limiting the reactions that are taking place.

A similar relationship was observed for the Mg-Ca-Zn alloys in the various media (Figure 7-14). Compared with HBSS, the MEM resulted in a large increase in the cathodic reaction rate for all Mg-*x*Ca-*y*Zn alloys, as well as a minor decrease in the anodic reaction rate. Thus the amino acids have a similar effect for these alloys as they do for the Mg-Zn, slowing the anodic reactions of the α-Mg slightly while causing increased cathodic activity. However, proteins appeared to have a greater effect on the anodic reaction rate for the Mg-Ca-Zn alloys, resulting in a similar decrease in both anodic and cathodic reactions. This lead to a decreased i_{corr} at a similar E_{corr} for MEM+FBS compared with MEM.

7.5. Conclusions

The (micro)electrochemical corrosion of Mg alloys

By increasing the content of Ca in binary Mg alloys to levels greater than the solubility limit a considerable rise in measured i_{corr} occurred (Figure 7-9). For the highly alloyed Mg, the corrosion rates found were greater than for any Mg alloy reported in the bio-Mg literature. This is primarily due to the highly reactive nature of the secondary Mg_2Ca phase. Over a wide range of potentials, Mg_2Ca sustains dissolution rates about an order of magnitude greater than Mg, which is already very reactive (Figure 7-15). This is posited to be owing to the chemistry and crystal structure of Mg_2Ca, and concomitant PBR<<1 which is expected, allowing the phase to be very reactive.

The presence of proteins principally affects the anodic reaction kinetics of Mg-Ca alloys, reducing the rate of metallic dissolution (Figure 7-10). This translates to an inhibitive effect

on overall dissolution. However, longer term immersion and electrochemical experiments on a range of Mg alloys reported in this work (Chapter 6.5) indicates that this may not be the case over the entire life of the material. It is unknown whether the positive effects that Ca might have on bone growth and osteoconduction would counterbalance the rapid corrosion. Hence, *in vivo* studies are needed to compare the results of the current *in vitro* tests.

It has been shown in this work and the literature that increasing the Ca content up to the solid solubility limit slightly alters the overall corrosion rate of Mg while additions above this significantly increase the corrosion rate [48]. This is seen clearly in Figure 7-9A, whereby following additions greater than a C_s (the solid solubility limit of Ca in Mg) of ~1.34 wt. % Ca, the corrosion rate increases monotonically.

Increasing the level of Zn up to and above its solid solubility in Mg resulted in large increases in the rate of the cathodic reactions in all media (Figure 7-11). However, the Zn in solid solution, and especially when a secondary phase was present, exhibited little effect on the anodic reaction rate, which appeared to be similar at higher currents. This indicates that the Zn increases the efficiency of the cathode, a behaviour which was confirmed by analysis of the individual Mg_xZn_y phase (Figure 7-15). This behaviour is in line with all other known Mg intermetallics, with the exception of Mg_2Ca. Consequently the Mg_xZn_y phase acts as the cathode, and controls the overall reaction rate of the alloy.

The corrosion of the Mg-Ca-Zn alloys appears to be almost entirely controlled by the Zn content (Figure 7-13). A higher concentration (6 wt. % versus 3 wt. %) leads to increased cathodic reaction rates and a coinciding increase in i_{corr}. The Ca, which in binary alloys was found to control the anodic reaction rates, appears to have little effect on the overall corrosion mechanisms. In the different media, all Mg-Ca-Zn alloys behaved in a similar fashion to the Mg-Zn alloys, with a cathodically controlled increase in reaction rates due to the addition of amino acids. However, proteins resulted in a decrease in both reaction rates and a subsequent reduction in i_{corr}.

The precise quantification of corrosion rates in the human body is a major challenge that lies ahead for the design and clinical adoption of Mg biomaterials. However, the work described herein reveals that it is possible to develop criteria for the design of suitable materials by deconvolving the microstructure and its electrochemistry.

Summary

This work reveals how control of alloying Mg with Ca and Zn can influence its biocorrosion behaviour. By understanding the microstructural electrochemical response of these additions they may be deployed in an engineering sense as functional additions capable of controlling the dissolution rates of Mg alloys. This is not only important in the field, but gives significant creed to the notion of using the deconstruction approach herein for unlocking the microstructure-corrosion relationships that will enable functional (i.e. customisable) implants to be developed.

7.6. References

[1] Buchheit, R.G. *A Compilation of Corrosion Potentials Reported for Intermetallic Phases in Aluminum Alloys*. Journal of the Electrochemical Society 1995;142:3994.

[2] Birbilis, N., R.G. Buchheit. *Electrochemical Characteristics of Intermetallic Phases in Aluminum Alloys*. Journal of the Electrochemical Society 2005;152:B140.

[3] Suter, T., H. Böhni. *Microelectrodes for Studies of Localized Corrosion Processes.* Electrochimica Acta 1998;43:2843.

[4] Lohrengel, M.M. *Electrochemical Capillary Cells*. Corrosion Engineering, Science and Technology 2004;39:53.

[5] Birbilis, N., B.N. Padgett, R.G. Buchheit. *Limitations in Microelectrochemical Capillary Cell Testing and Transformation of Electrochemical Transients for Acquisition of Microcell Impedance Data*. Electrochimica Acta 2005;50:3536.

[6] Pistorius, P.C., G.T. Burstein. *Detailed Investigation of Current Transiences from Metastable Pitting Events on Stainless Steel - the Transition to Stability*. Electrochemical Methods in Corrosion Research 1992;111-112:429.

[7] Nascimento, M., W. Mueller, A. Carvalho, H. Tomás. *Electrochemical Characterization of Titanium Biomaterials Using the Mini-Cell System*. Journal of Materials Science 2006;41:3323.

[8] Nascimento, M.L., W.-D. Mueller, A.C. Carvalho, H. Tomás. *Electrochemical Characterization of Cobalt-Based Alloys Using the Mini-Cell System*. Dental Materials 2007;23:369.

[9] Mueller, W.-D., C. Schoepf, M.L. Nascimento, A.C. Carvalho, M. Moisel, A. Schenk, F. Scholz, K.P. Lange. *Electrochemical Characterisation of Dental Alloys: Its Possibilities and Limitations*. Analytical and Bioanalytical Chemistry 2005;381:1520.

[10] Mueller, W.D., M.L. Nascimento, M. Zeddies, M. Córsico, L.M. Gassa, M.A.F.L. de Mele. *Magnesium and Its Alloys as Degradable Biomaterials: Corrosion Studies Using Potentiodynamic and Eis Electrochemical Techniques*. Materials Research 2007;10:5.

[11] Mueller, W.D., M.F.L. de Mele, M.L. Nascimento, M. Zeddies. *Degradation of Magnesium and Its Alloys: Dependence on the Composition of the Synthetic Biological Media*. Journal of Biomedical Materials Research Part A 2009;90A:487.

[12] Lunder, O., J.E. Lein, T.K. Aune, K. Nisancioglu. Role of Mg17al12 *Phase in the Corrosion of Mg Alloy Az91*. Corrosion 1989;45:741.

[13] Renkema, K.Y., R.T. Alexander, R.J. Bindels, J.G. Hoenderop. *Calcium and Phosphate Homeostasis: Concerted Interplay of New Regulators.* Annals of Internal Medicine 2008;40:82.

[14] Ilich, J.Z., J.E. Kerstetter. *Nutrition in Bone Health Revisited : A Story Beyond Calcium*. Journal of the American College of Nutrition 2000;19:715.

[15] Hassel, T., F.W. Bach, A.N. Golovko, A. Krause. *Investigation of the Mechanical Properties and the Corosion Behaviour of Low Alloyed Magnesium-Calcium-Alloys for Use as Absorbable Biomaterial in the Implant Technique*. In: Pekguleryuz, M., editor. Conference of Metallurgists : Magnesium Technology in the Global Age. Montreal, Quebec, Canada, 2006. p.359.

[16] Kannan, M.B., R.K.S. Raman. *In Vitro Degradation and Mechanical Integrity of Calcium-Containing Magnesium Alloys in Modified-Simulated Body Fluid*. Biomaterials 2008;29:2306.

[17] Kim, W.-C., J.-G. Kim, J.-Y. Lee, H.-K. Seok. *Influence of Ca on the Corrosion Properties of Magnesium for Biomaterials*. Materials Letters 2008;62:4146.

[18] Pietak, A.M., T. Mahoney, G. Dias, M.P. Staiger. *Bone-Like Matrix Formation on Magnesium and Magnesium Alloys*. Journal of Biomedical Materials Research 2007;19:407.

[19] Gu, X., Y. Zheng, Y. Cheng, S. Zhong, T. Xi. *In Vitro Corrosion and Biocompatibility of Binary Magnesium Alloys*. Biomaterials 2009;30:484.

[20] Shi, Z., G. Song, A. Atrens. *Corrosion Resistance of Anodised Single-Phase Mg Alloys*. Surface and Coatings Technology 2006;201:492.

[21] Zhang, S., X. Zhang, C. Zhao, J. Li, Y. Song, C. Xie, H. Tao, Y. Zhang, Y. He, Y. Jiang, Y. Bian. *Research of Mg-Zn Alloy as Degradable Biomaterial*. Acta Biomaterialia 2010;6:626.

[22] Li, J., Y. Song, S. Zhang, C. Zhao, F. Zhang, X. Zhang, L. Cao, Q. Fan, T. Tang. *In Vitro Responses of Human Bone Marrow Stromal Cells to a Fluoridated Hydroxyapatite Coated Biodegradable Mg-Zn Alloy*. Biomaterials 2010;31:5782.

[23] Chen, Y., S. Zhang, J. Li, Y. Song, C. Zhao, X. Zhang. *Dynamic Degradation Behavior of Mgzn Alloy in Circulating M-Sbf*. Materials Letters 2010;64.

[24] Abidin, N.I.Z., D. Martin, A. Atrens. *Corrosion of High Purity Mg, Az91, Ze41 and Mg2zn0.2mn in Hank's Solution at Room Temperature*. Corrosion Science;In Press, Accepted Manuscript.

[25] Song, G. *Control of Biodegradation of Biocompatable Magnesium Alloys*. Corrosion Science 2007;49:1696.

[26] Wang, X., H.M. Lu, X.L. Li, L. Li, Y.F. Zhenh. *Effect of Cooling Rate and Composition on Microstructures and Properties of Zn-Mg Alloys*. Transactions of Nonferrous Metals Society of China 2007;17:S122.

[27] Das, A., G. Liu, Z. Fan. *Investigation on the Microstructural Refinement of an Mg-6 wt.% Zn Alloy*. Materials Science and Engineering: A 2006;419:349.

[28] Zhang, S., J. Li, Y. Song, C. Zhao, X. Zhang, C. Xie, Y. Zhang, H. Tao, Y. He, Y. Jiang, Y. Bian. *In Vitro Degradation, Hemolysis and Mc3t3-E1 Cell Adhesion of Biodegradable Mg-Zn Alloy*. Materials Science and Engineering: C 2009;29:1907.

[29] Bamberger, M., G. Levi, J.B. Vander Sande. *Precipitation Hardening in Mg-Ca-Zn Alloys*. Metallurgical and Materials Transactions A: Physical Metallurgy and Materials Science 2006;37:481.

[30] Brar, H.S., M.V. Manuel. *The Dissolution Behaviour of a Mg-Zn-Ca Allow for Biomedical Applications*. In: Agnew, S.R., Neelameggham, N.R., Nyberg, E.A., Sillekens, W.H., editors. Magnesium Technology. Seatle, WA, USA: TMS, 2010. p.647.

[31] Guan, R., T. Zhao, L.L. Wang, T. Cui. *New Magnesium Alloys for Potential Application of Implantation Biomaterial.* Advanced Materials Research 2009;79:1443.

[32] Rosalbino, F., S. De Negri, A. Saccone, E. Angelini, S. Delfino. *Bio-Corrosion Characterization of Mg–Zn–X (X = Ca, Mn, Si) Alloys for Biomedical Applications*. Journal of Materials Science: Materials in Medicine 2010;21:1091.

[33] Wang, H.X., S.K. Guan, X. Wang, C.X. Ren, L.G. Wang. *In Vitro Degradation and Mechanical Integrity of Mg-Zn-Ca Alloy Coated with Ca-Deficient Hydroxyapatite by the Pulse Electrodeposition Process.* Acta Biomaterialia 2010;6:1743.

[34] Zberg, B., P.J. Uggowitzer, J.F. Loffler. *Mgznca Glasses without Clinically Observable Hydrogen Evolution for Biodegradable Implants*. Nature Materials 2009;8:887.

[35] Merrit, K., S.A. Brown, N.A. Sharkey. *The Binding of Metal Salts and Corrosion Products to Cells and Proteins in Vitro*. Journal of Biomedical Materials Research 1984;18:1005.

[36] Clarke, E.G.C. *In Vitro Aspects of Metallic Corrosion in Tissue Fluids*. Proceedings of the Royal Society of Medicine 1953;46:17.

[37] Yamamoto, A., S. Hiromoto. *Effect of Inorganic Salts, Amino Acids and Proteins on the Degradation of Pure Magnesium in Vitro*. Materials Science and Engineering: C 2009;29:1559.

[38] Rettig, R., S. Virtanen. *Time-Dependent Electrochemical Characterization of the Corrosion of a Magnesium Rare-Earth Alloy in Simulated Body Fluids*. Journal of Biomedical Materials Research Part A 2008;85A:167.

[39] Nie, J.F., B.C. Muddle. *Precipitation Hardening of Mg-Ca(-Zn) Alloys*. Acta Metallurgica Sinica 1997;37:1475.

[40] Li, Z., X. Gu, S. Lou, Y. Zheng. *The Development of Binary Mg-Ca Alloys for Use as Biodegradable Materials within Bone*. Biomaterials 2008;29:1329.

[41] Nayeb-Hashemi, A.A. *The Ca-Mg (Calcium-Magnesium) System*. In: International, A., editor. Bulletin of Alloy Phase Diagrams, vol. 8. 1987. p.58.

[42] ASM International. *Binary Alloy Phase Diagrams*. Materials Park, OH: ASM International, 1996.

[43] Buha, J. *Reduced Temperature (22-100 °C) Ageing of an Mg-Zn Alloy*. Materials Science and Engineering: A 2008;492:11.

[44] ASM International. *Corrosion : Fundamentals*, Testing and Protection. Materials Park: ASM International, 1987.

[45] Cui, F.Z., J.X. Yang, Y.P. Jiao, Q.S. Yin, Y. Zhang. *Calcium Phosphate Coating on Magnesium Alloy for Modification of Degradation Behavior*. Frontiers of Material Science in China 2008;2:143.

[46] Cheng, X., S.G. Roscoe. *Corrosion Behavior of Titanium in the Presence of Calcium Phosphate and Serum Proteins*. Biomaterials 2005;26:7350.

[47] Sharpe, J.R., R.L. Sammons, P.M. Marquis. *Effect of Ph on Protein Adsorption to Hydroxyapatite and Tricalcium Phosphate Ceramics*. Biomaterials 1997;18:471.

[48] Wan, Y., G. Xiong, H. Luo, F. He, Y. Huang, X. Zhou. *Preparation and Characterization of a New Biomedical Magnesium-Calcium Alloy*. Materials & Design 2008;29:2034.

CHAPTER 8: Development of Topologically Ordered Porous Magnesium

8.1. Introduction

The need for a process to safely produce ordered Mg structures has been well established (see Chapter 2.2.8.). The potential benefits for such a structure include improved integration with the body [1, 2] and tailoring of mechanical properties (***e.g.*** stiffness) for a variety of applications [3].

Random foams, although capable of being produced non-toxically employing an NaCl route, have an intrinsically wider variance of mechanical properties than ordered structures and cannot be used to create a variety of designs [4, 5]. Current methods that are able to synthesise topologically ordered porous Mg (TOPM) use a plaster porogen that is difficult to completely remove from the surface of the Mg, causing potential biocompatibility issues [6, 7]. Thus, a simple process is required to produce TOPM for Mg-based implants using only biocompatible materials.

The aim of this study was to create and investigate a suitable production method for TOPM using only biocompatible materials. Investigation of processing parameters would be necessary, as would study of the surface topology and mechanical performance. An understanding of the effect that the production method has on corrosion rates was also required.

8.1.1. Synthesis of topologically ordered porous Mg

A fabrication method was developed for producing TOPM structures ***via*** a rapid prototyping and salt (NaCl) casting process. The present work demonstrates the application of a multistep process for the fabrication of porous magnesium that can be used to control the cellular architecture at different topology scales. The high flammability of Mg in the powdered form means that powder processing routes such as selective laser sintering are a formidable and dangerous task. This has prompted the development of a new liquid metal casting route for cellular Mg that involves the infiltration of a NaCl template having a desired ordered

architecture. NaCl is an ideal porogen material for casting Mg due to its: (i) high thermal stability and strength, (ii) non-reactive nature with Mg, (iii) ability to be formed into complex, ordered structures, (iv) biocompatibility and (iv) the ease with which NaCl is removed from the cast material.

8.2. Experimental methods

8.2.1. Preparation of ordered NaCl template and TOPM

NaCl particles (Ø = 45-63 µm) were infiltrated into cylindrical polymer templates fabricated from a computer aided design (CAD) model using a commercial rapid prototyping (RP) machine (InVision® HR 3D Modeller, VisiJet® HR 200, 3D Systems, Rock Hill, SC, USA). Polymeric RP templates (Ø20 × 20 mm) were produced for NaCl infiltration (Figure 8-1). The RP templates were infiltrated with a paste based on NaCl powder and a supersaturated solution of NaCl. Upon removal of the water by drying in an oven a NaCl lattice structure was formed. The polymer template was carefully removed by combustion in air, using a burnout cycle with 690°C as the maximum temperature.

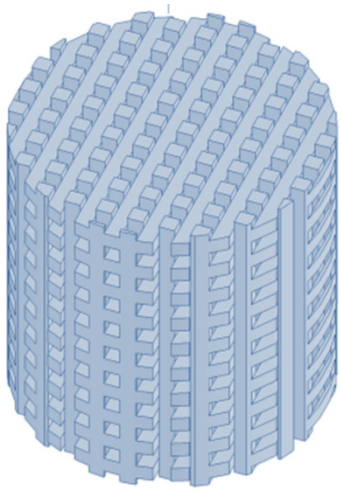

Figure 8-1 : Image of the CAD model of a 1 × 1 mm lattice structure.

The NaCl templates were cut horizontally into three equal sized samples. Each of these was infiltrated with high purity (99.98%) liquid Mg using low pressure casting in a 10 kW induction furnace under a high purity Ar atmosphere (Grade 0) at 700°C. Infiltration pressures (P_i) of 1.4, 1.5, 1.6, 1.7, 1.8 and 1.85 bar (±5 mbar) were investigated. Following

solidification of the Mg, the NaCl was removed by washing in a sodium hydroxide solution with pH > 11.8 to limit corrosion of the Mg. The process resulted in a Mg casting having an open lattice-type architecture that is referred to as TOPM in this study. A schematic of the entire process for the synthesis of TOPM is given in Figure 8-2A, and a cross-section schematic of the crucible with scaffold is shown in Figure 8-2B. Photographs of the sample at each stage of the process can be seen in Figure 8-3.

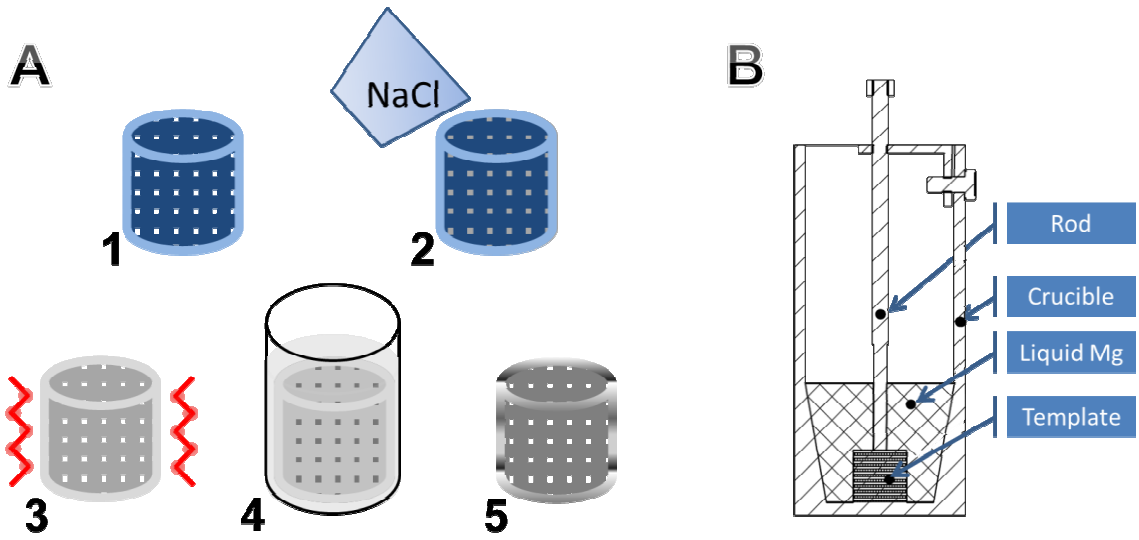

Figure 8-2 : (A) Schematic of the RP fabrication process: (1) polymeric RP template, (2) infiltration of RP with NaCl paste, (3) polymer template burn-out and subsequent sintering of NaCl, (4) low-pressure casting of Mg into the NaCl template, and (5) final TOPM following NaCl removal by dissolution. (B) Cross-section of crucible with NaCl template.

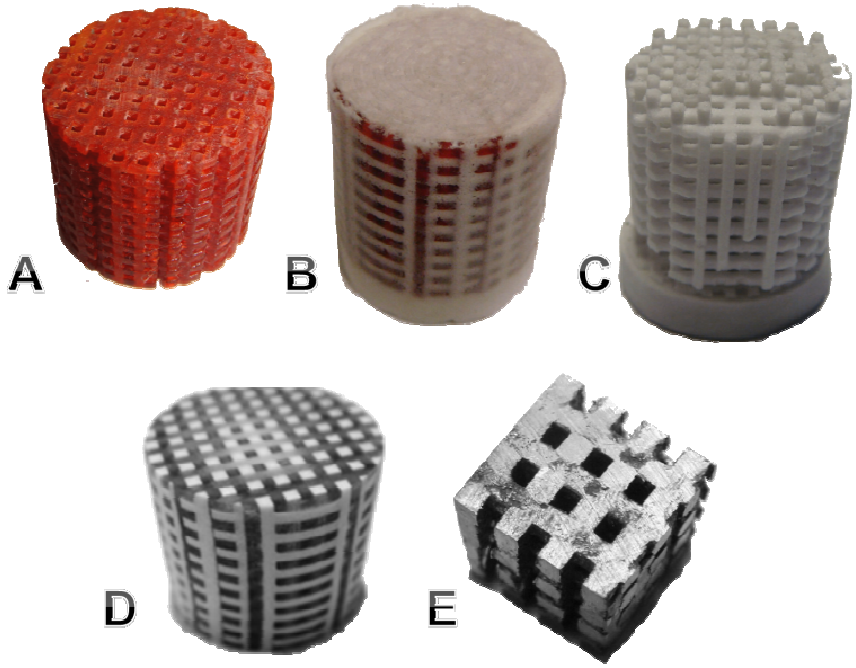

Figure 8-3 : Photographs of a sample at different stages of the infiltration process: (A) RP template, (B) RP infiltrated with NaCl, (C) salt template after removal of the RP, (D) NaCl infiltrated with Mg, (E) a piece of the final Mg scaffold after removing the NaCl.

8.2.2. Corrosion experiments

H_2^{evo} tests were carried out to study the corrosion performance of the TOPM samples. Instead of using the 3D TOPM structure, flat samples of Mg were prepared to ensure a controllable surface area for corrosion testing. To create flat Mg samples, NaCl discs were prepared in the same manner as for 3D lattice-type structures. Liquid Mg was then cast onto the flat NaCl discs using a P_i of 1.8 bar, by means of the same apparatus as for TOPM. The as-cast surface was referred to as template roughened Mg (TR). A sample of bulk Mg was also taken from the same ingot, polished to 1200 grit and then investigated for comparison. All samples were tested for 6 hrs in HBSS at T_{phy} and at a pH of 7.4 using the setup described in Chapter 4.2.2.

PDP and EIS were carried out on samples produced in the same way as for the H_2^{evo} experiment. The normal electrochemical setup was used as described in Chapter 4.3 in HBSS at T_{phy} and at a pH of 7.4.

8.2.3. Mechanical performance of TOPM

Compressive tests of selected samples were carried out using an initial strain rate of 10^{-3} s^{-1} on a MTS® 810 Material Test System (MTS, Eden Drive, MN, USA) equipped with a 100 kN load cell. Samples were prepared according to ASTM E9-89a with dimensions of 5 × 5 × 9 mm (depth × width × height) [8]. The maximum compressive stress of TOPM was determined from the first stress peak in the stress-strain curve after Ashby *et al.* [9]. The compressive strength of TOPM samples was compared to bulk Mg considering samples of equivalent cross sectional area. The cross sectional area of the TOPM samples was based solely on the area of the vertical columns in the lattice structure (Figure 8-1).

8.2.4. Microstructural analysis

The TOPM samples were initially observed under an Olympus B061 upright optical microscope and photographed using a digital camera (G10, Canon Inc., Tokyo, Japan). A JEOL 7000F FE-SEM was used with EDS to analyse the surface morphology and composition. Confocal microscopy (Leica® TCS-SP5) was used to characterize the surface topology of the final as-cast TOPM at different pressures. The confocal micrographs were analysed with specially-developed in-house software, based on well-defined techniques [10, 11] from the University of Canterbury, to obtain surface roughness (R_a) values. The software used a large number of confocal images (100+) to calculate the mean "depth" from which the R_a is obtained.

8.3. Results and discussion

8.3.1. Effect of casting pressure on the infiltration and surface roughness of TOPM

Initial trials demonstrated that the NaCl structures could not be infiltrated by liquid Mg in the absence of an applied pressure. This suggested a lack of wetting between the Mg and NaCl as well as an indication of the significant surface tension that hinders infiltration into the 1 × 1 mm pores. A lack of infiltration pressure results in smooth, curved surfaces (Figure 8-4A). A P_i of 1.4 and 1.5 bar resulted in only partial infiltration of the NaCl lattice structure (Figure 8-4B & C). At a P_i of 1.6, 1.7 and 1.8 bar the scaffolds were fully infiltrated (Figure 8-4D, E,

F). It was observed that a greater P_i resulted in a rougher surface than a lower P_i, indicating that the process could be modified to produce a range of different R_a.

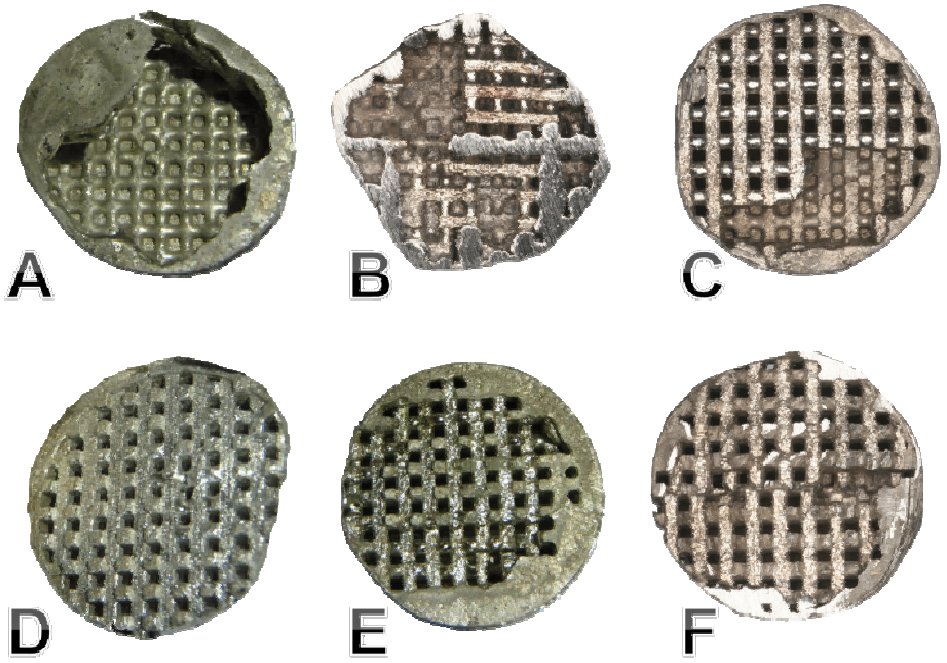

Figure 8-4 : Photographs of TOPM produced with P_i of: (A) 1 bar, (B) 1.4 bar, (C) 1.5 bar, (D) 1.6 bar, (E) 1.7 bar and (F) 1.8 bar.

A P_i above 1.8 bar was found to cause a “random” infiltration due to Mg permeation in between the salt grains within the struts of the NaCl structure. This is visible in the photograph of a 1.85 bar structure (Figure 8-5A), and is even more apparent when viewed with the SEM (Figure 8-5B). This highlights the importance of carefully controlling the P_i at all points during the synthesis of TOPM.

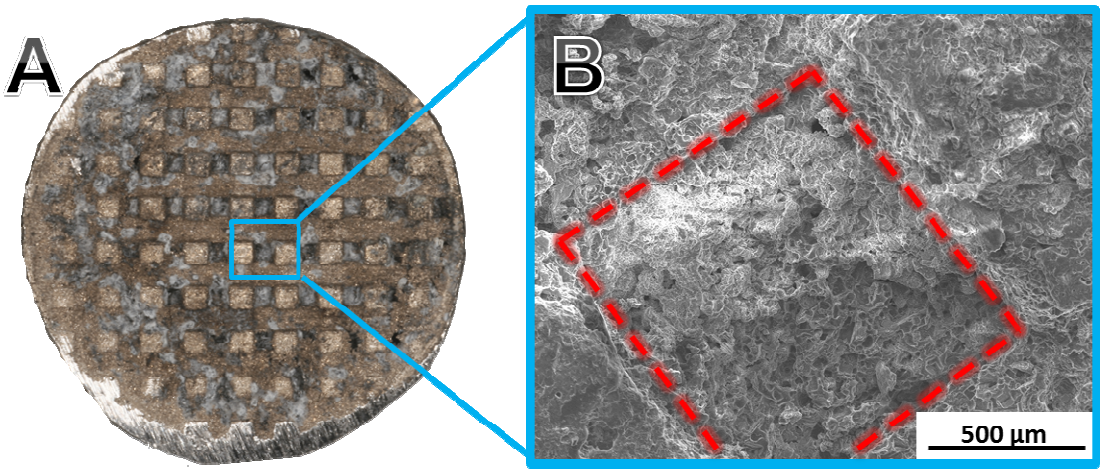

Figure 8-5 : (A) Photograph of TOPM using a P_i of 1.85 bar and (B) scanning electron micrograph of over-infiltrated strut with red rectangle indicating area of Mg infiltration where the original NaCl strut was positioned before washing.

It was observed that the roughness of the surface increased significantly as the P_i increased (Figure 8-6). For example, the surface roughness of TOPM with a P_i of 1.8 bar is more than twice that of a sample produced using a P_i of 1.4 bar (Table 8-1). The Mg was found to wet the salt, leaving reverse imprints of the salt grains on the surfaces of the struts. This suggests that the NaCl particle size and distribution could be selected to tailor the desired R_a.

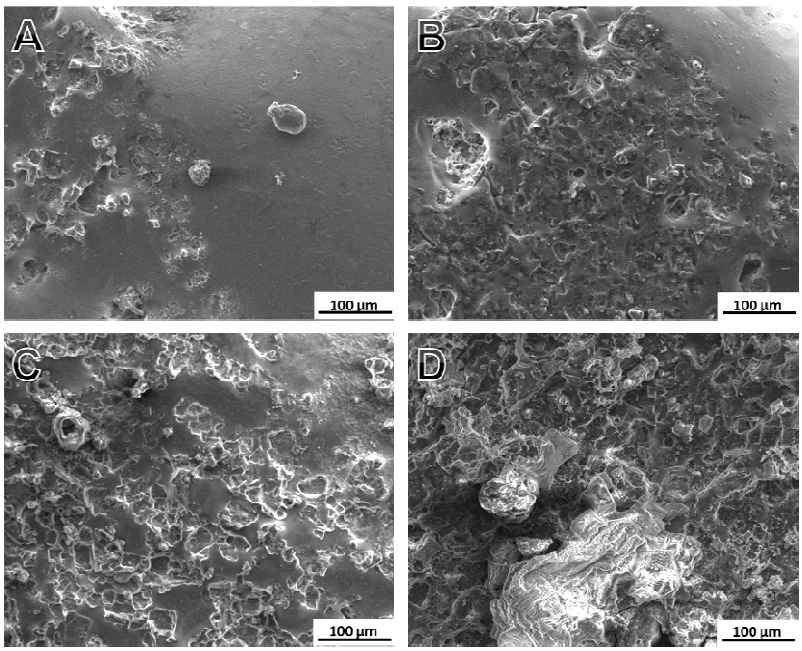

Figure 8-6 : Scanning electron micrographs of the surface of TOPM cast as a function of P_i: (A) 1.4 bar, (B) 1.6 bar, (C) 1.8 bar, (D) 1.85 bar.

Table 8-1 : Surface roughness values of TOPM samples as a function of P_i.

P_i (bar)	R_a (µm)
1.4	11.07
1.5	11.49
1.6	17.54
1.8	23.36

This roughness may provide both positive and negative effects in biological situations. Firstly, it has been shown that increased roughness can significantly enhance the corrosion rate of Mg alloys [12, 13]. However, the surface micro-architecture or topology of orthopaedic implant devices is recognized as an important parameter for encouraging new tissue formation [14-18]. For example, Schwartz ***et al.*** found that implants with surface roughness values (R_a) of 3 to 6 µm increase cell proliferation by up to 9 times compared with a smooth surface (R_a = 0.2 µm) [17]. Wilson ***et al.*** found that "valleys" 40 µm wide and 20 µm deep had a positive effect on proliferation of bone cells when compared to smooth surfaces [19]. The RP moulds used to create the inverse salt templates displayed a topology containing micro-valleys ranging from 10-30 µm across (Figure 8-7A). These micro-valleys appear to be partially transferred to the inverse salt mould (Figure 8-7B), although the size of the NaCl particles (45-63 µm) resulted in limited penetration. The amount of penetration by the NaCl is not clear in the electron micrographs due to the large size and random orientation of the salt grains. However, it was clear from the TOPM sample at the higher infiltration pressures (1.8 bar) that some of the original features of the RP mould had been transferred (Figure 8-7A versus C). This indicates that through careful design and control of processing parameters both the roughness and microarchitecture may be altered, allowing a variety of surface topologies.

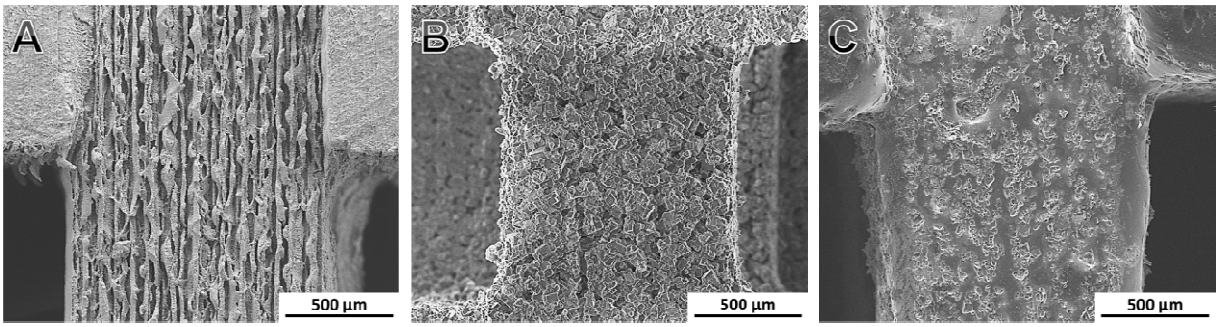

Figure 8-7 : Scanning electron micrographs of (A) the micro-valley architecture of the positive polymeric template that is partially transferred to (B) the negative NaCl template and subsequently to (C) the TOPM surface.

8.3.2. Improvements in compressive mechanical behaviour of TOPM over random foams

The ability to control the surface topology of cellular Mg is important for mechanical properties, since it will affect crack propagation and load transmission through the introduction of "defects" and stress raisers at the surface. The periodic (1×1 mm) samples exhibited ultimate compressive strengths (~13 MPa) equivalent to or slightly higher than bulk Mg samples (~11 MPa) (Figure 8-8). This was somewhat unexpected since it was thought that the introduction of sharp corners into the lattice structure might have decreased the strength. However, the contribution of the horizontal struts in supporting the vertical columns is presumed to help strengthen the lattice structure.

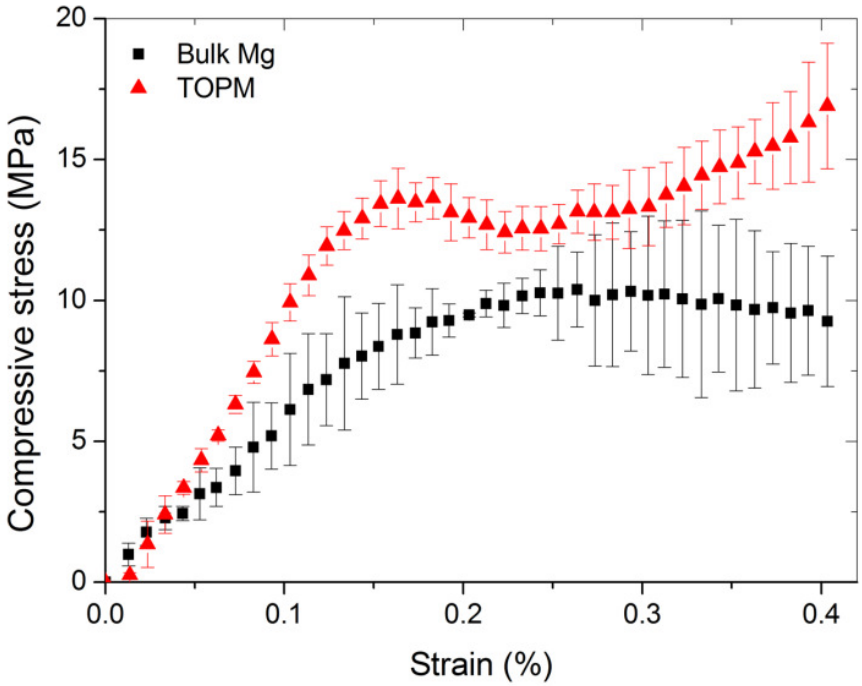

Figure 8-8 : Compressive stress-strain behaviour of bulk Mg and TOPM with equivalent cross-sectional areas.

Interestingly, TOPM with a theoretical porosity of 41% exhibited compressive strengths just below that of random porous Mg foams reported in the literature [20]. Wen *et al.* reported a compressive strength of 15 MPa for random Mg foam with a porosity of 41%. They also noted that the pore size of the foams influenced the strength, with larger pores resulting in reduced mechanical properties. On this basis, considering the trend of decreased strength as pore size increases, if the TOPM could be considered to have an effective pore size of 1 mm it would yield a compressive strength almost 40% higher than equivalent random foams that Wen *et al.* tested (Figure 8-9). Thus, in theory, the properties of TOPM exhibit a significant mechanical efficiency over the random porous structures.

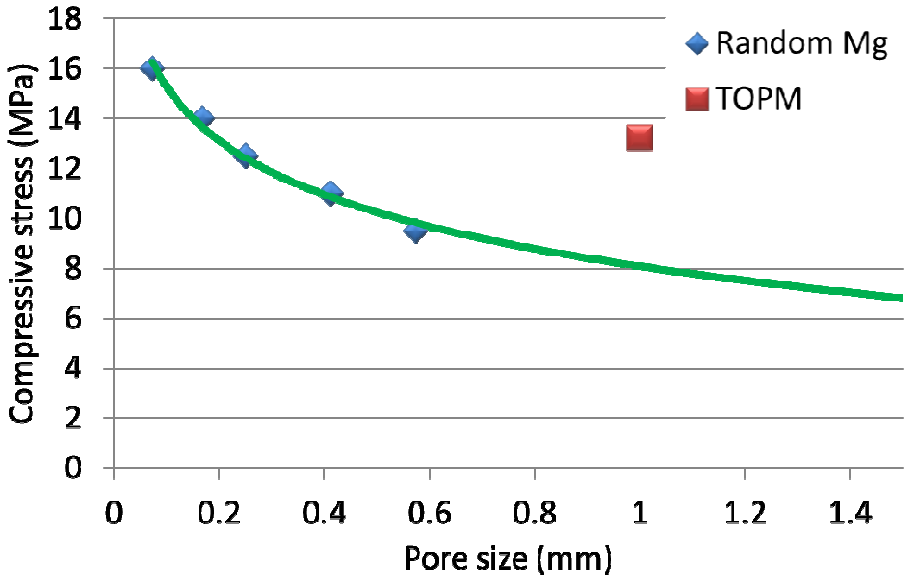

Figure 8-9 : Compressive stress as a function of pore size, including the extrapolated data of random porous foams and measured TOPM performance.

8.3.3. Rapid hydrogen evolution of template-roughened Mg

A significant amount of H_2 was observed to evolve from the template roughened Mg (TR) samples over 6 hrs (Figure 8-10). The rate of evolution increased in the first 4 hrs, indicating intensified corrosion on the surface of the sample. Between 4-6 hrs this rate appeared to flatten, which is consistent with the electrochemical results (Figure 8-11). After 6 hrs the evolution rate was approximately 10 × faster for the TR samples than for those polished to 1200 grit. It is likely that the H_2 evolution was effectively occurring at its maximum rate for the TR samples after 6 hrs, and the entire surface of the sample was observed to be covered in H_2 bubbles.

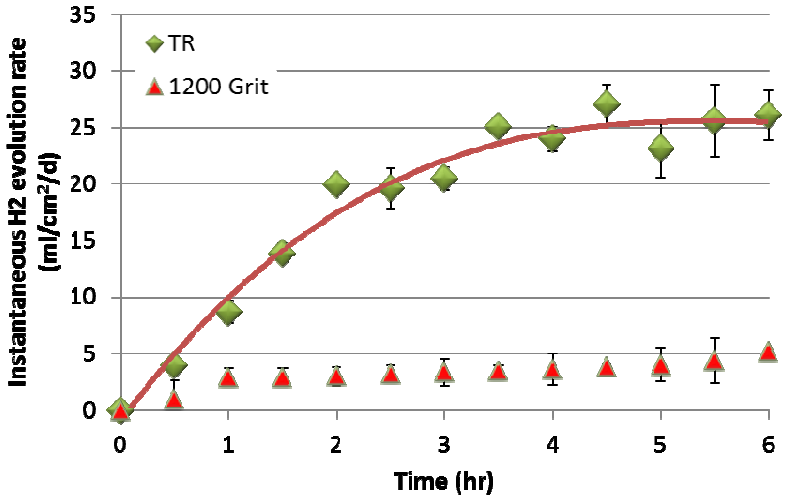

Figure 8-10 : Instantaneous H_2 evolution rate of TR and 1200 grit polished samples over 6 hrs. (HBSS, T_{phy}, 7.4)

8.3.4. Electrochemical analysis of template-roughened Mg

The TR samples displayed a considerably different electrochemical response when compared with pure Mg polished to 1200 grit (Figure 8-11). While the polished samples gradually displayed a lower i_{corr}, TR samples exhibited the opposite trend with a quickly increasing $i_{corr.}$ The final i_{corr} for the TR after 24 hrs (360 µA/cm^2) was over 7 × higher than that of the 1200 grit Mg (50 µA/cm^2). This is potentially a result of an increased surface area as the corrosion proceeded, due to rapid corrosion in the initial period. However, given only 1 cm^2 of surface was in contact with the test solution, the levelling of corrosion current density for this sample may simply be due to the sample reaching its maximum corrosion rate for the available area.

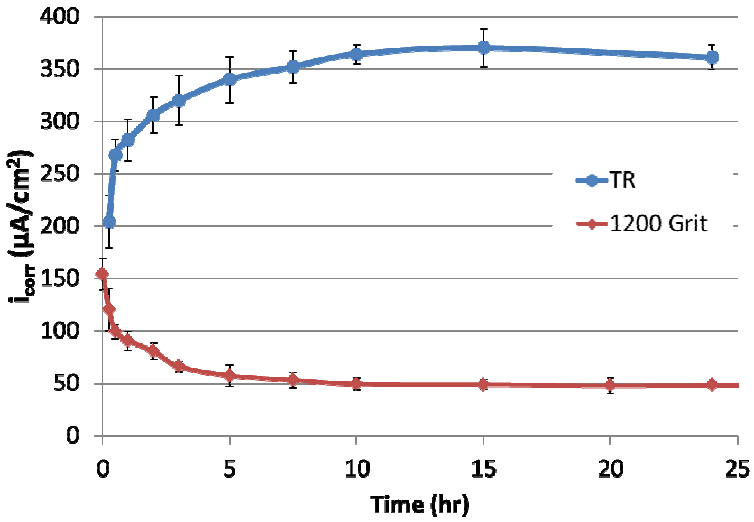

Figure 8-11 : i_{corr} of TR and 1200 grit polished Mg samples. (HBSS, T_{phy}, 7.4)

The physical imprints of the salt grains on the Mg surface that were visible on the surface of the as-cast TR (Figure 8-12A) disappeared after 24 hrs of immersion, revealing the underlying Mg grain boundaries (Figure 8-12C). The typical $Mg(OH)_2$ / CaP surface dry-earth corrosion layer, as shown for the polished sample (Figure 8-12D), was not visible on the TR surface. EDS analysis of the surface confirmed only Mg and O were present on the TR surface compared with considerable amounts of Ca and P (Ca = 7 wt.%, P = 9 wt. %) on the polished sample (Figure 8-13). This indicates that the corrosion of the polished samples was partially limited by the build-up of a $Mg(OH)_2$ / CaP layer on the surface. The corrosion rate of the TR samples was not limited by any layer, and consequently proceeded rapidly.

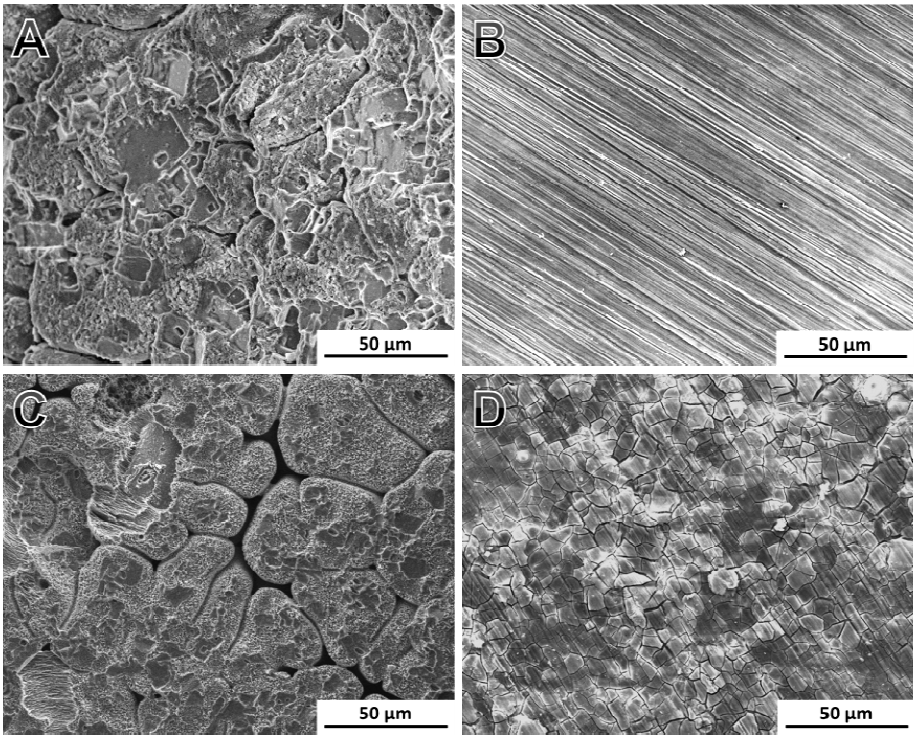

Figure 8-12 : Scanning electron micrographs (2000 ×) of the TR and 1200 grit polished surfaces before (A&B) and after (C&D) 24 hrs immersion. (HBSS, T_{phy}, 7.4)

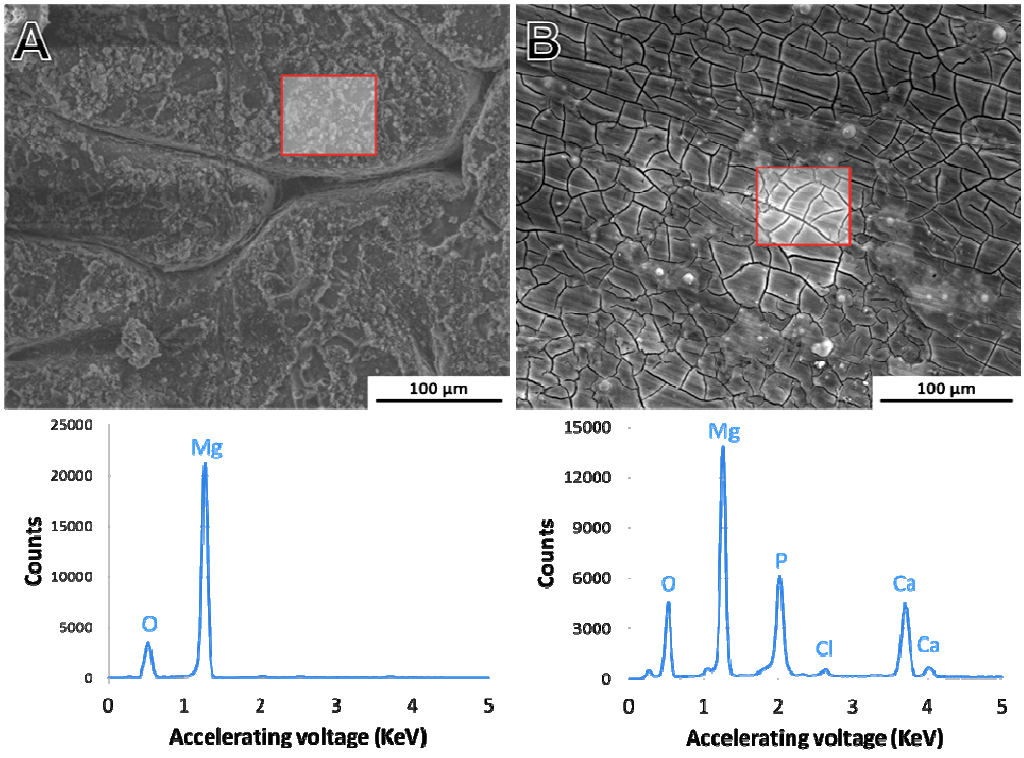

Figure 8-13 : Scanning electron micrographs (1000 ×) of surface after 24 hrs immersion of (A) TR and (B) 1200 grit polished surfaces and corresponding EDS analysis. (HBSS, T_{phy}, 7.4)

To further analyse this phenomenon, EIS experiments were performed over a shorter time period (6 hrs) to limit the effect that corrosion may be having on the surface morphology. As expected the TR samples displayed significantly lower R_{tot} than the polished samples (Figure 8-14A). Analysis of the curves over time on the Nyquist plot revealed a single time constant behaviour for the TR samples at each time point over the 6 hrs (Figure 8-14B). The 1200 grit samples displayed a single time constant initially, however a second eventually developed, which, based on previous analyses in this work, is due presumably to a $Mg(OH)_2$ / CaP layer.

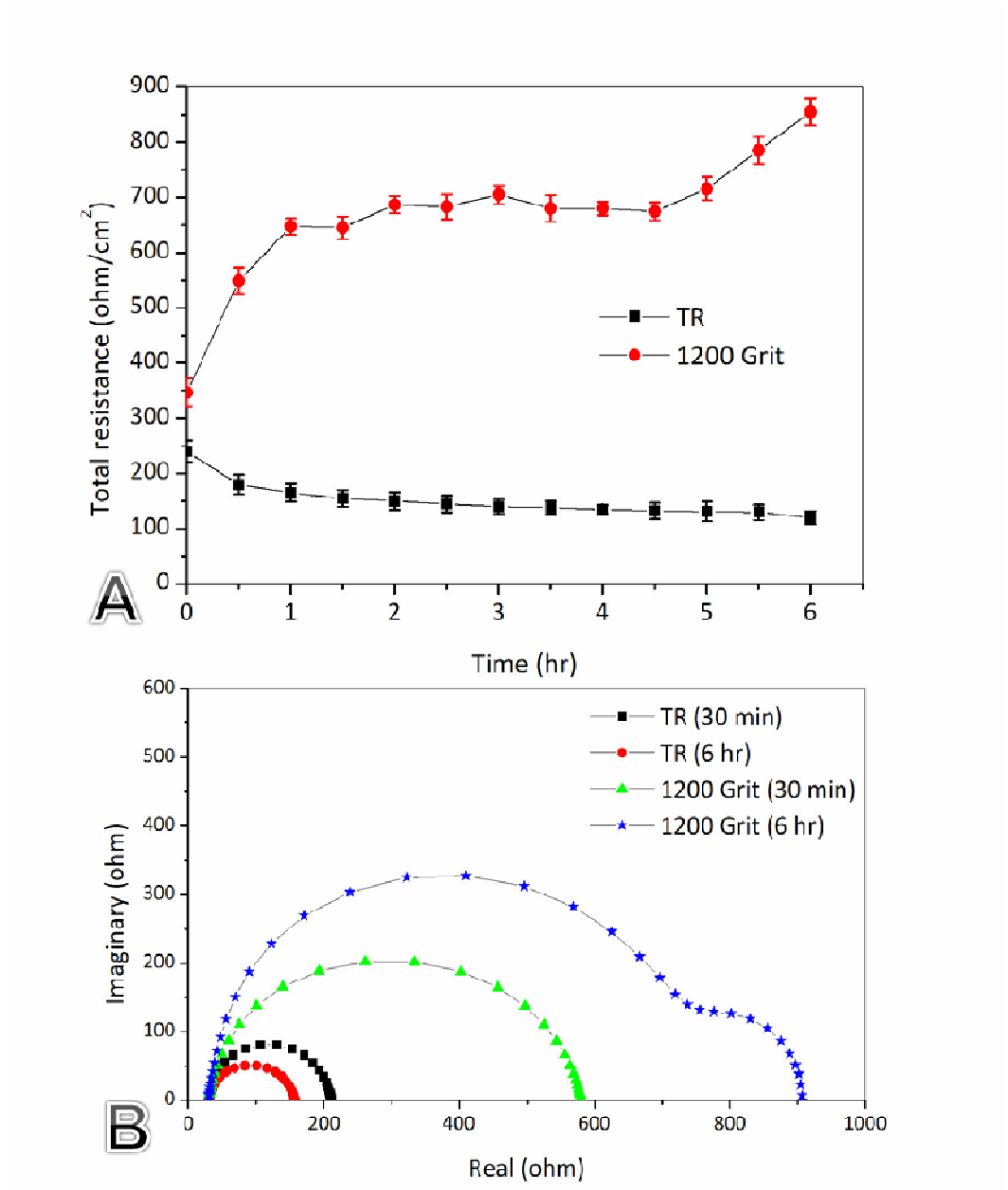

Figure 8-14 : (A) R_{tot} over 6 hrs for TR and polished Mg and (B) corresponding Nyquist plots at 30 min and 6 hrs. (HBSS, T_{phy}, 7.4)

Considering the rapid corrosion rates (Figure 8-10, Figure 8-11) and significantly different morphology (Figure 8-12) with a complete lack of the CaP layer (Figure 8-13), it appears that the TOPM structure may not be suitable in its current form for use *in vivo*. There is potential that the slower rates of corrosion that have been observed *in vivo* rather than *in vitro* may help partially alleviate this problem [21-23], but it is likely that the rates observed are too rapid for most applications. However, given the novelty of the process, there are many improvements (*e.g.* lower pressures) that might be made that could reduce the corrosion rate to acceptable levels.

8.4. Conclusions

A porous NaCl template with controlled internal structure was synthesised using existing rapid prototyping methods. This process could be used to create ordered structures, currently with a minimum pore size of 0.3 x 0.3 mm [24]. The potential of such a technique for Mg is clear, as ordered cellular metal has been shown to have many benefits over solid structures.

The surface of the structure may be controlled by altering casting conditions during processing. It was found that the casting pressure had a considerable affect not only on the infiltration success and mechanical integrity, but also on the surface texture and wetting of the liquid Mg with NaCl. Although higher pressures improved some of these characteristics, they could also lead to uncontrollable effects such as infiltration between the NaCl grains. Control of this surface, including the average roughness and creation of the "valley" architecture, is crucial as it can yield a topology that is specially designed for cell attachment. Combined with effective channelling of the new bone growth attributable to the overall structure design, the potential for more effective and faster healing in orthopaedic applications is significant.

However, sizeable challenges remain, primarily due to the increased corrosion rate that occurs due to the rougher surface. Unlike polished surfaces, no significant corrosion layer appears to effectively form on the surface of the TR/TOPM. This layer has been seen to form on every non-TR alloy investigated in BSS in this work, and consequently indicates a departure from this "normal" layer formation behaviour. It is likely that the primary reason for the lack of a CaP layer is due to the rapid corrosion that occurs soon after immersion,

between 7 × (Figure 8-11) and 10 × (Figure 8-10) faster than 1200-grit polished Mg, preventing the build-up of any corrosion product. It is important to consider that the increased corrosion may be due in part to a number of factors including: (i) impurities pickup during the casting process, (ii) NaCl embedded into the Mg struts (resulting in an increase in Cl^- concentration near the surface), and (iii) variance in grain size (and grain boundary volume) due to the difference in cooling conditions for the TOPM structure compared with the normal casting method. These factors, although not investigated in this study, nonetheless constitute future areas of work for this method. However, although TOPM currently corrodes too quickly for virtually any biomaterial application, the properties may be altered by careful processing control, balancing the potential favourable surface properties for cell attachment with corrosion regulation. The use of coatings also may prove highly beneficial in slowing this initial corrosion, which may in turn allow protein/cellular attachment to further slow degradation.

8.5. References

[1] Alvarez, K., H. Nakajima. *Metallic Scaffolds for Bone Regeneration*. Materials 2009;2:790.

[2] Karageorgiou, Vassilis, Kaplan, David. *Porosity of 3d Biomaterial Scaffolds and Osteogenesis*. Oxford, ROYAUME-UNI: Elsevier, 2005.

[3] Hutmacher, D.W., D.F. Williams. *Scaffolds in Tissue Engineering Bone and Cartilage*. The Biomaterials: Silver Jubilee Compendium. Oxford: Elsevier Science, 2006. p.175.

[4] Witte, F., H. Ulrich, C. Palm, E. Willbold. *Biodegradable Magnesium Scaffolds: Part 2: Peri-Implant Bone Remodeling*. Journal of Biomedical Materials Research Part A 2007;81A:757.

[5] Witte, F., H. Ulrich, M. Rudert, E. Willbold. *Biodegradable Magnesium Scaffolds: Part 1: Appropriate Inflammatory Response*. Journal of Biomedical Materials Research Part A 2007:748.

[6] Yamada, Y., C. Wen, K. Shimojima, H. Hosokawa, Y. Chino, M. Mabuchi. *Compressive Deformation Characteristics of Open-Cell Mg Alloys with Controlled Cell Structure*. Materials Transactions 2002;43:1298.

[7] Yamada, Y., K. Shimojima, Y. Sakaguchi, M. Mabuchi, M. Nakamura, T. Asahina, T. Mukai, H. Kanahashi, K. Higashi. *Processing of an Open-Cellular Az91 Magnesium Alloy with a Low Density of 0.05 G/Cm(3)*. Journal of Materials Science Letters 1999;18:1477.

[8] ASTM International. Astm Standard E9-89a, "Standard Test Methods of Compression Testing of Metallic Materials at Room Temperature". 2000.

[9] Ashby, M.F., A. Evans, N.A. Fleck, L.J. Gibson, J.W. Hutchinson, H.N.G. Wadley. *Metal Foams: A Design Guide*. Woburn, MA: Butterworth Heinemann, 2000.

[10] Whitehouse, D. *Surfaces and Their Measurement*. London: Kogan Page Science, 2004.

[11] Udupa, G., M. Singaperumal, R.S. Sirohi, M.P. Kothiyal. *Assessment of Surface Geometry Using Confocal Scanning Optical Microscope*. Mechatronics 1998;8:187.

[12] Yoo, B., K.R. Shin, D.Y. Hwang, D.H. Lee, D.H. Shin. *Effect of Surface Roughness on Leakage Current and Corrosion Resistance of Oxide Layer on Az91 Mg Alloy Prepared by Plasma Electrolytic Oxidation*. Applied Surface Science 2010;256:6667.

[13] Song, G., D. St John, T. Abbott. *Corrosion Behaviour of a Pressure Die Cast Magnesium Alloy*. International Journal of Cast Metals Research 2005;18:174.

[14] Gogolewski, S. *Bioresorbable Polymers in Trauma and Bone Surgery*. Injury 2000;31:D28.

[15] Kasemo, B., J. Gold. *Implant Surfaces and Interface Processes*. Adv Dent Res 1999;13:8.

[16] Pebe, P., R. Bardot, J. Trinidad, A. Pesquara, J. Lucente, R. Nishimura, H. Nasr. *Countertorque Testing and Histomorphometric Analysis of Various Implant Surfaces in Canines: A Pilot Study*. Implant Dentistry 1997;6:256.

[17] Schwartz, Z., C.H. Lohmann, J. Oefinger, L.F. Bonewald, D.D. Dean, B.D. Boyan. *Implant Surface Characteristics Modulate Differentiation Behavior of Cells in the Osteoblastic Lineage*. Advanced Dental Research 1999;13:38.

[18] Gentile, F., L. Tirinato, E. Battista, F. Causa, C. Liberale, E.M. di Fabrizio, P. Decuzzi. *Cells Preferentially Grow on Rough Substrates*. Biomaterials 2010;31:7205.

[19] Wilson, C.E., J.D. De Bruijn, C.A. Van Blitterswijk, A.J. Verbout, W.J.A. Dhert. *Design and Fabrication of Standardized Hydroxyapatite Scaffolds with a Defined Macro-Architecture by Rapid Prototyping for Bone-Tissue-Engineering Research*. Journal of Biomedical Materials Research - Part A 2004;68:123.

[20] Wen, C.E., Y. Yamada, K. Shimojima, Y. Chino, H. Hosokawa, M. Mabuchi. *Compressibiltity of Porous Magnesium Foam: Dependency on Porosity and Pore Size*. Materials Letters 2004;58:357.

[21] Li, Z., X. Gu, S. Lou, Y. Zheng. *The Development of Binary Mg-Ca Alloys for Use as Biodegradable Materials within Bone*. Biomaterials 2008;29:1329.

[22] Witte, F., J. Nellesen, H.-A. Crostack, V. Kaese, A. Pisch, F. Beckmann, H. Windhagen. *In Vitro and in Vivo Corrosion Measurements of Magnesium Alloys*. Biomaterials 2006;27:1013.

[23] Wong, H.M., K.W.K. Yeung, K.O. Lam, V. Tam, P.K. Chu, K.D.K. Luk, K.M.C. Cheung. *A Biodegradable Polymer-Based Coating to Control the Performance of Magnesium Alloy Orthopaedic Implants*. Biomaterials 2010;31:2084.

[24] Staiger, M.P., I. Kolbeinsson, N.T. Kirkland, T. Nguyen, G. Dias, T.B.F. Woodfield. *Synthesis of Topologically-Ordered Open-Cell Porous Magnesium*. Materials Letters 2010;64:2572.

CHAPTER 9: Summary and Concluding Remarks

9.1. Summary of findings and achievements

9.1.1. In vitro experimental techniques

- Although mass loss experiments provide data on overall corrosion rates, they do not elucidate information on the corrosion mechanisms that are occurring. However, they are the only method that consistently and reliably provides information on the exact amount of corrosion that has occurred, and consequently are a vital part of almost any assessment of biodegradation of Mg and its alloys.

- Hydrogen evolution may be used to clarify the physical corrosion rate over time without the need for the multiple samples/end points that would be required to obtain the same information using mass loss. However, the experimental setup and assumptions required necessitate a large number of considerations that must be taken into account to accurately predict the physical mass loss of the sample. This makes it difficult to make comparisons between data obtained from different experimental setups. Thus, careful consideration and analysis of the experimental setup must be made when drawing conclusions for hydrogen evolution experiments.

- The monitoring of solution pH as a technique of measuring Mg corrosion is inappropriate for use in Mg *in vitro* tests. It requires the pH of the medium to deviate significantly from physiological levels to allow for quantitative measurements. This undermines the validity of the method and, as such, pH monitoring cannot be recommended as a tool for investigating Mg biocorrosion.

- Potentiodynamic polarisation can be used to provide data on the instantaneous corrosion current density of a given alloy, which is related to its corrosion rate.

PDP is a crucial technique for use in determining the mechanistic causes of corrosion and how they change depending on the environment or alloy choice. However, the corrosion rates obtained by PDP should not be considered absolute, but rather indicative of the amount of corrosion taking place. Although care should be taken when drawing conclusions from extrapolated short-term data, PDP should be considered an indispensable technique for most Mg biodegradation studies.

- Electrochemical impedance spectroscopy can be used to elucidate changes that are occurring at the interface between the substrate and corrosion medium. EIS can detect the formation of calcium phosphates and other biocorrosion layers directly at the surface of a Mg sample. Consequently, it can also determine how much protection this layer is providing to the Mg subsurface, and whether it is growing or degrading. This information is vital as these layers are crucial to the success of any Mg alloy, and in their absence corrosion typically proceeds rapidly. However, care must be taken when properly analysing the data, as the selection of an equivalent circuit is crucial to understanding the reactions taking place. The rapid biodegradation of Mg in SBFs also results in problems when recording lower frequencies, as they may affect the accuracy of the calculated results. In spite of this, overall EIS offers vital insight into the biodegradation of Mg alloys, primarily due to its use in analysis of layer formation, and should be considered a core technique for most Mg studies.

9.1.2. Effect of in vitro variables on the biocorrosion of Mg alloys

- The change from room temperature to the physiological temperature resulted in a substantially increased rate of corrosion for a range of Mg alloys. i_{corr} was found to rise by up to 840% (for AZ91) and there was a 130% increase in total H_2 evolved (for Mg-1Zn) over a 72 hr period. Analysis of the polarisation curves indicated that the increase in i_{corr} was almost entirely due to faster rates of oxidation reaction, displaying a shift in the anodic curve for all alloys. The cathodic reaction was relatively unaffected by the temperature increase. The magnitude of the increase in corrosion is both alloy and solution dependant, preventing conversion of data obtained at one temperature to another. Hence,

it is crucial that all *in vitro* experiments be performed at the normal body temperature of 37 °C.

- The control of pH to physiological levels *in vitro* is crucial to the biodegradation of Mg alloys. Deviations in pH of only ± 0.3 outside the physiological range can result in up to a 300% change in corrosion rate and can lead to significant morphological and chemical changes of the surface layer. pH variation may also affect the surface adsorption of proteins and amino acids. Thus the control of the pH of a medium *in vitro* to between 7.4 to 7.6 is required for an appropriate test design to attempt to mimic the body's environment.

- It is highly recommended that a buffering agent be utilised in all *in vitro* experiments. An unbuffered solution creates an unrealistic environment for corrosion to occur and dramatically alters the degradation process of Mg alloys. Chemical buffers provide a method of controlling the pH in situations where an incubator and CO_2 environment are not available or feasible. However, they may react with the Mg itself, causing increased corrosion. Ideally all corrosion experiments should be performed using a physiological concentration of sodium bicarbonate in a 5 % (or similar) CO_2 atmosphere, the closest *in vitro* condition to that of the body.

- Choice of an appropriate medium is perhaps the most crucial aspect of any *in vitro* experiment. NaCl solutions should not be utilised as they do not contain critically important elements that have been shown to influence the corrosion rate of Mg. Hanks and other balanced salt solutions provide a more realistic inorganic environment. Moreover, the use of a medium specially designed to contain appropriate levels of the most important elements, such as Kirkland's biocorrosion medium (KBM), is recommended. The organic components that are present *in vivo,* such as amino acids and proteins, increase the physiological relevance of the medium and have been shown in this work to influence the corrosion rate of Mg. Therefore it can be concluded that it is important to incorporate these components into the *in vitro* test design. However, the mechanisms of adsorption for these organic components are still

not fully understood in light of Mg biocorrosion and further work is required before they may be appropriately employed *in vitro*. Further, comparisons with *in vivo* data are also essential before any valid conclusions can be made regarding the most appropriate way in which to utilise organic components *in vitro*.

- Near-physiological flow rates were found in this work to result in significant increases in the corrosion rate for pure Mg. The flow primarily affected the corrosion layer formation, effectively stopping any calcium phosphate layer nucleating on the Mg surface. However, more work is required to better simulate *in vivo* conditions. Further, it is also not clear how long an implant will be subjected to a flow *in vivo* after cell attachment and tissue encapsulation.

- Although sample surface preparation may affect Mg corrosion, its relationship is not linear with increasing surface roughness. A range of different corrosion behaviours were found depending on the polish of the Mg surface. It is recommended that a standard preparation method be developed and used by an experimenter throughout all *in vitro* tests, allowing for comparison of work. Ideally, this process would be adopted by the biomedical magnesium community as a whole, allowing greater transparency and more effective use of the literature.

9.1.3. Influence of alloying additions on Mg biodegradation

- Calcium was found to contribute significantly to the corrosion rate of Mg when alloyed above the solid solubility limit, creating a secondary Mg_2Ca phase. As the concentration of Ca increased, the anodic reaction rate became more rapid, while the cathodic curve did not move. This indicates that the Mg_2Ca is a more efficient anode than the α-Mg, a behaviour which has not been reported for any other Mg β-phase. The Mg_2Ca is also highly reactive, and can sustain dissolution rates an order of magnitude greater than Mg. This is suggested to be due to the chemistry and crystal structure of the phase.

- All Mg-Ca alloys displayed a trend towards a reduced corrosion rate as the solution more closely mimicked the *in vivo* environment. The presence of amino acids and FBS both primarily affected the anodic reaction kinetics of Mg-Ca alloys, reducing the rate of metallic dissolution. This indicates that these organic components principally affect the Mg_2Ca phase, as there was minimal shift in the cathode (which would be α-Mg in this case).

- The addition of Zn to Mg was found to result in large cathodic shifts to faster reaction rates. The E_{corr} rose as the amount of Zn increased, both below and above the solid solubility limit. This indicates that the secondary phase of Mg_xZn_y is a more efficient cathode than the α-Mg, typical of the behaviour of intermetallic particles in Mg alloys.

- Changing the solution from HBSS to MEM primarily resulted in a shift of the cathode of all Mg-Zn alloys to faster reaction rates, although a small decrease in the anodic curve was also observed. This indicates that the amino acids were having a greater effect on the β-phase, but were also providing some protection to the α-Mg. The addition of FBS to the MEM resulted in a minor decrease in the anodic curve but a larger reduction in the cathodic reaction rates, resulting in a lower i_{corr}.

- The ternary Mg-Ca-Zn alloys, although containing a range of Ca additions, appeared to have their electrochemical response controlled almost entirely by the Zn content. Increased levels of Zn lead to a shift in the cathodic curve to faster rates of reaction, as seen for the Mg-Zn binary alloys. In contrast, the Ca additions did not result in any perceived shift in the anodic curve. This indicates that it is the Zn content which is most crucial to the mechanistic control of Mg-Ca-Zn biocorrosion.

- The Mg-Ca-Zn alloys displayed very similar behaviour to Mg-Zn alloys when immersed in different media. The amino acids resulted in an increase in the reaction rates at the cathode with a small anodic shift to lower rates. However, for these alloys the addition of FBS was found to decrease both the cathodic and anodic reaction rates by similar amounts.

9.1.4. Ordered Mg structures for biomedical applications

- A process to create topologically-ordered porous Mg (TOPM) was described as a potential route for the production of biomedical devices based on Mg. It is capable of producing structures using only biocompatible materials and methods.

- The surface topology of the TOPM structures is controllable by altering the infiltration pressure during production. It is possible to manipulate the surface roughness and, at larger scales, create "micro-valleys" on the surface. It is foreseeable that the tailoring of such surface features could be potentially used to influence the cell-substrate attachment and biodegradation rates of Mg-based implants.

- The mechanical performance of the TOPM was found to be superior to random cellular Mg with a similar porosity. Although the test was preliminary, this highlights one of the benefits which greater control over the macrostructure can provide.

- The rougher surfaces of the TOPM created by the infiltration method lead to increased rates of hydrogen evolution. The structures produced by the current process degrade too rapidly for virtually any biomedical application. However, further refinement of the process will likely allow greater control of this rate. Overall, it will be necessary to balance the increase in corrosion rate with the potential improvements for biomedical applications presented by the rougher surface.

9.2. Concluding remarks

The primary objective of this research was to clarify the influence of *in vitro* experiments and variables in the context of their use for screening potential Mg biomaterials.

A number of *in vitro* techniques and analytic methods were used to determine the effects that a variety of variables have on the degradation performance of Mg alloys. When possible, suggestions were made for idealised ranges of values for these variables which would not only allow for more realistic representation of the biological environment but also for greater comparison and consistency in interpreting the validity of findings in the literature. In addition, the primary benefits and drawbacks of the most common *in vitro* techniques for testing Mg biomaterials were examined and discussed. A collation of some of the most important considerations when performing these tests was also presented. These were explained in light of each technique, with the aim of improving future experiments and minimising experimental error.

Several biocompatible alloying systems were investigated using a microelectrochemical (μCell) technique. The concentration of the alloying element, and subsequent secondary phases, was found to result in distinct and potentially controllable shifts in the reaction rates of both the cathode and the anode. Mg_2Ca was found to be unique in its role as an anode, increasing the corrosion rate of Mg alloy significantly. Mg_xZn_y displayed the opposite behaviour, controlling the cathodic reaction rate, and the Mg-Ca-Zn alloys were found to have their electrochemical behaviour dominated by the addition of Zn. This present work provided an initial investigation into these alloying effects in SBF for the first time. Further inquiry is warranted, however, to more fully develop an understanding of these alloying effects for a variety of other compositions.

A technique for the production of topologically-ordered porous Mg was presented. The effect of casting pressure as a means of controlling the surface topology was examined, and the corrosion rate of the structures was investigated. It was found that the process could be tailored to create a range of roughness and microarchitectures on the surface of the Mg. Although current corrosion rates are too high, there is potential that further refinement of the process could result in a suitable structure with an optimised morphology for cellular adsorption.

CHAPTER 10: Future Work

10.1. Effect of chemical buffers on Mg corrosion

Results gathered from these investigations suggest that solutions buffered with HEPES corroded considerably faster than those without added buffer. This can be attributed to a number of factors, including the neutralisation of hydroxyl ions, as suggested by Rettig and Virtanen [1]. Additionally, the maintenance of pH neutrality at the surface of the Mg obstructs the formation of an $Mg(OH)_2$ / CaP layer, allowing corrosion to proceed more rapidly. However, it is not apparent if the HEPES itself interacts with the Mg to further increase the corrosion rate.

In this thesis, it was found that HEPES has a significant negative impact on the corrosion performance of pure Mg when added to both Hanks and distilled water. It was suggested that HEPES and other chemical buffers may form complexes with the Mg, actively attaching to the Mg^{2+}. Certain techniques, such as nuclear magnetic resonance (NMR), should be used to help determine whether interactions are taking place between Mg and HEPES. By varying buffer and Mg^{2+} concentrations, it should be possible to determine what complexes are forming. This would be fundamental in helping to determine how the chemical buffers may be affecting the Mg corrosion.

It should also be considered that the effect of the buffer may not be a question of thermodynamic stability of the complexes, but rather a kinetic issue where the HEPES provides a mechanism to assist the dissolution of oxide coatings. The amount of MgO dissolved over time needs to be determined both in the presence and absence of HEPES and other buffers.

10.2. Development of electrochemical perfusion bio-cell

The flow of biological fluids around an implant is an area of study that has received relatively little attention in the design of *in vitro* tests for Mg alloys. It has been shown both in this work and in the literature [2, 3] that flow can have a considerable effect on corrosion.

However, faster flow rates do not necessarily result in increased corrosion [4]. Fluid flow in the body can also affect bone adsorption, and consequently may play a vital role in the success or failure of a given implant [5]. Mg biodegradation studies have used a number of methods to induce flow, including rotating electrodes [4, 6], shaking platforms [3], and sheer-stress controlled flow parallel to the sample surface [2, 7]. Levesque ***et al.*** created perhaps the most realistic flow cell for degradable metallic biomaterials to date [2]. However, the setup was designed to determine the performance of materials for stent applications in coronary arteries rather than orthopaedic applications for which significantly slower flow rates are observed.

Bioreactors offer ideal test conditions for the flow rates that may be encountered in orthopaedic applications. They provide a controlled environment, in which variables crucial to Mg corrosion, such as pH and temperature, may be monitored and adjusted. The creation of a bioreactor specifically designed for Mg or metallic biomaterials would be required in which electrochemical measurements could be carried out while the experiment is running. This would allow for an environment that could be used to simulate a range of flow conditions that may be encountered in the body while permitting analysis of the chemical reactions occurring at the surface. It would also allow for more effective study of protein and cell interactions with Mg, as the adsorption and desorption of these organic components is affected by flow and induced sheer stress at the surface [8].

10.3. Investigation into the effect of organic compounds on Mg corrosion

The effect of amino acids and proteins on the corrosion of Mg remains unclear. Therefore, it is not possible to recommend the manner in which these organic compounds should be used in the ***in vitro*** prediction of Mg implant performance. In this work, attempts were made to determine some of the more basic characteristics (e.g. adsorption/desorption rate, quantity adsorbed) of the interactions between proteins and Mg using a variety of techniques with limited success. However, techniques such as quartz crystal microbalance (QCM) show significant promise if a better coating method for the crystals can be found, allowing slower Mg corrosion rates. There is also the possibility for other experiments, such as attenuated total reflectance Fourier transform infrared spectroscopy (ATR-FTIR), which may help detect

protein attachment without modification of the surface after immersion. Atomic force microscopy (AFM) also shows promise in detecting the attraction of proteins to a Mg surface, although the corrosion of Mg may remain an issue. A more comprehensive study of the effect of organic compounds on Mg corrosion will require a multi-disciplinary approach based on biomolecular chemistry and electrochemistry.

10.4. Microelectrochemical behaviour of biocompatible Mg alloys and media

Further systematic studies of the microelectrochemical behaviour of biocompatible Mg alloys are warranted. The work herein found the behaviour of the alloyed Mg to vary significantly depending on the alloying element and its concentration. For example, the Mg_2Ca phase was found to act as an anode to the α-Mg, whilst the Mg_xZn_y phase acted as a cathode. A larger and more fundamental study is warranted on the performance of a wide range of Mg alloys using microelectrochemical techniques, thereby expanding the knowledge presented in the present work.

It is also crucial that future studies investigate the effect of the different microstructure in solutions containing proteins and even cells, as the varying microstructures may have currently unknown effects on these organic components. For example, in this study, proteins were found to primarily effect the anodic reactions of Mg-Ca alloys, while slowing the cathodic reactions of Mg-Zn alloys. Knowledge garnered from future investigations could then be used to effectively design alloys with known corrosion performance *in vitro*.

10.5. Refinement of TOPM process

Topologically-ordered porous Mg (TOPM) will show promise for open porous biomedical Mg devices if the problems of excessive hydrogen evolution (and consequently corrosion) can be solved. This is currently the primary issue facing this production technique, and therefore warrants the focus of future work.

The use of different rapid prototype materials and manufacturing machines should also be investigated to see if the "valley" architecture or surface roughness is altered. It is possible that the surface topology could even be controlled by incorporating it into the design of the RP if a higher resolution production process were used. It may also be possible to control the surface of the TOPM by using finer NaCl particles, as they would better replicate the shape of the original RP. These would all affect the corrosion rate, and subsequently the suitability of the TOPM process.

In addition, the use of a variety of pore topologies would allow for greater understanding of the limitations and resolution of the current production method. This would be necessary for the eventual production of biomedical devices, as it would determine possible designs that could be produced. Overall, there remains significant promise for this production method.

10.6. References

[1] Rettig, R., S. Virtanen. *Time-Dependent Electrochemical Characterization of the Corrosion of a Magnesium Rare-Earth Alloy in Simulated Body Fluids*. Journal of Biomedical Materials Research Part A 2008;85A:167.

[2] Levesque, J., H. Hermawan, D. Dube, D. Mantovani. *Design of a Pseudo-Physiological Test Bench Specific to the Development of Biodegradable Metallic Biomaterials*. Acta Biomaterialia 2008;4:284.

[3] Yang, J.X., F.Z. Cui, Q.S. Yin, T. Zhang, X.M. Wang. *Characterization and Degradation Study of Calcium Phosphate Coating on Magnesium Alloy Bone Implant in Vitro*. Plasma Science, IEEE Transactions on 2009;37:1161.

[4] Hiromoto, S., A. Yamamoto, N. Maruyama, H. Somekawa, T. Mukai. *Polarization Behavior of Pure Magnesium under a Controlled Flow in a Nacl Solution*. Materials Transactions 2008;49:1456.

[5] Johansson, L., U. Edlund, A. Fahlgren, P. Aspenberg. *Bone Resorption Induced by Fluid Flow*. Journal of Biomechanical Engineering 2009;131:094505.

[6] Hiromoto, S., A. Yamamoto, N. Maruyama, H. Somekawa, T. Mukai. *Influence of Ph and Flow on the Polarisation Behaviour of Pure Magnesium in Borate Buffer Solutions*. Corrosion Science 2008;50:3561.

[7] Chen, Y., S. Zhang, J. Li, Y. Song, C. Zhao, X. Zhang. *Dynamic Degradation Behavior of Mgzn Alloy in Circulating M-Sbf*. Materials Letters 2010;64.

[8] McIntire, L.V., J.E. Wagner, M. Papadaki, P.A. Whitson, S.G. Eskin. *Effect of Flow on Gene Regulation in Smooth Muscle Cells and Macromolecular Transport across Endothelial Cell Monolayers*. Biol Bull 1998;194:394.

APPENDIX A : CONDITIONS FOR THE AVERAGE HUMAN

Table 10-1 : Macroscopic parameters of the reference human.

General Parameters:	
Weight (kg): 70	Surface Area (m^2): 1.88
Height (m): 1.80	Volume (m^3): 0.065
Basal metabolic rate: 37 (/kcal*m^2/h)	
Composition:	**Density**:
Water: 60% (42 l)	Fat: 0.9 g/cm^3
Solid: 40% (28 kg)	Whole Body: 1.07 g/cm^3
Distribution of Tissue Types (% of Body Weight)	
Muscle:	43
Bone:	30
Blood:	7.2 (5 l)
Skin:	7
Internal Organs	
Viscera:	5.6
Brain:	2.3
Liver:	2
Lungs	1.6
Kidneys (2):	0.5
Heart	0.4
Spleen:	0.2
Adapted from [1]	

Table 10-2 : Mechanical and physiochemical conditions in humans.

Physiochemical	**Value**	**Location**
pH	1.0	Gastric contents
	4.5-6.0	Urine
	6.8	Intracellular
	7.0	Interstitial
	7.15-7.45	Blood
Temperature (°C)	37	Normal core
	20-42.5	Deviations due to disease
	28	Normal skin
	0-45	Skin extremities
pO_2 (mmHg)	2-40	Interstitial
	12	Intramedullary
	40	Venous
	100	Arterial
	160	Atmospheric
pCO_2 (mmHg)	40	Alveolar
	2	Atmospheric
Mechanical	**Stress (MPa)**	**Tissues**
	0.08-0.1	Across aortic valve
	0.12-0.16	Across mitral valve
	0-0.4	Cancellous bone
	0-4	Cortical bone
	4	Muscle (peak stress)
	40	Tendon (peak stress)
	80	Ligament (peak stress)
	Stress Cycles (/ y)	**Activity**
	3×10^5	Finger joint motion
	$0.1\text{-}1 \times 10^6$	Walking
	$1\text{-}2 \times 10^6$	Peristalsis
	3×10^6	Swallowing
	$0.5\text{-}4 \times 10^7$	Heart contraction

Data from [2, 3], adapted from [2]

APPENDIX B : COLLECTED *IN VIVO* STUDIES

Alloy	Animal Model	Area of Implantation	Coating/ Prework	Concurrent *In Vitro*	Cleaning Fluid	Time	Experiments	Ref
Pure Mg								
Pure Mg	Rabbits	Femura	-	Yes	Chromic Acid	1, 5 Weeks	SEM, EDS	[4]
AZ Alloys								
AZ31	Sheep	Hip Bones	Extrusion	-	-	3 months	SEM, EDX,	[5]
AZ31	Rabbits	Femura	-	Yes	Chromic Acid	1, 9 Weeks	SEM, EDS	[6]
AZ31	Guinea Pigs	Intradermal injection, Topical Induction	-	-	-	24 days	Histomorphological Analysis, ICPAES	[7]
AZ31	Guinea Pigs	Femora	-	-	-	6,18 weeks	SEM, EDX, XRD, Fluorescence Microscopy,	[8]
AZ91	New Zealand White Rabbits	Trochanter	Polymer Coating	Yes	-	1,2 months	Histological Analysis, x-Ray, Mg Ion Concentration, Flourescence, uCT	[9]
AZ91 (Foam)	New Zealand White Rabbits	Knee	-	-	-	12 weeks	uCT,	[10]
AZ91	Guinea Pigs	Femura	-	-	-	18 weeks	Synchrotron-radiation uCT, Volume Loss	[11]
AZ91	Guinea Pigs	Intradermal injection, Topical Induction	-	-	-	24 days	Histomorphological Analysis, ICPAES	[7]
AZ91	Guinea Pigs	Femora	-	-	-	6,18 weeks	SEM, EDX, XRD, Fluorescence Microscopy,	[8]
AZ91	Guinea Pigs	Femora	-	Yes	-	18 weeks	3D Volume Analysis, SEM, EDX	[12]
AZ91	New Zealand White Rabbits	Knee	-	-	-	12, 24 weeks	Compression Tests, uCT, Histomorphological Analysis	[13]
AZ91D	New Zealand White Rabbits	Knee	Foam	-	-	3, 6 months	Histological Analysis, Staining, Optical,	[14]
AZ91D	New Zealand	Knee	Foam	-	-	3, 6	Histological Analysis, Staining, Optical,	[15]

Alloy	Animal Model	Area of Implantation	Coating/ Prework	Concurrent *In Vitro*	Cleaning Fluid	Time	Experiments	Ref
	White Rabbits					months		
				Ca Binary Alloys				
Mg-0.4Ca	New Zealand White Rabbits	Femura	Surface Modified	-	-	6 weeks	Radiographs, X-Ray, Gas Analysis	[16]
Mg-0.8Ca	New Zealand White Rabbits	Femura	Surface Modified	-	-	6 weeks	Radiographs, X-Ray, Gas Analysis	[16]
Mg-0.8Ca	New Zealand White Rabbits	Femura	Extruded, Surface Modified	-	-	3,6 months	Radiographs, X-Ray, Gas Analysis, uCT	[17]
Mg-0.8Ca	New Zealand White Rabbits	Tibias	-	-	40% HF Acid	3, 6 months	3-Point Bend, Mass Loss, uCT, SEM, EDX,	[18]
Mg-0.8Ca	New Zealand White Rabbits	Tibae	-	-	-	3,6 months	Mass/Volume Loss, Radiographs, uCT	[19]
Mg-0.8Ca	New Zealand White Rabbits	Femura	Extruded, Surface Modified	-	-	3,6 months	Radiographs, EDX,	[20]
Mg-1Ca	New Zealand White Rabbits	Femura	Rolling / Extrusion	Yes	-	3 months	Radiographs, Mass Loss, Serum Mg Levels, Optical	[21]
Mg-1.2Ca	New Zealand White Rabbits	Femura	Surface Modified	-	-	6 weeks	Radiographs, X-Ray, Gas Analysis	[16]
Mg-2Ca	New Zealand White Rabbits	Femura	Surface Modified	-	-	6 weeks	Radiographs, X-Ray, Gas Analysis	[16]
				Zn Binary Alloys				
Mg-6Zn	New Zealand White Rabbits	Femora	-	Yes	-	14 weeks	Histological Analysis, Blood Testing, Staining	[22]
				LAE442 (9)				
LAE442	New Zealand White Rabbits	Tibias	-	-	40% HF Acid	3, 6 months	3-Point Bend, Mass Loss, uCT, SEM, EDX,	[18]
LAE442	Guinea Pigs	Femura	-	-	-	18 weeks	Synchrotron-radiation uCT, Volume Loss	[11]
LAE442	New Zealand White Rabbits	Femura	-	-	-	12 weeks	ICP-MS, Optical, Spot Ablation, PIXE	[23]

Alloy	Animal Model	Area of Implantation	Coating/ Prework	Concurrent *In Vitro*	Cleaning Fluid	Time	Experiments	Ref
LAE442	New Zealand White Rabbits	Tibae	-	-	-	3,6 months	Mass/Volume Loss, Radiographs, uCT	[19]
LAE442	Guinea Pigs	Intradermal injection, Topical Induction	-	-	-	24 days	Histomorphological Analysis, ICPAES	[7]
LAE442	New Zealand White Rabbits	Femura	-	-	-	2,4,6,12 weeks	uCT, Particle Induced Gamma Emissions, Histopathological Analysis, X-Rays, SEM, EDX, ICP-MS	[24]
LAE442	Guinea Pigs	Femora	-	-	-	6,18 weeks	SEM, EDX, XRD, Fluorescence Microscopy,	[8]
LAE442	Guinea Pigs	Femora	-	Yes	-	18 weeks	3D Volume Analysis, uCT, SEM, EDX	[12]
				WE43 (4)				
WE43	New Zealand White Rabbits	Tibias	-	-	40% HF Acid	3, 6 months	3-Point Bend, Mass Loss, uCT, SEM, EDX,	[18]
WE43	Guinea Pigs	Femura	-	-	-	18 weeks	Synchrotron-radiation uCT, Volume Loss	[11]
WE43	Guinea Pigs	Intradermal injection, Topical Induction	-	-	-	24 days	Histomorphological Analysis, ICPAES	[7]
WE43	Guinea Pigs	Femora	-	-	-	6,18 weeks	SEM, EDX, XRD, Fluorescence Microscopy,	[8]
				Mg-Zn-Mn (4)				
Mg-1Zn-0.8Mn	Rats	Femora	-	-	-	5-26 weeks	Histological Analysis, Blood Testing, Cross Area Measurement, SEM, EDS	[25]
Mg-1.2Mn-1Zn	Japanese Big-Ear Rabbits	Femora	Ca-P Coating	Yes	-	1,2,3,4 weeks	Fluorescence Microscopy, Staining, Immunohistochemistry, SEM, EDX, XPS	[26]
Mg-1.2Mn-1Zn	Rats	Femora	-	-	-	9,18 weeks	Optical, SEM, EDX, Histological Analysis, Blood Ion Testing	[27]
Mg-1.2Mn-1Zn	Japanese Big-Ear Rabbits	Femora	Ca-P Coating	Yes	-	1,2,3,4 weeks	Fluorescence Microscopy, Immunohistochemistry, SEM, EDX, XPS, XRD	[28]
AMS Mg*	Human Baby	Stent	-	-	-	?	Angiograms	[29]
AE21	Pig	Corronary Stent	-	-	-	56 days	Optical, Digitized Images For Analysis	[30]

Alloy	Animal Model	Area of Implantation	Coating/ Prework	Concurrent *In Vitro*	Cleaning Fluid	Time	Experiments	Ref
MBA Mg Filler**	Dogs	Distal Phalanges	-	-	-	21 days	Histological, Tensile, Bone Density	[31]

* = Unknown composition metal from Biotronik™, Germany.
** = Osteocrete from Bone Solutuons, Inc. Dallas, TX.

APPENDIX C : COLLECTED *IN VITRO* STUDIES

Alloy	Solution	Buffer	Coating/ Prework	Atmos-phere	Temp (°C)	pH Control	Time	Experiments	Ref.
				Pure Mg					
99.8% Mg	MEM + 15% FBS	N/S	-	5% CO2	37	N/S	8 days	Mass Loss, Cytotoxicity, Total Protein Assay, Alkaline Phosphatase Test, SEM, EDX, Confocal Microscopy	[32]
99.87% Mg	Model Saliva	N/S	Sand/Mold Cast, Extruded	-	20	Yes, N/S	164 hours	Mass Loss, Vickers Hardness, Tensile, Optical, SEM, EDX	[33]
99.9% Mg	Hanks (±Ca, Mg)	N/S	½ Oxidised	-	20	N/S	1080 hours	Mass Loss, SEM, XRD, Optical	[34]
99.9% Mg	Hanks	N/S	Na_2CO_3 / $NaHCO_3$	N/S	25	No (12)	75 days	Mass Loss, SEM, EDX, XRD	[35]
99.9% Mg	NaCl (±HEPES, $NaHCO_3$), Earles, MEM (±10% FBS)	HEPES	-	5% CO2	37	7.4, Yes	14 days	Mg Ion Measurement, EDX, Optical	[36]
99.9% Mg	Hanks	N/S	Heat Treated	N/S	20	N/S	625 hours	SEM, XRD, EDX,	[37]
99.9% Mg	0.6% NaCl	N/S	Rotating disk	N/S	37	No, 6	6 hours	PDP, OCP, EIS, Optical,	[38]
99.9% Mg	0.6% NaCl	Borate Buffer	Rotating Disk	N/S	37	Yes, 6.7, 7.6, 9.3	6 hours	EIS, OCP, XPS, Optical,	[39]
99.9% Mg	PSS	-	Foam	-	37	N/S	144 hours	Mass Loss, pH Recording, Compression, Optical, SEM, XRD	[40]
99.9% Mg	Basic SBF	HEPES	Solution Treated	-	37	Yes, 7.4, 9	5 days	Cytotoxicity, Wettability, Laser Profilometer, SEM, EDX,	[41]
99.9% Mg	Basic SBF	N/S	± Calcium Phosphate Coating	-	37	No, 7.4	21 days	Mass Loss, pH Recording, Atomic Absorption, SEM, EDX, XRD	[42]
99.9% Mg	Basic SBF	N/S	Annealed	-	37	No, 7.6	21 days	Mass Loss, pH recording Optical, SEM, EDX, XRD	[43]
99.9% Mg	Basic SBF (± Cl)	N/S	Solution / Heat	N/S	37	No	14 days	Mass Loss, pH Recording, Cytotoxicity, SEM, XRD, XPS	[44]

Alloy	Solution	Buffer	Coating/ Prework	Atmos-phere	Temp (°C)	pH Control	Time	Experiments	Ref.
			Treated						
99.92% Mg	0.9% NaCl	N/S	Ti Coating	-	25	N/S	-	PDP, SEM, EDX, XRD	[45]
99.947% Mg	Basic SBF	HEPES	-	N/S	37	7.4	N/S	PDP, EIS, SEM	[46]
99.946% Mg	Hanks	N/S	Impurity Levels	N/S	20	No, 7.4	180 hours	Hydrogen Evolution, ICP, SEM, EDX, XPS,	[47]
99.95% Mg	Hanks (±Ca, Mg)	N/S	-	-	37	N/S	4 days	Hydrogen Evolution, SEM, ICP	[48]
99.95% Mg	PBS, Dionized Water, McCoys Culture + 5% FBS	N/S	-	-	37	N/S	5 days	Mass Loss, OCP, Cytotoxicity, EIS, EDX, SEM,	[49]
99.95% Mg	1 % NaCl	Borate Buffer	-	N/S	25	Yes, 6.5, 9	168 hours	Mass Loss, pH Recording,	[50]
99.96% Mg	Basic SBF	HEPES	Solution / Heat Treated	N/S	37	No, 7.4	40 days	Mass Loss, pH Recording, SEM, EDX, XRD, ICP	[51]
99.96% Mg	Hanks	N/S	pH Test	-	37	5.5-8, yes	7 days	Hydrogen Evolution, Mg Ion Measurement, PDP, EIS, Optical, SEM,	[52]
99.96% Mg	Hanks	N/S	Conversion in HF	Air	37	N/S	2 days	EIS, PDP, SEM, AFM, XRD, XPS,	[53]
99.96% Mg	Hanks	Citric Acid Based	Steric Acid Coating	-	37	Yes, 7.4	24 hours, 80 days	PDP. EIS, Optical, SEM, FTIR, XRD	[54]
99.96% Mg	Hanks	Tris Buffer	± Sol-Gel Coating	-	37	Yes, 7.4	15 days	EIS, SEM, EDX, XRD,	[55]
99.96% Mg	Hanks	N/S	± Anodized	-	37	No, 6	30 days	PDP, EIS, Hydrogen Evolution, pH Recording, Optical	[56]
99.96% Mg	Basic SBF	N/S	Heat Treated	-	20	N/S	N/S	PDP, SEM, Optical, XRD, 3-Point-Bend,	[57]
99.967% Mg	Hanks	N/S	Impurity Levels	N/S	20	No, 7.4	180 hours	Hydrogen Evolution, ICP, SEM, EDX, XPS,	[47]
99.976% Mg	m-SBF	HEPES	-	-	37	No, 7.4	24 days	Mass Loss, PDP, EIS, SEM, EDX	[58]
99.98% Mg	5,10,35 g/L NaCl, PBS ±	N/S	-	-	N/S	N/S	5 mins	PDP, EIS, MircoCell, Optical, SEM, EDX	[59]

Alloy	Solution	Buffer	Coating/ Prework	Atmos-phere	Temp (°C)	pH Control	Time	Experiments	Ref.
	0.1/1/10 g/L BSA								
99.98% Mg	0.9% NaCl, PBS ± 1/10 g/L BSA	N/S	-	-	N/S	N/S	N/S	PDP, EIS, Optical, SEM, EDX, MicroCell	[60]
99.98% Mg	0.1M NaCl	-	-	-	N/S	7, No	22 days	Mass Loss, OCP, Linear Polarization, Optical, XRD	[61]
99.99% Mg	Basic SBF	N/S	Solution Treated	-	37	No, 7.44	3, 30 days	PDP, EIS, Mass Loss, Tensile, Compression, ICP-AES, SEM, EDX, XRD (In Vivo Also)	[22]
99.99% Mg	Hanks	N/S	-	-	37	Yes, 7.5	30 days	Mass Loss, Hydrogen Evolution, Kinetic Clotting Time Test, pH Recording, SEM, EDS (+ In Vivo)	[4]
99.993% Mg	Hanks	N/S	Impurity Levels	N/S	20	No, 7.4	180 hours	Hydrogen Evolution, ICP, SEM, EDX, XPS,	[47]
99.998% Mg	MEM	SB	-	5% CO2	37	No, 7.4	14 days	Mass Loss, PDP, SEM,	[62]
99.9999% Mg	1 % NaCl	Borate Buffer	-	N/S	25	Yes, 6.5, 9	168 hours	Mass Loss, pH Recording,	[50]
CP Mg	Hanks	N/S	± Anodized	-	37	N/S	30 days	Hydrogen Evolution	[63]
HP Mg	Hanks	N/S	± Anodized	-	37	N/S	30 days	Hydrogen Evolution	[63]
“Pure” Mg	Cell Culture + 10% FBS	In culture	-	N/S	37	7.4, Yes	3,6 days	Dendritic Cell Viability, Mg & Ca Ion Measurement, Mixed Leukocyte Reaction, Chemotaxis Assay	[64]
HP Mg	Hanks	N/S	Anodized, Static/Dynamic Flow	-	N/S	7, Yes	20 days	Mass Loss, EIS, Optical	[65]
				Ca Binary Alloys					
Mg-0.4Ca	MEM	SB	-	5% CO2	37	No, 7.4	14 days	Mass Loss, PDP, SEM,	[62]
Mg-0.4Ca	0.05 - 5% NaCl	TRIS	Extruded	-	21	Yes, 7.4	900 h	OCP, PDP, Hydrogen Evolution, Tensile	[66]
Mg-0.4Ca	5% NaCl	TRIS	Extruded	-	21	Yes, 7.4	900 h	OCP, PDP, Hydrogen Evolution, Tensile	[67]
Mg-0.4Ca	5% NaCl		½ Heat Treated	N/S	N/S	N/S	72 h	Mass Loss	[68]
Mg-0.4Ca	N/S	N/S	± Heat Treatment	-	N/S	N/S	72 hours	Mass Loss	[68]
Mg-0.5Ca	MEM + 15% FBS	N/S	-	5% CO2	37	No	8/17 days	Mass Loss, Cytotoxicity, Total Protein Assay, Alkaline Phosphatase Activity, SEM, EDX, Confocal	[32]
Mg-0.5Ca	MEM + 15%	N/S	-	5% CO2	37	N/S	8 days	Mass Loss, Cytotoxicity, Total Protein Assay,	[32]

Alloy	Solution	Buffer	Coating/ Prework	Atmos-phere	Temp (°C)	pH Control	Time	Experiments	Ref.
	FBS							Alkaline Phosphatase Test, SEM, EDX, Confocal Microscopy	
Mg-0.6Ca	Cell Culture + 10% FBS	In culture	-	N/S	37	7.4, Yes	3,6 days	Dendritic Cell Viability, Mg & Ca Ion Measurement, Mixed Leukocyte Reaction, Chemotaxis Assay	[64]
Mg-0.6Ca	Basic SBF	N/S	Heat Treated	-	20	N/S	N/S	PDP, SEM, Optical, XRD, 3-Point-Bend,	[57]
Mg-0.6Ca	Basic SBF	N/S	Heat Treated, Ion Implanted (Zinc)	-	20	N/S	N/S	PDP, SEM, EDX, Nano Indentation	[69]
Mg-0.6Ca	0.05 - 5% NaCl	TRIS	Extruded	-	21	Yes, 7.4	900 h	OCP, PDP, Hydrogen Evolution, Tensile	[66]
Mg-0.6Ca	5% NaCl	TRIS	Extruded	-	21	Yes, 7.4	900 h	OCP, PDP, Hydrogen Evolution, Tensile	[67]
Mg-0.8Ca	5% NaCl	TRIS	Extruded	-	21	Yes, 7.4	900 h	OCP, PDP, Hydrogen Evolution, Tensile	[67]
Mg-0.8Ca	Cell Culture + 10% FBS	In culture	-	N/S	37	7.4, Yes	3,6 days	Dendritic Cell Viability, Mg & Ca Ion Measurement, Mixed Leukocyte Reaction, Chemotaxis Assay	[64]
Mg-0.8Ca	5% NaCl		½ Heat Treated	N/S	N/S	N/S	72 h	Mass Loss	[68]
Mg-0.8Ca	Hanks	N/S	-	N/S	N/S	N/S	4 hours	Hydrogen Evolution, XRD,	[70]
Mg-0.8Ca	MEM + 15% FBS	N/S	-	5% CO2	37	N/S	8 days	Mass Loss, Cytotoxicity, Total Protein Assay, Alkaline Phosphatase Test, SEM, EDX, Confocal Microscopy	[32]
Mg-0.8Ca	0.05 - 5% NaCl	TRIS	Extruded	-	21	Yes, 7.4	900 h	OCP, PDP, Hydrogen Evolution, Tensile	[66]
Mg-0.8Ca	N/S	N/S	± Heat Treatment	-	N/S	N/S	72 hours	Mass Loss	[68]
Mg-0.8Ca	MEM + 15% FBS	N/S	-	5% CO2	37	No	8/17 days	Mass Loss, Cytotoxicity, Total Protein Assay, Alkaline Phosphatase Activity, SEM, EDX, Confocal	[32]
Mg-1Ca	5% NaCl	TRIS	Extruded	-	21	Yes, 7.4	900 h	OCP, PDP, Hydrogen Evolution, Tensile	[67]
Mg-1Ca	0.05 - 5% NaCl	TRIS	Extruded	-	21	Yes, 7.4	900 h	OCP, PDP, Hydrogen Evolution, Tensile	[66]
Mg-1Ca	Hanks, MEM, MEM+FBS	N/S	-	N/S	37	N/S	7 days	Linear Polarization, OCP, EIS, SEM, EDX,	[71]
Mg-1Ca	Basic SBF	N/S	Rolling / Extrusion	N/S	37	No, 7.4	250 hours	Hydrogen Evolution, pH Recording, PDP, Cytotoxicity, EDX, XRD, Optical, Tensile (In Vivo Concurrently)	[21]

Alloy	Solution	Buffer	Coating/ Prework	Atmos-phere	Temp (°C)	pH Control	Time	Experiments	Ref.
Mg-1Ca	0.1M NaCl	-	-	-	N/S	7, No	22 days	Mass Loss, OCP, Linear Polarization, Optical, XRD	[61]
Mg-1Ca	0.1 M NaCl		-	-	20	No	22 days	Mass Loss, OCP, PDP, XRD	[72]
Mg-1Ca	MEM	N/S	Powder Metallurgy	-	37	N/S	1,3,12, 72 hours	EIS, PDP, OCP, Tensile, Ion Measurement, Cytotoxicity, SEM, EDX, IXP-AES, XRD	[73]
Mg-1Ca	Cell Culture + 10% FBS	In culture	-	N/S	37	7.4, Yes	3,6 days	Dendritic Cell Viability, Mg & Ca Ion Measurement, Mixed Leukocyte Reaction, Chemotaxis Assay	[64]
Mg-1Ca	Hanks	N/S	Hot Extruded, Ca-P Coatings	-	20	No, 7.4	70, 250 hours	OCP, PDP, Hydrogen Evolution, SEM, XRD, EDX	[74]
Mg-1.2Ca	Cell Culture + 10% FBS	In culture	-	N/S	37	7.4, Yes	3,6 days	Dendritic Cell Viability, Mg & Ca Ion Measurement, Mixed Leukocyte Reaction, Chemotaxis Assay	[64]
Mg-1.2Ca	Basic SBF	N/S	Heat Treated	-	20	N/S	N/S	PDP, SEM, Optical, XRD, 3-Point-Bend,	[57]
Mg-1.2Ca	Basic SBF	N/S	Heat Treated, Ion Implanted (Zinc)	-	20	N/S	N/S	PDP, SEM, EDX, Nano Indentation	[69]
Mg-1.34Ca	MEM	SB	-	5% CO2	37	No, 7.4	14 days	Mass Loss, PDP, SEM,	[62]
Mg-1.5Ca	5% NaCl	TRIS	Extruded	-	21	Yes, 7.4	900 h	OCP, PDP, Hydrogen Evolution, Tensile	[67]
Mg-1.5Ca	0.05 - 5% NaCl	TRIS	Extruded	-	21	Yes, 7.4	900 h	OCP, PDP, Hydrogen Evolution, Tensile	[66]
Mg-1.6Ca	Basic SBF	N/S	Heat Treated, Ion Implanted (Zinc)	-	20	N/S	N/S	PDP, SEM, EDX, Nano Indentation	[69]
Mg-1.6Ca	Basic SBF	N/S	Heat Treated	-	20	N/S	N/S	PDP, SEM, Optical, XRD, 3-Point-Bend,	[57]
Mg-1.7Ca	5% NaCl	TRIS	Extruded	-	21	Yes, 7.4	900 h	OCP, PDP, Hydrogen Evolution, Tensile	[67]
Mg-1.7Ca	0.05 - 5% NaCl	TRIS	Extruded	-	21	Yes, 7.4	900 h	OCP, PDP, Hydrogen Evolution, Tensile	[66]
Mg-2Ca	0.05 - 5% NaCl	TRIS	Extruded	-	21	Yes, 7.4	900 h	OCP, PDP, Hydrogen Evolution, Tensile	[66]
Mg-2Ca	N/S	N/S	± Heat Treatment	-	N/S	N/S	72 hours	Mass Loss	[68]
Mg-2Ca	5% NaCl		½ Heat Treated	N/S	N/S	N/S	72 h	Mass Loss	[68]

Alloy	Solution	Buffer	Coating/ Prework	Atmos-phere	Temp (°C)	pH Control	Time	Experiments	Ref.
Mg-2Ca	Basic SBF	N/S	Heat Treated	-	20	N/S	N/S	PDP, SEM, Optical, XRD, 3-Point-Bend,	[57]
Mg-2Ca	Basic SBF	N/S	Rolling / Extrusion	N/S	37	No, 7.4	250 hours	Hydrogen Evolution, pH Recording, PDP, Cytotoxicity, EDX, XRD, Optical, Tensile (In Vivo Concurrently)	[21]
Mg-2Ca	5% NaCl	TRIS	Extruded	-	21	Yes, 7.4	900 h	OCP, PDP, Hydrogen Evolution, Tensile	[67]
Mg-2.5Ca	5% NaCl	TRIS	Extruded	-	21	Yes, 7.4	900 h	OCP, PDP, Hydrogen Evolution, Tensile	[67]
Mg-2.5Ca	0.05 - 5% NaCl	TRIS	Extruded	-	21	Yes, 7.4	900 h	OCP, PDP, Hydrogen Evolution, Tensile	[66]
Mg-3Ca	0.05 - 5% NaCl	TRIS	Extruded	-	21	Yes, 7.4	900 h	OCP, PDP, Hydrogen Evolution, Tensile	[66]
Mg-3Ca	Basic SBF	N/S	Rolling / Extrusion	N/S	37	No, 7.4	250 hours	Hydrogen Evolution, pH Recording, PDP, Cytotoxicity, EDX, XRD, Optical, Tensile (In Vivo Concurrently)	[21]
Mg-3Ca	0.9% NaCl	N/S	Surface Roughness Modifications	-	20	Yes (flow)	16 days	Mass Loss, Hydrogen Evolution,	[75]
Mg-3Ca	5% NaCl	TRIS	Extruded	-	21	Yes, 7.4	900 h	OCP, PDP, Hydrogen Evolution, Tensile	[67]
Mg-4Ca	5% NaCl	TRIS	Extruded	-	21	Yes, 7.4	900 h	OCP, PDP, Hydrogen Evolution, Tensile	[67]
Mg-4Ca	0.05 - 5% NaCl	TRIS	Extruded	-	21	Yes, 7.4	900 h	OCP, PDP, Hydrogen Evolution, Tensile	[66]
Mg-5Ca	Model Saliva	N/S	Sand/Mold Cast, Extruded	-	20	Yes, N/S	164 hours	Mass Loss, Vickers Hardness, Tensile, Optical, SEM, EDX	[33]
Mg-5Ca	MEM	N/S	Powder Metallurgy	-	37	N/S	1,3,12, 72 hours	EIS, PDP, OCP, Tensile, Ion Measurement, Cytotoxicity, SEM, EDX, IXP-AES, XRD	[73]
Mg-5Ca	MEM	SB	-	5% CO2	37	No, 7.4	14 days	Mass Loss, PDP, SEM,	[62]
Mg-5Ca	Hanks	N/S	-	N/S	N/S	N/S	4 hours	Hydrogen Evolution, XRD,	[70]
Mg-10Ca	MEM	N/S	Powder Metallurgy	-	37	N/S	1,3,12, 72 hours	EIS, PDP, OCP, Tensile, Ion Measurement, Cytotoxicity, SEM, EDX, ICP-AES, XRD	[73]
Mg-16.2Ca	MEM	SB	-	5% CO2	37	No, 7.4	14 days	Mass Loss, PDP, SEM,	[62]
Zn Binary Alloys									
Mg-1Zn	Hanks	N/S	± Anodized	-	37	N/S	30 days	Hydrogen Evolution	[63]
Mg-1Zn	0.1 M NaCl		-	-	20	No	22 days	Mass Loss, OCP, PDP, XRD	[72]
Mg-1Zn	0.1M NaCl	-	-	-	N/S	7, No	22 days	Mass Loss, OCP, Linear Polarization, Optical, XRD	[61]
Mg-1Zn	Hanks, Basic SBF		-	N/S	37	N/S	20 days	H_2 Evolution, Mg Ion Concentration, PDP, Tensile, Cytotoxicity, Hemolysis, Platlet Adhesion	[76]

Alloy	Solution	Buffer	Coating/ Prework	Atmos-phere	Temp (°C)	pH Control	Time	Experiments	Ref.
Mg-3Zn	MEM	SB	-	5% CO2	37	No, 7.4	14 days	Mass Loss, PDP, SEM,	[62]
Mg-6Zn	Basic SBF	-	-	-	37	No, 7.4	3,30 days	PDP, EIS, Hemolysis, XRD, EDX, SEM	[77]
Mg-6Zn	Basic SBF	N/S	Solution Treated	-	37	No, 7.44	3, 30 days	PDP, EIS, Mass Loss, Tensile, Compression, ICP-AES, SEM, EDX, XRD (In Vivo Also)	[22]
Mg-6.2Zn	MEM	SB	-	5% CO2	37	No, 7.4	14 days	Mass Loss, PDP, SEM,	[62]
Mg-10Zn	MEM	SB	-	5% CO2	37	No, 7.4	14 days	Mass Loss, PDP, SEM,	[62]
Al, Mn, Si, Zr, Li Binary Alloys									
Mg-3Al	MEM	SB	-	5% CO2	37	No, 7.4	14 days	Mass Loss, PDP, SEM,	[62]
Mg-1Mn	Hanks, Basic SBF		-	N/S	37	N/S	20 days	H_2 Evolution, Mg Ion Concentration, PDP, Tensile, Cytotoxicity, Hemolysis, Platlet Adhesion	[76]
Mg1-Zr	Hanks, Basic SBF		-	N/S	37	N/S	20 days	H_2 Evolution, Mg Ion Concentration, PDP, Tensile, Cytotoxicity, Hemolysis, Platlet Adhesion	[76]
Mg-1Si	Hanks, Basic SBF		-	N/S	37	N/S	20 days	H_2 Evolution, Mg Ion Concentration, PDP, Tensile, Cytotoxicity, Hemolysis, Platlet Adhesion	[76]
Mg-12Li	0.1 M NaCl		-	-	20	No	22 days	Mass Loss, OCP, PDP, XRD	[72]
Mg-12Li	0.1M NaCl	-	-	-	N/S	7, No	22 days	Mass Loss, OCP, Linear Polarization, Optical, XRD	[61]
RE Binary Alloys									
Mg-4Ce	MEM	SB	-	5% CO2	37	No, 7.4	14 days	Mass Loss, PDP, SEM,	[62]
Mg-0.5Y	MEM	SB	-	5% CO2	37	No, 7.4	14 days	Mass Loss, PDP, SEM,	[62]
Mg-0.1Sr	MEM	SB	-	5% CO2	37	No, 7.4	14 days	Mass Loss, PDP, SEM,	[62]
Mg-1La	MEM	SB	-	5% CO2	37	No, 7.4	14 days	Mass Loss, PDP, SEM,	[62]
Mg-2Y	MEM	SB	-	5% CO2	37	No, 7.4	14 days	Mass Loss, PDP, SEM,	[62]
Mg-4La	MEM	SB	-	5% CO2	37	No, 7.4	14 days	Mass Loss, PDP, SEM,	[62]
Mg-4Nd	MEM	SB	-	5% CO2	37	No, 7.4	14 days	Mass Loss, PDP, SEM,	[62]
Mg-8Y	3.5% NaCl	-	Zone Solidified	-	N/S	N/S	10 Min	PDP, Vickers Hardness, Optical, SEM, EDX, XFS	[78]
Mg-1Nd	MEM	SB	-	5% CO2	37	No, 7.4	14 days	Mass Loss, PDP, SEM,	[62]
Mg-0.05Sn	MEM	SB	-	5% CO2	37	No, 7.4	14 days	Mass Loss, PDP, SEM,	[62]
Mg-1Ce	MEM	SB	-	5% CO2	37	No, 7.4	14 days	Mass Loss, PDP, SEM,	[62]
Mg-1Sn	Hanks, Basic SBF		-	N/S	37	N/S	20 days	H_2 Evolution, Mg Ion Concentration, PDP, Tensile, Cytotoxicity, Hemolysis, Platlet Adhesion	[76]

Alloy	Solution	Buffer	Coating/ Prework	Atmos-phere	Temp (°C)	pH Control	Time	Experiments	Ref.
Mg-1Y	Hanks, Basic SBF		-	N/S	37	N/S	20 days	H_2 Evolution, Mg Ion Concentration, PDP, Tensile, Cytotoxicity, Hemolysis, Platlet Adhesion	[76]
Mg-2Gd	1% NaCl	N/S	Heat Treated	N/S	22	No, 6.5	N/S	Hydrogen Evolution, Mass Loss, Optical, SEM, EDX, TEM, XRD, Tensile, Compression	[79]
Mg-5Gd	1% NaCl	N/S	Heat Treated	N/S	22	No, 6.5	N/S	Hydrogen Evolution, Mass Loss, Optical, SEM, EDX, TEM, XRD, Tensile, Compression	[79]
Mg-10Gd	1% NaCl	N/S	Heat Treated	N/S	22	No, 6.5	N/S	Hydrogen Evolution, Mass Loss, Optical, SEM, EDX, TEM, XRD, Tensile, Compression	[79]
Mg-15Gd	1% NaCl	N/S	Heat Treated	N/S	22	No, 6.5	N/S	Hydrogen Evolution, Mass Loss, Optical, SEM, EDX, TEM, XRD, Tensile, Compression	[79]
AZ Alloys									
AZ21	MEM + 15% FBS	N/S	-	5% CO2	37	N/S	8 days	Mass Loss, Cytotoxicity, Total Protein Assay, Alkaline Phosphatase Test, SEM, EDX, Confocal Microscopy	[32]
AZ21	MEM + 15% FBS	N/S	-	5% CO2	37	No	8/17 days	Mass Loss, Cytotoxicity, Total Protein Assay, Alkaline Phosphatase Activity, SEM, EDX, Confocal	[32]
AZ31B	Basic SBF	N/S	Fluoride Treatment	5% CO2	37	7.4, Yes	168 hours	PDP, pH Recording, Three-Point Bend, SEM, EDX, XRD	[80]
AZ31	Basic SBF	N/S	Ca-P Coating, Shaken	-	37	7.3, Yes	3,5,7,11, 15 days	Mass Loss, SEM, EDX, XRD	[81]
AZ31	0.1M NaCl	-	-	-	N/S	7, No	22 days	Mass Loss, OCP, Linear Polarization, Optical, XRD	[61]
AZ31	Hanks (±Ca, Mg)	N/S	½ Oxidised	-	20	N/S	1080 hours	Mass Loss, SEM, XRD, Optical	[34]
AZ31	3% NaCl	N/S	Calcium Phosphate Coating	-	37	N/S	15 days	Mass Loss, Tensile, SEM, EDX, XRD, FTIR	[82]
AZ31	Hanks (±Ca, Mg)	N/S	½ Oxidised	-	20	N/S	1080 h	Mass Loss, SEM, XRD,	[18]
AZ31	8 g/l NaCl, PBS	N/S	Heat Treated / Rolled / ECAP	-	20	N/S	6 Days	OCP, PDP, EIS, SEM, EDX, FTIR, Grain Size	[83]
AZ31	0.1 M NaCl		-	-	20	No	22 days	Mass Loss, OCP, PDP, XRD	[72]

Alloy	Solution	Buffer	Coating/ Prework	Atmos-phere	Temp (°C)	pH Control	Time	Experiments	Ref.
AZ31	Hanks, MEM, MEM+FBS	N/S	-	N/S	37	N/S	7 days	Linear Polarization, OCP, EIS, SEM, EDX,	[71]
AZ31	1 % NaCl	Borate Buffer	-	N/S	25	Yes, 6.5, 9	168 hours	Mass Loss, pH Recording,	[50]
AZ31	MEM	SB	-	5% CO2	37	No, 7.4	14 days	Mass Loss, PDP, SEM,	[62]
AZ31	0.9% NaCl, PBS ± 1/10 g/L BSA	N/S	-	-	N/S	N/S	N/S	PDP, EIS, Optical, SEM, EDX, MicroCell	[60]
AZ31	5,10,35 g/L NaCl, PBS ± 0.1/1/10 g/L BSA	N/S	-	-	N/S	N/S	5 mins	PDP, EIS, MircoCell, Optical, SEM, EDX	[59]
AZ31	Hanks	N/S	-	-	37	Yes, 7.5	30 days	Mass Loss, Hydrogen Evolution, SEM, EDS (+ In Vivo)	[6]
AZ31	0.5-3.5% NaCl, PBS (±0-10 g/l BSA), McCoys Media	HEPES	-	-	20	N/S	N/S	PDP, EIS, MicroCell,	[84]
AZ31	Basic SBF	N/S	-	-	37	Yes, N/S	72 hours	EIS, Optical, SEM, EDX, XPS	[85]
AZ31	Hanks	N/S	Hot Extruded, Ca-P Coatings	-	20	No, 7.4	70, 250 hours	OCP, PDP, Hydrogen Evolution, SEM, XRD, EDX	[74]
AZ31	0.9% NaCl	N/S	Macro-Arc Oxidation	-	20/37	N/S	90 mins	OCP, PDP, Optical,	[86]
AZ31	m-SBF	HEPES	-	-	37	No, 7.4	24 days	Mass Loss, PDP, EIS, SEM, EDX	[58]
AZ31	Hanks	N/S	Squeeze Cast, Hot Rolled, ECAP	-	N/S	7, Yes	20 days	Mass Loss, EIS, Fatigue Test, SEM, TEM, Optical	[87]
AZ31	Hanks	N/S	Squeeze Cast, Hot Rolled, ECAP	-	N/S	7, Yes	20 Days	Mass Loss, Optical, TEM	[88]
AZ31	Hanks	N/S	Anodized, Static/Dynamic Flow	-	N/S	7, Yes	20 days	Mass Loss, EIS, Optical	[65]

Alloy	Solution	Buffer	Coating/ Prework	Atmos-phere	Temp (°C)	pH Control	Time	Experiments	Ref.
AZ61	m-SBF	HEPES	-	-	37	No, 7.4	24 days	Mass Loss, PDP, EIS, SEM, EDX	[58]
AZ61	Hanks (±Ca, Mg)	N/S	½ Oxidised	-	20	N/S	1080 hours	Mass Loss, SEM, XRD, Optical	[34]
AZ61	Hanks (±Ca, Mg)	N/S	½ Oxidised	-	20	N/S	1080 h	Mass Loss, SEM, XRD,	[18]
AZ61+0.4Ca	Basic SBF	HEPES	-	N/S	37	7.4	N/S	PDP, EIS, Slow Strain Rate Test, SEM, EDX,	[89]
AZ63	0.9% NaCl, Thyrode's	N/S	Solution / Heat Treated	N/S	37	Yes, 7.2	14 days	Mass Loss, OCP, pH Recording, Optical, Atomic Absorption,	[90]
AZ91	0.9% NaCl	N/S	Macro-Arc Oxidation	-	20/37	N/S	90 mins	OCP, PDP, Optical,	[86]
AZ91D	Basic SBF	N/S	HA Coating,	-	37	7.4, No	48 hours	PDP, EIS, SEM, EDX, XRD,	[91]
AZ91	Model Saliva	N/S	Sand/Mold Cast, Extruded	-	20	Yes, N/S	164 hours	Mass Loss, Vickers Hardness, Tensile, Optical, SEM, EDX	[33]
AZ91	m-SBF	HEPES	-	-	37	No, 7.4	24 days	Mass Loss, PDP, EIS, SEM, EDX	[58]
AZ91	MEM	SB	-	5% CO2	37	No, 7.4	14 days	Mass Loss, PDP, SEM,	[62]
AZ91	Hanks	N/S	± Anodized	-	37	N/S	30 days	Hydrogen Evolution	[63]
AZ91	Hanks	N/S	± Anodized	-	37	No, 6	30 days	PDP, EIS, Hydrogen Evolution, pH Recording, Optical	[56]
AZ91D	Basic SBF	N/S	Heat Treatment	-	37	7.3-7.4	168 hours	Mass Loss, PDP, SEM, EDX, Optical	[92]
AZ91	Basic SBF (± 1 g/l BSA)	HEPES	-	N/S	37	Yes, 5, 7.2	7 days	Mass Loss, OCP, PDP, EIS, SEM, EDX, FTIR	[93]
AZ91	Hanks	HEPES	Static/Dynamic Environment	N/S	37	Yes, 7.3-7.5	168 hours	Atomic Absorption, SEM, EDX, XRD, EPMA, FTIR, Optical	[94]
AZ91	Basic SBF	HEPES	Sand Cast	N/S	37	7.4	N/S	PDP, Slow Strain Rate Test, ICPAES, SEM	[95]
AZ91	Hanks, MEM, MEM+FBS	N/S	-	N/S	37	N/S	7 days	Linear Polarization, OCP, EIS, SEM, EDX,	[71]
AZ91	Hanks (±Ca, Mg)	N/S	½ Oxidised	-	20	N/S	1080 hours	Mass Loss, SEM, XRD, Optical	[34]
AZ91	Basic SBF	N/S	-	Air	37	N/S	35 hours	EIS, PDP, SEM	[96]

Alloy	Solution	Buffer	Coating/ Prework	Atmos-phere	Temp (°C)	pH Control	Time	Experiments	Ref.
AZ91	0.9% NaCl, Hanks, ±FBS	N/S	-	N/S	37	Yes	N/S	Linear Polarization, PDP, EIS,	[97]
AZ91D	Substitute Sea Water	-	-	Air	20	-	240 hours	PDP, SEM, EDX (In Vivo Concurrently)	[12]
AZ91	Basic SBF	-	Polymer Coating	N/S	37	No, 7.4	2 months	PDP, Mass Loss, Cytotoxicity, Compression Tests, pH Measurement, ICPMS, SEM	[9]
AZ91	Basic SBF	N/S	Zr Coating	-	N/S	N/S	N/S	PDP, EIS, SEM, XRD, XPS	[98]
AZ91	Basic SBF	N/S	Al_2O_3 Coating	-	N/S	N/S	18 hours	PDP. EIS, XPS, SEM	[99]
AZ91	Basic SBF	N/S	-	-	N/S	N/S	1,4,7 days	Mass Loss, Hydrogen Evolution, OCP, EIS, Optical, SEM, EDX, FTIR, XPS	[100]
AZ91	5% NaCl		½ Heat Treated	N/S	N/S	N/S	72 h	Mass Loss, Mechanical	[68]
AZ91	N/S	N/S	± Heat Treatment	-	N/S	N/S	72 hours	Mass Loss	[68]
AZ91	Hanks (±Ca, Mg)	N/S	½ Oxidised	-	20	N/S	1080 h	Mass Loss, SEM, XRD,	[18]
AZ91	1 % NaCl	Borate Buffer	-	N/S	25	Yes, 6.5, 9	168 hours	Mass Loss, pH Recording,	[50]
AZ91	Basic SBF	HEPES	Sand/Die Cast	N/S	37	7.4	N/S	PDP, EIS, SEM	[46]
AZ91	Basic SBF	HEPES	-	N/S	37	7.4	N/S	PDP, EIS, Slow Strain Rate Test, SEM, EDX,	[89]
AZ91+1Ca	Basic SBF	HEPES	-	N/S	37	7.4	N/S	PDP, EIS, Slow Strain Rate Test, SEM, EDX,	[89]
AZ91 + 20% HA	Sea Water, MEM (±10% FBS)	N/S	-	N/S	37	N/S	24, 72 hours	PDP, EIS, Mass Loss, Vickers Hardness, Nano Indentation, Cytotoxicity, Optical, SEM, EDX, XRD	[101]
RE Ternary Alloys (LAE442, WE43, and others)									
LAE442	Substitute Sea Water	-	-	Air	20	-	240 hours	PDP, SEM, EDX (In Vivo Concurrently)	[12]
LAE442	0.5-3.5% NaCl, PBS (±0-10 g/l BSA), McCoys Media	HEPES	-	-	20	N/S	N/S	PDP, EIS, MicroCell,	[84]
LAE442	0.9% NaCl, PBS	N/S	-	-	N/S	N/S	N/S	PDP, EIS, Optical, SEM, EDX, MicroCell	[60]

Alloy	Solution	Buffer	Coating/ Prework	Atmos-phere	Temp (°C)	pH Control	Time	Experiments	Ref.
	± 1/10 g/L BSA								
LAE442	5,10,35 g/L NaCl, PBS ± 0.1/1/10 g/L BSA	N/S	-	-	N/S	N/S	5 mins	PDP, EIS, MircoCell, Optical, SEM, EDX	[59]
WE43	NaCl (±$CaCl_2$, K_2HPO_4), m-SBF (± 40g/L BSA)	HEPES	-	-	20 / 37	No, 7.4	2 weeks	PDP, EIS, OCP,	[102]
WE43	NaCl (±$CaCl_2$, K_2HPO_4), m-SBF (± 40g/L BSA)	HEPES	Extrusion,	-	37	Yes, 7.4	2-5 days	SEM, OPTICAL, EDX, XRD, FTIR	[103]
WE43	SBF with 3 Cell Lines	N/S	-	N/S	37	N/S	48 hours	Cell Study	[104]
WE43	Hanks	HEPES	Static/Dynamic Environment	N/S	37	Yes, 7.3-7.5	168 hours	Atomic Absorption, SEM, EDX, XRD, EPMA, FTIR, Optical	[94]
WE43	3% NaCl, Basic SBF, Artificial Plasma	N/S	Extruded, ± Heat Treated	N/S	20	No, 6, 7.4	24 hours	EIS, Tensile, SEM, Optical, EDX, AES	[105]
WE43	0.9% NaCl	N/S	Macro-Arc Oxidation	-	20/37	N/S	90 mins	OCP, PDP, Optical,	[86]
ZE41	MEM	SB	-	5% CO2	37	No, 7.4	14 days	Mass Loss, PDP, SEM,	[62]
ZE41	Hanks	N/S	± Anodized	-	37	N/S	30 days	Hydrogen Evolution	[63]
AE44	MEM	SB	-	5% CO2	37	No, 7.4	14 days	Mass Loss, PDP, SEM,	[62]
ZW21	Basic SBF		-	N/S	20	Yes, below 8	7 Days	Hydrogen Evolution, Tensile Test,	[106]
WZ21	Basic SBF		-	N/S	20	Yes, below 8	7 Days	Hydrogen Evolution, Tensile Test,	[106]
ZX152	Hanks (±Ca, Mg)	N/S	-	-	37	N/S	4 days	Hydrogen Evolution, SEM, ICP	[48]
AX53	0.9 % NaCl (±0.7 g/l $NaHCO_3$),	N/S	-	-	20	N/S	6, 24 hours	PSP, Mass Loss, SEM, EDX, XRD	[107]

Alloy	Solution	Buffer	Coating/ Prework	Atmos-phere	Temp (°C)	pH Control	Time	Experiments	Ref.
	Hanks								
Mg-4Y-2Nd	Basic SBF, Artificial Plasma	Tris Buffer	± Anodized	-	37	No	24 hours	EIS, pH Recording, SEM, AES, Optical,	[108]
				Mg-Mn-Zn , Mg-Ca-Zn, AM Alloys					
Mg-0.4Ca-3Zn	MEM	SB	-	5% CO2	37	No, 7.4	14 days	Mass Loss, PDP, SEM,	[62]
Mg-0.4Ca-10Zn	MEM	SB	-	5% CO2	37	No, 7.4	14 days	Mass Loss, PDP, SEM,	[62]
Mg-Zn-Ca (N/S)	Basic SBF	N/S	Ca-Deficient Ha Coating	-	37	N/S	1 hour	PDP, SEM, EDX, Slow Strain Rate Test, XRD	[109]
Mg-1Zn-1Mn	Basic SBF	-	-	-	37	-	-	PDP, Cytotoxicity, Hemolysis, Tensile, SEM, Optical	[110]
Mg-2Zn-0.2Mn	Hanks	N/S	± Anodized	-	37	N/S	30 days	Hydrogen Evolution	[63]
Mg-2Zn-1Mn	Basic SBF	-	-	-	37	-	-	PDP, Cytotoxicity, Hemolysis, Tensile, SEM, Optical	[110]
Mg-2Zn-1Mn	Hanks	N/S	Extruded	N/S	37	No, 7.4	24 hours	PDP, pH Recording, OCP, SEM, XRD, XPS, EDX	[111]
Mg-3Zn-1Mn	Basic SBF	-	-	-	37	-	-	PDP, Cytotoxicity, Hemolysis, Tensile, SEM, Optical	[110]
Mg-1Mn-1Zn	Hanks, Simulated Blood Plasma	N/S	-	Air	N/S	N/S, No	288 hours	Mass Loss, OCP, pH Recording, PDP, SEM, EDX, XRD	[112]
Mg-1.2Mn-1Zn	PRMI1640 Medium	N/S	Ca-P Coating	5% CO2	37	N/S	5 days	Cytotoxicity, SEM, XRD, XPS, EDX	[28]
Mg-1.2Mn-1Zn	PRMI1640 Media	N/S	Ca-P Coating	5% CO2	37	Yes, 7.4	5 days	Cytotoxicity, Cell Count, SEM, XRD, XPS	[26]
Mg-1.2Mn-1Zn	0.9% NaCl	N/S	Phosphate Coating	-	37	No, 7.4	1,2,4,9 days	PDP, SEM, EDX, SAXS, XRD, XPS	[113]
AM50	0.9% NaCl, Hanks, ±FBS	N/S	-	N/S	37	Yes	N/S	Linear Polarization, PDP, EIS,	[97]
AM50	Model Saliva	N/S	Sand/Mold Cast,	-	20	Yes, N/S	164 hours	Mass Loss, Vickers Hardness, Tensile, Optical, SEM, EDX	[33]

Alloy	Solution	Buffer	Coating/ Prework	Atmos-phere	Temp (°C)	pH Control	Time	Experiments	Ref.
			Extruded						
AM60	Hanks	HEPES	Static/Dynamic Environment	N/S	37	Yes, 7.3-7.5	168 hours	Atomic Absorption, SEM, EDX, XRD, EPMA, FTIR, Optical	[94]
Other Ternary, Quad, and Bulk metallic glass									
Mg-7Al-0.05Ti	MEM	SB	-	5% CO2	37	No, 7.4	14 days	Mass Loss, PDP, SEM,	[62]
Mg-2Zn-1Mn-0.4Y	Hanks	N/S	Extruded	N/S	37	No, 7.4	24 hours	PDP, pH Recording, OCP, SEM, XRD, XPS, EDX	[111]
Mg-2Zn-1Mn-0.8Y	Hanks	N/S	Extruded	N/S	37	No, 7.4	24 hours	PDP, pH Recording, OCP, SEM, XRD, XPS, EDX	[111]
Mg-2Zn-1Mn-1.5Y	Hanks	N/S	Extruded	N/S	37	No, 7.4	24 hours	PDP, pH Recording, OCP, SEM, XRD, XPS, EDX	[111]
Mg-2Zn-1Mn-0.3Ca	Hanks	-	-	-	37	N/S	15 mins	Volume Fraction, PDP, Tensile, SEM, EDX, ICP-AES	[114]
Mg-2Zn-1Mn-0.5Ca	Hanks	-	-	-	37	N/S	15 mins	Volume Fraction, PDP, Tensile, SEM, EDX, ICP-AES	[114]
Mg-1.5Zn-1Mn-1Ca	Hanks	-	-	-	37	N/S	15 mins	Volume Fraction, PDP, Tensile, SEM, EDX, ICP-AES	[114]
Mg Bulk Metallic Glass	Basic SBF,			5% CO2	37	N/S	30 days	pH Change, PDP, Cytotoxicty, SEM, XPS Compression, Cell Test, Optical	[115]
Mg Bulk Metallic Glasses	PBS	N/S	-	Aireated wtih O2/N2	37	7.4	N/S	PDP, OCP, SEM, EDX, XRD, Optical,	[116]
Mg Bulk Metallic Glass	Basic SBF	N/S	Bulk Metallic Glass	-	N/S	7.3-7.4, No	4 days	Hydrogen Evolution, PDP, EIS, OCP, SEM, EDX, XRD	[117]

N/S indicates values were not stated.

APPENDIX D : ELEMENTAL COMPOSITION OF INVESTIGATED ALLOYS

Alloy Designation	Mg	Ca	Al	Zn	Mn	Zr	Fe	Sr	Cu	Ni	Be	Cr	Pb	Sn
Pure Mg	Balance	< 0.002	< 0.005	< 0.005	< 0.002	< 0.002	< 0.001	< 0.001	< 0.002	< 0.001	< 0.0001	< 0.001	< 0.002	< 0.002
Mg-0.4Ca	Balance	0.42					< 0.002							
Mg-0.8Ca	Balance	0.84					< 0.002							
Mg-1.34Ca	Balance	1.5					< 0.002							
Mg-5Ca	Balance	4.55					< 0.002							
Mg-10Ca	Balance	10.2					< 0.002							
Mg-16.2Ca	Balance	16.2					< 0.002							
Mg-28Ca	Balance	28					< 0.005							
Mg-1Zn	Balance			0.99			< 0.002							
Mg-3Zn	Balance			2.87			< 0.001							
Mg-6.2Zn	Balance			5.96			< 0.005							
Mg-10Zn	Balance			9.68			< 0.009							
Mg-20Zn	Balance			20.03			< 0.009							
Mg-0.5Mn	Balance				0.61		0.012							
Mg-1Mn	Balance				1.13		0.015							
Mg-2.2Mn	Balance				2.31		0.016							
Mg-5Mn	Balance				4.97		0.004							
Mg-10Mn	Balance				8.75		0.002							

Alloy Designation	Mg	Ca	Al	Zn	Mn	Zr	Fe	Sr	Cu	Ni	Be	Cr	Pb	Sn
Mg-0.3Zr	Balance					0.32	< 0.002							
Mg-0.57Zr	Balance					0.58	< 0.001							
Mg-1Zr	Balance					0.97	0.004							
Mg-2Zr	Balance					1.73	0.009							
Mg-0.4Ca-3Zn	Balance	0.41	2.95				< 0.002							
Mg-0.4Ca-6.2Zn	Balance	0.42	9.87				< 0.002							
Mg-1.34Ca-3Zn	Balance	1.25	3.12				< 0.002							
Mg-1.34Ca-6.2Zn	Balance	1.38	6.2				< 0.002							
Mg-5Ca-3Zn	Balance	5.31	2.99				< 0.001							
Mg-5Ca-6.2Zn	Balance	5.17	6.15				< 0.002							
Master Alloys / Elements														
Pure Zn				Balance			< 0.001							
Mg-33.3Zr	Balance					35.42	0.015							
Mg-30Ca	Balance	29.97	0.005	< 0.005	< 0.002	< 0.002	< 0.005	0.022	< 0.002	< 0.001	< 0.0001	< 0.001	< 0.002	< 0.002

Values reported are weight %.

APPENDIX E : PREPARATION OF KIRKLAND'S BIOCORROSION MEDIUM

1. Cleaning of glassware
    a. Use only new glassware and keep securely stored solely for production of KBM.
    b. All bottles, flasks, beakers and other glassware should be cleaned with distilled water 3-4 times. Following this they should be washed with high purity ethanol (99.8%) 2-3 times.
    c. If required, immerse bottles in dilute HCl solution for 4-6 hours. Remove from solution and repeat above steps.
2. Creation of media
    a. All dissolution of chemicals should take place in a flow hood to minimise dust pickup.
    b. Pour 900 ml of distilled water into a 1 L beaker. Place a clean magnetic stirrer bar in the beaker and place on a heated magnetic plate.
    c. Adjust heated plate so temperature of bulk solution is 37 °C ± 1.
    d. Add the chemicals given in Table E-1 one-by-one in the order provided. Ensure each is completely dissolved before adding the next.
    e. Buffer choice depends on the intended experimental atmosphere. Both may be added if desired. Add the buffer (Table E-2) in 1 gram amounts to minimise localised changes in pH.
    f. Finally, add distilled water to the beaker until 1 L is reached (typically 95 ml).
3. pH adjustment for HEPES
    a. Before any pH measurement, calibrate the pH meter to a minimum of two points (*e.g.* 7 and 10).
    b. Re-check the temperature of the solution to ensure it is 37 °C ± 1.
    c. Measure the pH of the KBM and add 1 M NaOH in 0.25 mL portions until a pH of 7.4 is reached.
4. pH adjustment for $NaHCO_3$
    a. The concentration of CO_2 in the incubator will determine the pH of the media.
    b. Adjust the volume % CO_2 of the incubator to 5% and allow solution to stabilise over 4 hours. Measure the pH of the media and raise CO_2 level if pH is too high (and lower CO_2 level if pH is too low).
    c. Let settle again for 4 hours and measure pH again. Typically 4.7%-5.1% CO_2 results in a pH of 7.4.

5. Storage
    a. After pH adjustment decant the KBM into a 1 L Schott bottle or similar.
    b. Store in a refrigerator at 5-10 °C.
    c. Use within 2 weeks of creation.

Table 10-3 : Components and concentrations of KBM.

Compound	**Amount (g/L)**
NaCl	5.4
D-Glucose ($C_6H_{12}O_6$)	0.9
KCl	0.38
$CaCl_2$	0.28
Na_2HPO_4 (Anhydrous)	0.122
$MgSO_4$	0.06
Phenol Red ($C_{19}H_{14}O_5S$)	0.011

Table 10-4 : Buffers and concentrations for addition to KBM.

Buffer	**Amount (g/L)**
SB ($NaHCO_3$)	2.2
HEPES ($C_8H_{18}N_2O_4S$)	5.96

APPENDIX F : COMMON EXPERIMENTAL TECHNIQUES TO DETERMINE PROTEIN ADHESION

Test	Use	Procedure	Comments
X-ray photoelectron spectroscopy (XPS)	Elemental composition	Surface is irradiated by beam of monochromatic x-rays, released photoelectrons are captured	• Widely used • Non-destructive • Not useful for multi-protein studies
Secondary ion mass spectroscopy (SIMS)	Elemental & molecular composition	Bombardment of surface with focused beam of ions/atoms resulting in emission of secondary particles	• Widely used • Good protein resolution
Time-of-flight secondary ion mass spectroscopy (ToF-SIMS)	Elemental & molecular composition	Similar to SIMS, secondary ions are accelerated through field-free drift region, which separates heavy/light ions	• Greater resolution • Increased sensitivity
Fourier transform infrared spectroscopy (FTIR)	Chemical bonds & conformation	IR beam is reflected from a surface and spectrum is developed from IR absorbance at different frequencies	• Very common • Limited use in multi-protein studies (complicated spectra) • Quick
Attenuated total frequency (ATR-FTIR)	Chemical bonds & conformation	Similar to FTIR, total internal reflection of IR beam back into detector along region of contact with sample surface	• Reduced surface area required
Solute-depletion test	Amount adsorbed	Changes in bulk concentration of protein in a solution is measured over time	• Assumes all protein loss is due to material attachment
Protein labelling, staining & florescence	Amount adsorbed and areas	Proteins labelled with fluorescent or radioactive probes, concentration of adsorbed protein deterred on surface	• Easy to perform
Immunoassay (eg. ELISA)	Presence and bioactivity	An antibody is directed against a protein, bonding to specific portions of the target protein	• Widely used
Ellipsometry	Layer thickness	Polarised light is directed at surface at an angle, then reflected back to detector. Changes in reflected light provide information on interface	• Very common • Nanometre resolution
Surface plasmon resonance (SPR) & Neutron reflectivity	Layer thickness	Similar to ellipsometry, but uses excitation of surface plasmons and beam of neutrons, respectively.	• More complicated • NR is not widely used due to equipment and potential radiation problems

(NR)			
Quartz crystal microbalance (QCM)	Protein adsorption over time	Measure change in frequency for coated quartz crystal as a solution comes into contact	• Real-time measurement of protein attachment • Quantitative values obtained • Easy to setup
Matrix-assisted laser / desorption / ionisation time-of-flight (MALDI-ToF)	Protein identification	Matrix molecules are added to surface prior to irradiation with pulse laser.	• Difficult sample preparation • Matrix fluid required • Very low detection limits • Poor ability to resolve larger proteins
Scanning and transmission electron microscopy (SEM / TEM)	Elemental & layer analysis	Surface analysed under electron microscope	• Sample preparation (drying, coating) may cause serious issues • Poor quantitative analysis
Atomic force microscopy (AFM)	Protein attraction, layer property	"Feels" surface with a very sharp micro-scale cantilevered tip	• Allows tests in situ • Can be very hard to setup
Scanning tunnelling microscopy (STM)	Protein attraction, layer property	Measures quantum mechanical tunnelling of current between conductive surface and very sharp metallic tip.	• Can capture extremely fine changes in height • Lateral information not available from AFM
Surface-enhanced infrared adsorption spectroscopy (SEIRA)	Protein functionality	IR technique, amplifies received signal by two orders	• Not widely used

APPENDIX G : APPENDIX REFERENCES

[1] Lentner, C. *Geigy Scientific Tables*. Basle: Ciba-Geigy, 1981.

[2] Black, J. *Biological Performance of Materials: Fundamentals of Biocompatibility*. New York: Marcel Dekker, 2006.

[3] Park, J.B., R.S. Lakes. *Biomaterials : An Introduction*. New York: Springer, 2007.

[4] Ren, Y., H. Wang, J. Huang, B. Zhang, K. Yang. *Study of Biodegradation of Pure Magnesium.* Key Engineering Materials 2007;342-343:601.

[5] Duygulu, O., R.A. Kaya, G. Oktay, A.A. Kaya. *Investigation on the Potential of Magnesium Alloy Az31 as a Bone Implant*. Materials Science Forum 2007;546-549:421.

[6] Ren, Y., J. Huang, B. Zhang, K. Yang. *Preliminary Study of Biodegradation of Az31b Magnesium Alloy*. Frontiers of Material Science in China 2007;1:401.

[7] Witte, F., I. Abeln, E. Switzer, V. Kaese, A. Meyer-Lindenberg, H. Windhagen. *Evaluation of the Skin Sensitizing Potential of Biodegradable Magnesium Alloys*. Journal of Biomedical Materials Research Part A 2008;86A:1041.

[8] Witte, F., V. Kaese, H. Haferkamp, E. Switzer, A. Meyer-Lindenberg, C.J. Wirth, H. Windhagen. *In Vivo Corrosion of Four Magnesium Alloys and the Associated Bone Response*. Biomaterials 2005;26:3557.

[9] Wong, H.M., K.W.K. Yeung, K.O. Lam, V. Tam, P.K. Chu, K.D.K. Luk, K.M.C. Cheung. *A Biodegradable Polymer-Based Coating to Control the Performance of Magnesium Alloy Orthopaedic Implants*. Biomaterials 2010;31:2084.

[10] Reifenrath, J., C. Palm, P. Muller, H. Hauser, H.A. Crostack, J. Nellesen, F.W. Bach, D. Besdo, M. Rudert, F. Witte. *Subchondral Plate Reconstruction by Fast Degrading Magnesium Scaffolds Influence Cartilage Repair in Osteochondral Defects*. In: Society, O.R., editor. 51st Annual Meeting of the Orthopaedic Research Society, vol. 30: Orthopaedic Research Society, 2005.

[11] Witte, F., J. Fischer, J. Nellesen, F. Beckmann. *Microtomography of Magnesium Implants in Bone and Their Degradation*. vol. 6318. San Diego, CA, United States: International Society for Optical Engineering, Bellingham WA, WA 98227-0010, United States, 2006. p.631806.

[12] Witte, F., J. Nellesen, H.-A. Crostack, V. Kaese, A. Pisch, F. Beckmann, H. Windhagen. *In Vitro and in Vivo Corrosion Measurements of Magnesium Alloys*. Biomaterials 2006;27:1013.

[13] Witte, F., J. Reifenrath, P.P. Müller, H.A. Crostack, J. Nellesen, F.W. Bach, D. Bormann, M. Rudert. *Cartilage Repair on Magnesium Scaffolds Used as a Subchondral Bone Replacement*. Materialwissenschaft und Werkstofftechnik 2006;37:504.

[14] Witte, F., H. Ulrich, C. Palm, E. Willbold. *Biodegradable Magnesium Scaffolds: Part 2: Peri-Implant Bone Remodeling.* Journal of Biomedical Materials Research Part A 2007;81A:757.

[15] Witte, F., H. Ulrich, M. Rudert, E. Willbold. *Biodegradable Magnesium Scaffolds: Part 1: Appropriate Inflammatory Response*. Journal of Biomedical Materials Research Part A 2007:748.

[16] Von Der Höh, N., A. Krause, C. Hackenbroich, D. Bormann, A. Lucas, A. Meyer-Lindenberg. *The Influence of Difference Surface Machining Treatments of Resorbable Implants of Different Magnesium Alloys - a Primary Study in Rabbits*. Biomaterialien 2006;7:122.

[17] Von Der Höh, N., D. Bormann, A. Lucas, B. Denkena, C. Hackenbroich, A. Meyer-Lindenberg. *Influence of Different Surface Machining Treatments of Magnesium-Based*

Resorbable Implants on the Degradation Behavior in Rabbits. Advanced Engineering Materials 2009;11:B47.

[18] Krause, C., D. Bormann, T. Hassel, F.W. Bach, H. Windhagen, A. Krause, C. Hackenbroich, A. Meyer-Lindenberg. *Mechanical Properties of Degradable Magnesium Implants in Dependence of the Implantation Duration.* In: Pekguleryuz, M., editor. Conference of Metallurgists : Magnesium Technology in the Global Age. Montreal, Quebec, Canada, 2006. p.329.

[19] Thomann, M., C. Krause, D. Bormann, N. von der Höh, H. Windhagen, A. Meyer-Lindenberg. *Comparison of the Resorbable Magnesium Alloys Lae442 and Mgca0.8 Concerning Their Mechanical Properties, Their Progress of Degradation and the Bone-Implant-Contact after 12 Months Implantation Duration in a Rabbit Model*. Materialwissenschaft und Werkstofftechnik 2009;40:82.

[20] Von Der Höh, N., B. von Rechenberg, D. Bormann, A. Lucas, A. Meyer-Lindenberg. *Influence of Different Surface Machining Treatments of Resorbable Magnesium Alloy Implants on Degradation - Edx-Analysis and Histology Results*. Materialwissenschaft und Werkstofftechnik 2009;40:88.

[21] Li, Z., X. Gu, S. Lou, Y. Zheng. The Development of Binary Mg-Ca *Alloys for Use as Biodegradable Materials within Bone*. Biomaterials 2008;29:1329.

[22] Zhang, S., X. Zhang, C. Zhao, J. Li, Y. Song, C. Xie, H. Tao, Y. Zhang, Y. He, Y. Jiang, Y. Bian. *Research of Mg-Zn Alloy as Degradable Biomaterial*. Acta Biomaterialia 2010;6:626.

[23] Gruhl, S., F. Witte, J. Vogt, C. Vogt. *Determination of Concentration Gradients in Bone Tissue Generated by a Biologically Degradable Magnesium Implant*. Journal of Analytical Atomic Spectrometry 2009;24:181.

[24] Witte, F., J. Fischer, J. Nellesen, C. Vogt, J. Vogt, T. Donath, F. Beckmann. *In Vivo Corrosion and Corrosion Protection of Magnesium Alloy Lae442*. Acta Biomaterialia 2010;6:1792.

[25] Zhang, E.L., L.P. Xu, G.N. Yu, F. Pan, K. Yang. *In Vivo Evaluation of Biodegradable Magnesium Alloy Bone Implant in the First 6 Months Implantation*. Journal of Biomedical Materials Research Part A 2009;90A:882.

[26] Xin, Y., K. Huo, H. Tao, G. Tang, P.K. Chu. *Influence of Aggressive Ions on the Degradation Behavior of Biomedical Magnesium Alloy in Physiological Environment*. Acta Biomaterialia 2008;4:2008.

[27] Xu, L., G. Yu, E. Zhang, F. Pan, K. Yang. *In Vivo Corrosion Behavior of Mg-Mn-Zn Alloy for Bone Implant Application*. Journal of Biomedical Materials Research - Part A 2007;83:703.

[28] Xu, L., F. Pan, G. Yu, L. Yang, E. Zhang, K. Yang. *In Vitro and in Vivo Evaluation of the Surface Bioactivity of a Calcium Phosphate Coated Magnesium Alloy*. Biomaterials 2009;30:1512.

[29] Schranz, D., P. Zartner, I. Michel-Behnke, H. Akintürk. *Bioabsorbable Metal Stents for Percutaneous Treatment of Critical Recoarctation of the Aorta in a Newborn*. Catheterization and Cardiovascular Interventions 2006;67:671.

[30] Heublein, B., R. Rohde, V. Kaese, M. Niemeyer, W. Hartung, A. Haverich. *Biocorrosion of Magnesium Alloys: A New Principle in Cardiovascular Implant Technology?* Heart 2003;89:651.

[31] Thomopoulos, S., E. Zampiakis, R. Das, H.M. Kim, M.J. Silva, N. Havlioglu, R.H. Gelberman. *Use of a Magnesium-Based Bone Adhesive for Flexor Tendon-to-Bone Healing*. The Journal of Hand Surgery;34:1066.

[32] Pietak, A.M., T. Mahoney, G. Dias, M.P. Staiger. Bone-Like Matrix Formation on Magnesium and Magnesium Alloys. Journal of Biomedical Materials Research 2007;19:407.

[33] Vojtěch, D., H. Čížová, K. Volenec. *Investigation of Magnesium-Based Alloys for Biomedical Applications*. Kovove Mater 2006:211.

[34] Kuwahara, H., Y. Al-Abdullat, M. Ohta, S. Tsutsumi, K. Ikeuchi, N. Mazaki, T. Aizawa. *Surface Reaction of Magnesium in Hank's Solutions*. vol. 350-351. Nagaoka City, Japan: Trans Tech Publications, 2000. p.349.

[35] Al-Abdullat, Y., S. Tsutsumi, N. Nakajima, M. Ohta, H. Kuwahara, K. Ikeuchi. *Surface Modification of Magnesium by Nahco3 and Corrosion Behavior in Hank's Solution for New Biomaterial Applications*. Materials Transactions 2001;42:1777.

[36] Yamamoto, A., S. Hiromoto. *Effect of Inorganic Salts, Amino Acids and Proteins on the Degradation of Pure Magnesium in Vitro*. Materials Science and Engineering: C 2009;29:1559.

[37] Kuwahara, H., Y. Al-Abdullat, N. Mazaki, S. Tsutsumi, T. Aizawa. *Precipitation of Magnesium Apatite on Pure Magnesium Surface During Immersing in Hank's Solution*. Materials Transactions 2001;42:1317.

[38] Hiromoto, S., A. Yamamoto, N. Maruyama, H. Somekawa, T. Mukai. *Polarization Behavior of Pure Magnesium under a Controlled Flow in a Nacl Solution*. Materials Transactions 2008;49:1456.

[39] Hiromoto, S., A. Yamamoto, N. Maruyama, H. Somekawa, T. Mukai. *Influence of Ph and Flow on the Polarisation Behaviour of Pure Magnesium in Borate Buffer Solutions*. Corrosion Science 2008;50:3561.

[40] Zhuang, H., Y. Han, A. Feng. Preparation, *Mechanical Properties and in Vitro Biodegradation of Porous Magnesium Scaffolds*. Materials Science and Engineering: C 2008;28:1462.

[41] Lorenz, C., J.G. Brunner, P. Kollmannsberger, L. Jaafar, B. Fabry, S. Virtanen. *Effect of Surface Pre-Treatments on Biocompatibility of Magnesium*. Acta Biomaterialia 2009;5:2783.

[42] Wang, Y., M. Wei, J. Gao. *Improve Corrosion Resistance of Magnesium in Simulated Body Fluid by Dicalcium Phosphate Dihydrate Coating*. Materials Science and Engineering: C 2009;29:1311.

[43] Wang, Y., M. Wei, J. Gao, J. Hu, Y. Zhang. *Corrosion Process of Pure Magnesium in Simulated Body Fluid*. Materials Letters 2008;62:2185.

[44] Li, L., J. Gao, Y. Wang. *Evaluation of Cyto-Toxicity and Corrosion Behavior of Alkali-Heat-Treated Magnesium in Simulated Body Fluid*. Surface and Coatings Technology 2004;185:92.

[45] Zhang, E., L. Xu, K. Yang. *Formation by Ion Plating of Ti-Coating on Pure Mg for Biomedical Applications*. Scripta Materialia 2005;53:523.

[46] Kannan, M.B. *Influence of Microstructure on the in-Vitro Degradation Behaviour of Magnesium Alloys*. Materials Letters 2010;64:739.

[47] Lee, J.-Y., G. Han, Y.-C. Kim, J.-Y. Byun, J.-i. Jang, H.-K. Seok, S.-J. Yang. *Effects of Impurities on the Biodegradation Behavior of Pure Magnesium*. Metals and Materials International 2009;15:955.

[48] Brar, H.S., M.O. Platt, M. Sarntinoranont, P.I. Martin, M.V. Manuel. *Magnesium as a Biodegradable and Bioabsorbable Material for Medical Implants*. Jom 2009;61:31.

[49] Yun, Y., Z. Dong, D. Yang, M.J. Schulz, V.N. Shanov, S. Yarmolenko, Z. Xu, P. Kumta, C. Sfeir. *Biodegradable Mg Corrosion and Osteoblast Cell Culture Studies*. Materials Science and Engineering: C 2009;29:1814.

[50] Inoue, H., K. Sugahara, A. Yamamoto, H. Tsubakino. *Corrosion Rate of Magnesium and Its Alloys in Buffered Chloride Solutions*. Corrosion Science 2002;44:603.

[51] Lopez, H.Y., D.A. Cortes, S. Escobedo, D. Mantovani. *In Vitro Bioactivity Assessment of Metallic Magnesium*. Key Engineering Materials 2006;309-311:453.

[52] Ng, W.F., K.Y. Chiu, F.T. Cheng. *Effect of Ph on the in Vitro Corrosion Rate of Magnesium Degradable Implant Material.* Materials Science and Engineering: C 2010;30:898.

[53] Chiu, K.Y., M.H. Wong, F.T. Cheng, H.C. Man. *Characterization and Corrosion Studies of Fluoride Conversion Coating on Degradable Mg Implants*. Surface and Coatings Technology 2007;202:590.

[54] Ng, W.F., M.H. Wong, F.T. Cheng. *Stearic Acid Coating on Magnesium for Enhancing Corrosion Resistance in Hanks' Solution.* Surface and Coatings Technology 2010;204:1823.

[55] Shi, P., W.F. Ng, M.H. Wong, F.T. Cheng. *Improvement of Corrosion Resistance of Pure Magnesium in Hank's Solution by Microarc Oxidation with Sol-Gel Tio2 Sealing*. Journal of Alloys and Compounds 2007.

[56] Song, G., S. Song. *A Possible Biodegradable Magnesium Implant Material*. Advanced Engineering Materials 2007;9:298.

[57] Wan, Y., G. Xiong, H. Luo, F. He, Y. Huang, X. Zhou. *Preparation and Characterization of a New Biomedical Magnesium-Calcium Alloy.* Materials & Design 2008;29:2034.

[58] Wen, Z., C. Wu, C. Dai, F. Yang. *Corrosion Behaviors of Mg and Its Alloys with Different Al Contents in a Modified Simulated Body Fluid*. Journal of Alloys and Compounds 2009;488:392.

[59] Mueller, W.D., M.F.L. de Mele, M.L. Nascimento, M. Zeddies. *Degradation of Magnesium and Its Alloys: Dependence on the Composition of the Synthetic Biological Media*. Journal of Biomedical Materials Research Part A 2009;90A:487.

[60] Mueller, W.D., M.L. Nascimento, M. Zeddies, M. Córsico, L.M. Gassa, M.A.F.L. de Mele. *Magnesium and Its Alloys as Degradable Biomaterials: Corrosion Studies Using Potentiodynamic and Eis Electrochemical Techniques*. Materials Research 2007;10:5.

[61] Yfantis, C.D., D.K. Yfantis, J. Anastassopoulou, T. Theophanides, M.P. Staiger. *New Magnesium Alloys for Bone Tissue Engineering: In Vitro Corrosion Testing*. WSEAS transactions on Environment and Development 2006;2:1110.

[62] Kirkland, N.T., J. Lespagnol, N. Birbilis, M.P. Staiger. *A Survey of Bio-Corrosion Rates of Magnesium Alloys*. Corrosion Science 2010;52:287.

[63] Song, G. *Control of Biodegradation of Biocompatable Magnesium Alloys*. Corrosion Science 2007;49:1696.

[64] Feser, K., M. Kietzmann, W. Baumer, C. Krause, F.W. Bach. *Effects of Degradable Mg-Ca Alloys on Dendritic Cell Function*. J Biomater Appl 2010:0885328209360424.

[65] Wang, H., Z.M. Shi, K. Yang. *Magnesium and Magnesium Alloys as Degradable Metallic Biomaterials*. Advanced Materials Research 2008;32:207.

[66] Hassel, T., F.W. Bach, C. Krause. *Influence of the Alloy Composition on the Mechanical and Electrochemical Properties of Binary Mg-Ca Alloys and Its Corrosion Behaviour in Solutions at Different Chloride Concentrations.* In: Kainer, K.U., editor. Magnesium : Proceedings of the 7th International Conference on Magnesium Alloys and Their Applications: Wiley-VCH, 2007. p.789.

[67] Hassel, T., F.W. Bach, A.N. Golovko, A. Krause. *Investigation of the Mechanical Properties and the Corosion Behaviour of Low Alloyed Magnesium-Calcium-Alloys for Use as Absorbable Biomaterial in the Implant Technique*. In: Pekguleryuz, M., editor. Conference of

Metallurgists : Magnesium Technology in the Global Age. Montreal, Quebec, Canada, 2006. p.359.

[68] Denkena, B., C. Podolsky, A. Lucas, T. Hassel, F. Witte, O. Palm, C. Hurschler. *Degradable Implants Made of Magnesium Alloys*. 5th Euspen International Conference, vol. 6. Montpellier, France, 2005.

[69] Wan, Y.Z., G.Y. Xiong, H.L. Luo, F. He, Y. Huang, Y.L. Wang. *Influence of Zinc Ion Implantation on Surface Nanomechanical Performance and Corrosion Resistance of Biomedical Magnesium-Calcium Alloys*. Applied Surface Science 2008;254:5514.

[70] Kim, W.-C., J.-G. Kim, J.-Y. Lee, H.-K. Seok. *Influence of Ca on the Corrosion Properties of Magnesium for Biomaterials*. Materials Letters 2008;62:4146.

[71] Gu, X.N., Y.F. Zheng, L.J. Chen. *Influence of Artificial Biological Fluid Composition on the Biocorrosion of Potential Orthopedic Mg-Ca, Az31, Az91 Alloys*. Biomedical Materials 2009;4:8.

[72] Yfantis, C.D., D.K. Yfantis, J. Anastassopoulou, T. Theophanides, M.P. Staiger. *In Vitro Corrosion Behaviour of New Magnesium Alloys for Bone Regeneration*. World Scientific and Engineering Academy and Society, 2006.

[73] Zheng, Y.F., X.N. Gu, Y.L. Xi, D.L. Chai. *In Vitro Degradation and Cytotoxicity of Mg/Ca Composites Produced by Powder Metallurgy*. Acta Biomaterialia 2010;6:1783.

[74] Zhang, C.-Y., R.-C. Zeng, C.-L. Liu, J.-C. Gao. *Comparison of Calcium Phosphate Coatings on Mg-Al and Mg-Ca Alloys and Their Corrosion Behavior in Hank's Solution*. Surface and Coatings Technology 2010;204(21):3636.

[75] Denkena, B., A. Lucas. *Biocompatible Magnesium Alloys as Absorbable Implant Materials - Adjusted Surface and Subsurface Properties by Machining Processes*. CIRP Annals - Manufacturing Technology 2007;56:113.

[76] Gu, X., Y. Zheng, Y. Cheng, S. Zhong, T. Xi. *In Vitro Corrosion and Biocompatibility of Binary Magnesium Alloys*. Biomaterials 2009;30:484.

[77] Zhang, S., J. Li, Y. Song, C. Zhao, X. Zhang, C. Xie, Y. Zhang, H. Tao, Y. He, Y. Jiang, Y. Bian. *In Vitro Degradation, Hemolysis and Mc3t3-E1 Cell Adhesion of Biodegradable Mg-Zn Alloy*. Materials Science and Engineering: C 2009;29:1907.

[78] Peng, Q., Y. Huang, L. Zhou, N. Hort, K.U. Kainer. *Preparation and Properties of High Purity Mg-Y Biomaterials*. Biomaterials 2010;31(3):398.

[79] Hort, N., Y. Huang, D. Fechner, M. Störmer, C. Blawert, F. Witte, C. Vogt, H. Drücker, R. Willumeit, K.U. Kainer, F. Feyerabend. *Magnesium Alloys as Implant Materials - Principles of Property Design for Mg-Re Alloys*. Acta Biomaterialia 2010;6:1714.

[80] Yan, T., L. Tan, D. Xiong, X. Liu, B. Zhang, K. Yang. *Fluoride Treatment and in Vitro Corrosion Behavior of an Az31b Magnesium Alloy*. Materials Science and Engineering: C;In Press, Accepted Manuscript.

[81] Yang, J.X., F.Z. Cui, Q.S. Yin, T. Zhang, X.M. Wang. *Characterization and Degradation Study of Calcium Phosphate Coating on Magnesium Alloy Bone Implant in Vitro*. Plasma Science, IEEE Transactions on 2009;37:1161.

[82] Cui, F.Z., J.X. Yang, Y.P. Jiao, Q.S. Yin, Y. Zhang. *Calcium Phosphate Coating on Magnesium Alloy for Modification of Degradation Behavior*. Frontiers of Material Science in China 2008;2:143.

[83] Alvarez-Lopez, M., M.D. Pereda, J.A. del Valle, M. Fernandez-Lorenzo, M.C. Garcia-Alonso, O.A. Ruano, M.L. Escudero. *Corrosion Behaviour of Az31 Magnesium Alloy with Different*

Grain Sizes in Simulated Biological Fluids. Acta Biomaterialia 2009;In Press, Corrected Proof.

[84] Mueller, W.D., M. Lucia Nascimento, M.F. Lorenzo de Mele. *Critical Discussion of the Results from Different Corrosion Studies of Mg and Mg Alloys for Biomaterial Applications*. Acta Biomaterialia 2010;6:1749.

[85] Song, Y., D. Shan, R. Chen, F. Zhang, E.-H. Han. *Biodegradable Behaviors of Az31 Magnesium Alloy in Simulated Body Fluid*. Materials Science and Engineering: C 2009;29:1039.

[86] Zeng, R.C., J. Chen, W. Dietzel, N. Hort, K.U. Kainer. *Electrochemical Behavior of Magnesium Alloys in Simulated Body Fluids*. Transactions of Nonferrous Metals Society of China 2007;17:S166.

[87] Wang, H., Y. Estrin, H. Fu, g. Song, Z. Zúberová. *The Effect of Pre-Processing and Grain Structure on the Bio-Corrosion and Fatigue Resistance of Magnesium Alloy Az31*. Advanced Engineering Materials 2007;9:967.

[88] Wang, H., Y. Estrin, Z. Zúberová. *Bio-Corrosion of a Magnesium Alloy with Different Processing Histories*. Materials Letters 2008;62:2476.

[89] Kannan, M.B., R.K.S. Raman. *In Vitro Degradation and Mechanical Integrity of Calcium-Containing Magnesium Alloys in Modified-Simulated Body Fluid*. Biomaterials 2008;29:2306.

[90] Liu, C., Y. Xin, G. Tang, P.K. Chu. *Influence of Heat Treatment on Degradation Behavior of Bio-Degradable Die-Cast Az63 Magnesium Alloy in Simulated Body Fluid*. Materials Science and Engineering: A 2007;456:350.

[91] Song, Y.W., D.Y. Shan, E.H. Han. *Electrodeposition of Hydroxyapatite Coating on Az91d Magnesium Alloy for Biomaterial Application*. Materials Letters 2008;62:3276.

[92] Zhou, W., T. Shen, N.N. Aung. *Effect of Heat Treatment on Corrosion Behaviour of Magnesium Alloy Az91d in Simulated Body Fluid*. Corrosion Science 2010;52:1035.

[93] Liu, C., Y. Xin, X. Tian, P.K. Chu. *Degradation Susceptibility of Surgical Magnesium Alloy in Artificial Biological Fluid Containing Albumin*. Journal of Materials Research 2007;22:1806.

[94] Levesque, J., H. Hermawan, D. Dube, D. Mantovani. *Design of a Pseudo-Physiological Test Bench Specific to the Development of Biodegradable Metallic Biomaterials*. Acta Biomaterialia 2008;4:284.

[95] Kannan, M.B., R.K.S. Raman. *Evaluating the Stress Corrosion Cracking Susceptibility of Mg-Al-Zn Alloy in Modified-Simulated Body Fluid for Orthopaedic Implant Application*. Scripta Materialia 2008;59:175.

[96] Fekry, A.M., R.M. El-Sherif. *Electrochemical Corrosion Behavior of Magnesium and Titanium Alloys in Simulated Body Fluid*. Electrochimica Acta 2009;54:7280.

[97] Eliezer, A., F. Witte. *Corrosion Behaviour of Magnesium Alloys in Biomedical Environments*. Advanced Materials Research 2010;95:17.

[98] Xin, Y., C. Liu, K. Huo, G. Tang, X. Tian, P.K. Chu. *Corrosion Behavior of Zrn/Zr Coated Biomedical Az91 Magnesium Alloy*. Surface and Coatings Technology 2009;203:2554.

[99] Xin, Y., C. Liu, W. Zhang, J. Jiang, G. Tang, X. Tian, P.K. Chu. *Electrochemical Behavior Al2o3/Al Coated Surgical Az91 Magnesium Alloy in Simulated Body Fluids*. Journal of the Electrochemical Society 2008;155:178.

[100] Xin, Y., C. Liu, X. Zhang, G. Tang, X. Tian, P.K. Chu. *Corrosion Behavior of Biomedical Az91 Magnesium Alloy in Simulated Body Fluids*. Journal of Materials Research 2007;22:2004.

[101] Witte, F., F. Feyerabend, P. Maier, J. Fischer, M. Stormer, C. Blawert, W. Dietzel, N. Hort. *Biodegradable Magnesium-Hydroxyapatite Metal Matrix Composites*. Biomaterials 2007;28:2163.

[102] Rettig, R., S. Virtanen. *Time-Dependent Electrochemical Characterization of the Corrosion of a Magnesium Rare-Earth Alloy in Simulated Body Fluids*. Journal of Biomedical Materials Research Part A 2008;85A:167.

[103] Rettig, R., S. Virtanen. *Composition of Corrosion Layers on a Magnesium Rare-Earth Alloy in Simulated Body Fluids*. Journal of Biomedical Materials Research - Part A 2009;88:359.

[104] Feyerabend, F., J. Fischer, J. Holtz, F. Witte, R. Willumeit, H. Drücker, C. Vogt, N. Hort. *Evaluation of Short-Term Effects of Rare Earth and Other Elements Used in Magnesium Alloys on Primary Cells and Cell Lines*. Acta Biomaterialia;In Press, Corrected Proof.

[105] Gunde, P., F. Angela, C.H. Anja, S. Patrik, J.U. Peter. *The Influence of Heat Treatment and Plastic Deformation on the Bio-Degradation of a Mg-Y-Re Alloy*. Journal of Biomedical Materials Research Part A 2010;92A:409.

[106] Hänzi, A.C., M.M. Weder, B. Gerold, P.J. Uggowitzer. *New Bio-Absorbable Magnesium Alloys for Medical Applications*. Light Metals Technology Conference. Canada, 2007.

[107] Wang, J., R. Zeng, J. Chen, R. Chen. *Corrosion Behaviour of Magnesium Alloy Az53 in Simulated Body Fluids*. Material Science Forum 2009;610-613:1174.

[108] Quach, N.-C., P.J. Uggowitzer, P. Schmutz. *Corrosion Behaviour of an Mg-Y-Re Alloy Used in Biomedical Applications Studied by Electrochemical Techniques*. Comptes Rendus Chimie 2008;11:1043.

[109] Wang, H.X., S.K. Guan, X. Wang, C.X. Ren, L.G. Wang. *In Vitro Degradation and Mechanical Integrity of Mg-Zn-Ca Alloy Coated with Ca-Deficient Hydroxyapatite by the Pulse Electrodeposition Process.* Acta Biomaterialia 2010;6:1743.

[110] Zhang, E., D. Yin, L. Xu, L. Yang, K. Yang. *Microstructure, Mechanical and Corrosion Properties and Biocompatibility of Mg-Zn-Mn Alloys for Biomedical Application*. Materials Science and Engineering: C 2009;29:987.

[111] He, W., E. Zhang, K. Yang. *Effect of Y on the Bio-Corrosion Behavior of Extruded Mg-Zn-Mn Alloy in Hank's Solution*. Materials Science and Engineering: C 2009;30:167.

[112] Yang, L., E. Zhang. *Biocorrosion Behavior of Magnesium Alloy in Different Simulated Fluids for Biomedical Application*. Materials Science and Engineering: C 2009;29:1691.

[113] Xu, L., E. Zhang, K. Yang. *Phosphating Treatment and Corrosion Properties of Mg–Mn–Zn Alloy for Biomedical Application*. Journal of Materials Science: Materials in Medicine 2009;20:859.

[114] Zhang, E., L. Yang. Microstructure, *Mechanical Properties and Bio-Corrosion Properties of Mg-Zn-Mn-Ca Alloy for Biomedical Application*. Materials Science and Engineering: A 2008;497:111.

[115] Gu, X., Y. Zheng, S. Zhong, T. Xi, J. Wang, W. Wang. *Corrosion of, and Cellular Responses to Mg-Zn-Ca Bulk Metallic Glasses*. Biomaterials 2010;31:1093.

[116] Huang, L., D. Qiao, B.A. Green, P.K. Liaw, J. Wang, S. Pang, T. Zhang. *Bio-Corrosion Study on Zirconium-Based Bulk-Metallic Glasses*. Intermetallics 2009;17:195.

[117] Zberg, B., P.J. Uggowitzer, J.F. Loffler. *Mgznca Glasses without Clinically Observable Hydrogen Evolution for Biodegradable Implants*. Nature Materials 2009;8:887.